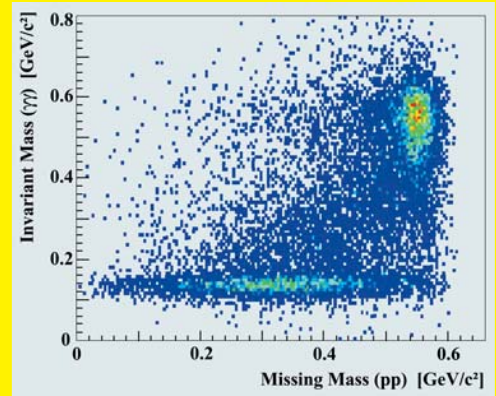
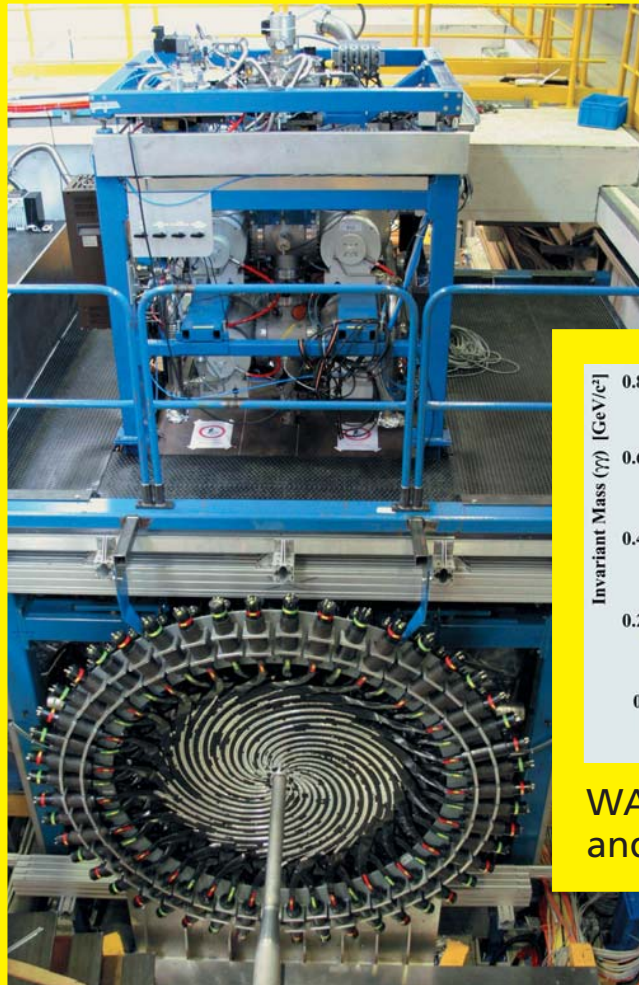




Institut für Kernphysik
COSY



WASA at COSY: Installation
and First Measurements

ANNUAL REPORT 2006

Annual Report 2006

Institut für Kernphysik / COSY

DIRECTORS AT THE IKP:

Experimental Hadron Structure (IKP-1):

Experimental Hadron Dynamics (IKP-2):

Theoretical Nuclear Physics (IKP-3):

Large-Scale Nuclear Physics Equipment (IKP-4):

Prof. Dr. James Ritman

Prof. Dr. Hans Ströher

Prof. Dr. Ulf-G. Meißner

Prof. Dr. Rudolf Maier (managing director)

EDITORIAL BOARD:

Priv. Doz. Dr. Markus Büscher

Priv. Doz. Dr. Christoph Hanhart

Prof. Dr. Siegfried Krewald

Prof. Dr. Hartmut Machner

Prof. Dr. Rudolf Maier

Prof. Dr. Ulf-G. Meißner

Prof. Dr. James Ritman

Dr. Hans Stockhorst

Prof. Dr. Hans Ströher

Cover picture:

One and a half years after starting the dismantling at CELSIUS, the WASA detector has been installed and successfully commissioned at COSY. The photograph shows the spiral elements of the Jülich quirl, encircling the COSY beam line (bottom), and the pellet generator above the interaction point in the course of the installation phase. First data on the reaction $pp \rightarrow pp\eta$ ($\rightarrow \gamma\gamma$) have been reconstructed during commissioning from the WASA forward- and central-detector information (abscissa and ordinate of the experimental spectrum, respectively).

Preface

The past year 2006 has been a very successful one for the institute: first off, a major milestone has been achieved with the in-time installation of the WASA detector at an internal target station of COSY and its subsequent commissioning. WASA-at-COSY is ready to take data and the collaboration is looking forward to its first data production run, approved by the COSY-PAC and scheduled for spring 2007. Furthermore, after very productive scientific programs, the internal experiment COSY-11 and the external beam experiments at BIG KARL have finished their data taking phases, and are now completing the analysis of the existing data.

The following highlights top the list of the important scientific results:

- Pentaquark studies: the TOF-collaboration has very carefully analysed their dedicated high-statistics data sample, and did not find a signal for the $\Theta^+(1540)$. This finding has been supported by the ANKE-collaboration in a different final state.
- Bound η -nucleus states: data with unprecedented precision for the ${}^3\text{He}\eta$ system have been obtained both at ANKE and at COSY-11 in the dp -reaction, exploiting the unique possibilities at the internal COSY beam during the ramp-up of the energy. The very rapid rise of the total cross section close to threshold implies a very large ${}^3\text{He}\eta$ scattering length and hence the presence of a quasi-bound state extremely close to threshold.
- Hyperon-nucleon interactions: chiral effective field theory has successfully been applied to the interactions between nucleons and hyperons. This paves the way to a model-independent approach of strange quark effects in nuclei.
- Accelerator studies: the COSY accelerator has been used for spin manipulations of a polarized deuteron beam, and clear indications for a deuteron spin resonance have been obtained.

All results mentioned have recently been submitted for publication. More details and further results can be found in the main text.

In addition to WASA, the two other major installations continue to be developed further:

- ANKE has taken an important step towards double polarization experiments with the first installation and commissioning of the polarized internal target.
- TOF is preparing for an upgrade with straw-detectors to further improve the tracking resolution. In view of the non-confirmation of the pentaquark at COSY and elsewhere, the earlier plans to implement a polarized target have been dropped.

As the FAIR project at GSI Darmstadt is taking shape, the IKP continues to become more and more involved in the preparations for the hadron physics program with antiproton beams:

- The accelerator group plays the dominant role in the international consortium of FZJ, TSL Uppsala and GSI Darmstadt to design the High Energy Storage Ring at FAIR. The ion optical design of the HESR, the RF systems, beam diagnostics, magnet and cryo-design and the stochastic cooling system are in the responsibility of the Jülich accelerator group.
- Beam-dynamics investigations in the equilibrium of internal targets and beam cooling have been carried out at COSY.
- The experimental groups are widely engaged in the design of the PANDA detector at HESR, with projects and commitments ranging from inner tracking to the pellet target. In particular, a cleanroom has been installed to develop the silicon pixel microvertex detector, and the IKP straw concept has been adapted by PANDA as the basis for the proposed Straw Tube Tracker. Furthermore, the IKP-Moscow group has taken a leading role in the pellet-target development.
- The possibilities to effectively produce polarized antiprotons for a later upgrade are being pursued by the PAX collaboration with essential test measurements at COSY (and possibly elsewhere).

We are looking forward to the constitution of the FAIR GmbH and the formal start of the project, and we hope for the timely flow of investment money in order to prepare and build the accelerator and detector components as planned.

Within the new funding opportunities by the Helmholtz association, IKP has succeeded in:

- A virtual institute “Spin and strong QCD”, headed by Prof. U.-G. Meißner , has been installed.
- A HGF-University junior-researcher position on “Few-Nucleon Systems in Chiral Effective Field Theory” has been raised in collaboration with Bonn University by Prof. E. Epelbaum.

More than 20 teaching positions at 11 Universities demonstrate the strong dedication of the institute for the education of students and young researchers. In this respect I want to emphasize that in 2006 the 3rd COSY Summer School took place which was attended by more than 30 Diploma and Ph.D. students from 9 countries.

Finally I would like to express my sincere gratitude to all our colleagues and co-workers, since without their help and support, we would not have been able to achieve our milestones. For WASA-at-COSY, our special thanks go to the former WASA-collaboration and to ZAT and ZEL. We also acknowledge the continuous support by the board of management of the Research Center and HGF.

Jülich, January 2007

Rudolf Maier

Contents

Cover	i
Titlepage	i
Preface	iii
Contents	viii
1 Experimental Hadron Physics	1
1.1 Analysis of $pp \rightarrow pK^0\pi^+\Lambda$. Search for the Pentaquark	2
1.2 $\Lambda(1405)$ production in pp collisions	3
1.3 The $pp \rightarrow K^+n\Sigma^+$ reaction near threshold	4
1.4 Investigation of the Reaction $dd \rightarrow {}^4\text{He}K^+K^-$ with ANKE	5
1.5 Production of the 1S_0 diproton in the $pN \rightarrow pp\pi^0$ reaction in the GeV region	6
1.6 Investigation of the ${}^3\text{He}\eta$ Final State in dp -Reactions at ANKE	7
1.7 Study of the ABC effect in the reaction $d+p \rightarrow {}^3\text{He}+\pi^++\pi^-$ close to the η -production threshold at ANKE	9
1.8 The reaction $d+p \rightarrow {}^3\text{He}+\pi^0$ close to the η production threshold at ANKE	10
1.9 The Polarized Internal Target at ANKE	11
1.10 Determination of the polarization of the ANKE polarized hydrogen storage cell target using the quasi-free $n\bar{p} \rightarrow d\pi^0$ reaction	13
1.11 Comparison of two implementations for timing by STT	15
1.12 Improved study of a possible Θ^+ production in the $pp \rightarrow pK^0\Sigma^+$ reaction with the COSY-TOF spectrometer	17
1.13 The Analysis Program “typeCase”	19
1.14 π^0 Production in pp Collisions at 0.95 GeV/c	20
1.15 Tests of the WASA-at-COSY Electromagnetic Calorimeter with a radioactive source	21
1.16 Test of the WASA Plastic Scintillator Barrel	23
1.17 Energy calibration of the WASA Plastic Scintillator Barrel	24
1.18 In-beam efficiency study of the WASA Trigger Hodoscope	26
1.19 Measurements on the light attenuation in the elements of the WASA-at-COSY Forward Trigger Hodoscope	27
1.20 First analysis of π^+ -tracks in the WASA Mini Drift Chamber	28
1.21 Test of the WASA Forward Proportional Chamber	29
1.22 The light pulser and light pulser monitoring system of WASA-at-COSY	30
1.23 Development of the new DAQ System for WASA at COSY	31
1.24 Status of the pellet target for the WASA-at-COSY experiment	32
1.25 A Pellet Tracking System for WASA at COSY	33
1.26 Evaluation of the missing mass resolution for the FRH extensions with DIRC and Time-of-Flight detectors	34
1.27 Upgrade of the Forward Range Hodoscope of the WASA-at-COSY facility	35
1.28 A Cherenkov detector for WASA-at-COSY	36
1.29 Monte Carlo studies for a RICH detector	37
1.30 Near threshold production mechanism of the η meson	39
1.31 Acceptance corrections of the two proton correlation function determined for the $pp \rightarrow pp\eta$ reaction	40
1.32 Measurement of the $dp \rightarrow {}^3\text{He}\eta$ reaction close to threshold	41
1.33 Near threshold η meson production via $dp \rightarrow dp\eta$ reaction	42
1.34 Measurement of the $pp \rightarrow pp\eta'$ reaction aiming at determination of the natural width of the η' meson	43
1.35 Study of the proton- η' interaction: analysis status	44
1.36 Status of the analysis of the $pn \rightarrow pn\eta'$ reaction	45
1.37 Measurement of the $pn \rightarrow d\eta'$ reaction at COSY-11	46
1.38 Close to threshold Λ production at COSY-11 with a polarized proton beam	47
1.39 Micro-Collimators for internal Cluster-Jet Targets	48
1.40 Wire device for the measurement of the dimensions of the COSY-11 cluster-jet target	49
1.41 Study of the $p+{}^6\text{Li} \rightarrow \eta+{}^7\text{Be}$ reaction close to threshold	50
1.42 Search for η -bound nuclei	51
1.43 Measurement of the Deuteron-Proton Breakup at 130 MeV	52
1.44 High Resolution Study of the $p+p \rightarrow K^++X$ reaction	53
1.45 The K^+K^- interaction in the reaction $pd \rightarrow {}^3\text{He}K^+K^-$ near threshold	54
1.46 Measurement of spectra of intermediate mass fragments from Au+p reaction by means of Bragg curve detectors	55
1.47 Do Unpolarized Electrons Affect the Polarization of a Stored Proton Beam?	56

1.48	A Polarized Target for Spin Filtering Tests at COSY and AD	58
1.49	Detector concept development for the spin-filtering experiment at COSY	59
1.50	High statistics measurement of the $K\beta$ transition in pionic deuterium	61
2	Theoretical Physics	63
2.1	Novel evaluation of the two-pion contribution to the nucleon isovector form-factors	64
2.2	Improved analysis of J/ψ decays into a vector meson and two pseudoscalars	65
2.3	Chiral corrections to the Roper mass	66
2.4	On the chiral effective meson-baryon Lagrangian at third order	67
2.5	K^-p scattering length from scattering experiments	68
2.6	On the extraction of the quark mass ratio $(m_d - m_u)/m_s$ from $\Gamma(\eta' \rightarrow \pi^0\pi^+\pi^-)/\Gamma(\eta' \rightarrow \eta\pi^+\pi^-)$	69
2.7	T-odd correlations in radiative K_{l3}^+ decays and chiral perturbation theory	70
2.8	$B_{s,d} \rightarrow \gamma\gamma$ decay in the model with one universal extra dimension	71
2.9	The Triton and three-nucleon force in nuclear lattice simulations	72
2.10	Testing the nature of the $\Lambda(1520)$ resonance in proton-induced production	73
2.11	The reaction $\pi N \rightarrow \pi\pi N$ in a meson-exchange approach	74
2.12	Omega-phi mixing in chiral perturbation theory	75
2.13	The nucleon axial-vector coupling beyond one loop	76
2.14	Isospin-breaking corrections in the pion-deuteron scattering length	77
2.15	Kaon-nucleon scattering lengths from kaonic deuterium experiments	78
2.16	Resonances and final state interactions in the reaction $pp \rightarrow pK^+\Lambda$	79
2.17	Aspects of ϕ -meson production in proton-proton collisions	80
2.18	Near threshold $p\bar{p}$ enhancement in B and J/Ψ decay	81
2.19	Comment on 'Mass and $K\Lambda$ coupling of the $N^*(1535)$ '	82
2.20	On the strong energy dependence of the $e^+e^- \leftrightarrow p\bar{p}$ amplitude near threshold	83
2.21	Phenomenology of the Λ/Σ^0 production ratio in pp collisions	84
2.22	Kaon-Deuteron Scattering at Low Energies	85
2.23	Dynamics of 1S_0 diproton formation in the $pd \rightarrow \{pp\}_s n$ and $pN \rightarrow \{pp\}_s \pi$ reactions in the GeV region	86
2.24	Insights on scalar mesons from their radiative decays	87
2.25	Hyperon-nucleon interactions – a chiral effective field theory approach	88
2.26	On the sign of the $\pi\rho\omega$ coupling constant	89
2.27	Unitarity cutting rules for the nucleus excitation and topological cross sections in hard production off nuclei from nonlinear k_t -factorization	90
2.28	Quenching of Leading Jets and Particles: the p_t Dependent Landau-Pomeranchuk-Migdal effect from Nonlinear k_t -Factorization	91
2.29	Glue in the pomeron from nonlinear k_\perp -factorization	92
2.30	Investigation of subthreshold resonances with the Trojan Horse Method	93
2.31	High-energy direct reactions with exotic nuclei and low-energy nuclear astrophysics	94
2.32	Electromagnetic strength of one- and two-neutron halo nuclei	95
2.33	Transverse momentum distribution of vector mesons produced in ultraperipheral relativistic heavy ion collisions	96
2.34	How accurate are the pionium breakup calculations?	97
2.35	Scalar Casimir effect between Dirichlet spheres or a plate and a sphere	98
2.36	Neutron-proton mass difference in nuclear matter	99
2.37	Periodic orbits in scattering from elastic voids	100
2.38	A force from nothing onto nothing: Casimir effect between bubbles in the Fermi sea	101
2.39	Casimir interaction between normal or superfluid grains in the Fermi sea	102
2.40	Hyperon-nucleon interactions in effective field theory	103
2.41	Three-nucleon force effects in the analyzing powers of the d(pol.) p breakup at 130 MeV	104
2.42	Compton Scattering on ^3He	105
2.43	More on the infrared renormalization group limit cycle in QCD	106
2.44	Lorentz boosted nucleon-nucleon potential applied to the ^3He -polarized(e-polarized, e^+ p)pn and ^3He -polarized(e-polarized, e^+ n)pp processes	107
2.45	Cross sections and tensor analyzing powers A_{yy} of the reaction $^1\text{H}(d, pp)n$ in 'symmetric constant relative energy' geometries at $E_d = 19$ MeV.	108
2.46	Measurement of the $^2\text{H}(n, \gamma)^3\text{H}$ reaction cross section between 10 and 550 keV	109
2.47	New data for total $^3\text{He}(\gamma, p)\text{D}$ and $^3\text{He}(\gamma, pp)n$ cross sections compared to current theory	110
2.48	Realistic few-body physics in the $dd \rightarrow \alpha \pi^0$ reaction	111
2.49	Application of chiral nuclear forces to light nuclei	112

2.50	A First estimation of chiral four-nucleon force effects in ^4He	113
2.51	Nucleon-deuteron capture with chiral potentials	114
2.52	Testing nuclear forces by polarization transfer coefficients in d(polarized-p, polarized-p)d and d(polarized-p, polarized-d)p reactions $E_{p,lab} = 22.7 \text{ MeV}$	115
2.53	Density matrix functional theory that includes pairing correlations	116
2.54	Gauge-invariant approach to meson photoproduction including the final-state interaction	117
2.55	Dispersive and absorptive corrections to the pion deuteron scattering length	118
2.56	Towards a field theoretic understanding of $NN \rightarrow NN\pi$	119
3	Accelerator Division	120
3.1	Longitudinal Stochastic Cooling Simulations in Comparison with Cooling Experiments at COSY	121
3.2	Experiments on Proton Beam Ordering by Electron Cooling	126
3.3	Loss Phenomena of Electron Cooled Ion Beams	128
3.4	Proposed 2 MeV Electron Cooler for COSY-Jülich	129
3.5	Study of a Pulsed Hydrogen Dissociator for the COSY Polarized Ion Source	131
3.6	Operation of the Injector Cyclotron and Ion Sources at COSY/Jülich	133
3.7	Substitute of Power Supplies and Improving of Water Cooling Circuits	135
3.8	Radiation Protection	136
4	Preparations for FAIR	138
4.1	Maximum Luminosities with Nuclear Targets in HESR	139
4.2	Ring-Slot Coupler for the HESR Stochastic Cooling System	140
4.3	Printed Loop Coupler for the HESR Stochastic Cooling System	141
4.4	Investigation of the Operation Regimes with the Moscow-Jülich Pellet Target	143
4.5	Modifications of the HESR Layout for Polarized Antiproton-Proton Physics	145
4.6	Lattice studies for low-beta sections at COSY and AD of CERN for spin-filtering studies	146
4.7	Simulation of antiproton interaction with silicon	148
5	Technical Developments	149
5.1	Gas Electron Multipliers as candidates for fast tracking detectors	150
5.2	Development of a Large-Volume Si(Li) Compton Polarimeter	151
5.3	Position-Sensitive Si(Li) Transmission Detectors for the EXL-Experiments at GSI-Darmstadt	152
5.4	Electronics Laboratory	153
A	Councils	154
A.1	Hadron Physics Program Advisory Council	154
A.2	COSY Program Advisory Committee	154
B	Publications 2006	155
C	Diploma and Ph.D. Theses	163
D	Invited Talks and Colloquia	164
E	Awards & Offers for Professorships	172
F	Funded Projects	173
G	COSY-FFE Projects	174
H	COSY Summer School CSS2006	175
I	Conferences (co-)organized by the IKP	176
I.1	HPC ² , Lanzhou (China)	176
I.2	International Workshop on η Physics	176
I.3	MESON2006, Cracow (Poland)	177
I.4	CGSWHP2006, Tbilisi (Georgia)	177
I.5	Carolina Isospin Violation Workshop	177
J	Teaching Positions	178

K	Beam Time at COSY 2006	179
L	Personnel	180
	L.1 Scientific Staff	180
	L.2 Technical and Administrative Staff	182
M	List of Authors	186

1 Experimental Hadron Physics

Analysis of $pp \rightarrow pK^0\pi^+\Lambda$. Search for the Pentaquark.

M. Nekipelov for the ANKE collaboration

The reaction $pp \rightarrow pK^0\pi^+\Lambda$, measured at ANKE at a beam momentum of $p_p = 3.65$ GeV/c, allows one to investigate the Kp system, which attracted a lot of attention due to its putative coupling to the pentaquark baryon $\Theta^+(1540)$ [1]. Its current status is reviewed in [2]. There is no theoretical investigation that reconciles both the positive and the negative observations, and it is believed that hadronic experiments at low energies can be crucial to clarify the situation.

The reaction at ANKE has been identified by detecting four particles simultaneously, the π^+ coming from the reaction vertex, the proton from vertex/ Θ^+ decay, and the products of the Λ decay: proton and π^- . Besides individual particle identification, the final state is fixed by the missing mass technique. A sizable background remains after cuts on masses are made, and this background is removed by the side band subtraction method.

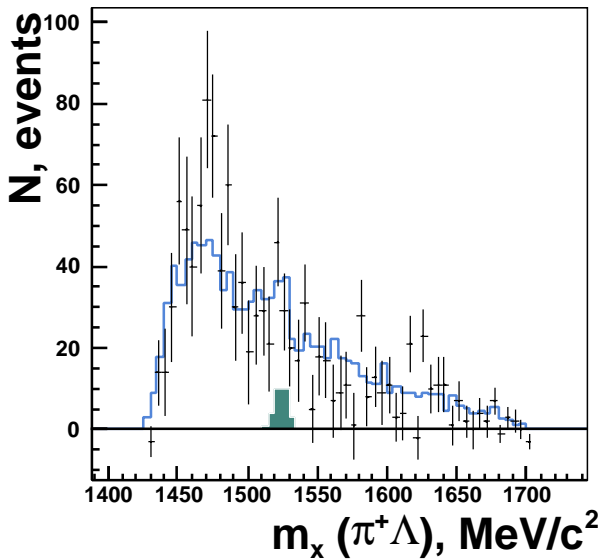


Fig. 1: Missing mass spectrum of $\pi^+\Lambda$ system. The solid line denotes the sum of all the contributions. The black region corresponds to the maximum permissible $\Theta^+(1540)$ signal.

The missing mass distribution $m(\pi^+\Lambda)$, presented in Fig. 1, is the one where the signal from the pentaquark is expected to appear. The solid line includes contribution from non-resonant production as well as contribution from the formation of an intermediate $\Delta^{++}(1232)$, inclusion of which is dictated by other differential distributions. The black area in Fig. 1 corresponds to the possible signal expected from the Θ^+ production. The fit results in a Θ^+ peak area, comparable with the statistical fluctuation of the background. Therefore, only an upper limit for the possible Θ^+ production is deduced:

$$\sigma_{\Theta^+\pi^+\Lambda} < 0.058 \mu\text{b}.$$

Since the acceptances of both four-body phase-space production and production with an intermediate $\Delta^{++}(1232)$ are very similar, a total cross section for the $pK^0\pi^+\Lambda$ final state can be calculated independent of the decomposition into separate channels. After the normalisation and efficiency corrections,

the following total cross section for the $pK^0\pi^+\Lambda$ final state has been deduced:

$$\sigma_{\text{tot}} = 1.41 \pm 0.05 \pm 0.33 \mu\text{b},$$

where the first error is statistical, while the second is systematic. The systematic uncertainty is mostly coming from the error of $\sigma_{pK^+\Lambda}$ [3], which has been used for the normalisation.

The total cross sections for the non-resonant channel and the channel with the $\Delta^{++}(1232)$ excitation have also been evaluated:

$$\begin{aligned} \sigma_{pK^0\pi^+\Lambda}^{\text{non-resonant}} &= 0.92 \pm 0.16 \pm 0.21 \mu\text{b}, \\ \sigma_{\Delta^{++}K^0\Lambda} &= 0.49 \pm 0.14 \pm 0.11 \mu\text{b}. \end{aligned}$$

The measured cross section for the $pp \rightarrow \Delta^{++}K^0\Lambda$ reaction is significantly lower than a model prediction, $\sigma \approx 6 \mu\text{b}$ [4]. However, this model overestimates as well the data available at high energies.

It is not possible to directly compare the Θ^+ production cross section obtained at ANKE with the one for $pp \rightarrow \Theta^+\Sigma^+$ measured at $p_p = 2.95$ GeV/c by the COSY-TOF collaboration [5] (see also Ref. [6] for the results of an improved study of this channel). Not to mention a difference in beam momentum of ~ 700 MeV/c, the exit channels are distinct and even the number of particles in the final state differs.

The details of the analysis can be found in Ref. [7].

References:

- [1] D. Diakonov, V. Petrov, and M. Polyakov, *Z. Phys. A* **359**, (1997) 305.
- [2] W.-M. Yao *et al.* (Particle Data Group), *J. Phys. G* **33**, (2006) 1.
- [3] R. I. Louttit *et al.* *Phys. Rev.* **123**, (1961) 1465.
- [4] K. Tsushima *et al.* *Phys. Rev. C* **59**, (1999) 369.
- [5] M. Abdel-Bary *et al.* *Phys. Lett. B* **595**, (2004) 127.
- [6] M. Abdel-Bary *et al.*; hep-ex/0612048.
- [7] M. Nekipelov *et al.*, *J. Phys. G: Nucl. Part. Phys.* **34**, (2007) 627.

$\Lambda(1405)$ production in pp collisions

I.Zychor^a for the ANKE Collaboration

The $\Lambda(1405)$ is a particularly interesting baryonic state because its structure is not yet understood and it is difficult to obtain in quark models. The $\Lambda(1405)$ can be the spin-multiplet partner of $J^P = 3/2^-$ $\Lambda(1520)$, or a meson-baryon resonance, or $\bar{K}N$ quasibound state. The first indication about a resonance now known as the $\Lambda(1405)$ has been presented in 1960 [1]. In 1985 after the measurement of the $\Lambda(1405)$ in K^-p reactions [2] there has been a hope that "the debate as to whether the $\Lambda(1405)$ is a pure quark state or a $\bar{K}N$ bound state may soon be clarified." Recent theoretical investigations based on chiral dynamics predict two poles for the $\Lambda(1405)$, one with a mass $1390 \text{ MeV}/c^2$ and a width of about $130 \text{ MeV}/c^2$ coupling strongly to $\pi\Sigma$ states and the other one with a mass around $1425 \text{ MeV}/c^2$ and a width of about $30 \text{ MeV}/c^2$ coupling mostly to $\bar{K}N$ states [3]. Earlier references could be found in the Review of Particle Physics 2000 Edition [4].

We report on measurements done with the ANKE spectrometer at COSY-Jülich. The reaction $pp \rightarrow pK^+Y^{0*}$ has been studied at a beam momentum of $3.65 \text{ GeV}/c$ to investigate the production of excited hyperon resonances Y^{0*} decaying via $\Sigma^0\pi^0$. In case of $\Lambda(1405)$ production in pp collisions there are two protons, one positively charged kaon and negatively charged pion in the final state: $pp \rightarrow pK^+\Lambda(1405) \rightarrow pK^+\Sigma^0\pi^0 \rightarrow pK^+\Lambda\gamma\pi^0 \rightarrow pK^+p\pi^-\pi^0\gamma$. At ANKE those particles are measured with *different* parts of the detection system: a positively charged kaon is registered in a telescope, a vertex proton in a forward detector, a decay proton in a positive-side detector (telescope or side-wall counter) and a negatively charged pion in a negative counter. In Fig. 1 the missing-mass distribution $MM(p_{FD}K^+)$ vs $MM(pK^+p\pi^-)$ is shown for the $3.65 \text{ GeV}/c$ pp collisions.

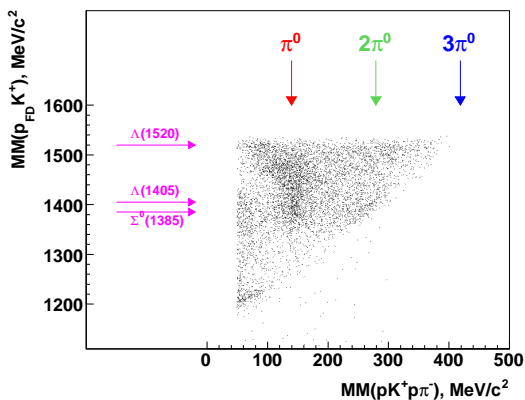


Fig. 1: The missing-mass distribution $MM(p_{FD}K^+)$ vs $MM(pK^+p\pi^-)$ for the $3.65 \text{ GeV}/c$ pp collisions.

The triangular shape of the distributions is due to the combination of kinematics and ANKE acceptance. The missing and invariant mass techniques are used to identify the $\Lambda(1405)$ resonance. Cutting on the invari-

ant mass of $p\pi^-$ we detect protons and negative pions from Λ decay. Furthermore we request the missing mass $MM(pK^+p\pi^-)$ to be higher than a mass of π^0 to separate the $\Lambda(1405)$ hyperon.

In Fig. 2 the missing-mass $MM(p_{FD}K^+)$ spectrum measured under above conditions is shown. The most prominent peak corresponds to the $\Lambda(1405)$.

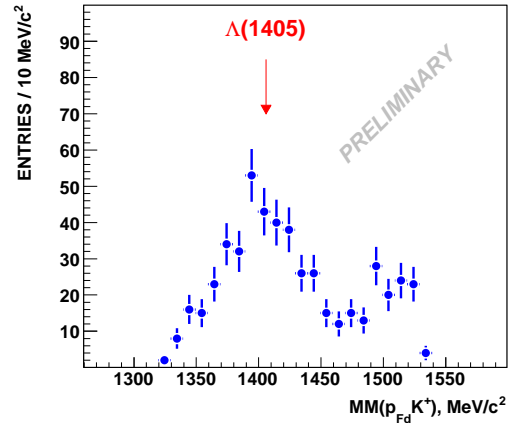


Fig. 2: The missing-mass $MM(p_{FD}K^+)$ distribution with a peak corresponding to the $\Lambda(1405)$ mass.

It is the first observation of the direct production of $\Lambda(1405)$ in pp collisions decaying via $\Sigma^0\pi^0$. Preliminary number of events in the $\Lambda(1405)$ peak is 250 ± 50 .

In the next step, the missing-mass spectra both $MM(p_{FD}K^+)$ and $MM(pK^+p\pi^-)$ will be analysed and compared with extensive Monte Carlo simulations. The phase-space distribution as well as the $\Lambda(1405)$ mass distribution for the $\Sigma^0\pi^0$ decay channel obtained in a chiral unitary model [5] will be exploited.

References:

- [1] R.H.Dalitz and S.F.Tuan, *Annals of Physics* **3**, 307 (1960)
- [2] R.J. Hemingway, *Nucl. Phys.* **B253**,742 (1985)
- [3] V.K.Magas *et al*, *Phys. Rev. Lett.* **95**, 052301 (2005)
- [4] D.E. Groom *et al*, *Eur. Phys. Jour.* **C15**,1 (2000)
- [5] J.C.Nacher *et al*, *Phys. Lett.* **B455**, 55 (1999)

^aThe Andrzej Sołtan Institute for Nuclear Studies, Świerk, Poland

The energy dependence for the total production cross sections of the Λ and Σ^0 hyperons in the COSY energy range is well known. It can be described by three-body phase-space, modified in the Λ case by strong $p\Lambda$ final state interaction (FSI) [1]. However, there are only three published experimental data points for the $pp \rightarrow K^+ n \Sigma^+$ reaction [2, 3]. Recent close-to-threshold measurements of this reaction channel at excitation energies of $\epsilon = 13$ and 60 MeV shows $\sigma(\Sigma^+)$ roughly equal to $\sigma(\Lambda)$ [2] at these energies. These result contradicts phenomenological analyses of the inclusive K^+ spectra which show that $\sigma(pp \rightarrow K^+ n \Sigma^+) \sim \sigma(pp \rightarrow K^+ p \Sigma^0)$ [4] at somewhat higher energies. But available K^+ inclusive data are restricted to the energies higher then 2.3 GeV and therefore have no direct bearing on the COSY-11 result. Thus, the unexpected energy behavior of the Σ^+ production total cross section needs further investigation.

We analyzed ANKE data collected at 2.16 GeV proton beam energy (correspond to $\epsilon = 128$ MeV) trying to fix the total cross section for Σ^+ production, using both K^+ inclusive spectra and K^+p , $K^+\pi^+$ correlations. Here we only present our analysis of the correlation spectra using relative normalization. For details of the analysis we refer to a forthcoming publication Ref. [5].

The resulting K^+p missing-mass spectrum is presented in Fig. 1. Two peaks corresponding to the Λ and Σ^0 ground states are very prominent. In addition there is a continuum which originates from the $\Lambda \rightarrow \pi^- p$ and $\Sigma^0 \rightarrow \gamma \Lambda \rightarrow \gamma p \pi^-$ decays, as well as a contribution from the $\Sigma^+ \rightarrow p \pi^0$ (BR 51.6%) decay. This continuum is well described by our simulations. The ratio of the Σ^0/Λ count rates, N_{Σ^0}/N_{Λ} , is prac-

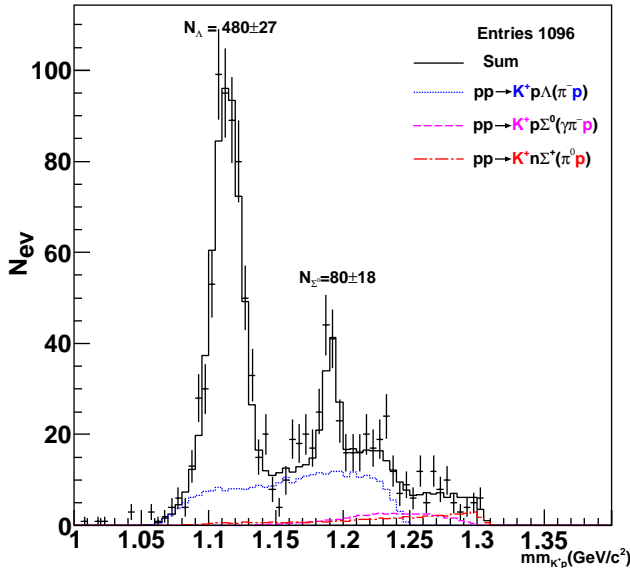


Fig. 1: Missing mass distribution of K^+p pairs produced in pp collisions at 2.16 GeV. In addition to the two peaks corresponding to direct protons from the $pp \rightarrow K^+ p \Lambda/\Sigma^0$ reactions, there are secondary protons arising from the $pp \rightarrow K^+ p (\Lambda \rightarrow \pi^- p)$ (dotted histogram), $pp \rightarrow K^+ p (\Sigma^0 \rightarrow \gamma \Lambda \rightarrow \gamma \pi^- p)$ (dashed histogram), and $pp \rightarrow K^+ n (\Sigma^+ \rightarrow \pi^0 p)$ (chain histogram). The sum of all contributions shown by the solid histogram.

tically independent of the conditions of the experiment (luminosity, telescope efficiencies), but depends on the acceptances and the total cross section in the combination:

$$N_{\Sigma^0}/N_{\Lambda} \times \text{acc}_{K^+p(\Lambda)}/\text{acc}_{K^+p(\Sigma^0)} = \frac{\sigma_{\text{tot}}(\Sigma^0)}{\sigma_{\text{tot}}(\Lambda)}. \quad (1)$$

The ratio of the acceptances was calculated using the phase-space model with a $p\Lambda$ FSI for $pp \rightarrow K^+ p \Lambda$ reaction and without any $p\Sigma^0$ FSI for the $pp \rightarrow K^+ p \Sigma^0$ reaction. This leads to the following estimates: $\text{acc}_{K^+p(\Lambda)} = 1.6 \times 10^{-4}$ and $\text{acc}_{K^+p(\Sigma^0)} = 4.6 \times 10^{-4}$. Thus:

$$\frac{\sigma_{\text{tot}}(\Sigma^0)}{\sigma_{\text{tot}}(\Lambda)} = \frac{80}{480} \times \frac{1.8 \times 10^{-4}}{4.6 \times 10^{-4}} = \frac{1}{(15 \pm 4)}. \quad (2)$$

Using the known value of the total cross section for Λ production of $\sigma_{\text{tot}}(\Lambda) = (23.9 \pm 1.2) \mu\text{b}$, the ratio leads to $\sigma_{\text{tot}}(\Sigma^0) = (1.7 \pm 0.4) \mu\text{b}$ at $T_p = 2.16$ GeV. This value is consistent with the parameterization presented in Ref. [1].

Using the known number of observed $K^+\pi^+$ correlation events from the ratio:

$$\text{BR}_{\Sigma^+ \rightarrow \pi^+ n} \times \frac{\sigma_{\text{tot}}(\Sigma^+)}{\sigma_{\text{tot}}(\Sigma^0)} = \frac{N_{K^+\pi^+(\Sigma^+)}}{N_{K^+p(\Sigma^0)}} \times \frac{\text{acc}_{K^+p(\Sigma^0)}}{\text{acc}_{K^+\pi^+(\Sigma^+)}}. \quad (3)$$

we obtain the following values of the ratio of Σ^+/Σ^0 total cross section:

$$\frac{\sigma_{\text{tot}}(\Sigma^+)}{\sigma_{\text{tot}}(\Sigma^0)} = \frac{40}{80} \times \frac{4.6 \times 10^{-4}}{3.8 \times 10^{-4}} \times \frac{1}{0.48} = 1.3 \pm 0.4. \quad (4)$$

Using the ratio of number of events and total acceptances in the K^+p and $K^+\pi^+$ spectra, the total cross section for $\sigma(\Sigma^+) = 2.2 \pm 0.3 \mu\text{b}$ at $\epsilon = 128$ MeV is obtained, which is more than an order of magnitude lower than that at $\epsilon = 60$ MeV reported in Ref. [2]. This only can be explained if there is a very strong close-to-threshold anomaly. It should be noted that the results for the total Σ^0 production cross section extracted from the analysis of K^+p correlations is in good agreement with the World data.

References:

- [1] A. Sibirtsev, J. Haidenbauer, H.-W. Hammer and S. Krewald, Eur. Phys. J. A 27 (2006) 269.
- [2] T. Rożek et al., Phys. Lett. B 643 (2006) 251.
- [3] R.I. Louttit et al., Phys. Rev. 123 (1961) 1465.
- [4] A. Sibirtsev, J. Haidenbauer, H.-W. Hammer and Ulf-G. Meißner, hep-ph/0701269, FZJ-IKP(TH)-2007-07.
- [5] Yu. Valdau et al., to be submitted to PLB.

1 High Energy Physics Department, Petersburg Nuclear Physics Institute, 188350 Gatchina, Russia

2 Institut für Kernphysik, Forschungszentrum Jülich, 52425 Jülich, Germany

Investigation of the Reaction $dd \rightarrow {}^4\text{He}K^+K^-$ with ANKE*

M.Büscher, A.Dzyuba^a, V.Koptev^a, M.Nekipelov, X.Yuan

A central goal of the COSY scalar-meson program is the extraction of the a_0 - f_0 mixing amplitude from a measurement of the isospin-violating reaction $dd \rightarrow {}^4\text{He}\pi^0\eta$ with WASA. An important step to reach this goal to measure the reaction $dd \rightarrow {}^4\text{He}K^+K^-$ with ANKE; from the analysis of these data the f_0 production amplitude can be determined which is later needed to determine the mixing strength [1].

In the analysis of the latter experiment a partial wave decomposition should be performed in order to isolate the $K\bar{K}$ s -wave contribution that may be identified with f_0 production. A similar analysis has been performed for $pp \rightarrow dK^+\bar{K}^0$ data at two beam energies [2, 3].

The measurement of the reaction $dd \rightarrow {}^4\text{He}K^+K^-$ has been performed in April 2006 (four weeks of beamtime) at 3.7 GeV/c deuteron-beam momentum, corresponding to 38 MeV excess energy. Positively charged kaons are detected in the side detection system, using time-of-flight (TOF) measurements. High momentum particles (d , t , ${}^3\text{He}$ and ${}^4\text{He}$) detected in coincidence with the kaons (online trigger condition) are detected by a forward detection (FD) system. In order to suppress the huge background from breakup protons the energy losses of the high momentum particles in the FD have been included into the online trigger. In order to determine the luminosity, using the known dd quasielastic cross section ($d\sigma/d\Omega$ at 6°), an additional prescaled single forward trigger has been added to the data stream.

In Fig. 1 the momentum distribution of the high momentum particles at $\theta = 6^\circ$ is presented for the second trigger. A clean peak from the deuteron quasielastic reaction is clearly visible at the expected position, and contains virtually no background.

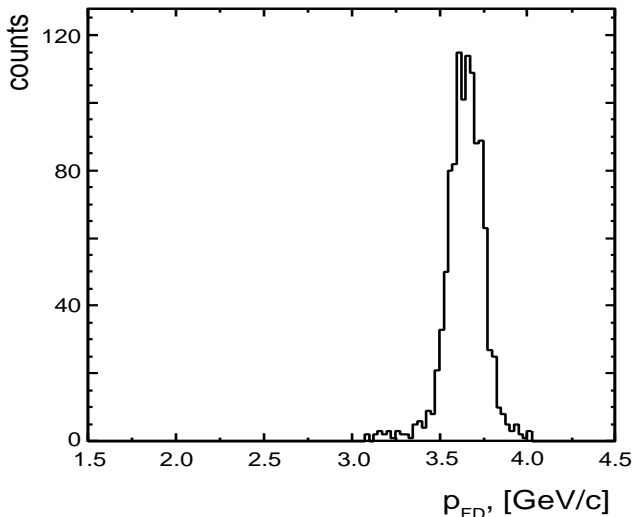


Fig. 1: Momentum of forward particle for prescaled forward trigger and $\theta = [5, 7]^\circ$.

The first step towards identifying the events from the ${}^4\text{He}K^+K^-$ final state was a careful investigation of ${}^4\text{He}\pi^+$ correlations. Since both mass and charge of ${}^4\text{He}$ are twice larger than for deuterons, the bands from $d\pi^+$ and ${}^4\text{He}\pi^+$ correlations coincide in a rigidity-*vs.*-time-difference spectrum (see Fig. 2a). versus A cut on this band suppresses ${}^3\text{He}\pi^+$ events and a ${}^4\text{He}\pi^+$ band becomes visible in a

rigidity-*vs.*-energy-loss in the FD (Fig. 2b,c). An additional cut on energy loss in another layer of scintillators (which was placed behind the FD) suppresses scattered background (Fig. 2d). This procedure allows us to select about 5000 ${}^3\text{He}\pi^+$ and 500 ${}^4\text{He}\pi^+$ coincidence events.

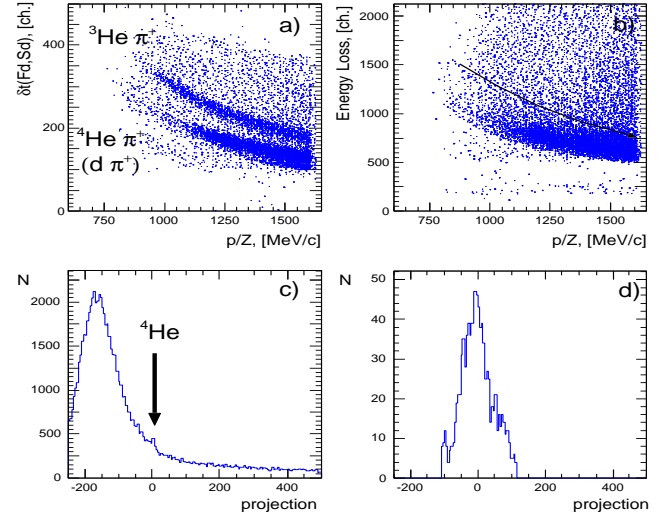


Fig. 2: Measured distributions for ${}^{2,3,4}\text{A}\pi^+$ events: a) Rigidity *vs.* (Sd-Fd) time difference (see text for details); b) Rigidity *vs.* energy loss in the FD; c) Projection on the ${}^4\text{He}$ band for spectrum (solid line in spectrum b)) with cut on deuteron band in spectrum a); d) Same projection but with cut on energy losses in another scintillator layer.

As a first step to identify the K^+ mesons in the ANKE side detectors, the delayed-veto technique has been applied. This leads to a very clean kaon identification, however, the efficiency of this method is only between 10 and 20%. Nevertheless, about 100 dK^+ coincidence events have been observed. This allows for a first rough estimate of ≤ 100 $dd \rightarrow {}^4\text{He}K^+K^-$ events in the full data set.

The next steps of the analysis will be a precise calibration of the forward-side time difference spectra, in order to identify ${}^4\text{He}K^+$ correlations, and acceptance corrections based on GEANT simulations. It is planned to finish the data analysis in 2007.

References:

- [1] M.Büscher *et al.*, COSY Proposal #140.
- [2] V. Kleber *et al.*, Phys. Rev. Lett. **91**, (2004) 172304.
- [3] A. Dzyuba *et al.*, Eur. Phys. J. A **29**, (2006) 245.

^a PNPI, Gatchina, Russia

* supported by DAAD, DFG, RFFI, COSY-FFE program

Production of the 1S_0 diproton in the $pN \rightarrow pp\pi^0$ reaction in the GeV region

S. Dymov^a, V. Kurbatov^a, A. Kulikov^a, V. Komarov^a, G. Macharashvili^a, D. Tsirkov^a, and Yu. Uzikov^a
for ANKE collaboration

Single pion production in NN collisions in the GeV region is attracting increasing attention in both theory and experiment [1, 2]. The $pp \rightarrow \{pp\}_s\pi^0$ reaction is of special interest for low excitation energy of the pp -system, $E_{pp} < 3$ MeV, when the 1S_0 final state dominates. Kinematically this reaction is very close to the well investigated $pp \rightarrow d\pi^+$ reaction [3]. However, the final $\{pp\}_s$ -pair is an isotriplet partner of the unbound virtual deuteron, whereas the 3S_1 - 3D_1 deuteron is an isosinglet. The different spin-isospin values lead to different transitions in the NN system that could significantly change the mechanism of the $pp \rightarrow \{pp\}_s\pi^0$ reaction as compared to that of $pp \rightarrow d\pi^+$. This gives us an opportunity to get more insight into the underlying meson-baryon dynamics by analyzing both reactions together. Unfortunately, experimental data on the $pp \rightarrow \{pp\}_s\pi^0$ reaction are very scarce (see Ref. [4] and references therein).

The unpolarized cross section of the $pp \rightarrow \{pp\}_s\pi^0$ reaction has recently been measured at COSY-ANKE at 0.8 GeV for diproton cm angles between 0 and 15.4° [4]. The absolute value of the measured cross section was found to be two orders of magnitude smaller than that of $pp \rightarrow d\pi^+$. Furthermore, an unusual angular dependence of the cross section was observed for this reaction. Both these peculiarities were qualitatively explained within a phenomenological model [5], which explicitly includes the Δ -isobar excitation in the intermediate state. Within this approach, a very strong energy dependence of the differential cross section and spin observables is expected below 1 GeV. This behaviour will soon be tested at COSY [6]. Here we report on the preliminary results of an analysis of data obtained at 1.1 GeV under similar conditions to those in Ref. [4].

For the analysis, events with two charged particle tracks crossing the Forward Detector of ANKE [7], were selected and the identification of the process was done on the basis of the missing-mass criterion. In total about 2000 events were obtained with $E_{pp} \leq 3$ MeV for the angular interval $0^\circ \leq \theta \leq 21.0^\circ$, where θ is the ejection angle of the pp system in the centre of mass of the reaction. The integral luminosity needed for normalization was found by simultaneous detecting $pp \rightarrow pp$ events and comparing the results with experimental data [8] and phase shift analysis [3].

In Fig. 1 the differential cross section is shown as a function of $\cos^2\theta$. The fit to the linear function $a(1 + b\sin^2\theta)$ gives $a = (186.8 \pm 15.5)$ nb/sr and $b = 9.74 \pm 2.64$, where the errors are pure statistical. Though the measured cross section demonstrates the same type of angular dependence as at 0.8 GeV, it is a factor 3.8 lower in the forward direction [4]. This seems to be in contradiction to the main trend expected in the GeV region within the ΔN model [5].

The ratio of the $pp \rightarrow \{pp\}_s\pi^0$ and $pp \rightarrow d\pi^+$ cross sections at 1.1 GeV and angle zero is $R(\pi^0/\pi^+) = 4.5 \times 10^{-3}$, which is very close to that found at 0.8

GeV. This is also very similar to the ratio of backward diproton production in the $pd \rightarrow \{pp\}_sn$ reaction to the deuteron in $pd \rightarrow dp$ in the GeV region [9]. Using the $pp \rightarrow \{pp\}_s\pi^0$ data at 0.8 GeV [4], agreement with the experimental results on the deuteron breakup $pd \rightarrow \{pp\}_sn$ [9] and the one-pion-exchange model involving the subprocess $pN \rightarrow \{pp\}_s\pi$ was found [10], where a baryon (or Reggeon) exchange mechanism was assumed for the $pN \rightarrow \{pp\}_s\pi$ reaction. Using the present data at 1.1 GeV, one can also find [11] similar agreement with the deuteron breakup data, interpolated between 0.95 and 1.35 GeV [9]. As noted in Ref. [10], in order to distinguish between baryon exchange and Δ -isobar mechanisms it is necessary to measure the ratio of π^- and π^0 production in the $pN \rightarrow \{pp\}_s\pi$ reaction.

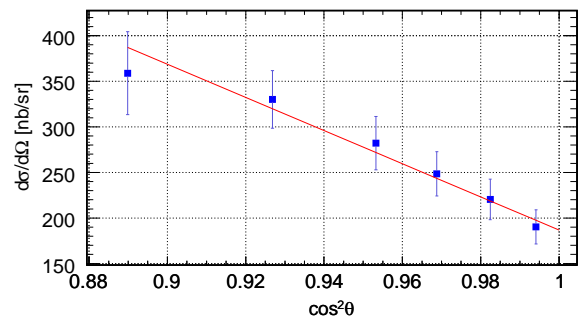


Fig. 1: The measured differential cross section of the $pp \rightarrow \{pp\}_s\pi^0$ reaction at 1.1 GeV versus $\cos^2\theta$, where θ is the angle of the momentum of the diproton system relative to direction of the beam in the cm system.

References:

- [1] V. Lensky *et al.*, Eur. Phys. J. **A 27**, 37 (2006).
- [2] C. Hanhart, Phys. Rep. **397**, 215 (2004)
- [3] R.A. Arndt, I.I. Strakovsky, R.L. Workman, and D.V. Bugg, Phys. Rev. C **48**, 1926 (1993); <http://gwdac.phys.gwu.edu>
- [4] S. Dymov *et al.*, Phys. Lett. B **635** (2006) 270.
- [5] J.A. Niskanen, Phys. Lett. B **642**, 34 (2006).
- [6] A. Kulikov *et al.*, *Measurement of the cross section and analyzing power of the $\bar{p}p \rightarrow \{pp\}_s\pi^0$ reaction*, COSY proposal No. 158 (2006).
- [7] S. Barsov *et al.* Nucl. Instrum. Methods. A **462**, 364, (2001).
- [8] F. Shimizu *et al.*, Nucl. Phys. A **389**, 445 (1982).
- [9] V.I. Komarov *et al.*, Phys. Lett. B **553** (2003) 179.
- [10] Yu.N. Uzikov, J. Haidenbauer, and C. Wilkin, Phys. Rev. C **75**, 014008 (2007).
- [11] Yu.N. Uzikov *et al.* (*in preparation*).

^a Joint Institute for Nuclear Research, Dubna, Russia

Investigation of the ^3He η Final State in dp -Reactions at ANKE*

T. Mersmann¹, A. Khoukaz¹, M. Mielke¹, M. Papenbrock¹, T. Rausmann¹ and A. Taeschner¹ for the ANKE-Collaboration

The existence of η -mesic nuclei is still an open issue of research. To investigate the possibility of the formation of such bound systems, production measurements with one η meson and one light nucleus in the final state are of great interest. By studying the final state interaction at low excess energies, information about the scattering length of the η -nucleus system can be gained. The latter one is closely related to the properties of such a possible bound state and has to be determined with high precision. The available data sets in the close vicinity of the threshold expose discrepancies, which currently forbid the extraction of scattering length information with sufficient precision [1].

Therefore, the reaction $d+p \rightarrow ^3\text{He} + \eta$ has been investigated at the ANKE spectrometer using a continuously ramped accelerator beam at excess energies ranging from below threshold at $Q = -5.1$ MeV up to $Q = +11.3$ MeV. Additionally, data at excess energies of $Q = 20, 40$ and 60 MeV have been recorded in order to determine total cross sections and to investigate contributions from higher partial waves [2]. For the analysis of the continuous ramp all data were sorted by the time information in the ramp. The resulting width of the excess energy interval is 72 keV.

To search for the events of the reaction channel of interest the ^3He nuclei are selected using the ANKE forward detector. The production of η -mesons is identified via the missing mass technique. For the reconstruction of the momenta via the magnetic spectrometer the information of the three drift- and multi-wire proportional chambers are used.

The particle identification is achieved by an energy loss versus momentum plot ($\Delta E/p$) for three segmented scintillation walls, two of the forward system and an additional side wall frame of the positive detector placed behind the forward system. A simultaneous cut on the expected region for ^3He nuclei in the ($\Delta E/p$) plot in the three scintillation walls allows for a clear identification of the ^3He band. The reactions can be identified by plotting the transversal versus the longitudinal reconstructed center of mass (CMS) momenta. For a reaction with two particles in the exit channel one expects a momentum ellipse with a fixed radius.

In the near threshold region the CMS-momenta of the ^3He nuclei are small. Due to this fact the scattering angles ϑ^{LS} for the ^3He nuclei after the Lorentz transformation into the laboratory system are small and all ^3He nuclei of the reaction channel of interest are in the geometrical acceptance of the wire chambers of the forward system. For this reason the dp kinematic was used for the beamtime, leading to a full geometrical acceptance in the wire chambers up to an excess energy of 20 MeV. The result is a characteristic image of the hit position in all chambers.

The identification of the η events is done using the missing mass distribution shown in figure 1b). The challenge of the extraction of the η peak from the background near the kinematical limit can impressively be met by using subthreshold data as it was done in [3]. The background reactions, namely the multi pion production and misidentified protons from breakup reactions, have a high excess energy and vary only slowly with the excess energy for the η -production. Subthreshold data of the continuous ramp analysed with the same

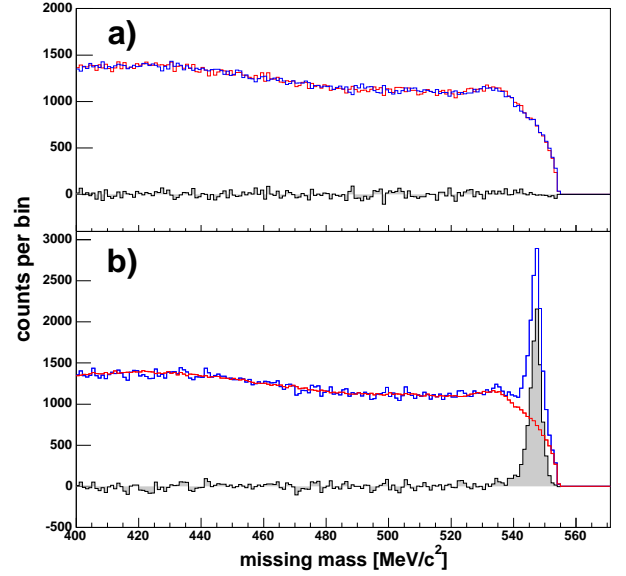


Fig. 1: a) Comparison of the data at $Q = -4.75$ MeV (blue line) and $Q = -0.6$ MeV (red line). The difference shown is consistent with zero (blue filled histogram). b) Missing mass distribution (blue line) at an excess energy of $Q = 6.95$ MeV. The subtraction of the scaled background description (red line) using all the sub-threshold data results in a clean η peak (filled histogram).

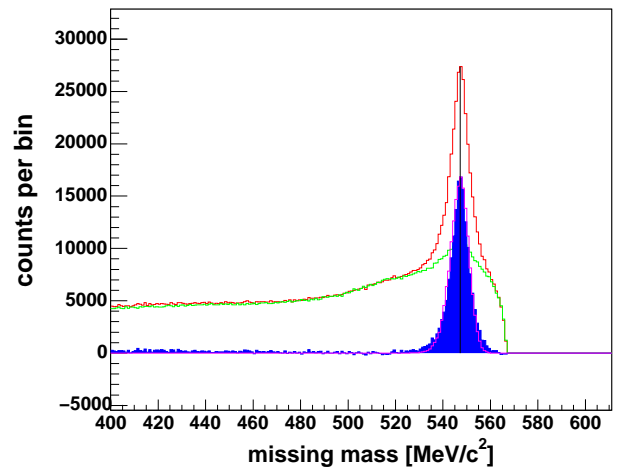


Fig. 2: Preliminary missing mass plot (red line) at an excess energy of $Q = 20$ MeV. The background description (green line), the subtracted η signal (blue filled histogram) and a Monte-Carlo simulation (pink line) of the η -peak are added.

kinematical conditions as the analysed data are expected to give a good description of the background behaviour. The data of the chosen excess energy interval and the sub-threshold data were analysed assuming an excess energy of $Q = 6.95$ MeV. The reconstructed ^3He momenta were scaled

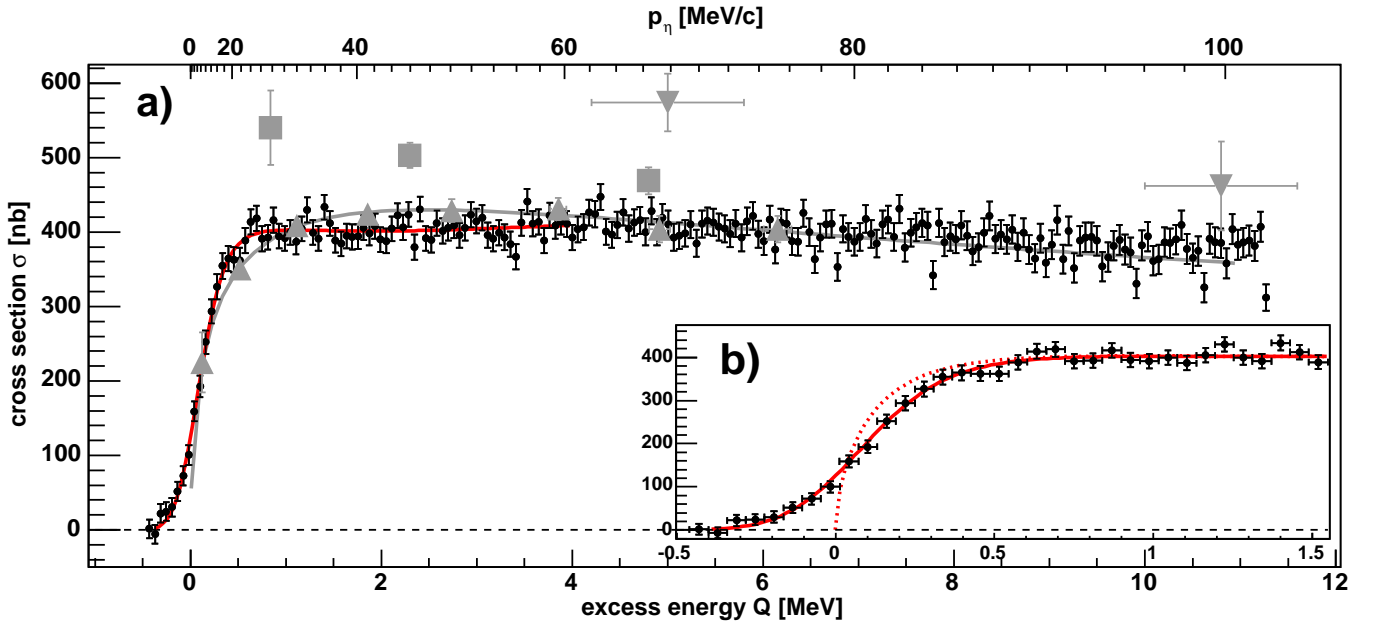


Fig. 3: Comparison of the extracted total cross section data (circles) with data from Ref.[4](squares), Ref.[5](triangles) and Ref.[6](inverted triangles). The red curve is the fit to our data for $Q < 4$ MeV. The grey curve is the SpesII fit to their own data [5]. Not shown are overall uncertainties arising from data normalization.

to the same conditions. In figure 1b) the red line shows the resulting missing mass distribution of the data at $Q = 6.95$ MeV and the green one of the subthreshold data scaled to the red line. The difference, plotted as the filled histogram, corresponds to pure η production.

A check of the method to describe the background is possible by the comparison of the data obtained at $Q = -4.75$ MeV (green line) and $Q = -0.6$ MeV (red line) in figure 1a) where both were analyzed assuming a value of $Q = +6.95$ MeV. The difference of the scaled curves (blue filled histogram) vanish, therefore the shape of the background does not vary within the first eighty seconds of the ramp. Thus it can be assumed that this behaviour does not change for the following 180 seconds.

The $d+p \rightarrow {}^3\text{He}+\eta$ total cross sections obtained at 195 bins in excess energy Q are displayed in figure 3. The minimal relative systematic errors resulting from the measurement of the excitation function in a single experiment form a robust data set for any analysis. In 3b) one can see the surprisingly steep rise of the total cross section near threshold that indicates a very strong final state interaction. The shape of the η production below the nominal threshold is well understood and it is a very sensitive measurement of the finite width of the COSY beam. It was also possible to extract the differential cross sections for each excess energy bin and therefore to determine the angular asymmetry parameter α , defined as

$$\left(\frac{d\sigma}{d\Omega}\right)_{\text{c.m.}} = \frac{\sigma_{\text{tot}}}{4\pi} [1 + \alpha \cos\theta_{\text{c.m.}}] \quad (1)$$

The results show a contribution from higher partial waves already above an excess energy of $Q = 4$ MeV.

The data taken at higher excess energies of $Q = 20, 40$ and 60 MeV are as well currently analysed. A preliminary missing mass plot is shown in figure 2. Total cross sections as well as differential cross sections will be determined for this energies. Together with the results from the continuous ramp data this will form a complete differential and total cross section

sample from threshold up to 60 MeV excess energy for the $d+p \rightarrow {}^3\text{He}+\eta$ reaction.

References:

- [1] A. Sibirtsev, J. Haidenbauer, C. Hanhart and J. A. Niskanen, *The $\eta^3\text{He}$ scattering length revisited*, Eur. Phys. J. A 22, 495-502 (2004)
- [2] A. Khoukaz, T. Mersmann, *Investigation of the ${}^3\text{He}$ η final state in the reaction $d+p \rightarrow {}^3\text{He}+\eta$ at ANKE*, COSY-Proposal, 2004
- [3] A. Wronska, *Near threshold eta meson production in the $d+d \rightarrow {}^4\text{He}+\eta$ reaction*, doctoral thesis, Jagiellonian University, Cracow, 2005
- [4] J. Berger et al., Phys. Rev. Lett. 61, 919 (1988)
- [5] B. Mayer et al., Phys. Rev. C 53, 2068 (1996)
- [6] H.-H. Adam et al., Phys. Rev. C (*in press*)

¹ Institut für Kernphysik Westfälische Wilhelms-Universität, 48149 Münster, Germany

* Supported by FZ-Jülich FFE

Study of the ABC effect in the reaction $d+p \rightarrow {}^3\text{He} + \pi^+ + \pi^-$ close to the η -production threshold at ANKE*

M. Mielke¹, A. Khoukaz¹, T. Mersmann¹, M. Papenbrock¹, T. Rausmann¹ and A. Täschner¹ for the ANKE-Collaboration

In 2005 the reaction $d+p \rightarrow {}^3\text{He} + \eta$ was studied at ANKE. Due to the fact that the reaction of interest was measured by detection of the ${}^3\text{He}$ nuclei and reconstruction of the η meson via the missing mass technique, data on the multi pion production near the η threshold was additionally obtained with the same trigger.

For this purpose supplementary to the forward detector used for the ${}^3\text{He}$ detection, the negative system of the ANKE experimental setup was used to detect π^- mesons.

Investigation of ${}^3\text{He}$ events with a coincident π^- meson allows for a systematic study of the multi pion production near the η threshold which is required for the separation of the η signal from the background. Furthermore the investigation of the two pion production is interesting by itself since it offers the possibility to study the ABC effect occurring in the reaction $d+p \rightarrow {}^3\text{He} + \pi^+ + \pi^-$ similar to recent measurements at CELSIUS [2].

The data presented here was obtained at an excess energy of $Q = 20$ MeV relative to the η threshold and a fixed beam momentum of 3.223 GeV/c.

In the following analysis only events with a coincident ${}^3\text{He}$ nucleus in the forward detector and a π^- meson in the negative system are used. The ${}^3\text{He}$ nuclei were identified as described in [1]. At the used beam energy particles detected by the negative system in coincidence with a ${}^3\text{He}$ nucleus in the forward system can only be pions or leptonic background.

Multi pion production can be identified in the squared missing mass distribution of the ${}^3\text{He} \pi^-$ system (figure 1a). The production of two charged pions leads to the left hand peak at the squared mass of the π^+ meson. The structure on the right hand side of the spectrum can approximately be reproduced by ANKE Root Monte Carlo simulations of the reactions $d+p \rightarrow {}^3\text{He} + \eta [\eta \rightarrow \pi^+ + \pi^- + \pi^0]$ and $d+p \rightarrow {}^3\text{He} + \pi^+ + \pi^- + \pi^0$. Therefore, figure 1a demonstrates the possibility to select a clean sample of two pion events.

For the investigation of the ABC effect in the reaction $d+p \rightarrow {}^3\text{He} + \pi^+ + \pi^-$ it is necessary to separate the two pion production from the multi pion background. To achieve this the invariant mass spectrum of the two pion system $M_{\pi^+\pi^-}$ is divided into finite mass intervals. For each interval the content of the π^+ peak in the respective squared missing mass distribution of the ${}^3\text{He} \pi^-$ system is determined.

The results after correction for geometrical acceptance are shown in figure 1b. Pure phase space distribution considering the finite ANKE momentum reconstruction is given by the shaded area. The uncertainties correspond purely to statistical errors. As expected the ABC effect manifests itself in an enhancement at low invariant masses $M_{\pi^+\pi^-}$.

Its size becomes clear from the ratio of measured data and simulations (figure 1d), where the low-invariant mass region shows a strong deviation from phase space considerations.

Since low invariant masses belong to pion pairs with small relative momentum, the opening angle $\delta_{\pi^+\pi^-}$ between these pions in the overall cms must be small. This can be seen in figure 1c, which is derived in the same way as figure 1b.

In the Dalitz plot of $M_{3\text{He}\pi^-}$ and $M_{3\text{He}\pi^+}$ (figure 2) the ABC effect is clearly visible as a strong enhancement in the region corresponding to minimum invariant masses $M_{\pi^+\pi^-}$.

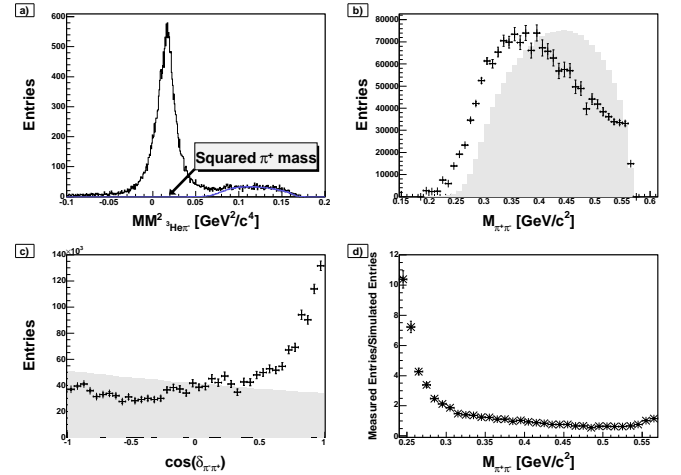


Fig. 1: a) Squared missing mass distribution of the ${}^3\text{He} \pi^-$ system; blue curve shows ANKE Root Monte Carlo simulations of multi pion background
b) Opening angle $\delta_{\pi^+\pi^-}$ between the two pions in $d+p \rightarrow {}^3\text{He} + \pi^+ + \pi^-$
c) Invariant mass spectrum $M_{\pi^+\pi^-}$ of the two pion system in $d+p \rightarrow {}^3\text{He} + \pi^+ + \pi^-$
d) Ratio of measured and simulated invariant mass $M_{\pi^+\pi^-}$.

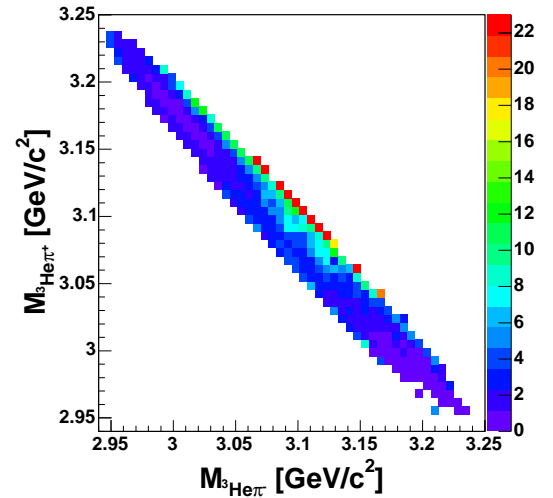


Fig. 2: Dalitz plot of $M_{3\text{He}\pi^-}$ and $M_{3\text{He}\pi^+}$ system, corrected for the geometrical acceptance of ANKE.

References:

- [1] T. Mersmann et al., *ibidem*, *Investigation of the ${}^3\text{He} \eta$ Final State in dp -Reaction $d+p \rightarrow {}^3\text{He} + \eta$ at ANKE*
- [2] M. Bashkanov et al., *Exclusive Measurements of $pd \rightarrow {}^3\text{He} + \pi\pi$: the ABC effect revisited*, *Phys. Lett. B* **637**, 223-228, (2006)

¹ Institut für Kernphysik Westfälische Wilhelms-Universität, 48149 Münster, Germany

* Supported by FZ-Jülich FFE

The reaction $d+p \rightarrow {}^3\text{He} + \pi^0$ close to the η production threshold at ANKE*

M. Papenbrock¹, A. Khoukaz¹, T. Mersmann¹, M. Mielke¹, T. Rausmann¹, and A. Täschner¹ for the ANKE-Collaboration

In 2005 the reaction $d+p \rightarrow {}^3\text{He} + \eta$ was studied at the ANKE experimental setup [1]. This reaction is of great interest as it allows the investigation of the final state interaction of an η meson and the ${}^3\text{He}$ nucleus and thus a possible bound state of the η - ${}^3\text{He}$ system. Due to the fact that the reaction of interest was measured by detection of the ${}^3\text{He}$ nuclei and reconstruction of the η meson via the missing mass technique, data on the π^0 production near the η threshold was additionally obtained with the same trigger. This data is of special interest as there may be a structure in the ${}^3\text{He} \pi^0$ production cross section close to the η production threshold. Here we present data obtained at a fixed excess energy of $Q = 20$ MeV ($p_d = 3.223$ GeV/c) relative to the η threshold, corresponding to $Q = 427$ MeV with respect to the π^0 threshold. This data set was used because it provides high statistics for a fixed beam momentum and thus is very suitable for understanding and handling the background.

The ${}^3\text{He}$ nuclei were identified using the ANKE forward detector system. The extracted transversal vs. longitudinal momentum plot in the center of mass system exhibits clear signals of both the exit channels ${}^3\text{He} + \pi + \pi$ and ${}^3\text{He} + \pi^0$. As can be seen in figure 1, the geometrical acceptance of the ANKE spectrometer is large for forward scattered ${}^3\text{He}$ nuclei in the center of mass system. The plot was filled with the reciprocal value of the transversal momentum as an event weight. The two curves indicate the kinematical limits for both the π^0 and the two-pion production.

Figure 2 shows the center of mass momentum of particles identified as ${}^3\text{He}$ nuclei for a certain $\cos(\vartheta_{{}^3\text{He}}^{\text{CMS}})$ interval. A clear π^0 signal is visible on top of background distributions, namely the multi pion production and misidentified protons from breakup reactions. To describe this background, Monte Carlo simulations for the reactions $d+p \rightarrow {}^3\text{He} + \pi + \pi$ and $d+p \rightarrow p+p+n$ are required. In the latter case forward scattered protons were assumed to be ${}^3\text{He}$ nuclei. The distribution of the deuteron breakup was scaled to fit the high momentum tail of the experimental data. Afterwards the multi pion productions were scaled to fit with the lower momenta of the data, while keeping the ratio between the $\pi^0\pi^0$ and the $\pi^+\pi^-$ production according to [2]. As can be seen in figure 2, there is a discrepancy between simulated and experimental data approaching the high momenta of the two pion productions. An approach to describe this gap is introduced with the ABC-effect [2], which is not considered in the shown simulations. This effect is expected to raise the distributions of the multi pion productions at lower invariant masses and therefore higher CMS momenta of the ${}^3\text{He}$ nuclei.

Further analyses are currently performed at ANKE to quantify the ABC-effect which will be included in the simulated multi pion productions [3]. These corrected simulations will then be subtracted from the experimental data and to separate the π^0 peak from the background.

This way, it will be possible to extract differential cross sections for the reaction $d+p \rightarrow {}^3\text{He} + \pi^0$. Furthermore, data obtained above and below the η -threshold will be analysed with respect to a possible structure in this cross section that may indicate the occurrence of a cusp effect.

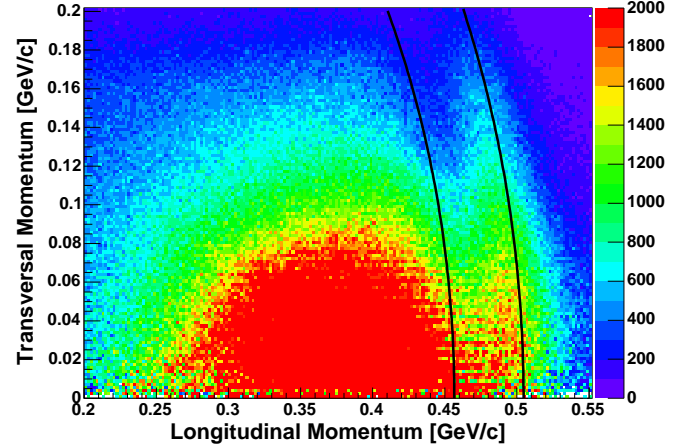


Fig. 1: Momentum plot of the ${}^3\text{He}$ CMS momenta. The solid lines indicate the kinematical limits of π^0 production (right) and the two pion productions (left).

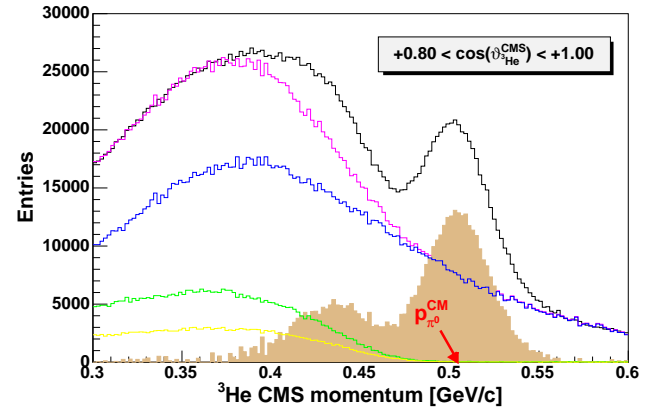


Fig. 2: Center of mass momentum distribution for several data sets: experimental data (black); simulated data for $d+p \rightarrow {}^3\text{He} + \pi^0 + \pi^0$ (yellow), $d+p \rightarrow {}^3\text{He} + \pi^+ + \pi^-$ (green), $d+p \rightarrow p+p+n$ (blue), sum of all simulated data (magenta); experimental data after background subtraction with simulated data (filled brown).

References:

- [1] A. Khoukaz, T. Mersmann, *Investigation of the ${}^3\text{He}$ η final state in the reaction $d+p \rightarrow {}^3\text{He} + \eta$ at ANKE*, COSY-Proposal 137, 2004
- [2] M. Bashkanov *et al.*, *Exclusive measurements of $p d \rightarrow \text{He-3} \pi^+ \pi^-$: The ABC effect revisited* arXiv:nucl-ex/0508011.
- [3] M. Mielke *et al.*, *ibidem*, *Study of the ABC effect in the reaction $d+p \rightarrow {}^3\text{He} + \pi^+ + \pi^-$ close to the η -production threshold at ANKE*

¹ Institut für Kernphysik Westfälische Wilhelms-Universität, 48149 Münster, Germany

* Supported by FZ-Jülich FFE

The Polarized Internal Target at ANKE

R. Engels, D. Chiladze¹, S. Dymov², K. Grigoryev³, P. Jansen⁴, A. Kacharava⁵, F. Klehr⁴, H. Kleines⁶, B. Lorentz, M. Mikirtychyants³, S. Mikirtychyants³, D. Prasuhn, F. Rathmann, J. Sarkadi, H. Seyfarth, and A. Vasilyev³

In a first stage of the double polarized measurements, to be performed at the magnet spectrometer ANKE, several $\vec{d}\vec{p}$ reactions of actual interest will be investigated with the polarized deuteron beam of COSY and the polarized hydrogen storage-cell target. These include the reactions $\vec{d}\vec{p} \rightarrow (2p)n$, $\vec{d}\vec{p} \rightarrow (2p)\Delta^0$, $\vec{d}\vec{p} \rightarrow dp$, $\vec{d}\vec{p} \rightarrow {}^3\text{He}\pi^0$, and $\vec{d}\vec{p} \rightarrow {}^3\text{He}\eta$ [1].

In order to maximize the figure of merit for double polarized experiments, two weeks of beam time in February and March 2006 were spent to study the use of stochastic cooling of the unpolarized proton beam circulating through the storage cell and to commission the polarized atomic beam source (ABS) at the ANKE target position near to the spectrometer dipole magnet D2.

Following the test measurements in November 2005 with a storage cell in the ANKE target chamber [2], the support frame with the cell was dismantled and a cryogenic catcher for the ABS beam was installed (Fig. 1). By its use, the

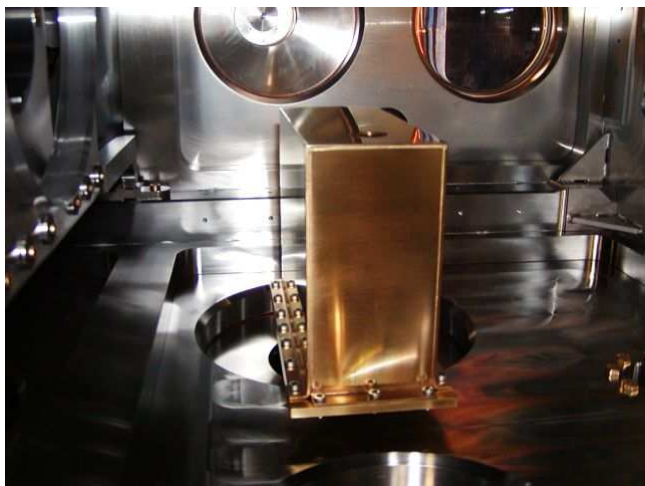


Fig. 1: Side view into the ANKE target chamber with the cryogenic catcher. The outer surface is polished and gold-plated to reduce the radiation-heat load. By a Cu heat bridge the catcher is connected to a cold head, mounted below the target chamber. The vertical beam from the ABS enters the catcher by the hole in the upper surface.

residual gas pressure in the ANKE target chamber could be reduced by one order of magnitude to 3.7×10^{-8} mbar. The measured thickness of the direct ABS jet without storage cell of $(1.5 \pm 0.1) \times 10^{11}$ H atoms/cm² (left-hand side of Fig. 2) is in perfect agreement with the calculated value of $(1.6 \pm 0.1) \times 10^{11}$ H atoms/cm².

During the measurements with the jet, the medium field transition unit (MFT) of the ABS was working properly. But it was observed that the polarization of the ABS beam could not be switched from the positive value (atoms in hyperfine state 1 / MFT on - WFT off) to the negative value (atoms in hyperfine state 3 / MFT on - WFT on) achieved earlier in the laboratory tests ($Q_z = 0.89$ and $Q_z = -0.90$, respectively). This could be explained by the insufficient shielding of the weak field rf transition unit (WFT) of the ABS, i.e., penetration of the magnetic stray field of the

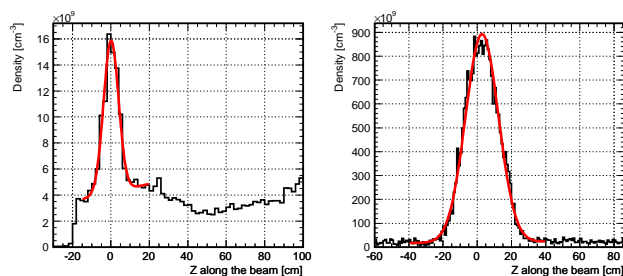


Fig. 2: Density distributions of the target gas along the COSY beam direction measured by use of the $pp \rightarrow d\pi^+$ reaction. The target-gas densities, given in the text, result from the summation over the peaks. Left-hand side: Measurement with the jet of H atoms and 600 MeV protons. Right-hand side: Measurement with H₂ gas in the storage cell of 20×20 mm² cross section, 380 mm length, and 831 MeV protons. The width of the distribution reflects the length of the storage cell.

magnet D2 into the transition unit [3]. To overcome this problem during the beam time, the direction of the magnetic gradient field in the medium field rf transition unit was reversed to populate the hyperfine state 2 of the H atoms in the ABS beam. According to the magnetic flux density of about 165 G in the interaction region of the COSY beam and the jet, the negative value of the polarization should be about $p_z = -0.31$. In this first measurement, however, only slightly more than 50% of the expected value of the polarization inversion could be achieved.

For the next beam time in March 2006, the ABS and the cryogenic catcher had to be dismantled. Two new storage cells with $20 \times 20 \times 380$ mm³ and $10 \times 10 \times 380$ mm³ were implemented. For COSY beam studies these cells were fed with H₂ gas fluxes equivalent to the H beam intensity of the ABS. The unpolarized COSY beam was electron-cooled and stacked during injection. This allowed to accelerate 1.6×10^{10} protons to 831 MeV flat top energy with the larger cell and with the COSY beam in the ANKE setup deflected by $\alpha = 8^\circ$. With the smaller cell only 2.5×10^9 protons could be injected, but they got lost during acceleration. The measured target-density distribution (right-hand side of Fig. 2) shows the triangular shape, expected due to the gas-density distribution in the storage cell along its axis.

In the flat top, the COSY beam was stochastically cooled to compensate the beam heating by the target gas. The effect of cooling was studied with the use of the count rate in the Forward-Detector system of ANKE. Without cooling, the beam heating results in a widening of the beam which leads to an increase of the beam interactions with the storage-cell wall (see Fig. 3). As seen in this figure, too, this effect is reduced by the application of stochastic cooling. The trigger rate in the ANKE Forward-Detector system follows the decrease of the COSY beam intensity. As a natural consequence, the life time of the COSY beam is increased by the beam cooling.

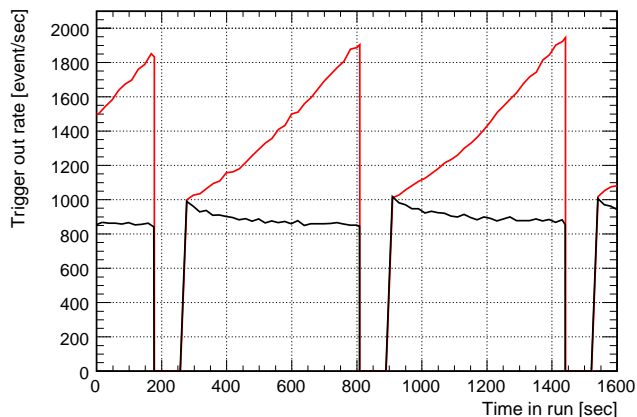


Fig. 3: Time dependence of the trigger rate of the ANKE Forward-Detector system in the 831 MeV flat top without (red) and with stochastic cooling.

For its use in tuning of the ABS, the Lamb-shift polarimeter (LSP) after a number of necessary modifications could be mounted with the ionizer and the 90° deflector below the ANKE target chamber. The Fig. 4 shows a part of the LSP components. In the present mode of installation, the LSP is used to measure the jet polarization as in the laboratory before [4].

With the ANKE magnet D2 set to magnetic field strengths,

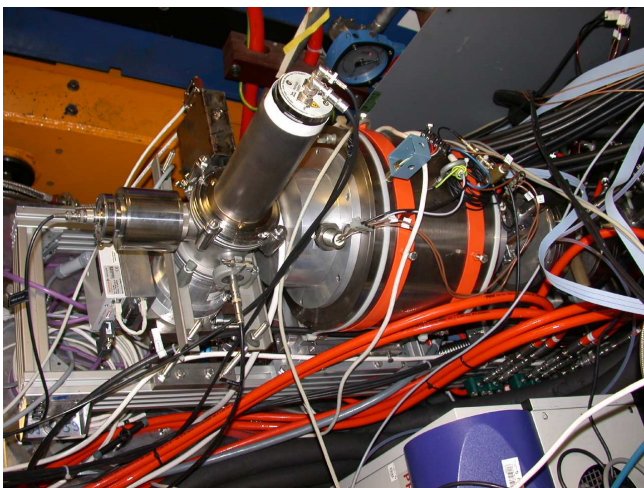


Fig. 4: The Lamb-shift polarimeter at ANKE. From left to right the visible components are the Faraday cup, the quench chamber with the photomultiplier, the spin-filter, and the cesium cell. The Wien filter, the 90° deflector, the ionizer, and the ANKE target chamber follow outside the right-hand edge of the figure.

requested in the beam times in 2007, in December 2006 the LSP could be commissioned. The peak ratios, however, in the Lamb-shift spectra (Fig. 5) were found to be about three times lower than expected. Furthermore, the polarization of the ABS jet resulted with a sign opposite to the expected one. This finding can be explained by the action of the magnetic stray field of the D2 magnet to the ions between the LSP ionizer and cesium cell, leading to changes in the precession of the polarized ions. A special problem was encountered by the variation of strength and probably also

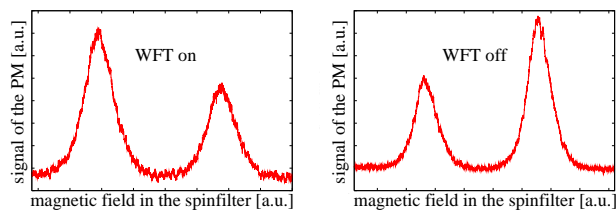


Fig. 5: Lamb-shift spectra measured with the LSP, when the weak field rf transition unit (WFT) was switched off (left-hand side) and on (right-hand side). The ratio of the two peaks in the spectra yield the polarization of the atomic beam.

the direction of the stray field with the field in the 20 cm gap of the D2 magnet. With additional shielding, the Wien filter, installed between the ionizer and the cesium cell, could be used to partly compensate the induced precession. In spite of the encountered problems, the measured asymmetries were found to be proportional to the polarization of the atomic hydrogen beam from the ABS and they thus could be used to monitor the polarization during the beam-time measurements.

Meanwhile, the insufficient magnetic shielding of the weak field rf transition unit, mentioned above, has been completed. Tests have shown that the operation of the unit now is not affected by the D2 stray field. Tuning of the rf transition units of the ABS is made possible with errors of about 1% in the achieved transition efficiencies. Now the polarization of the \vec{H} beam from the ABS can be switched between the maximum positive and negative values. The tuning procedures, switching of the polarization and monitoring of the system is done with the use of the slow-control system, developed in collaboration with the Zentralinstitut für Elektronik of FZJ [5].

The authors want to acknowledge the valuable help by the infrastructure division of IKP, by other divisions of FZJ, and by the members of the ANKE collaboration, who enabled the development, installation, and commissioning of the new setup. The authors thank E. Steffens, Universität Erlangen-Nürnberg, and H. Paetz gen. Schieck, Universität zu Köln, for contributions to the development of the PIT.

References:

- [1] A. Kacharava et al., Proposal for the Spin Physics from COSY to FAIR, nucl-ex/0511028, 2005.
 - [2] K. Grigoryev et al., IKP+COSY Ann. Rep. 2005.
 - [3] K. Grigoryev et al., Proc. 17th Int. Spin Physics Symposium (SPIN06), Kyoto, Japan, October 2006 (in press).
 - [4] R. Engels et al., Rev. Sci. Instrum. **76** (2005) 053305.
 - [5] H. Kleines et al., Nucl. Instr. Meth. A **560** (2006) 503.
- ¹ IHEPI, Tbilisi State University, 0186 Tbilisi, Georgia.
 - ² Joint Institute for Nuclear Research, 141980 Dubna, Russia.
 - ³ Petersburg Nuclear Physics Institute, 188350 Gatchina, Russia.
 - ⁴ Zentralabteilung Technologie, FZ Jülich.
 - ⁵ Universität Erlangen-Nürnberg, 91054 Erlangen, Germany.
 - ⁶ Zentralinstitut für Elektronik, FZ Jülich.

**Determination of the polarization of the ANKE polarized hydrogen storage cell target
using the quasi-free $n\bar{p} \rightarrow d\pi^0$ reaction***

D. Chiladze^{a,b}, S. Dymov^c, R. Engels, K. Grigoriev^a, A. Kacharava^{b,d}, M. Mikirtychiants^a, F. Rathmann, H. Seyfarht,
A. Vasilyev^e, and C. Wilkin^f for the ANKE collaboration

During one week of beam time in January 2007 allocated for the double-polarized Charge-Exchange reaction study [1, 2], we used a 1200 MeV polarized (unpolarized) deuteron beam and a polarized hydrogen storage cell target of size $20 \times 15 \times 390$ mm³. The preliminary results of the determination of the target polarization through the measurement of identified quasi-free $n\bar{p} \rightarrow d\pi^0$ events detected in the ANKE forward system, are presented.

Due to isospin invariance, the neutron analyzing power in the $\bar{n}p \rightarrow d\pi^0$ reaction should be identical to that of the proton in $\bar{p}p \rightarrow d\pi^+$, for which extensive data compilations are available (SAID). As shown by our earlier measurements with a polarized deuteron beam [3], the agreement of our results with the shape of the SAID predictions is very good for both small and large deuteron cm angles. This led to a determination of the vector polarization of the deuteron beam since, for the small Fermi momenta investigated here, there is a one-to-one relation between the deuteron and constituent neutron polarizations. The deduced value for P_z was completely consistent with that obtained from elastic $\vec{d}p$ scattering. Within small error bars, typically 2%, there was no sign of any effect arising from the tensor polarization of the deuteron beam.

For the January 2007 experiment using an unpolarized COSY deuteron beam and a polarized hydrogen storage cell target, the ϕ -dependence of the differential cross section $\sigma/\sigma_0 = 1 + Q_y A_y^p \cos \phi$ allowed us to extract the combination $Q_y A_y^p$. The known values of the proton analyzing power A_y^p of the $\bar{p}p \rightarrow d\pi^+$ leads to the determination of the hydrogen target polarization Q_y .

The Atomic Beam Source (ABS) of the ANKE polarized internal target (PIT) [4] has appeared in two spin modes: positive polarization Q_y^+ (spin-up, WFT is **off** and MFT is **on**) and negative polarization Q_y^- (spin-down, WFT is **on** and MFT is **on**). This has been managed by proper switching of the weak field transition (WFT) unit every 5 s **off** or **on**, while the medium field transition unit (MFT) was always switched **on**. In the following initial analysis it has assumed that $|Q_y^+| = |Q_y^-| = Q_y$.

The event identification has been done in the following way. Fig. 1 shows events from the $d\bar{p}$ interaction sample, where two charged particles were detected in the double-layer forward scintillation hodoscope. Polarized \bar{H} (unpolarized N_2) gas was used in the target cell and an incident deuteron beam of 1200 MeV energy employed. The figure shows the arrival-time differences for the two particles in the hodoscope (calculated after momentum and trajectory reconstruction under the assumption that both particles were protons) versus the measured difference of the two time signals from the scintillator. Thus, the two protons from the $dp \rightarrow (pp)n$ reaction should lie along the diagonal, with other pairs, such as dp_{sp} with a spectator proton from $dp \rightarrow dp_{sp}\pi^0$, being found elsewhere. Time-of-flight cuts applied to the distributions of Fig. 1 allow one to select the dp candidates and hence to derive the missing-mass squared distributions of the $dp \rightarrow dp\pi^0$ reactions presented in Fig. 2. For both the high deuteron momentum part (forward production in cm system), and the low momentum region (backward production),

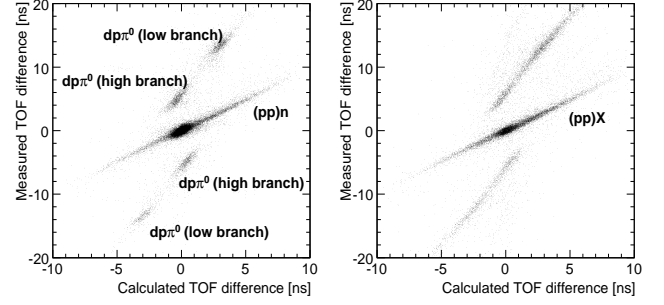


Fig. 1: Time difference of the two detected charged particles, calculated under the assumption that both particles are protons, versus the measured time difference for \bar{H} gas (left panel) and N_2 gas (right panel) in the storage cell.

the peaks corresponding to the unobserved π^0 are clearly seen. For small deuteron cm angles the spectrometer provides useful ϕ acceptance over the full angular range. However, for events in the backward hemisphere, this is restricted to $|\phi| < 60^\circ$, in order to get $|\cos \phi| \gg 0$.

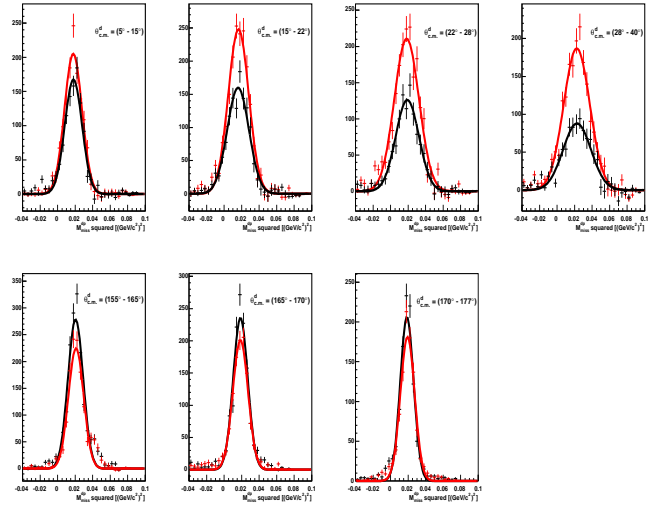


Fig. 2: Angular dependence of the missing-mass squared distribution for the reaction $d\bar{p} \rightarrow dp_{sp}X$ (upper row **High** branch, and lower row **Low** branch) measured with the storage cell and 1200 MeV deuteron beam. Red and black histograms stands, respectively, for data with target polarization 'spin-up' and 'spin-down', after background subtraction using N_2 data.

The background subtracted counts extracted from the different θ_{cm}^d angular intervals are listed in the Table 1 for two different spin states (N^+ and N^-). The background shape was taken from the N_2 data sample, as was discussed above.

Using the asymmetry value $\varepsilon = (N^+ - N^-)/(N^+ + N^-)$ determined for each individual θ_{cm}^d angular bin and the proper values for the averaged analyzing power $\langle A_y \rangle$ of

θ_{cm}^d	N^+	N^-	$\langle A_y \rangle$	$\langle \cos\phi \rangle$	Q_y
11.2	1286.5	1030.4	0.179	-0.826	-0.747 ± 0.297
19.5	1817.4	1239.4	0.293	-0.860	-0.750 ± 0.173
25.8	1855.1	1045.1	0.361	-0.894	-0.866 ± 0.154
32.7	1747.8	879.4	0.416	-0.902	-0.881 ± 0.140
161.5	1222.6	1523.1	0.186	0.896	-0.655 ± 0.237
167.9	1095.8	1230.3	0.127	0.864	-0.526 ± 0.345
172.7	926.7	988.0	0.078	0.852	-0.483 ± 0.640

Table 1: The target polarization Q_y extracted from the different θ_{cm}^d angular intervals.

protons from the SAID database, it was possible to extract the averaged target polarization value $\langle Q_y \rangle = \epsilon / \langle A_y \rangle \cdot \langle \cos\phi \rangle = 0.75 \pm 0.06$ with the $\chi^2/dof \approx 2/6$ (note that these results are PRELIMINARY).

References:

- [1] A. Kacharava, F. Rathmann, and C. Wilkin for the ANKE Collaboration, COSY Proposal #172 (2006).
- [2] D. Chiladze *et al.*, Phys. Lett. B **637** (2006) 170.
- [3] D. Chiladze *et al.*, Phys. Rev. ST Accel. Beams, **9** (2006) 050101.
- [4] R. Engels *et al.*, *ibidem*, *The Polarized Internal Target at ANKE*.

^a IKP FZJ, Germany

^b HEPI TSU, Tbilisi State University, Georgia

^c DLNP JINR, Dubna, Russia

^d Erlangen University, Germany

^e PNPI, Gatchina, Russia

^f University College London, U.K.

* supported by COSY–FFE

Comparison of two implementations for timing by STT

V. Leontyev^a, S. Merzliakov^b, D. Oellers^a, R. Schleichert^a and S. Trusov^c
for the ANKE-Collaboration.

The timing capability of the Silicon Tracking Telescopes can be realized with front-end electronics, based on either VA32TA2 or MATE3 chips. One chip-board is connected to one detector side for both solutions.

Each channel of the MATE3 based front-end electronics provides an individual time mark; a timing study with a prototype of a MATE3 chip card was presented in a previous report [1]. It was shown that the time resolution (σ) is about $0.3 ns$ for signal amplitudes $> 1.6 MeV$ in energy equivalent. The current setup of the VA32TA2 based front-end electronics contains 5 time output channels per chip-board (one per chip). Time marks are produced by fast amplifier-discriminator sections of the preamplifier channels. A common OR of these signals is delivered to the VME TDC. Data from laboratory measurements were used to develop a time calibration procedure for this solution and to study the timing performance. Results of the study are presented here.

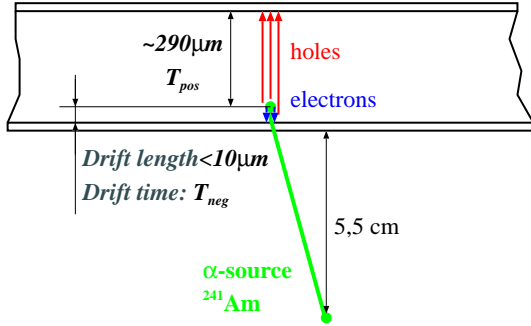


Fig. 1: Laboratory setup to study the timing of the VA32TA implementation. T_{neg} is a time mark produced when a collected charge of electrons exceeds a threshold. T_{pos} is a corresponding one for holes.

The laboratory setup (Fig. 1) comprised a detector of BaBar-IV type and an α -source placed in vacuum. Signals from one α -particle were obtained independently from both detector sides by two chip cards. The energy measurement information was applied to select events, when all produced charge was collected by one segment of a positive-doped (POS) side and one of a negative-doped (NEG) side. Practically the difference between T_{pos} and T_{neg} measured the drift time of holes to the positive side surface.

When the energy information is obtained, there is a simple method to define, which channel has produced the time signal. The signal with largest amplitude is the fastest, if channel thresholds are equal. So it is only necessary to sort the signal amplitudes and take the largest one. A cross-check is possible, comparing it with a signal from the other detector side.

Time measurements of all channels of one chip-board is presented in Fig. 2. It is seen, that if thresholds are adjusted, time distributions have the same shape. Only the peak positions are different, because each channel has an individual delay of a signal transmission to the VME TDC.

Fig. 3 presents the time difference measured using all capable channels of the detector read-out after a correction of the delay differences. A peak width $\sigma_{T_{diff}}$ is $0.65 ns$. It presents the resolution of this stand-alone measurement of charge car-

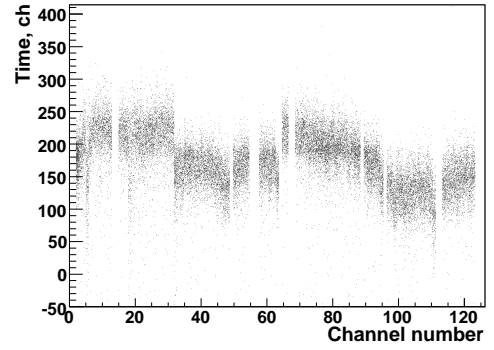


Fig. 2: Time difference between T_{pos} and T_{neg} versus number of fired channel on NEG side. A number of channel on the POS side is 33. One TDC channel corresponds $25 ps$.

rier drift time in the detector.

$\sigma_{T_{diff}}$ is the result of independent T_{pos} and T_{neg} resolutions:

$$\sigma_{T_{diff}} = \sqrt{\sigma_{T_{pos}}^2 + \sigma_{T_{neg}}^2} \quad (1)$$

T_{pos} and T_{neg} are obtained by the same equipment and for signals of the same amplitude. Thus $\sigma_{T_{pos}}$ and $\sigma_{T_{neg}}$ can to be assumed equal, because the influence of charge spreading is negligible for $300 \mu m$ of the carriers drift. So, $\sigma_{T_{neg}} = \sigma_{T_{diff}} / \sqrt{2} = 0.45 ns$.

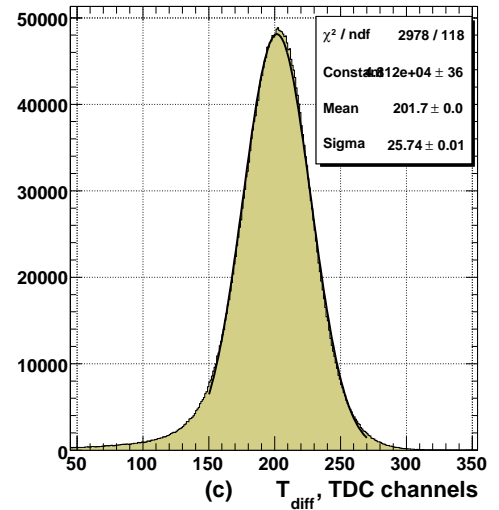


Fig. 3: Difference between the time marks from two detector sides. Peaks of α -particles is fitted by Gauss function.

Another selection of events was applied to study an influence of signal amplitude changes on the timing. The criterion to select events with a charge collection on a single segment was kept for NEG side. A charge distribution between any two adjacent segments was allowed for POS side, that provided a set of time measurements with different ranges of the signal amplitude for chosen (even) read-out channels. This study was a pure test of electronics, since all other significant conditions (the signal amplitude of NEG side, the drift times) were constant.

Figure 4 presents the dependence of the resolution σ_{Tdiff} on the signal amplitude and shows, that the time resolution is rather constant over the measured range of energies. The resolution of the single time mark measurement σ_{Tneg} was obtained from averaged σ_{Tdiff} , it is 0.52 ns for the data sample of the charge distribution.

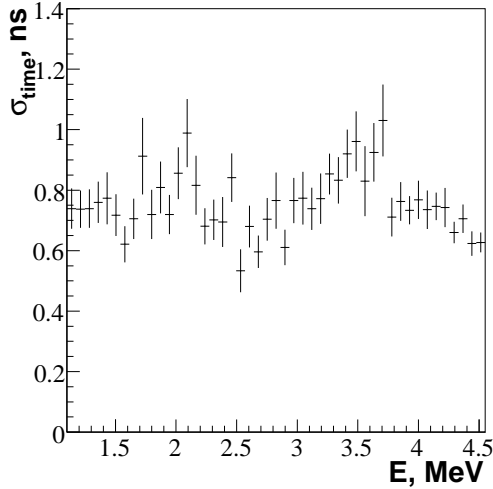


Fig. 4: Time resolution versus signal amplitude (in energy equivalent).

The same data sample was used to obtain the *time walk*, the dependence of the moment, when the time mark will be produced, on the signal amplitude. The reason is the difference between durations of the signal rising from zero to an operation threshold. The obtained time walk is presented in Fig. 5. It was fitted by a continuously decreasing function $p_0 + e^{(p_1 - p_2 * E)}$, where E is the energy equivalent in MeV and p_0, p_1, p_2 are parameters defined by the fit.

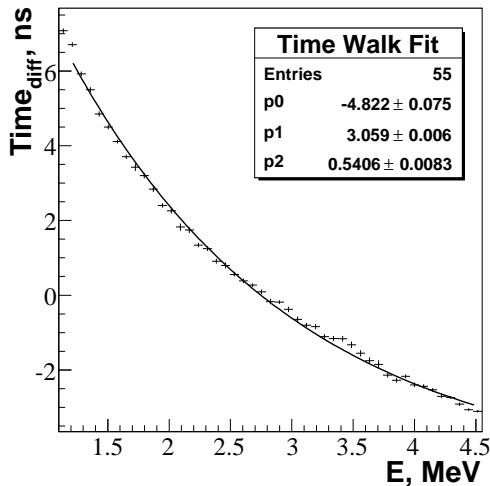


Fig. 5: Time walk, a dependence of a moment, when the time mark is produced, on the signal amplitude.

Another characteristics, which is quite different for the MATE3 and VA32TA2 implementations, is the threshold value. The nominal value of the MATE3 threshold is rather high (0.4 MeV). So it was especially interesting to study the possibility to set a VA32TA2 threshold as low as possible. It is needed in particular to calibrate a DAC, which control a level of the VA32TA2 threshold. Measurements were carried out with an α -source in the air, in order to provide a continuous spectrum of the measured energies. The time output was used for the read-out trigger and the minimum of the signal

amplitude, which exceeds the threshold, was defined for different values of the DAC. Fig. 6 illustrates a procedure of the definition.

It was shown (see Fig. 7), that the VA32TA2 threshold can be set as low as 100 keV of the energy equivalent. Thus, the MATE3 implementation provides the highest accuracy and the individual time read-out for each measuring element. But the high threshold limits its self-triggering capability. The timing accuracy of the VA32TA2 implementation is less convincing, but it has the lower threshold. An appropriate combination of these implementations provides a remarkable possibility to integrate the advantages as to overcome the difficulties.

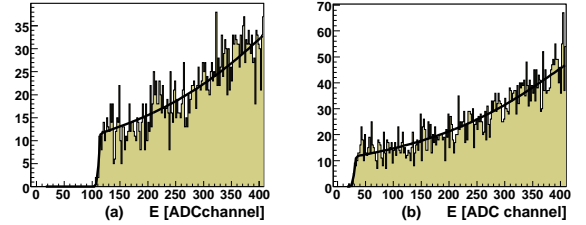


Fig. 6: α -source energy spectra in the air. A fit of the left edges of the spectra defines the threshold value. A position of the left edge depends on the value of the threshold DAC, which was 1850 for the picture (a), 2025 for the picture (b).

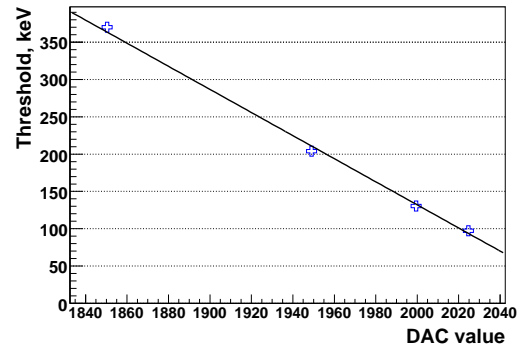


Fig. 7: Dependence of the VA32TA2 threshold on the DAC value.

It is planned that one side of each STT detector will be connected to the MATE3 based front-end electronics and another side to the VA32TA2 one. Experimental data obtained during January 2007 beam-time will provided a direct comparison of these timing implementations.

References:

- [1] V.Leontyev at al., Timing Performance of the ANKE Silicon Tracking Telescopes. IKP/COSY Annual Report 2005.

^a IKP FZ Jülich, Germany

^b JINR, Dubna, Russia

^c IKP FZ Rossendorf, Germany

The $pp \rightarrow pK^0\Sigma^+$ reaction was investigated with the COSY-TOF spectrometer. The main objective was to clarify whether or not a narrow exotic $S = +1$ resonance, the Θ^+ pentaquark, is populated at $1.53 \text{ GeV}/c^2$ in the pK^0 subsystem with a data sample of much higher statistical significance compared to the previously reported data in this channel.

The preceding measurement [1] was carried out at a beam momentum of $2.95 \text{ GeV}/c$, a slightly higher momentum of $3.059 \text{ GeV}/c$ was chosen for the new measurement. At this higher momentum the upper bound of the K^0p invariant mass is $1.597 \text{ GeV}/c^2$ and therefore a possible structure at $1.530 \text{ GeV}/c^2$ is further removed from the upper mass limit.

The analysis was carried out with three independent analysis programs (A, B,C), which differ in algorithms and event selection methods, but are based on a common calibration of all detector components. In order to cross-check each analysis the complete data sample was divided into two independent parts (events recorded with either even or odd number). The analysis procedures were developed using even events only and the odd events were analyzed only after the analysis procedures were frozen.

A $pK^0\Sigma^+$ event is identified by its topology, that is a prompt track emerging from the target (proton), a delayed decay (K^0) and optionally a kink in a charged track (Σ^+).

In all analyses an instrumental background from incorrectly reconstructed events in the data sample was investigated by various methods. The background was found to be smooth in the pK^0 , $p\Sigma^+$ and $K^0\Sigma^+$ invariant mass distributions. The background is determined to be 21% (A), 25% (B), 28% (C).

Elastically scattered events were recorded in parallel in order to determine the luminosity. Approximately 4000 $pK^0\Sigma^+$ events in analysis B,C, and 7900 events in analysis A, are reconstructed. Due to the different strategies of the analysis about 300 events are found both in B and C. For each combination A,B and A,C about 600 events are shared. Therefore, in total more than 12.000 independent $pK^0\Sigma^+$ events were reconstructed.

The invariant mass spectra of the subsystems pK^0 , $p\Sigma^+$, and $K^0\Sigma^+$ as extracted from the three analyses after background subtraction and acceptance correction agree within statistical uncertainties. No significant differences of spectra obtained from even and odd events were found. The resolution in the invariant mass distribution of the pK^0 subsystem is $\sigma = 6 \text{ MeV}/c^2$ for analyses A,C and $5 \text{ MeV}/c^2$ for analysis B as deduced from Monte Carlo. The pK^0 mass spectra are presented in Fig.1 together with a 3rd order polynomial parameterization in the mass region of $1.45 \text{ GeV}/c^2 < M_{pK^0} < 1.57 \text{ GeV}/c^2$. They were analyzed in order to determine the statistical significance with which a narrow structure might be present. A narrow structure was added to the polynomial described above. The shape of this narrow structure has been taken from Monte Carlo simulations of a resonance with a width negligible compared to the detector resolution. The mass of the resonance was varied in $1 \text{ MeV}/c^2$ steps over the M_{pK^0} range from $1.50 \text{ GeV}/c^2 - 1.55 \text{ GeV}/c^2$. The strength of the structure for each setting was varied between $-1 \mu\text{b} < \sigma_{\text{tot},X} < +1 \mu\text{b}$. These results are summarized in Fig.2.

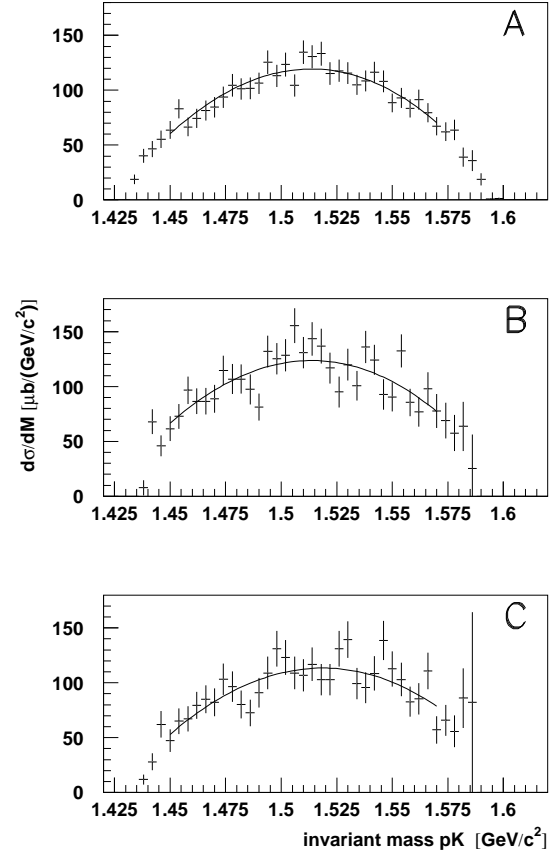


Fig. 1: The invariant masses of the pK^0 subsystem for the three analyses together with a 3rd order polynomial parameterization.

In this figure the value of $\sigma_{\text{tot},X}$ corresponding to the minimal value of χ^2 is represented by the central line of the band as a function of M_{pK^0} . The 95% confidence interval for an enhancement or suppression of the measured M_{pK^0} differential cross section is indicated by the width of the band. The results indicate that over the full M_{pK^0} range investigated here the parameterization assuming $\sigma_{\text{tot},X} = 0 \mu\text{b}$ is consistent with the measured data within the 95% confidence level. In particular, this new, higher statistics data do not contain positive evidence for a narrow structure at $M_{pK^0} = 1.530 \text{ GeV}/c^2$. The fluctuation of the central value of the 95% confidence intervals are not correlated between the different analyses. Based upon the smallest upper limit of the three 95% confidence intervals the maximum cross section for a narrow resonance $\sigma_{\text{tot},X} < 0.3 \mu\text{b}$ has been deduced over the full mass range. Further details of the new measurement are given in Ref [2]. These results also have to be compared with the positive evidence for a Θ^+ resonance found in the data of the first measurement. First of all the number of reconstructed events is much larger for the new measurement - about a factor of 4

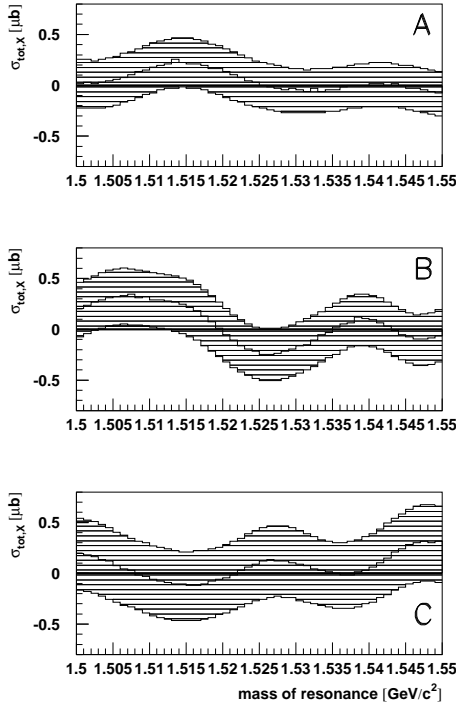


Fig. 2: 95% confidence range for the cross section of a narrow resonance as a function of M_{pK^0} for the A, B, C analyses in the top, center, and lower frames, respectively. The central lines of each band present the contribution of a hypothetical narrow resonance with the lowest χ^2 value.

for analyses B and C and about 8 for analysis A - this gives a strongly improved statistical accuracy. In addition, the three largely different analyses give a better understanding of systematic uncertainties. In the previous measurement the peak was located $32 \text{ MeV}/c^2$ below the upper kinematic limit of the populated pK^0 mass range and therefore resided on a continuum background with a steep negative slope. This caused uncertainties in the determination of the background. Therefore, in the present experiment a higher excess energy was chosen. Comparing the pK^0 spectra obtained in this work with the published one [1] a significant difference in the shape, which is more symmetric in the new measurement, is noticed. Since the pK^0 invariant mass distribution obtained in the new experiment is based on three independent analysis procedures including systematic studies of the instrumental background, we are confident in the symmetric shape of the pK^0 continuum. Using a continuum with this shape for the spectrum of the previous measurement the significance of the peak decreases substantially.

References:

- [1] COSY-TOF Collaboration: M. Abdel-Bary *et al.*, Phys. Lett. B **595** (2004) 127.
- [2] COSY-TOF Collaboration: M. Abdel-Bary *et al.*, hep-ex/0612048

* Physikalisches Institut, Universität Erlangen-Nuremberg, 91058 Erlangen, Germany

The Analysis Program "typeCase"

K. Ehrhardt* for the COSY-TOF-Collaboration
Physikalisches Institut Universität Tübingen

With the program "typeCase", a new analysis program has been developed to fit the needs of the extremely modular detector COSY-TOF. "typeCase" has been implemented in an Object-Oriented design, with a Graphical User Interface for parameter management and analysis control. Help-components have been added recently.

For the analysis of the recorded data several strategies and ways of analysis exist. "typeCase" was not designed to implement a new strategy, but to be able to make use of the work and ideas that have been done so far. It is a platform for analysis strategies. The actual analysis is divided into several algorithms, each performing an individual task, such as calibration, pixel-calculation or tracking. The user selects the algorithms he wants to use, defines the order in which to use them and then starts the analysis.

To provide maximum flexibility in detector setup and analy-

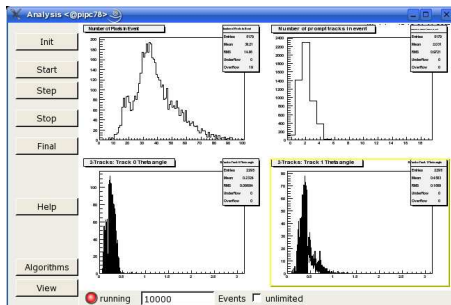


Fig. 1: Window displaying available algorithms in categories. They come with a description and parameters to modify.

sis strategies, storage and calculation of data have been separated. The user can adapt his own ideas/ algorithms easily to the nomenclature of the framework, a documentation of the used data structures is accessible (WWW). The Graphical User Interface helps with the installation of new algorithms as well as with the definition of the detector setup, the analysis parameters and the control of the actual analysis. These properties give rise to some interesting features: Users can exchange their algorithms, as they do with e.g. JPEG-pictures. Almost any detector setup can be analysed with this analysis framework and simulations can be treated in the same way as real data.

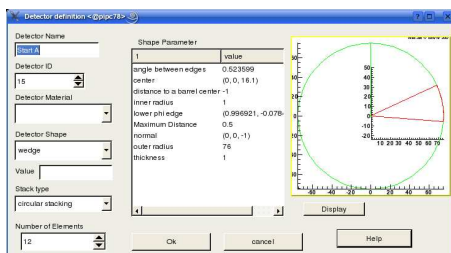


Fig. 2: Window to define a sub-detector of the setup. The shape of the first element and the envelope of the detector can be displayed

The program consists mainly of four parts: The containers, the defined classes, the algorithms and the Graphical User Interface.

To ensure maximum flexibility, the data and their build were separated. To fill these structures, the algorithms are used. A priori, the program does not know which algorithms the user chooses to use, no further compilation or linking is needed when switching to another analysis strategy. The analysis classes provide such functionality, using the inheritance feature of the Object-Oriented design.

To provide more flexibility, the user can pass parameters to the algorithms which gives an even improved handle on the actual analysis.

The "defined classes" are used for more specialized structures, such as shapes (e.g. cylinder or spiral) or reactions (e.g. pp-elastic or Λ -production), that have built in functionality (e.g. hit-point calculation).

These three parts are essential, the Graphical User Interface is optional, though it doesn't affect speed or performance. It is designed to guide the user through the analysis, providing descriptions, help and an overview over analysis-possibilities.

References:

- [1] ROOT: An Object-Oriented Data Analysis Framework (<http://root.cern.ch>)
- [2] Qt: The Cross-Platform C++ Development Framework by Trolltech (<http://www.trolltech.com>)

We report on the first kinematically complete high-statistics measurement of differential cross sections at a beam momentum of 0.95 GeV/c (corresponding to $T_p = 397$ MeV) for the reaction $pp \rightarrow pp\pi^0$ [1].

By use of the central calorimeter the COSY-TOF setup is capable of providing a reliable particle identification on the basis of the ΔE -E technique. In this way the different single pion production channels were separated. The results for the $d\pi^+$ channel agree well with previous results. For the $pp\pi^0$ channel significant deviations from previous investigations were obtained for angular distributions as well as for invariant mass spectra.

The data cover essentially the full available elliptical phase space areas and yield distributions, which are close to flat with just one pronounced excursion in the region of the pp FSI (small M_{pp}). This is visible in the experimental Dalitz plots of $M_{p\pi^0}^2$ versus M_{pp}^2 and $M_{p\pi^0}^2$ versus $M_{p\pi^0}^2$ displayed in Fig.1. Note that the plots are efficiency but not acceptance corrected, hence the tiny deviations from the elliptic circumference at the upper corners are due to the excluded beam-hole region. The data do not deviate vigorously from the flat phase space distributions, as we would expect, e.g. if Δ excitation would play a dominant role in this reaction channel.

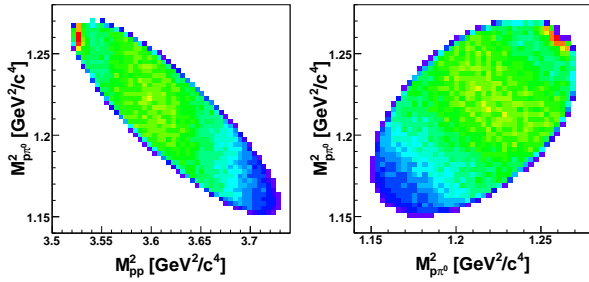


Fig. 1: Dalitz plots for the invariant mass combinations $M_{p\pi^0}^2$ versus M_{pp}^2 and $M_{p\pi^0}^2$ versus $M_{p\pi^0}^2$ as obtained from the data for the $pp \rightarrow pp\pi^0$ reaction.

The pion and proton angular distributions are shown in Fig.2, on the left for the pions denoted by their cm polar angles $\Theta_{\pi^0}^{cm}$ and on the right for protons in the pp subsystem (Jackson frame) denoted by Θ_p^{pp} , i.e. we use the same coordinate system scheme as defined in the IUCF publication [2].

The angular distributions were fitted using equation

$$\sigma(\Theta) \sim 1 + a_2 * (3 \cos^2\Theta - 1)/2, \quad (1)$$

The distributions are close to flat, exhibit, however, a clearly negative anisotropy parameter with $a_2 = -0.12(1)$ for pions and $a_2 = -0.10(1)$ for protons.

The negative anisotropy parameter observed in this experiment for the π^0 angular distribution comes as a surprise, since all previous experiments around $T_p \approx 400$ MeV gave - or indicated at least - a positive value for the pions, the most serious discrepancy being with the PROMICE/WASA results [3] of $a_2 = +0.127(7)$, since that measurement provided the

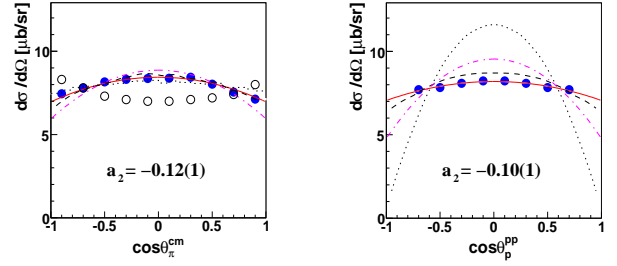


Fig. 2: Angular distributions of pions (overall cm system) and protons (pp subsystem, Jackson frame) for the $pp \rightarrow pp\pi^0$ reaction. Data of this work are shown by full circles, the fit to the data with eq. (1) by solid lines, the results of Ref. [3] by open circles and the prediction of Ref. [4] by the dash-dotted curve. Dashed and dotted lines give calculations with the ansatz eq. (4) [1] and the ansatz of [1, 5] respectively.

best statistics and phase space coverage of all previous experiments at this energy. Although Ref. [3] reports negative a_2 values for $T_p \leq 360$ MeV, positive values are found there for $T_p \geq 400$ MeV.

With our data we can demonstrate, that pions and protons exhibit q -dependent angular distributions [1]. Hence a full coverage of the phase space appears to be mandatory for reliable experimental results on this issue. For the lower q region angular distributions with negative a_2 parameter dominate pointing to the importance of proton spinflip transitions associated with π^0 s - and d -waves. In particular, we observe a pure $\sin^2\Theta$ distribution for $T_p^{pp} < 3$ MeV, which derives from a special combination of the spinflip transitions $^3P_0 \rightarrow ^1S_0s$ and $^3P_2 \rightarrow ^1S_0d$. Different from previous experiments this has been the first measurement at $T_p \approx 400$ MeV covering practically the full reaction phase space. The data thus may serve as a reliable basis for a comprehensive phase shift analysis of this reaction.

References:

- [1] S. Abd El-Samad et al., Eur.Phys.J.**A30** 443 (2006)
- [2] H. O. Meyer et al., Phys. Rev. **C63**, 064002 (2001) and references therein
- [3] R. Bilger et al., Nucl. Phys. **A693**, 633 (2001)
- [4] C. Hanhart, Phys. Rep. **397**, 155 (2004)
- [5] J. Zlomanczuk et al., Phys. Lett. **B436**, 251 (1998)

The WASA Scintillator Electromagnetic Calorimeter (SEC) has been used to measure electrons and photons up to 800MeV. It consists of 1012 CsI(Na) crystals shaped like truncated pyramids, each with active material of $16X_0$ (radiation lengths). The crystals are placed in 24 layers along the beam direction, covering angles from 20° to 169° . For a detailed description of the calorimeter see [1].

After the transport of the WASA detector from CELSIUS (Uppsala) to COSY in summer 2005, it was essential to establish the performance of all SEC channels. Prior to installation at COSY, measurements of individual components were done with a $^{241}\text{AmBe}$ radioactive source with a maximum of 4.4MeV in the photon energy distribution [2]. The source was pushed as closely as possible to the surface of the CsI crystals. In all measurements only one crystal was read out. The signals from the crystal were sampled by a SIS 3300 Flash ADC with a frequency of 100 MHz. After digitization data were read out with a data acquisition system provided by ZEL [3] and sent to a standard PC via PCI interface. The data were written to disk. During the measurements the spectra were monitored online using the RootSorter [4] analysis software.

The data were analysed event by event. For each pulse sampled by the Flash ADC the zero level was computed and subtracted from the original signal. Then, each signal was integrated within the selected gate. The further analysis was based on the calculation of the normalized integral. Two functions were fitted to the spectra, one describing the background (as exponential) and one describing the signal (as a Gauss function). Using this technique the peak position and the width of the signal were extracted from the data for each individual module (Fig. 1).

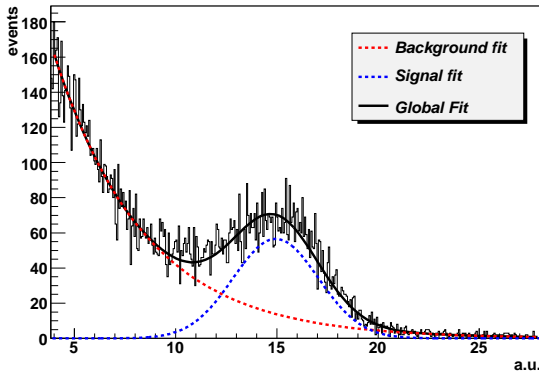


Fig. 1: Sample ADC spectrum, with fits to the 4.4MeV photon peak and background.

To check working conditions the peak position of the signal was plotted versus the photomultiplier high voltage (Fig. 2). The gains are adjusted to a similar working level by corrections to the HV settings (Fig. 3).

The relative peak width (standard deviation) is centered around 15% (Fig. 4). The peak width is a convolution of the experimental resolution and the photon spectral distribution from the source.

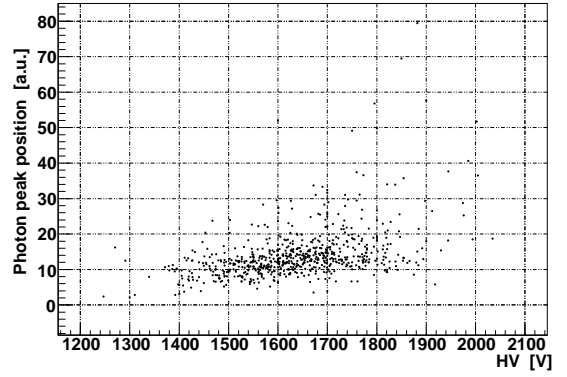


Fig. 2: Measured peak position of the photon signal versus high voltage for each individual crystal.

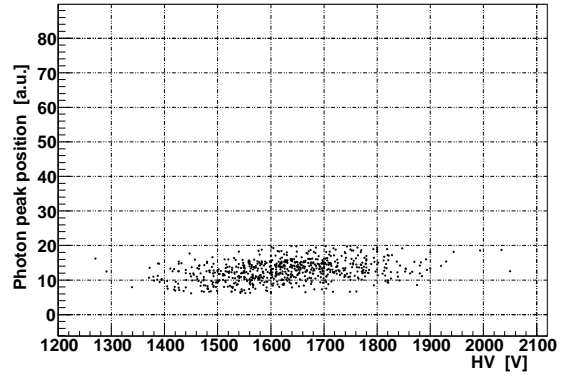


Fig. 3: Same as Fig. 2 after high voltage corrections.

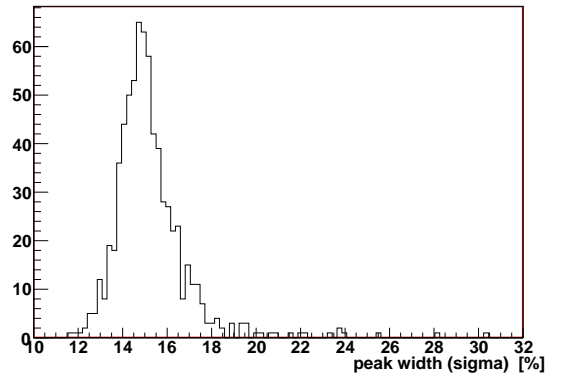


Fig. 4: Measured widths of the photon peak for each individual crystal.

In addition, the possibility to use cosmic muons for energy calibration was investigated. Detailed Monte-Carlo simulations using GEANT3 and measurements were performed. More information about the tests is given in [5].

References:

- [1] H.H. Adam et al., Proposal for the Wide Angle Shower Apparatus (WASA) at COSY-Jülich, COSY Proposal (2004), e-Print arXiv: nucl-ex/0411038.
- [2] H.R. Vega-Carrillo, E. Manzanares-Acuña, A.M. Becerra-Ferreiro, A. Carrillo-Núñez, Neutron and gamma-ray spectra of $^{238}\text{PuBe}$ and $^{241}\text{AmBe}$, Applied Radiation and Isotopes 57, 2002.
- [3] M. Drochner et al., IEEE Trans. Nucl. Sci. **45**, 1882 (1998).
- [4] V. Hejny M. Hartmann A. Mussgiller, RootSorter: A new analysis framework for ANKE, IKP/COSY Annual report 2002, Jül-4052.
- [5] B.R. Jany, Assembly and measurements of the Electromagnetic Calorimeter components for “WASA at COSY” setup, Master Thesis Jagiellonian University Cracow (2006), e-Print arXiv: physics/0606110.

^a IKP-2, Forschungszentrum Jülich

^b Nuclear Physics Department, Jagiellonian University, PL-30059 Kraków, Poland

Test of the WASA Plastic Scintillator Barrel

I. Keshelashvili^{a,b} and M. Mittag^a

Prior to reassembling of the Plastic Scintillator Barrel (PSB) of WASA at COSY tests have been performed to determine their physical parameters. The PSB, designed for use in the first level trigger logic consist of three parts of scintillation counters with a geometry allowing a close to 4π acceptance. Together with the mini drift chamber it is employed for charged particle identification by the $\Delta E - p$ and $\Delta E - E$ methods and as a veto for γ identification. The PSB is placed inside of the solenoid and surrounds the mini drift chamber. It consists of 48 forward, 50 central and 48 backward elements. For the laboratory test ^{207}Bi source has been used. It emits monochromatic electrons via electron capture with a maximum energy line at $E(e^-) = 1.047$ MeV. GEANT4 simulations shows that electrons from the source are stopped in the 8 mm thick PSB elements. All elements are enfolded with aluminum and mylar foils where the electrons lose $\text{MPV}=9$ keV. For the test measurements the read-out was self triggered using a discriminator which was adjusted to cut off the low energetic electrons from the source. Each scintillator is equipped with a PMT (FEU-115M)[1, 2] coupled to the ~ 50 cm long light guides which are glued to the active material. The peak of quantum efficiency for the photo-cathode and the peak of relative light output are consistent (see Fig. 1). For each module electrical, optical and

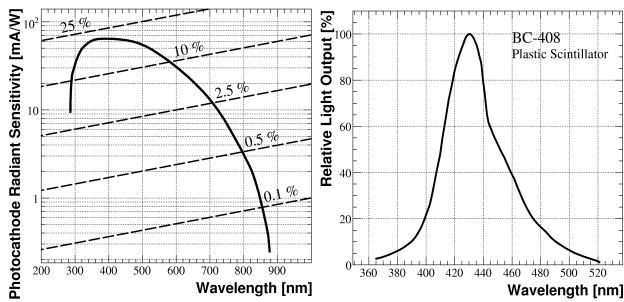


Fig. 1: Photo-cathode sensitivity and relative light output.

mechanical checks as well as maintenance have been done before assembling. After reassembly the amplitude changed by up to 20 % for certain elements. The high voltages for each PMT were given taken from later settings used during operation at CELSIUS.

Test of Forward Scintillators: The source was situated along each scintillator at seven equally shifted points. Each spectrum was fitted using the sum of an exponential and a Gaussian for background and signal, respectively. Using the mean value from the Gaussian parameters the dependence of light attenuation was extracted. Normally the light attenuation should exhibit an exponential decrease but in our case the dependence is more complicated. A deviation from an exponential decrease can be due to a complicated geometrical form or due to strong radiation and/or mechanical damages of the scintillation material. The fitting of the position dependence using a fourth order polynomial function is shown in Fig. 2. For different scintillators the position dependence differs for both the shape and the absolute light output.

Test of Central Scintillators: The central scintillators are ~ 50 cm long and the gain of PMTs was found insufficient.

Instead, a different type of the PMT (XP2972)[3] with higher gain was used. Using single-electron-spectrum (SES) we defined both gain and resolution for this PMT. From the SES the number of photoelectrons was estimated as $N_{ph.e.} \sim 30 - 120$. The shape of the position dependence is close to an exponential decrease. In Fig. 3 the light attenuation length is shown for different scintillators. The attenuation length is mostly below 100 cm whereas in case of spare elements the attenuation length is around 300 cm.

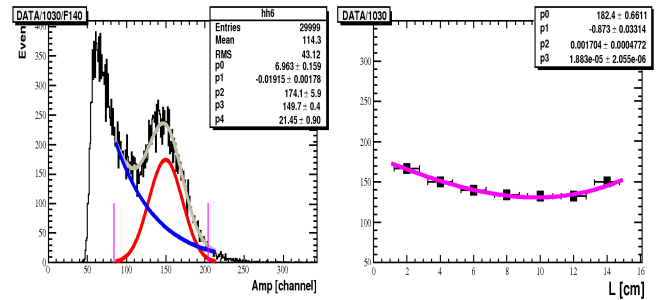


Fig. 2: Position dependence for one forward scintillator.

Test of Backward Scintillators: For the backward scintillators we have a situation very similar to the forward case. A huge spread in the position dependence shapes of different scintillators and a large deviation from an exponential function behavior where found. In conclusion, the present scintillator material is strongly damaged and needs to be replaced the sooner the better. All PMTs and HV dividers still work stable. The mechanical and electrical parts can also be used in future.

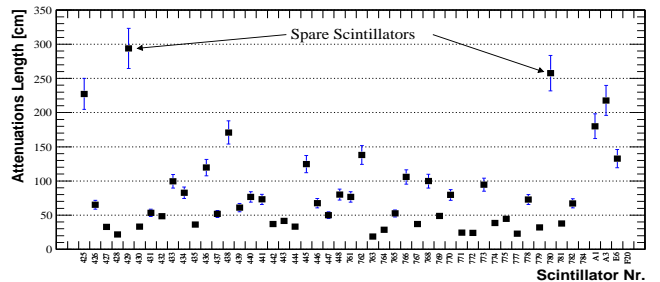


Fig. 3: Attenuation lengths for PSB central scintillators.

References:

- [1] <http://www.melz.ct.ru/eng/elect/>
- [2] V. Rykalin et al., Photo-multiplier with Improved Linearity and the Base of FEU-115, Preprint IHEP 95-12, Protvino (1995)
- [3] www.photonis.com/data/cms-resources/File/Photomultiplier_tubes/spec/XP2972.pdf

^a IKP FZJ, Jülich, Germany

^b HEPI TSU, Tbilisi, Georgia

The Plastic Scintillator Barrel (PSB) consists of a cylindrical part formed by 48 bars presented in fig. 1 and two end caps of 48 trapezoidal elements each.

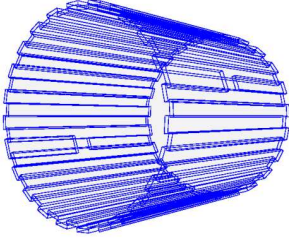


Fig. 1: Schematic view of the central part of PSB obtained from Monte Carlo, two elements are split to guarantee space for the pellet tube.

The detector is placed inside of the solenoid and surrounds the mini drift chamber (MDC). The main purpose of PSB is to provide a fast logic signal for the first level trigger (for separating neutral and charged tracks) and analog signals for particle identification, which can be done either via the ΔE -E or the ΔE -p technique, using the corresponding information from calorimeter and MDC, respectively[1].

The PSB was calibrated using $pp \rightarrow d\pi^+$ events selected from data measured with a proton beam of $E_{kin} = 600$ MeV.

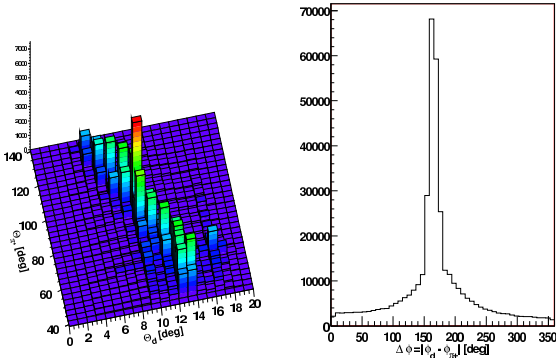


Fig. 2: Correlation between reconstructed polar angles of deuterons and pions (left), and the difference in the azimuthal angle (right).

For event selection the following criteria were applied:

- a trigger requiring one or more hits in the Forward Range Hodoscope
- a corresponding hit in the calorimeter (azimuthally matching the hit in PSB)
- one charged track in the Forward Detector
- cuts on the 2-body angular correlation shown in fig. 2.

As illustrated in fig. 3, the pions from $pp \rightarrow d\pi^+$ have a well defined correlation between energy deposit in PSB and scattering angle. As known from previous investigations, the light attenuation along the scintillator is significant and has to be taken into account[2]. Therefore, each element was divided into 10 angular bins and for each bin the measured ADC spectrum was compared to the energy spectrum obtained from MC simulation.

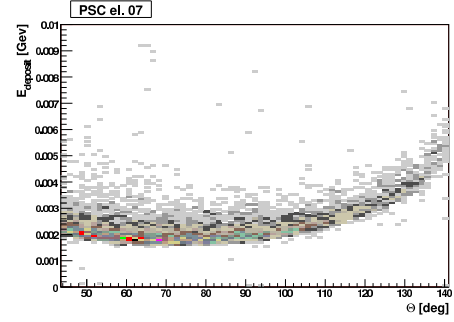


Fig. 3: Simulated energy deposition of pions in PSC as a function of the polar angle.

In both cases a Gaussian was fitted to the energy distributions and a linear calibration constant was extracted. For each module the average calibration constant and the angular dependence was separated (fig.4). The light attenuation can be derived by fitting an exponential function. The real energy

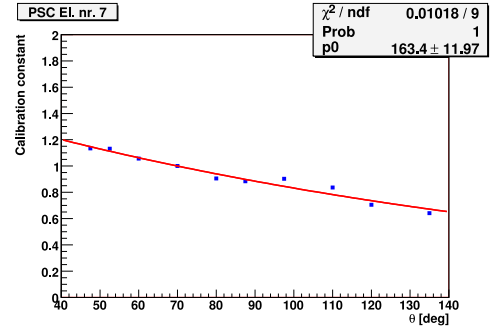


Fig. 4: ADC calibration and nonuniformity of individual PSC elements.

deposit is a function of the non-uniformity and the average calibration constants:

$$E_{dep} = ADC \cdot Calib_{const} \cdot NU(\theta) \quad (1)$$

A typical spectrum after applying the calibration procedure is presented in fig. 5. In addition the effective threshold of the corresponding discriminator is shown. Due to the light attenuation, this varies as a function of the polar angle θ .

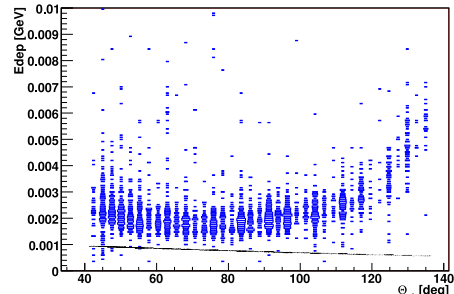


Fig. 5: Calibrated energy deposition of pions in PSC as a function of the polar angle.

References:

- [1] M.Jacewicz, Measurement of $pp \rightarrow pp\pi^+\pi^-\pi^0$ with CELSIUS/WASA at 1.36 GeV, PhD thesis, Uppsala University (2004).

[2] I.Keshelashvili, M. Mittag, Test of the WASA Plastic Scintillator Barrel, contribution to this Annual Report .

^a IKP-2, Forschungszentrum Jülich

^b Nuclear Physics Department, Jagiellonian University, Cracow, Poland

The Forward Trigger Hodoscope FTH is a three layered scintillator hodoscope situated in front of the WASA Forward Detector [1, 2]. The geometry is similar to the TOF quirl, consisting of one plane with 48 pie shaped elements, and two planes of each 24 Archimedean spiral elements. The FTH plays an important role in the WASA trigger system. It provides fast information on the multiplicity of charged tracks in the Forward Detector which is used for the first level trigger. By combining the hit information of all three layers even a reconstruction of scattering angles on trigger level is possible and proposed to further increase the trigger selectivity of the WASA experiment. High and well understood detection efficiency is thus necessary to obtain a well defined trigger acceptance.

The FTH was in operation for more then 12 years at the WASA-PROMICE and CELSIUS/WASA experiments. During this time severe aging effects of the detector could be observed, e.g. by comparing the non-uniformity parameters obtained for different periods in time. Prior to its reinstallation at WASA at COSY all scintillator elements were individually tested, several PM-tubes and one scintillator element were replaced by the only available spare, and high voltage settings were tuned in order to improve the detector performance (see [3] for details).

The goal of the study presented in this report was to make a final in-beam check of the detector performance and efficiency after these modifications, and to help judge if a complete replacement of the Trigger Hodoscope will be necessary, also in view of future trigger developments.

The measurement was performed using a selection of high energetic single track events in the WASA Forward Detector, based on data from the November commissioning run obtained at high kinetic beam energies (1450 MeV and 2500 MeV). Elastic proton proton scattering is the major contributing reaction channel, where the forward going proton is close to minimal ionizing when passing through the Trigger Hodoscope. The obtained results for the FTH detection efficiency thus define a lower limit.

The detection efficiency of each layer was derived using individual event samples, where the information of each other two layers was used for reconstruction of exact track coordinates. Based on these track coordinates the expected hit position and (rough) element number in the inspected layer could be determined. The efficiency for each bin was then obtained by counting the number of events per bin with missing hits in the investigated layer and by normalizing to the expected number of hits in each bin.

Some results of these studies are shown in figs. 1 and 2. Fig. 1 shows the obtained detection efficiency as a function of scattering angle and element number for the inner quirl plane, which showed the worst performance. Several elements reveal unefficiencies well above 10% for small scattering angles, and the overall distribution is strongly nonuniform. The bad efficiency of these elements also reflects as low light out-

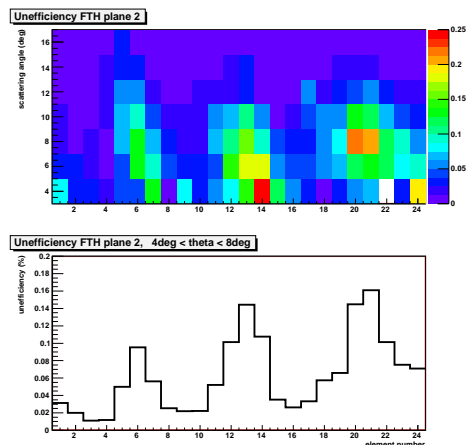


Fig. 1: FTH detection efficiency of the inner quirl layer for high energetic protons obtained at high beam energy ($T_{beam}=2500$ MeV) as a function of scattering angle and element number.

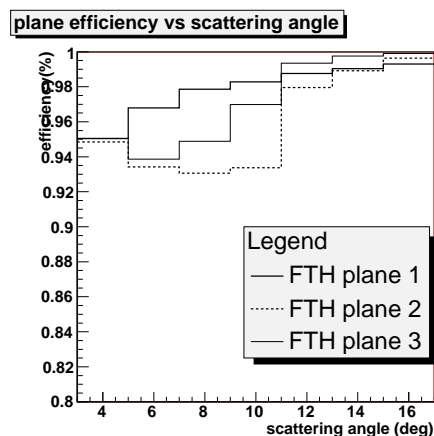


Fig. 2: Detection efficiency as function of scattering angle.

put and large position dependence in the measured light output non-uniformity.

Fig. 2 shows the averaged efficiency as function of scattering angle for all three layers. The expected unefficiency due to geometrical gaps between the elements should be much smaller according to the Monte Carlo simulation, and alone can not explain the observed behaviour for layer 2 and 3.

Based on these results and previous experience we plan for a complete exchange of all FTH scintillator elements in summer 2007.

References:

- [1] M. Dahmen, Nucl. Instrum. Meth. A **348**, 97-104 (1994)
- [2] H.-H. Adam et al, Proposal for the Wide Angle Shower Apparatus (WASA) at COSY-Jülich, COSY Proposal (2004), e-Print arXiv: nucl-ex/0411038
- [3] C. F. Redmer, Groß- und kleinflächige Szintillatorhodoskope in der Teilchen - und Atomphysik, Diplomarbeit, Ruhr-Universität Bochum, 2006, unpublished

The Forward Trigger Hodoscope (FTH) is the third forward wall component of the WASA-at-COSY detector setup. It is most important for the present first level trigger. Therefore it consists of three layers, each made of the fast plastic scintillator BICRON-404 of 5 mm thickness. The first layer is assembled from 48 wedge-shaped elements. The second and the third layer consist both of 24 curved elements. The shape of these elements follows an Archimedean spiral, where in one layer the spirals turn counterclockwise and in the other layer clockwise around the beam pipe. A projection in beam direction of all three layers results in a pixel structure that provides granularity for the hodoscope.

This 'quirl'-structure has already been used in the experiment PS202(JETSET) and is still employed in COSY-TOF. More detailed information is given in [1, 2].

Prior to installation at COSY, all of the 96 Elements of the FTH were checked and precalibrated. The measurements were performed with a ^{90}Sr source at different positions along each element. The light attenuation in the elements was studied in that way as well. Precalibration was achieved by tuning the high voltages of the photomultipliers of each element, starting with voltages used in the last experimental run at Uppsala.

Signals produced by the source in an FTH-Element and a small rectangular scintillator, located underneath, were recorded simultaneously. Triggering was done via an OR-logic. A cut on coincident signals selected only those of electrons that were minimum ionizing, when passing the FTH-element. Their spectrum follows a Landau distribution. Its mean value was extracted for further analysis.

This procedure has been repeated for all elements with four points of irradiation for the straight and five points for the longer bended elements. The extracted values are shown in Fig. 1 in dependence of the position they were measured.

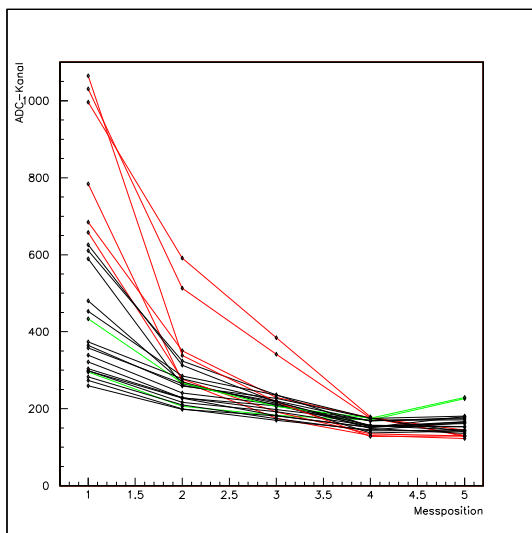


Fig. 1: Mean values of the signals of the elements in the second layer in dependence of the point of irradiation red: very bad elements, green: exchanged scintillators

It was found that signals of some elements were strongly position dependent. As it was already assumed before the tests

[2], most of those elements were part of the second layer of the FTH. They are marked as red lines in Fig 1. Although the voltage applied to the photomultiplier was already relatively high, signals produced far away from the photomultiplier were hardly separable from the background. This could be fixed for most of the elements with a further increase of the applied voltage.

On two elements of the second layer even increasing the voltage did not help to improve the signal quality. The scintillators of those elements were exchanged with spare parts produced at the same time as the whole FTH in 1992. In Fig. 1 their signals are highlighted in green. It can be seen that their position dependence is rather low, compared to the other elements. Additionally, signals produced at the end of the scintillator are quite high, as they should, due to the geometry.

To test if there were visible effects potentially influencing the light propagation in the material, the exchanged scintillators were unwrapped. Fig. 2 shows a substantial amount of micro cracks. Not seen on the photograph is a slight brownish de-colouring of the material in some regions which may be due to radiation damage in the material.



Fig. 2: Unwrapped scintillator of the FTH. Light is reflected from the microcracks.

Since the position dependence of the signal of the unwrapped scintillators is similar to many other elements, it was tried to anneal the unwrapped elements. After this procedure cracks were not visible and the elements were again wrapped and tested. Signals produced along the scintillator were much better but it was also observed, that the scintillators had bended during the process of annealing. More detailed informations on the tests are given in [3]

Due to the results of the tests, it was decided by the WASA-at-COSY-Collaboration to exchange all scintillators of the FTH in 2007.

References:

- [1] M.Dahmen, A. Empl et al, Nuclear Instruments and Methods A **348**, 97-104 (1994)
- [2] H.-H. Adam et al, Proposal for the Wide Angle Shower Apparatus (WASA) at COSY-Julich, COSY Proposal (2004), e-Print arXiv: nucl-ex/0411038
- [3] C. F. Redmer, Groß- und kleinflächige Szintillatorhodoskope in der Teilchen- und Atomphysik, Diplomarbeit, Ruhr-Universität Bochum, 2006, unpublished

First analysis of π^+ - tracks in the WASA Mini Drift Chamber

L.Yurev^{1,4}, P.Podkopał^{2,4}, M.Janusz^{2,4}, P.Kulesa³, H.Ohm⁴, K.Pysz³, V.Serdyuk^{1,4}, G.Ivanov¹, V.Tikhomirov¹, J.Majewski⁴

MDC setup. The Mini Drift Chamber was inspected under laboratory conditions after the transport of the WASA detector from the CELSIUS storage ring in Uppsala. New front-end electronics were applied based on the CMP-16[1] board and new readout electronics - TDC with F1 chip[2] - were first time operated during the experiment. The first commissioning phase was mainly used to debug the electronics, e.g. to fix overflow and software problems of the TDC.

From the second commissioning run data the behavior of the MDC was studied for π^+ mesons. The π^+ were selected according to the kinematics of the 2-body reaction $pp \rightarrow d\pi^+$ at 600 MeV. Several steps cut the events of interest:

- Trigger on deuteron in the Forward Range Hodoscope (FRH)
- ϕ angle in SEC and PSC - hits in elements of equal ϕ angle in the central part of the Calorimeter (SEC) and the plastic barrel (PSC)
- $\theta(\pi^+)$ and $\theta(d)$ are correlated as expected for a 2-body final state
- the sum of ϕ angles from PSC (π^+) and FRH(d) has to be close to 180° according to a 2-body reaction

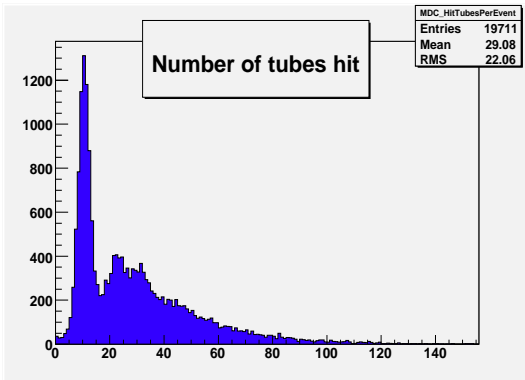


Fig. 1: Number of straw tubes(MDC) hit after $d\pi^+$ selection.

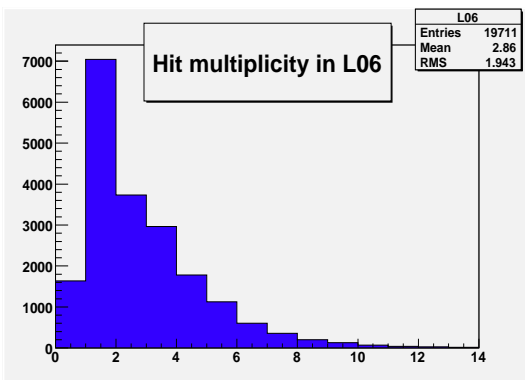


Fig. 2: Layer multiplicity after $d\pi^+$ selection.

Results. In figures 1 and 2 the histograms after $d\pi^+$ selection are presented. In figure 1 the distribution of straw tubes hit consists of several peaks: the dominant particles are π^+ -s, and additional hits from other events are accepted due to the wide time window of 1920 ns. The position of the dominant peak is located at 10 hit tubes out of 15 layers. In figure 2 the

hit multiplicity per layer indicates that events with one fired layer dominate.

For getting rid of the additional hits, coming from other events, the time window was reduced to 312 ns. The same histograms in figures 3 and 4 are extracted from the data with the reduced time window. The number of tubes hit shows a one peak structure with a maximum at 10 hit tubes. It can be interpreted as mostly one particle hitting MDC and PSC and in most cases 10 out of 15 layers fired. The background is seen suppressed by the time window cut. The hit multiplicity in figure 4 shows that for three quarters of events one layer fired. Using the event display program for the MDC, it is possible to see the tubes hit. From the comparison of real and MC data one can identify the MDC tracks as π^+ .

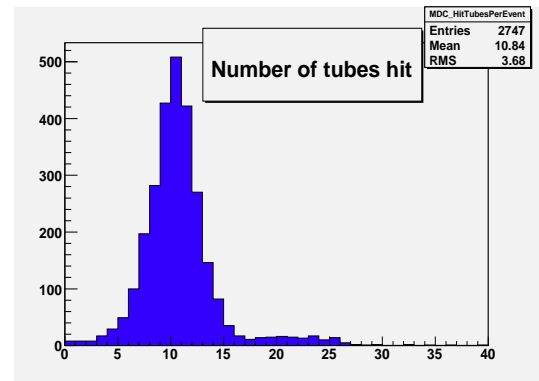


Fig. 3: The same as Figure 1, but after time window cut.

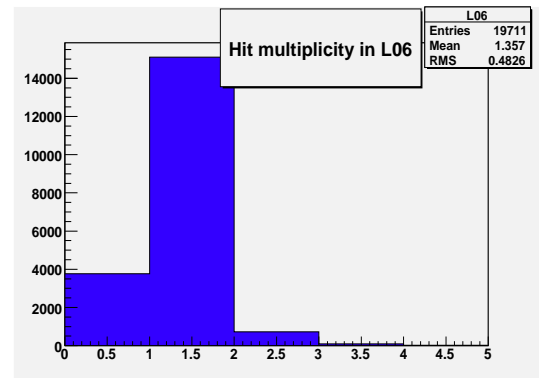


Fig. 4: The same as Figure 2, but after time window cut.

References:

- [1] <http://www-hep.phys.cmu.edu/cms>
- [2] H.Kleines et al., "Development of the new DAQ System for WASA at COSY", contribution to this Annual Report

¹ Joint Institute for Nuclear Research, Dubna, Russia

² Institute of Physics, Jagellonian University, Cracow, Poland

³ Department of Nuclear Reactions, Institute of Nuclear Physics PAS, Cracow, Poland

⁴IKP-2, Forschungszentrum Juelich

Test of the WASA Forward Proportional Chamber

M. Janusz^{1,2}, L. Yurev^{2,3}, M. Hodana¹, P. Kulesa^{2,4}, J. Majewski^{1,2}, K. Pysz^{2,4}, V. Serdyuk^{2,3}, H. Ohm²

The Forward Proportional Chamber (FPC) is a tracking detector for charged particles [1]. It consists of 4 planes of straw tubes with 448 straws each. These planes are subdivided in two identical halves. After transportation to Jülich they were inspected for possible aging effects due to the long operation at the CELSIUS accelerator and for possible damage during transportation. A series of tests were performed and new front-end electronics were developed and tested.

The performance of each straw tube was investigated by inspecting the shape and amplitude of analog signals. During these tests the straws were flushed with a 80/20 mixture of Ar and C₂H₆, and a voltage of 1.4 kV was applied. Since all measured signal amplitudes were found to be identical there is no indication of strong local aging effects occurred during previous operation. Moreover, the gas flow conditions of all chamber components are satisfactory.

During data taking with cosmic radiation prototype boards with CMP16 amplifier/discriminator chips [3] were connected to an FPC module. The main goal of this test was to check the interoperability of the prototype CMP16 chips with the chamber module. The test was based on a measurement of the time between the signal from a scintillation detector situated near the FPC and the signal from the FPC. The result is presented in fig.1. This time spectrum shows that the range of the drift time amounts approximately to 130 ns, a value which is in agreement with the maximum drift time of 150 ns. It was found that additional electric shielding of the straws is needed in order to reject pick-up of noise from external sources. Then it was possible to set the discriminator threshold to the very low level of about 30 fC.

In November one of the FPC modules was assembled at the WASA detector and tested under beam conditions. The main goal was to check the digital (F1) [2] and analog (CMP16) [3] electronic interoperability and all implemented functionalities. The collected data were used to test the acquisition system, to get experience in operation of the chamber and to establish working parameters. Results presented in fig.2 show that the range of the drift time is equal to 130 ns which is in agreement with the previous test performed with cosmic rays. In fig.2 one can notice background at a constant level which is likely to originate from imperfect screening of the detector module.

During the November commissioning run also the prototype of the gas system has been checked. In the future an analog device will be used as a gas supply for the FPC detector. The individual components (Ar and C₂H₆) of the gas mixture are delivered by mass flow controllers. The flow is subdivided into separate branches for each FPC module and the flow is monitored with flow sensors.

The complete detector is going to be installed for the first production run in April 2007.

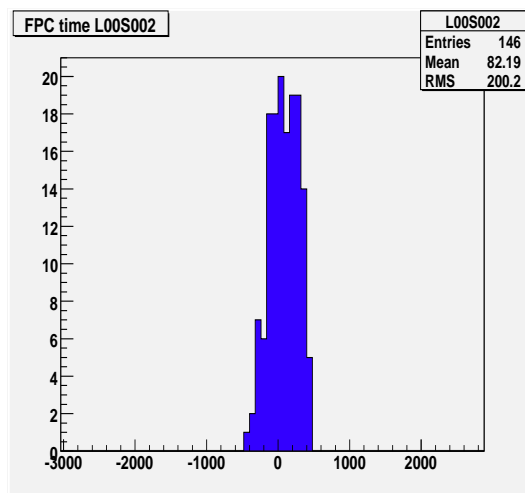


Fig. 1: Sample FPC spectrum received from the cosmic rays test. One channel corresponds to 130 ps.

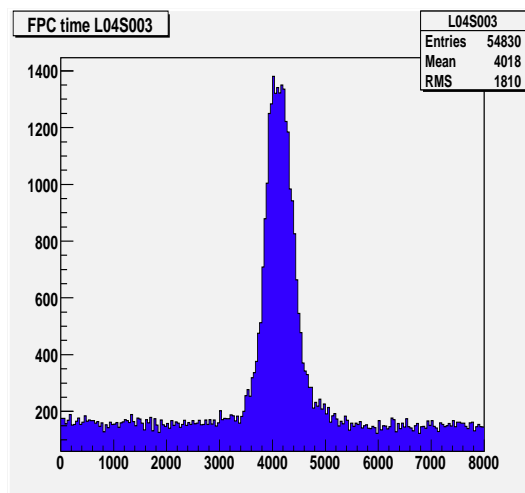


Fig. 2: Time spectra obtained during commissioning. One channel corresponds to 130 ps. The full width of the peak is equal to 130 ns.

References:

- [1] J. Zabierowski, Phys. Scripta, **T99**, 159, (2002).
- [2] H. Kleines et al., IEEE Trans. Nucl. Sci **53**, 893 (2006).
- [3] <http://www-hep.phys.cmu.edu/cms>

¹ Institute of Physics, Jagellonian University, PL 30-059 Cracow, Poland

² IKP-2, Forschungszentrum Jülich

³ Joint Institute for Nuclear Research, RU 141980 Dubna, Russia

⁴ Institute of Nuclear Physics, Polish Academy of Science, PL 31-342 Cracow, Poland

The light pulser and light pulser monitoring system of WASA-at-COSY

W. Węglorz^{1,2}

The WASA light pulser system (LP) was already used at the CELSIUS/WASA installation in Uppsala[1]. It allows to monitor the gain stability of the photomultipliers and, thus, simplifies the later data analysis. The light pulser system consists of two parts, the light sources and monitoring system. In total four common light sources are used; optical fibres are distributing the light pulses to the individual counters. Two types of light sources are in use: Xenon flash tubes and LED based fast light sources. Due to its high luminosity the Xenon flash tubes (XeLS) are used for the Scintillator Electromagnetic Calorimeter (SEC). The luminosity is crucial because the light is distributed from one central light source in a tree like way. Starting with quite thick optical fibres the light is led in two steps via distribution boxes to thin optical fibres ending at the individual detector modules. Although multiple sources would have made the setup more simple, this solution has two big advantages. First, fluctuations coming from the single light source are observed in the same way in all detector modules and, second, installing optical filters at one central place allows to control the amplitude for all modules at the same time (e.g. for linearity checks)[2].

For the plastic scintillators in total three fast light sources (FLS) based on common LEDs are in operation. Here, the light pulses are directly distributed to the individual counters via thin optical fibres. One source is used for the Plastic Barrel modules in the central detector, the other two for the whole forward detector.

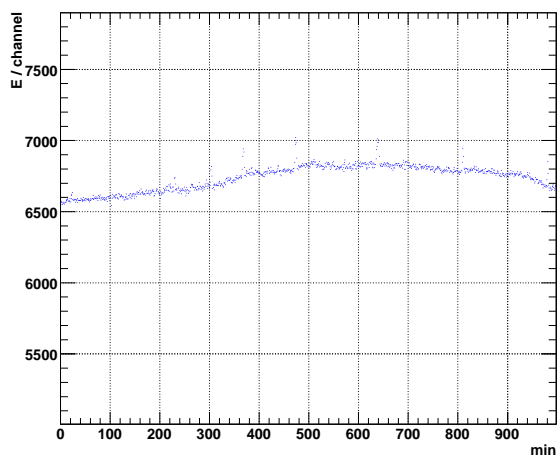


Fig. 1: XeLS stability observed during 1000 min test run.

The whole light pulser system is controlled via a dedicated monitor system. From each source one optical fibre is connected to a photodiode and further to an ADC channel of the data acquisition. The used photodiodes provide high stability and, thus, allow to obtain accurate data on the time stability

of the light source. In the data analysis these data are correlated with the response of each detector channel to eliminate the influence of time dependent changes of the amplitude of the light source. The remaining time dependence can then be assigned to the individual detector modules. The monitoring system has been completed and tested in December 2006. Results of the test are illustrated in Figs. 1 and 2.

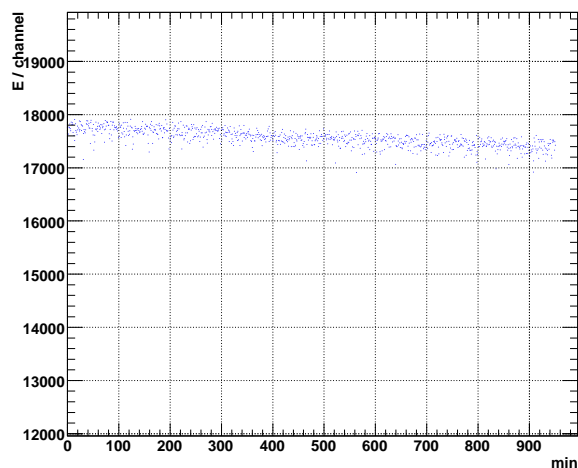


Fig. 2: FLS stability observed during 1000 min test run.

As one can see from the plots some long term fluctuations up to 10% are observed in case of the Xenon flash source. These can originate from the Xe lamp working parameters and from high voltage fluctuations of the pulse generator. In addition, short periods with increased light output (Fig. 1) are likely to come from the fact that the flash tube is operated close to the lower threshold parameters recommended by the producer (which was necessary to obtain the correct length of the light pulses). However, since the monitoring allows for correcting these effects, the light pulser system for WASA is an adequate tool to monitor the stability of the photomultiplier gain.

References:

- [1] J.Zabierowski et al. Phys.Scripta **T99**,159 (2002)
- [2] J.Zabierowski, Nucl. Instrum. Meth. **A338**, 577 (1994)

¹ Institute of Physics, University of Silesia, 40-007 Katowice, Poland

² IKP -2, Forschungszentrum Jülich

H. Kleines¹, K. Zwoll¹, P. Wüstner¹, W. Erven¹, P. Kämmerling¹, G. Kemmerling¹, H. Loevenich¹, A. Ackens¹, M. Wolke², V. Hejny², H. Ohm², T. Sefzick², R. Nellen², P. Marciniowski³, K. Fransson³, L. Gustafsson³, A. Kupsc³, H. Calen³

For the operation of the WASA detector system at COSY a new DAQ system was developed by the FZJ Central Institute for Electronics (ZEL) in close cooperation with IKP and the Department of Nuclear and Particle Physics of Uppsala University. Major reasons for the development of a new DAQ system were the increased performance requirements due to the higher luminosity at COSY and maintenance problems of the outdated electronics of WASA at CELSIUS [1].

Focus of the development work was the implementation of new digitalization modules (QDC and TDCs in Fig. 1) for all straw and scintillation detectors. Only the trigger system and parts of the front end electronics remained unchanged.

Due to the limited time of about one year the development project was extremely ambitious. The development work had to be interleaved with mass production of modules and it was impossible to do sufficient testing before the first test run in August, resulting in major technical risks.

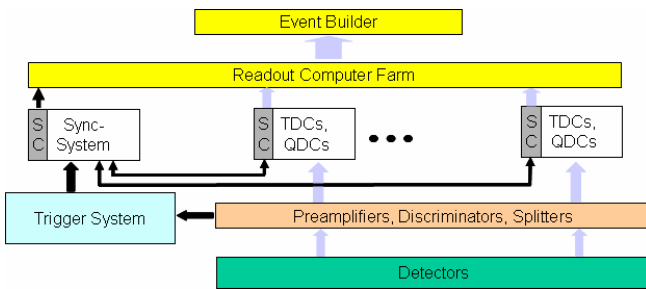


Fig. 1: Structure of the new DAQ system of WASA at COSY

The new DAQ system is based on the third generation of DAQ at COSY, with a purely hardware-based module readout, buffer and event management [2]. In the front-end modules latest state-of-art FPGAs are used enabling massively parallel operation, e.g. charge computation (integration) simultaneously for a group of ADCs. The system is completely “free-running”: All detector signals are digitized, time-stamped and stored in buffers in order to bridge trigger delays. As a consequence, crates with an optimized system bus for digitalization module readout (LVDS) and synchronization (ECL) had to be implemented.

According to Fig. 1 a System Controller (SC) is responsible for crate-wide synchronization and module readout. Via an optimized optical link (joint development with company SIS) the data is transferred from the SC to a readout PC. The event-builder buffers the data in a disk array before it finally arrives in a tape archive. A key component is the synchronization system [3], which distributes a common time base relative to the trigger point. It receives and distributes the trigger, generates event numbers, handles the module busy times and gathers performance statistics. All software implemented on readout PCs and the event-builder follows the EMS

framework thereby ensuring compatibility to all other COSY experiments.

Four types of digitalization modules have been developed: **SlowQDC:** The SlowQDC is designed for the readout of the Calorimeter PMTs (1084 channels) and does time-stamping in addition to charge computation. It is a 16 channel module based on 80 MHz FADCs.

FastQDC: The FastQDC is designed for the readout of detectors with plastic scintillators (PSB and Forward Detector, 564 channels). It is a 16 channel module based on 160 MHz FADCs.

FastTDC: The FastTDC is designed for the time-stamping of detectors with plastic scintillators. It is a 64 channel module based on the GPX ASIC from acam messelectronic gmbh.

SlowTDC: The SlowTDC is designed for the readout of straw tubes (4000 channels). It is an improved version of a module already developed for ANKE and TOF. It is equipped with LVDS inputs for the CMP16 based front-end electronics and distributes the threshold values serially to the DACs in the front-end. The SlowTDC is a 64 channel module based on the F1 ASIC from acam messelectronic gmbh.

For the test and commissioning beam times in August and November 2006 digitalization modules, crates and system controllers for all detector channels were available and the whole system could be tested successfully with an intermediate synchronization system. Since the software overhead of the intermediate synchronization system limited the readout time to about 80 μ s, the final performance goal could not be reached. This will only be possible with the final synchronization system, which is expected to be available before the first production beam time in 2007.

References:

[1] H. Kleines et al., IEEE Trans. Nucl. Sci., **53**, 893 (2006).
 [2] P. Wüstner et al., “System Development for COSY Experiments“, proc. 13th IEEE Real Time Conference, Montreal, Canada, May 2003.
 [3] P. Wüstner et. al., “A new synchronisation system for experiments at COSY“, proc. 14th IEEE Real Time Conference, Stockholm, June 2005

¹ ZEL, FZ Jülich

² IKP, FZ Jülich

³ Department of Nuclear and Particle Physics, Uppsala University

Status of the pellet target for the WASA-at-COSY experiment*

A. Winnemöller[#], A. Khoukaz[#], N. Milke[#], T. Rausmann[#], and A. Täschner[#]

After the transfer of the WASA-experiment from CELSIUS to COSY, the reassembly of the pellet target started in December 2005 at the test station at the Bermuda triangle. This target is the first and up to now only pellet target system running in an internal beam accelerator experiment [1,2]. Different tests and optimizations have been accomplished until the first droplet beam was obtained in April 2006 (figure 1). Shortly after that the first pellets were produced. The final installation of the pellet target at the COSY ring took place in summer 2006. Due to the new location inside the COSY hall (figure 2), a second control system was established close to the COSY control room in order to re-tune or adjust the target during a beam time without any radiation exposure of the personnel.

One of our major objectives after the installation at COSY was to reproduce the target performance (pellet rate, target thickness, stability, etc.) obtained at CELSIUS/Uppsala. This goal was reached during the commissioning phase in August 2006 [3] with a pellet target thickness of approx. $2.5 \cdot 10^{15}$ atoms \cdot cm $^{-2}$ calculated from the energy loss of the COSY beam. During the beam time in November 2006 the pellet beam was stable for more than a week until the end of the running period.

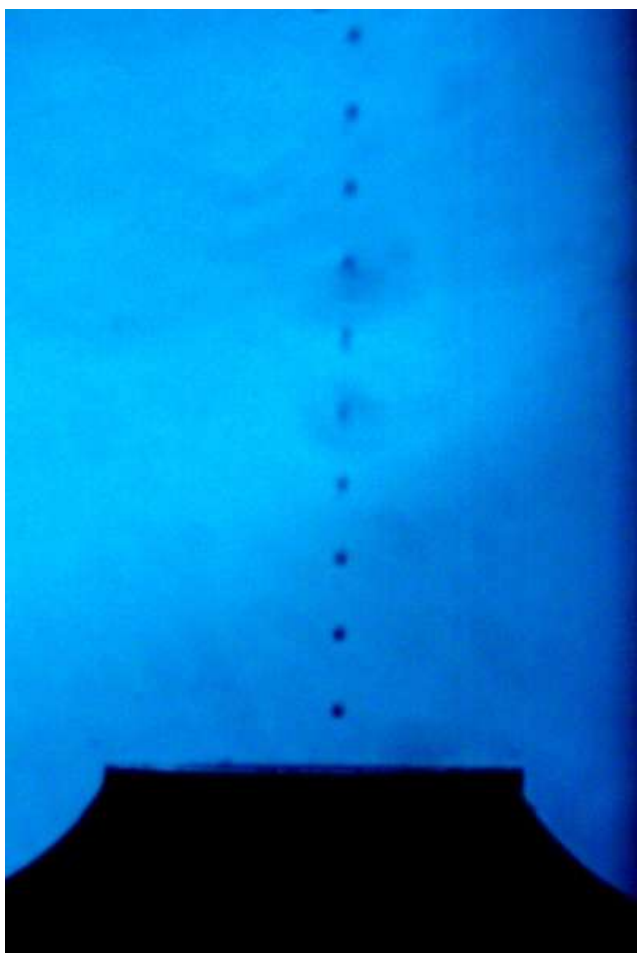


Fig. 1: Photo of the droplet beam before reaching the vacuum injection capillary.

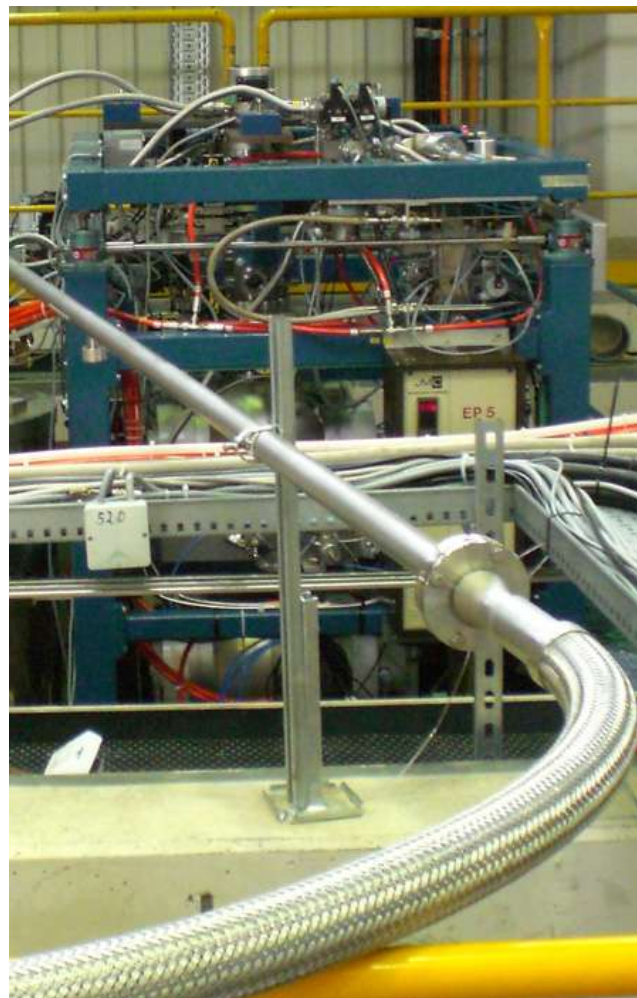


Fig.2: Photo of the pellet target at its new location at the COSY ring.

Furthermore, tests with deuterium have been started in December 2006, ending with the production of first deuterium pellets at COSY.

The target performance strongly depends on the quality of the glass nozzles and the vacuum injection capillaries. Therefore, a facility for the production of these parts has been established at the ZAT. The production started at the very end of 2006.

In the near future systematic studies on optimum pellet beam conditions using hydrogen as well as deuterium gas will be performed.

References:

- [1] B. Trostell, Nucl. Instr. and Meth. **A 362**, 41 (1995)
- [2] C. Ekström et al., Nucl. Instr. and Meth. **A371**, 572 (1996)
- [3] H.-H. Adam et al., *Proposal for WASA at COSY* COSY-PAC 29 (2004); nucl-ex/0411038

[#] Institut für Kernphysik, Universität Münster, 48149 Münster, Germany

A Pellet Tracking System (PTS) for WASA at COSY is proposed in order to determine the interaction point (the primary interaction vertex) between the COSY beam and the target pellets. The knowledge of this interaction vertex helps to reconstruct the paths of the different decay products and thus to improve the momentum resolution of the events. This will also be important for the study of D-mesons planned at the PANDA detector at the future accelerator facility FAIR in Darmstadt, Germany [1]. Furthermore the PTS gives information about the position distribution of the pellets below their place of production and below the interaction point, allowing the geometrical alignment of the system to be improved.

In previous work on the pellet tracker at Uppsala University a setup with one camera and one laser was used to study hair, wires as pellet simulator and pellets from a pellet test station. A one dimensional distribution of the pellets was measured, and found to be consistent with the expectations from the geometry of the system [1-3].

The main idea to determine the interaction point is to measure the x and z position of a pellet before and after the interaction point. That can be done by using a laser beam to light up the pellet and photographing it (using the scattered laser light from the pellet) by pairs of fast CCD line scan cameras, below and above the interaction point (fig.1). The cameras are arranged at 90° relative angle to each other. Then the pellet trajectories can be tracked from the position information from each plane and the relative timing.

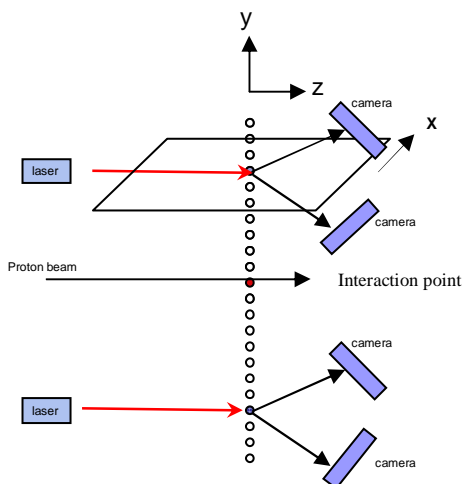


Fig.1 Proposed system to determine the x and z position of the individual pellets.

Equipment needed

- Laser: the laser used is an MFL Micro-Focus laser, 660 nm, 80 mW and 185 mm working distance with 1° fan angle [4].
- Line scan camera: the camera used is an AVIIVA M2 CL 0514 line scan camera, with maximum read out frequency of 98 KHz [5].
- Frame grabber and software programs to analyze the photos: DALSA CORECO frame grabber is used with the Spera CamExpert program for taking pictures with the

line scan camera. CommCam is used to control the camera [6].

Photographing a strand of hair

As a first test of the equipment’s capabilities, a strand of hair was photographed and its thickness was determined (figs. 2 and 3).



Fig.2 Photograph of the system used to determine the thickness a hair.

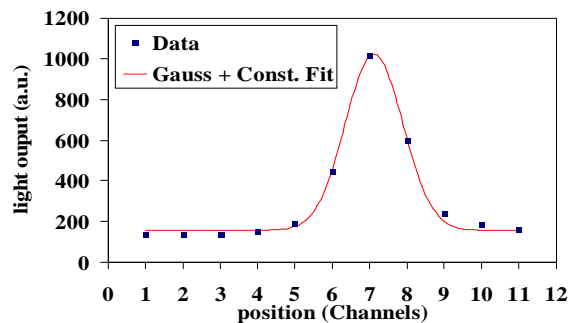


Fig.3 Gauss fit of the measured light intensity in the camera to the scattered light from a hair.

A strand of hair was fixed at distance of 175mm from the lens. At this distance the lens has a magnification factor of (0.4 ± 0.01) . As shown in fig.3 the FWHM of the measured light distribution was found to be (1.8 ± 0.06) channels. Using the pixel size of $14\mu\text{m}$ [5] the calculated thickness of the hair is found to be $(63.3 \pm 2)\mu\text{m}$, in agreement with the value $(70 \pm 5)\mu\text{m}$ measured directly with a micrometer.

References:

- [1] Ö. Nordhage et al., Nucl. Instrum. Meth. A **568**, 561 (2006).
- [2] Jonas Lith. Development of a Tracking System for Hydrogen Pellet Targets utilizing a Line-Scan Camera. Master thesis, Uppsala University (2006).
- [3] Matthias Schult. Development of a Pellet Tracking System. Project work, Uppsala University (2005).
- [4] LASER 2000. MFL Micro-Focus Laser users manual.
- [5] ATMEL. AVIIVA™ M2 Cl Cameralink™ Line Scan Camera, 2006, Data sheet.
- [6] DALSA CORECO. X64-CL iPro Series User’s Manual Edition 1.11.

The η' mesons for the rare decay studies at the WASA-at-COSY facility will be produced in the $pp \rightarrow pp\eta'$ reaction close to threshold. The identification of the $pp \rightarrow pp\eta'$ process will be performed by means of missing mass to the two outgoing protons measured in the Forward Range Hodoscope (FRH). Due to the large background originating from multipion production the statistical and systematical errors in the evaluations of cross sections and branching ratios of the investigated decay channels will strongly depend on the resolution of the missing mass reconstruction, which in turn will depend on the precision of the reconstruction of the momentum vectors of the registered protons. At present the determination of the energy of the protons is based on the energy loss measurement in the scintillation layers of the FRH. The resolution achieved with the setup used at the CELSIUS facility was about 1.5% ($\sigma(T)/T$) for protons with kinetic energy lower than $T = 300$ MeV, i.e. for protons stopped in the detector material. However, it worsens significantly for larger energies. The achieved accuracy was satisfactory for investigations of the η meson production and decay. However, it appears to be insufficient for studies of the η' meson due to a much higher background-to-signal ratio and due to higher energies of the outgoing protons than in case of the $pp \rightarrow pp\eta$ reaction. For the beam momentum of $P_{beam} = 3.35$ GeV/c, considered as an optimum for the production of the η' meson at the WASA-at-COSY facility [1], the kinetic energies of the protons are in the range between 300 MeV and 800 MeV (see figure 1(left)).

In order to improve the accuracy of the energy determination for forward scattered ejectiles the FRH was upgraded with two new scintillator layers each with a thickness of 15 cm [2]. The rough estimate of the energy resolution expected with the extended detector is shown in figure 1(right). With this accuracy the missing mass distribution has a width of about 3.5 MeV/ c^2 (FWHM) and tails as it is seen in figure 2(left). In the simulations contributions from the extension of the interaction region and the spread of the COSY beam momentum were not included. Presently, the overall contributions of these effects are estimated to be about 4 MeV/ c^2 (FWHM) [1]. In this report only the proton kinetic energy resolution is considered.

There are two suggestions for a possible future improvement of the energy measurement accuracy. One assumes installation of a DIRC detector which would enable to determine the velocity of protons with an accuracy of about $\sigma(\beta)/\beta = 0.003$. The second scenario foresees an extension of the forward detector which would allow to determine the time of flight [3] for protons passing through the FRH with a precision of $\sigma(TOF) = 100$ ps [4]. In order to facilitate comparison of the TOF, DIRC and energy loss techniques we expressed the properties of TOF and DIRC methods in terms of fractional kinetic energy resolution. The results are compared in figure 1(right). The figure shows that both DIRC and TOF would yield better resolution than that obtained only from energy loss. It is also evident, that the energy resolution of the DIRC detector is much better than the TOF method. It is, however, important to note, that TOF can be determined for protons which passed the whole detector ($T > \approx 360$ MeV), whereas a DIRC can deliver signals only for protons above

Cerenkov threshold which corresponds to 500 MeV. This implies that only a fraction of protons from the $pp \rightarrow pp\eta'$ reaction can be reconstructed by means of the DIRC or TOF detectors.

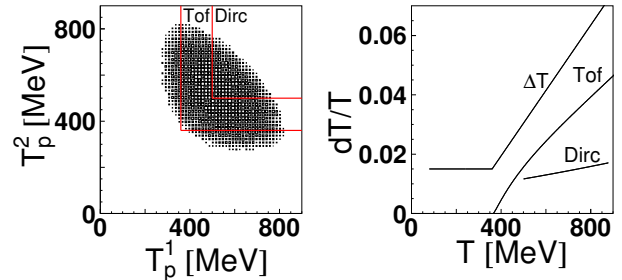


Fig. 1: **Left:** Kinetic energies of protons from the $pp \rightarrow pp\eta'$ reaction simulated for the beam momentum of 3.35 GeV/c. **Right:** Fractional kinetic energy resolution estimated for the three considered techniques.

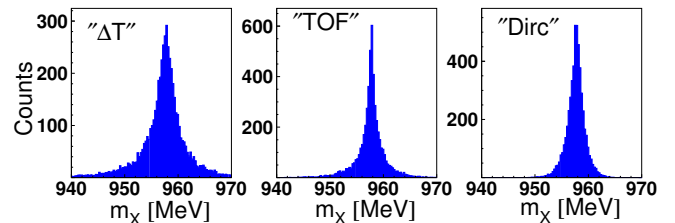


Fig. 2: Missing mass resolution for the $pp \rightarrow pp\eta'$ reaction reconstructed assuming the kinetic energy determination from energy loss measurement (left), TOF (middle), and DIRC (right), respectively.

Figure 1(left) shows that at a beam momentum of 3.35 GeV/c the energy of both protons from the $pp \rightarrow pp\eta'$ reaction can be reconstructed for only about 20% of events using the DIRC detector, and for about 70% of events using the TOF technique. In other cases the energy of either one or both protons must be determined using energy loss. Simulations of the missing mass distribution show that using the TOF or DIRC techniques for the energy reconstruction of protons would improve the resolution of the missing mass reconstruction by about a factor of two (see figures 2(middle) and 2(right)).

References:

- [1] A. Kupś, WASA-at-COSY Note/060122AK.
- [2] H. Calen et al., Ann. Rep., IKP, FZ-Jülich (2006).
- [3] P. Moskal, A. Kupś, J. Złomańczuk, WASA-at-COSY Note/061123PM.
- [4] T. Sugitate et al., Nucl. Instrum. Meth. **A249** 354 (1986).

^a Institute of Physics, Jagiellonian University, 30-059 Cracow, Poland

^b Department of Nuclear and Particle Physics, Uppsala University, 75121 Uppsala, Sweden

Upgrade of the Forward Range Hodoscope of the WASA-at-COSY facility

H. Calén^a, E. Czerwiński^b, R. Czyżykiewicz^b, D. Duniec^a, K. Fransson^a, A. Heczko^b, P. Klaja^{b,c}, A. Kupś^{c,a}, A. Malarz^b, W. Migdał^b, P. Moskal^{b,c}, A. Nawrot^d, N. Paul^c, C. Pauly^c, J. Przerwa^{b,c}, A. Pricking^e, M. Zieliński^b

In the CELSIUS/WASA experimental facility at TSL, the energy reconstruction of the forward scattered particles was based on the measurement of the energy losses in the Forward Range Hodoscope (FRH) which consisted of four layers of plastic scintillators each with a thickness of 11 cm [1]. The thickness was optimized for measurements of protons originating from the $pp \rightarrow pp\eta$ reaction ($T_p = 100\text{-}550$ MeV) at the beam energies in the range of the CELSIUS accelerator.

The transfer of the WASA detector from CELSIUS to COSY opened possibilities to study the production and decays of mesons heavier than the η meson, in particular the η' meson [2]. The resolution of the FRH appeared, however, to be insufficient for such investigations, in particular due to much higher background-to-signal ratio and due to higher energies of the outgoing protons than in the case of the $pp \rightarrow pp\eta$ reaction. For the beam momentum of $P_{beam} = 3.35$ GeV/c, anticipated as an optimum value for the studies of the η' mesons [3], the kinetic energy of protons ranges from 300 MeV to 800 MeV. The resolution with the setup used at the CELSIUS facility was about 1.5% ($\sigma(T)/T$) for protons with kinetic energy lower than $T = 300$ MeV, i.e. for protons stopped in the detector material. However, it worsens significantly for larger energies relevant for the studies of the η' meson. Therefore, in order to improve the accuracy of the FRH for the reconstruction of protons with energies higher than 300 MeV the effective thickness of the sensitive material of the detector was increased by 19 cm. This was achieved by adding two new layers each with a thickness of 15 cm at the downstream end. The first of the old layers had to be taken away due to a necessary extension of the Forward Proportional Chamber (FPC) for improving the reconstruction of the scattering angles of the particles. The configuration of the upgraded Forward Detector (FD) is shown in Fig. 1. A total thickness of the scintillation material in this detector amounts now to 68 cm and stops protons with kinetic energies up to 360 MeV. We expect that the upgrade of FRH will improve the accuracy of the determination of proton energies by about 25% (at the highest energies). By analogy to the design used at CELSIUS the new layers consist of 24 independent detection units, each built out of a cake-piece shaped plastic scintillator (see Fig. 2) with a photomultiplier tube attached at the outer edge. The scintillator material is of type EJ-200 produced by the ELJEN company and the PMTs are of type XP3540B with voltage dividers VD202K/T1 from the PHOTONIS company. No lightguides were used and the PMs were connected directly to the scintillator material using Bicon BC-630 optical grease.

The outer edge of the cake piece scintillator has a rectangular shape with dimension 23.7 cm x 15 cm which is much larger than the active area of the photomultiplier tube (diameter = 13 cm). Therefore, in order not to suffer from the inhomogeneities in the collection of light in the region close to the PMT, the length of the scintillator unit (radius of the sensitive area of the detection layer) is more than 5 cm bigger than necessary for full geometrical acceptance.

For light tightness the scintillators were wrapped with thin (26 μ m) aluminized mylar foil. In addition, black paper cov-

ers the front and rear surface of each detector layer. The light tightness was checked before the final assembly and installation.

The scintillator units in a detector layer are mechanically supported and kept together in between two 8 mm thick plexi-glass sheets with aluminium structures at the outer edge and at the central hole (for the beam pipe).

The first of the new layers was installed in summer 2006 and its functionality was proven during the commissioning runs in autumn. The second layer was installed in December.

The funding for the upgrade was provided by The Knut and Alice Wallenberg Foundation. The conceptual design was made at INS Warsaw and the final design and fabrication of the mechanical support details and PM housing were done at JU Cracow. The plexi sheets were water-beam cut by the Malarlaser company. Tests with accelerator beam for selecting the PM readout system were done at TSL Uppsala.

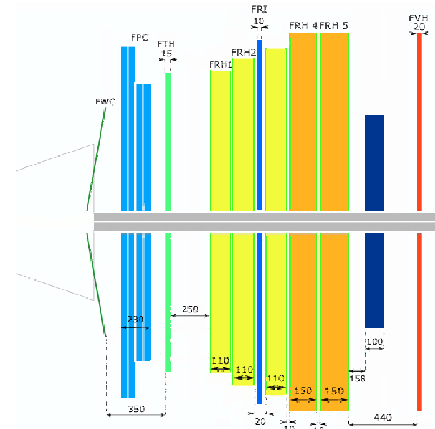


Fig. 1: Layout of the Forward Detector of WASA-at-COSY (measures are given in mm).

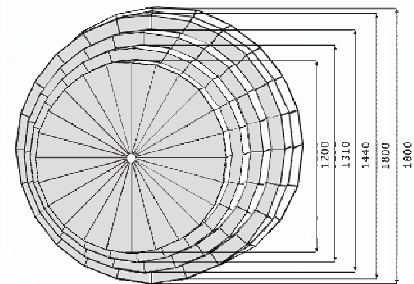


Fig. 2: Schematic view of the upgraded FRH (measures are given in mm).

References:

- [1] J. Zabierowski et al., Phys. Scripta. **T 99**, 159 (2002).
- [2] H. H. Adam et al., e-Print Archive: nucl-ex/0411038.
- [3] A. Kupś, WASA-at-COSY Note/060122AK.

^a Uppsala University (UU), Sweden

^b Jagiellonian University (JU), Cracow, Poland

^c IKP-1, Forschungszentrum Jülich, Germany

^d Institute for Nuclear Studies (INS), Warsaw, Poland

^e Tübingen University, Germany

The Forward Detector of the WASA at COSY[1] setup is essential to tag mesons by reconstructing the missing mass of recoil protons emitted in the forward direction. The original WASA[2] detector was designed to operate at beam energies up to 1.36 GeV for protons. At COSY it has to cope with higher energies (up to $T \sim 2.88$ GeV for protons) and increased event rates. As a result upgrades of several detector components were required. One such item is the Forward Range Hodoscope. In its original design the FRH is made of four planes of plastic scintillator which gives a kinetic energy resolution for stopped particles ($T_{stop} \leq 0.3$ GeV for protons) $\sigma_T/T \simeq 1.5\%$. At COSY the maximum kinetic energy of outgoing protons in the $pp \rightarrow pp\eta'$ will be about 1 GeV. This is too high to be measured by the existing FRH with sufficient energy resolution, therefore two additional layers of plastic scintillator have been constructed. At around 0.5 GeV protons kinetic energy the estimated resolution is about 3% and worsens to 10% at 0.9 GeV. To improve the energy measurements and provide particle identification of fast particles a Cherenkov detector has been proposed.

The Cherenkov detector design consists of 80 wedge shaped modules (length \times thickness $\simeq 600 \times 70$ mm²) placed radially around the beam axis and inclined in the beam direction. The radiator material is plexiglass ($n=1.5$) which is transparent in the UV region. The individual radiator modules are wrapped with reflective material. Charged particles with velocities higher than the Cherenkov threshold $\beta_{thr} = 1/n$ produce a cone of Cherenkov light. By means of total internal reflection and reflective material the light will be transferred to a photomultiplier tube located on the outside surface of the module. The signal amplitude of the PMT readout will give information about the velocity (or energy for a given mass hypothesis) of the particle. Fig.1 shows an artistic view of the proposed detector.

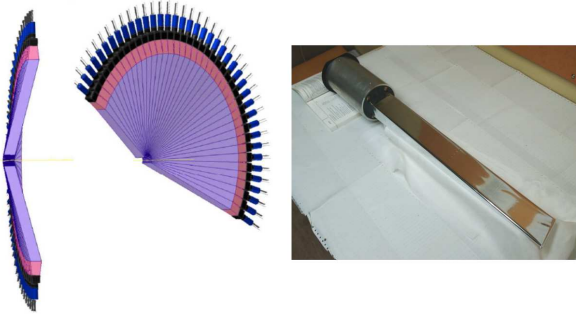


Fig. 1: Artistic view from two perspectives of one half of the detector (left) and a prototype module.

This design has been studied extensively with Geant4[3] - in order to estimate basic characteristics of the proposed detector. Properties of the material such as the absorption length, reflectivity of the wrapping material, properties of the PMT - quantum efficiency have been included as functions of wavelength of the emitted Cherenkov light. Assuming the Cherenkov detector placed in front of FRH, by combining the energy deposition of the particles in the FRH and the light output of the Cherenkov detector particle identification can

be performed. Noting γ_1 as a Lorentz factor measured with the Cherenkov detector and γ_2 measured by the FRH from $\gamma_2 = \gamma_1 - \frac{E_{dep}}{M_j}$, where M_j is the mass hypothesis of the given particle and E_{dep} is the deposited energy in the FRH, the experimental value of the mass of the particle is

$$M = \frac{z^2 \cdot \Delta X}{\frac{(\gamma_1 - 1)^2}{(\gamma_1 \cdot R_1)} - \frac{(\gamma_2 - 1)^2}{(\gamma_2 \cdot R_2)}}, \quad (1)$$

where ΔX [g/cm²] is the thickness of the FRH, z -is the charge of the particle and $R(\gamma)$ is a function derived from the Bethe-Bloch equation.

In November 2005 a prototype module with a plexi-glass radiator has been manufactured. In-beam measurements have been performed in cooperation with the HIRES collaboration[4]. During the tests with different particle momenta the light output and energy resolution were measured for different orientations of the prototype module. The kinetic energy resolution depends on the angle between the front side of the module and the particle trajectory (θ -inclination angle) and the entry point of the particle in the radiator. The kinetic energy resolution as a function of proton kinetic energy was determined for $\theta = 30^\circ$. The simulated and experimental values are shown in Fig.2. The open point for $T < 0.4$ GeV corresponds to measurements with protons and the results for $T > 0.4$ GeV were obtained using pions where the effective proton kinetic energy has been estimated from the pion velocity. The differences in the points are related to the different energy losses $\frac{dE}{dx}$ in radiator material.

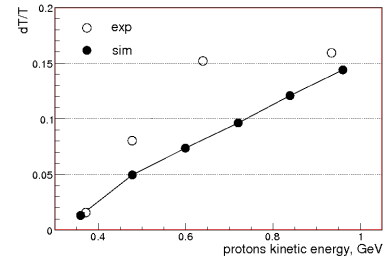


Fig. 2: Proton kinetic energy resolution. Results of simulation and experiment are shown with full and open points, respectively.

References:

- [1] H-H. Adam et al., nucl-ex/0411038
- [2] J.Zabierowski et al., **T99** 159-168 (2002)
- [3] Geant4, <http://geant4.web.cern.ch/geant4/>
- [4] HIRES Collaboration, <http://www.iskp.uni-bonn.de/gruppen/hires/index.html>

¹ IKP-1, Forschungszentrum Jülich, 52425 Jülich, Germany,

² Helmholtz-Insitut für Strahlen- und Kernphysik Rheinische Friedrich-Wilhelms-Universität, 53115 Bonn, Germany

³ Laboratory of High Energies, Joint Institute for Nuclear Research, 141980 Dubna, Russia

⁴ Institute of Nuclear Physics, Polish Academy of Science, 31342 Cracow, Poland

Čerenkov detectors are widely used in high energy physics. Depending on the task Čerenkov detectors could have different applications: particle identification, energy measurement, threshold detector for detecting specific type of particles in a definite energy range.

Our aim is to measure proton energy in an energy range from 400 MeV to 1000 MeV. In order to find proper radiator and photocathode Monte Carlo simulations were performed.

Different materials were tested as radiator: *LiF*, *CaF* and quartz. All materials have different refractive index (Fig. 1) and transmittance (Fig. 2) [1]. To measure particles with "low" energy radiator must have large refractive index. *LiF* has wider transmittance for UV range in comparison with *CaF* and Quartz. It gives possibility to build Čerenkov detector with *LiF* as radiator and proper photocathode for detecting photons in UV range. *LiF* radiator should be thin because of the low transmittance (large probability to absorb photon).

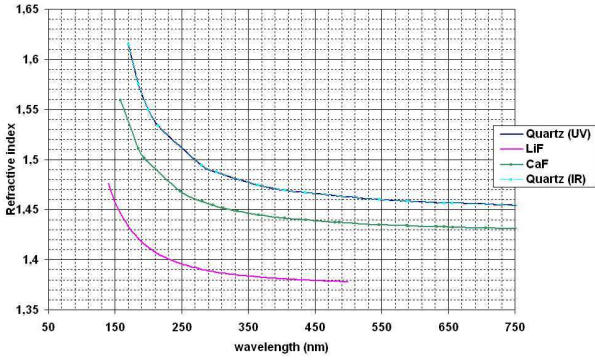


Fig. 1: Refractive index for quartz (UV-grade and IR-grade), *CaF* and *LiF*.

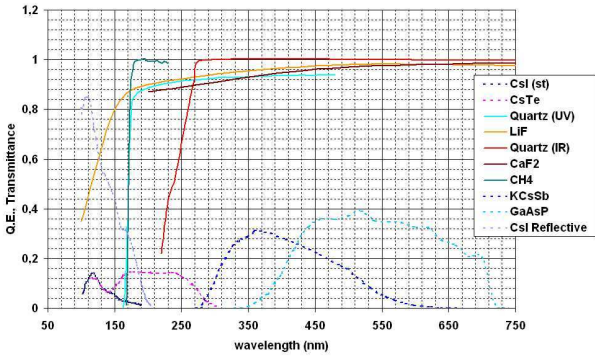


Fig. 2: Photocathode quantum efficiency (dotted curves) and radiator transmittance (solid curves).

Quantum efficiencies for different photocathode's types are shown in Fig. 2 [2–4]. *CsI* and *CsTe* are used for photon detecting in UV range. Bialkali (*KCsSb*) and multialkali (*GaAsP*) photocathodes are used for upper UV and visible light ranges. These types of photocathodes have large and broad shape of the quantum efficiency function. It could compensate smaller amount of emitted photons in this wave

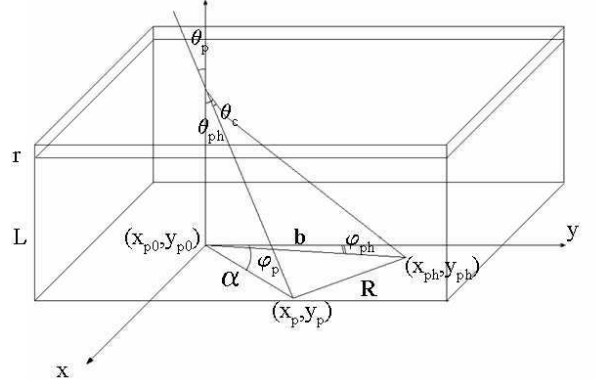


Fig. 3: Geometry and event reconstruction scheme.

range. A proximity focusing RICH detector with a radiator of thickness 1 cm is shown in Fig. 3. Emitted photons pass through a drift chamber with a thickness of 4 cm. The photocathode is placed on the back plane of the drift chamber. Photons produce photoelectrons, which could be detected in the drift chamber volume. Methane is used as active gas in the drift chamber.

The knowledge of particle direction (θ_p, φ_p) and photon position on the screen (x_{ph}, y_{ph}) are necessary for event reconstruction. The point from the particle hit should be also visible on the screen. In the reconstruction algorithm is assumed, that Čerenkov photons are emitted in the half thickness of the radiator. Knowing particle direction it is possible to define coordinates of this point (x_{p0}, y_{p0}). The event reconstruction algorithm is described by the following equations:

$$a = \left(\frac{r}{2} + L \right) \tan \theta_p \quad (1)$$

$$b = \frac{r}{2} \tan \theta_{ph} + L \frac{n_r \cdot \sin(\theta_{ph})}{\sqrt{n_L^2 - n_r^2 \sin^2(\theta_{ph})}} \quad (2)$$

$$\tan \varphi_{ph} = \frac{y_{ph} - y_{p0}}{x_{ph} - x_{p0}} \quad (3)$$

$$R^2 = [a \cdot \cos \varphi_p - b \cdot \cos \varphi_{ph}]^2 + [a \cdot \sin \varphi_p - b \cdot \sin \varphi_{ph}]^2 \quad (4)$$

$$\cos \theta_c = \cos \theta_p \cdot \cos \theta_{ph} + \sin \theta_p \cdot \sin \theta_{ph} \cdot \cos(\varphi_p - \varphi_{ph}) \quad (5)$$

Eq. (1) gives the distance from the particle hit on the screen to the (x_{p0}, y_{p0}), where r and R are the radiator and drift chamber thicknesses, respectively. The distance to the photon hit point is defined by Eq. (2), where θ_{ph} is the angle of the emitted photon to the normal, n_L and n_r are refractive indices for the drift chamber active gas and radiator, respectively. By solving Eq. (4) it is possible to find θ_{ph} . The Čerenkov angle θ_c can then be obtained from Eq. (5). More details are given in Ref. [5].

Results of Monte-Carlo simulations are shown on Fig. 4–6. The number of the detected photons for different configurations "radiator-photocathode" is shown in Fig. 4. For configuration quartz-*CsI* the lowest number of the converted photons was obtained. This can be explained by the low photocathode quantum efficiency and a narrow emitting-detecting

range which is limited by the radiator transmittance function from the left side and quantum efficiency function from the right side. For configurations with multialkali and bialkali photocathodes the number of detected photons is large. Čerenkov angle resolution (Fig. 5) and momentum resolution (Fig. 6) for quartz-*CsI* are worse than for radiators with multi- and bialkali photocathodes. Best results are obtained for a *LiF* radiator with multi- and bialkali photocathodes.

[4] R. Mirzoyan, D. Ferenc, E. Lorenz, Nucl. Instr. and Methods in Phys. Research A 442, 140 (2000).
 [5] ALICE Collaboration, Technical Design Report of the High Momentum Particle Identification Detector, CERN/LHCC 98-19.

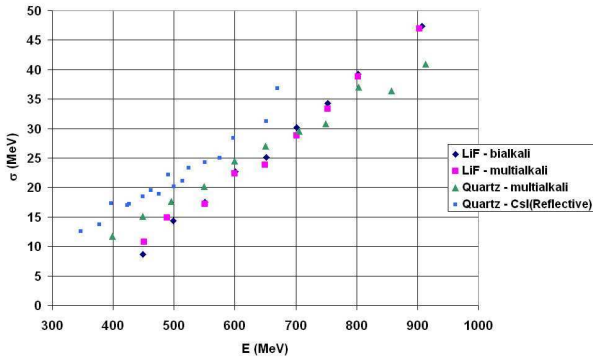


Fig. 4: Detected photon number for different configurations radiator-photocathode

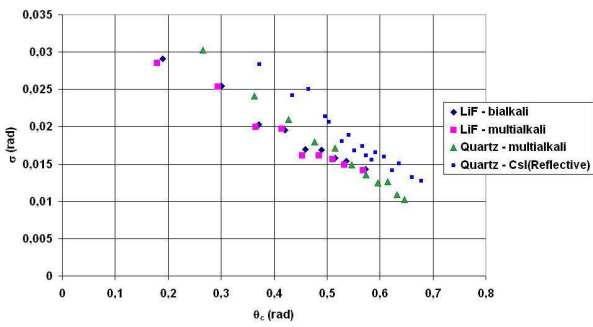


Fig. 5: Čerenkov angle resolution

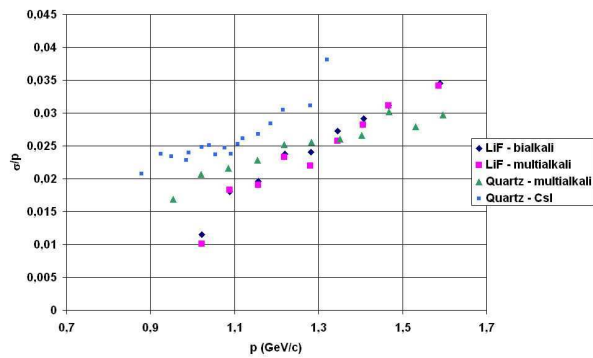


Fig. 6: Momentum resolution

References:

[1] SCHOTT optical glass data sheets.
 [2] A.Breskin, Nucl. Instr. and Methods in Phys. Research A 371, 116 (1996).
 [3] D.Mota and S.Schönert, arXiv:physics/0408075v1

From precise measurements of the total cross sections of the η meson production in the $pp \rightarrow pp\eta$ reaction [1, 2, 3, 4, 5, 6, 7, 8] it was concluded that this process proceeds through the excitation of one of the protons to the $S_{11}(1535)$ state which subsequently deexcites via the emission of the η meson (see Fig. 1). In practice, within the meson exchange

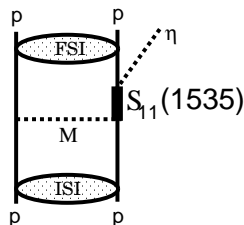


Fig. 1: The mechanism of the η meson production in nucleon-nucleon collisions. M denotes an intermediate pseudoscalar or vector meson, e.g. π , η , ω , ρ . ISI and FSI indicate initial and final state interaction between the nucleons.

picture, the excitation of the intermediate resonance can be induced by exchange of any of the pseudoscalar or vector ground state mesons between the nucleons. Based only on the excitation function it was, however, impossible to disentangle the contributions to the production process originating from the π , η , ω or ρ meson exchange.

More constraints to theoretical models [9, 10, 11, 12, 13, 14, 15, 16] have been deduced from the measurement of the isospin dependence of the total cross section by the WASA/PROMICE collaboration [17]. From the comparison of the η meson production in proton-proton and proton-neutron collisions it was inferred that the η meson is by a factor of twelve more copiously produced when the total isospin of the nucleons equals to zero with respect to the case when it equals to one. As a consequence only an isovector meson exchange is conceivable as being responsible for such a strong isospin dependence. It was a large step forward but still the relative contributions of the ρ and π mesons remained to be disentangled. For this purpose we have determined the analysing power for the $\vec{p}p \rightarrow pp\eta$ reaction since its theoretical value [11, 14] is sensitive to the assumption on the type of the meson being exchanged in order to excite one of the colliding nucleons to the $S_{11}(1535)$ state.

Measurements have been performed in the close-to-threshold region at beam momenta of $p_{beam} = 2.010$ and 2.085 GeV/c, corresponding to the excess energies of $Q=10$ and 36 MeV, respectively. The experimental method is presented elsewhere [18, 19], here we would only like to present the results of our measurements and the conclusions.

The values of analysing power determined for both excess energies are presented in Fig. 2. At the excess energy of $Q = 36$ MeV an insufficient statistics for the $\cos\theta_\eta \in (-1; -0.5)$ range resulted in an error larger than the allowed range of values and hence this point was omitted.

In order to verify the correctness of the models based on the dominance of the ρ or π meson exchanges, a χ^2 test has been performed [18, 19]. The reduced value of the χ^2 for the pseudoscalar meson exchange model was determined to be $\chi^2_{psc} = 0.54$, which corresponds to a significance level $\alpha_{psc} = 0.81$, whereas for the vector meson exchange model $\chi^2_{vec} = 2.76$, resulting in a significance level of $\alpha_{vec} = 0.006$. This result provides a strong evidence for the supposition that the production of the η mesons in nucleon-nucleon collision is dominated by the pion exchange.

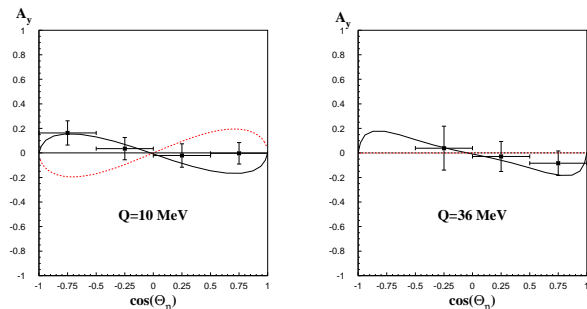


Fig. 2: Analysing powers for the $\vec{p}p \rightarrow pp\eta$ reaction as a function of the cosine of center-of-mass polar angle of the η meson for $Q = 10$ MeV (left panel) and $Q = 36$ MeV (right panel). Full lines are the predictions based on the pseudoscalar meson exchange model [14] whereas the dotted lines represent the results of the calculations based on the vector meson exchange [11]. In the right panel the dotted line is consistent with zero. Error bars in this figure show the statistical uncertainties only.

One should, however, keep in mind that the interference in the exchange of both types of mesons are not excluded and should be studied theoretically and experimentally by the measurement of further spin observables.

It is also worth to mention that the analysing powers of the $\vec{p}p \rightarrow pp\eta$ reaction for both excess energies studied are consistent with zero within one standard deviation. This may suggest that the η meson is predominantly produced in the s -wave, an observation which is in agreement with the results of the analysing power measurements performed by the DISTO collaboration [20] where, interestingly, in the far-from-threshold energy region the A_y were found to be also consistent with zero within one standard deviation.

References:

- [1] F. Hibou et al., Phys. Lett. **B 438** (1998) 41.
- [2] J. Smyrski et al., Phys. Lett. **B 474** (2000) 182.
- [3] A. M. Bergdolt et al., Phys. Rev. **D 48** (1993) 2969.
- [4] E. Chivassa et al., Phys. Lett. **B 322** (1994) 270.
- [5] H. Calén et al., Phys. Lett. **B 366** (1996) 39.
- [6] H. Calén et al., Phys. Rev. Lett. **79** (1997) 2642.
- [7] P. Moskal et al., Phys. Rev. **C 69** (2004) 025203.
- [8] M. Abdel-Bary et al., Eur. Phys. J. **A 16** (2003) 127.
- [9] J. F. Germond and C. Wilkin, Nucl. Phys. **A 518** (1990) 308;
- [10] J. M. Laget et al., Phys. Lett. **B 257** (1991) 254;
- [11] G. Fäldt and C. Wilkin, Phys. Scripta **64** (2001) 427.
- [12] A. Moalem et al., Nucl. Phys. **A 600** (1996) 445.
- [13] T. Vetter et al., Phys. Lett. **B 263** (1991) 153.
- [14] K. Nakayama et al., Phys. Rev. **C 65** (2002) 045210.
- [15] B. L. Alvaredo et al., Phys. Lett. **B 324** (1994) 125.
- [16] M. Batinic et al., Phys. Scripta **56** (1997) 321.
- [17] H. Calén et al., Phys. Rev. **C 58** (1998) 2667.
- [18] R. Czyżykiewicz, Ph.D. Dissertation, Jagellonian University (2006) submitted.
- [19] R. Czyżykiewicz et al., e-print Archive: hep-ex/0611015.
- [20] F. Balestra et al., Phys. Rev. **C 69** (2004) 064003.

¹ Institute of Physics, Jagellonian University, Poland

The high statistics data from the $pp \rightarrow pp\eta$ reaction measured by the COSY-11 collaboration [1] are now being evaluated using the correlation femtoscopy technique [2]. Our aim is to determine the proton-proton correlation function for the $pp \rightarrow pp\eta$ reaction free of the physical multi-pion background and corrected for the limited acceptance of the detection system. We think that the shape of this function will allow us to learn about the size of the interaction region from which protons are emitted. However, it is still a subject of discussions whether this information can be derived from the correlation function in case of the meson productions in the collisions of protons.

The two-proton correlation function $R(q)$ depends on the relative momentum between protons and can be defined [3] as a ratio of the reaction yield $Y_{pp\eta}(q)$ to the uncorrelated yield $Y^*(q)$:

$$R(q) + 1 = C^* \frac{Y_{pp\eta}(q)}{Y^*(q)}, \quad (1)$$

where $Y^*(q)$ can be calculated using the event mixing technique [4], and C^* denotes an appropriate normalization constant.

In the discussed $pp \rightarrow pp\eta$ experiment, only four-momenta of two protons were measured and the unobserved meson was identified via the missing mass technique [1]. Therefore, it is impossible to decide whether a given event corresponds to the η meson production or whether it is due to the multi-pion creation. In the reference [5] we have described a method which allows to separate contributions to the correlation function originating from the η meson and multi-pion production. In this report we would like to give an account on a next step of the analysis which was the correction for the acceptance and efficiency of the detector system.

First, we calculated the acceptance and efficiency of the COSY-11 system for the registration and reconstruction of the $pp \rightarrow pp\eta$ reaction as a function of the relative momentum of the outgoing protons. The result of the simulations is presented in the figure 1(left). We divided the relative

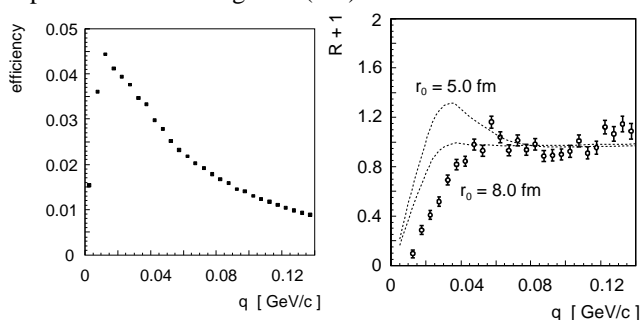


Fig. 1: **Left panel:** Overall detection efficiency (acceptance and efficiency) of the COSY-11 detection setup for the measurement of the $pp \rightarrow pp\eta$ reaction at the excess energy of $Q = 15.5$ MeV.

Right panel: The comparison of the acceptance corrected two-proton experimental correlation function for the $pp \rightarrow pp\eta$ reaction, represented by the open circles and theoretical calculations indicated as the two dashed lines for the reaction volume parametrized by the Gaussian distributions with $r_0 = 5.0$ fm and $r_0 = 8.0$ fm, respectively.

momentum range into bins with a width of 5 MeV/c. The

width of the bin was chosen to be in the order of the accuracy of the determination of the relative proton momentum ($\sigma(q) \approx 6$ MeV/c). Knowing the acceptance it would be straightforward to correct a nominator of equation 1(left), however the correction of the uncorrelated yield $Y^*(q)$ is not trivial since momenta of protons in the uncorrelated event originates from two independent real events which in general could correspond to different values of the detection efficiency.

Therefore, in order to derive a correlation function corrected for the acceptance we have created a sample of data as it would be measured with an ideal detector. For this aim we multiplied each reconstructed event so many times as it results from the known acceptance. This means that a given reconstructed $pp \rightarrow pp\eta$ event with a proton-proton relative momentum of q was added to the sample $1/A(q)$ times.

Based on this corrected data sample we calculated the two-proton correlation function according to the formula 1(left). In order to avoid mixing between the same events, a 'mixing step' in calculations was set to a value bigger than the inverse of the lowest acceptance value. The random repetition of the identical combinations was also omitted by increasing correspondingly a 'mixing step'. In particular, a k^{th} real event, from the acceptance corrected data sample, was "mixed" with a $(k+n)^{\text{th}}$ event, where $n > \max(1/A(q))$. If the $(k+1)^{\text{th}}$ event was the same as k^{th} , then this was mixed with a $(k+1+2n)$ event, etc. The two-proton background free correlation function corrected for the acceptance is presented in the figure 1(right).

The results are compared to the calculations, performed assuming a simultaneous emission of two protons and the η meson. The effective spatial shape of the reaction volume is approximated by a Gaussian distribution. A rough comparison between theoretical correlation and the experimental points indicates that the effective size of the emission source turns out to be large. However, as we stated at the beginning an interpretation of the results still remains a subject of discussions.

From figure 1(right) it is evident, that the calculated and experimental shapes differ at q lower than 0.05 GeV/c. This may be due to the neglect of the experimental resolution in the theoretical calculations or due to the approximations made in the estimation of the interactions of protons in the $pp\eta$ system. Therefore, as a next step of the analysis we plan to improve the theoretical calculations of the correlation function by taking into account the experimental resolution as well as the experimentally determined interaction between protons in the $pp\eta$ system [1].

References:

- [1] P. Moskal et al., Phys. Rev. **C 69**, 025203 (2004)
- [2] R. Lednický, Nukleonika **49** (Sup. 2), S3 (2004)
- [3] D. H. Boal et al., Rev. Mod. Phys. **62**, 553 (1990)
- [4] G. I. Kopylov, M. I. Podgoretsky, Sov. J. Nucl. Phys. **15**, 219 (1972)
- [5] P. Klaja et al., Acta Phys. Slovaca **56**, 251 (2006)

^a Institute of Physics, Jagellonian University, Poland

Measurement of the $dp \rightarrow {}^3\text{He}\eta$ reaction close to threshold

J. Smyrski* for the COSY-11 collaboration

Study of the $dp \rightarrow {}^3\text{He}\eta$ reaction is of high interest due to a very strong effect of the final state interaction which was observed in the near-threshold data measured at the SPES-4 [1] and the SPES-2 spectrometer [2]. This effect can be interpreted as a possible manifestation of the ${}^3\text{He} - \eta$ bound state [3]. The measured cross sections do not allow, however, for a reliable determination of the ${}^3\text{He} - \eta$ low energy scattering parameters due to inconsistencies between the data sets, and due to possible contributions from higher partial waves [4]. In order to resolve these inconsistencies and to check the possible onset of higher angular momenta, we performed high precision measurements of the total and differential cross sections of the $dp \rightarrow {}^3\text{He}\eta$ reaction.

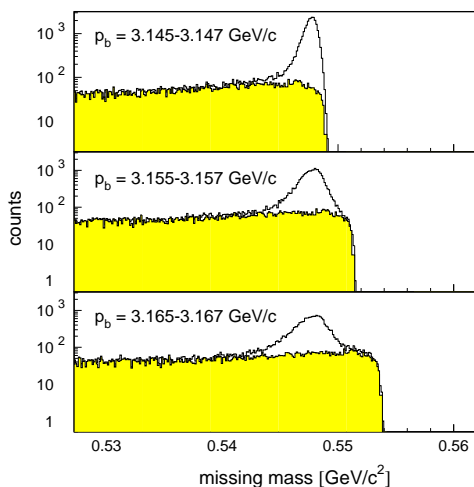


Fig. 1: Missing mass spectra for three different beam momentum intervals above the η production threshold.

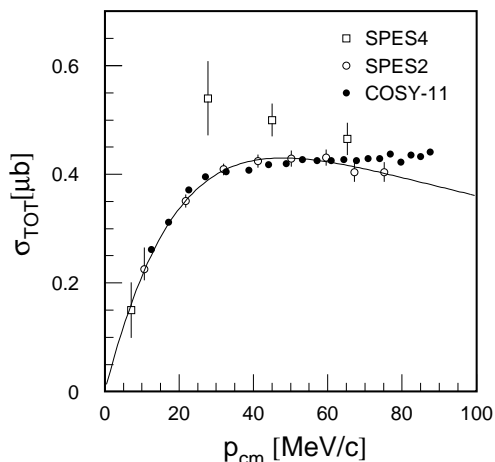


Fig. 2: Total cross section for the $dp \rightarrow {}^3\text{He}\eta$ reaction as a function of the ${}^3\text{He}$ c.m. momentum. The solid line represents the scattering length fit to the SPES-2 data.

The experiment was conducted with the internal deuteron beam of COSY scattered on a proton target of the cluster jet type and with the COSY-11 facility detecting the charged reaction products. For reduction of various possible systematical uncertainties, the measurements were performed during a slow acceleration of the beam with the nominal beam momentum continuously varied from 3.099 GeV/c to 3.179 GeV/c, crossing the threshold for the $dp \rightarrow {}^3\text{He}\eta$ reaction at 3.141 GeV/c. Identification of the ${}^3\text{He}$ ejectiles was based on the energy loss in scintillation counters and, independently, on the time-of-flight measured on a path of 9 m between two scintillation hodoscopes. The η mesons were identified via the missing mass technique (see Fig. 1). The luminosity was monitored using coincident measure-

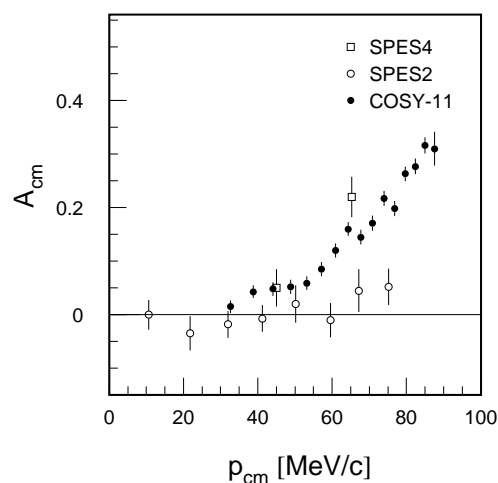


Fig. 3: Forward-backward asymmetries of angular distributions of ${}^3\text{He}$ in c.m. system.

ment of the elastic $d - p$ scattering and, independently, of the $p - p$ quasi-free scattering. The preliminary results on the total cross section dependence from the ${}^3\text{He}$ center-of-mass (c.m.) momentum are shown in Fig. 2. They are consistent with the SPES-2 results, however, at higher momenta, they deviate from the scattering length fit to the SPES-2 data [2]. The forward-backward asymmetries of the differential cross sections in the c.m. system are shown in Fig. 3. They deviate clearly from zero for c.m. momenta above about 40 MeV/c. This effect indicates a presence of higher partial waves in the final state and it can result from the S- and P-wave interference.

References:

- [1] J. Berger et al., Phys. Rev. Lett. **61**, 919 (1988).
- [2] B. Mayer et al., Phys. Rev. **C 53**, 2068 (1996).
- [3] C. Wilkin, Phys. Rev. **C 47**, R938 (1993)
- [4] A. Sibirtsev et al., Eur. Phys. J. **A 22**, 495 (2004).

* Institute of Physics, Jagiellonian University, 30-059 Cracow, Poland

Recently the $d - \eta$ and ${}^3\text{He} - \eta$ interaction was intensively studied on the theoretical ground. This interaction is of special interest due to the possible existence of the η -nucleus bound states. From the experimental point of view, the η meson production near threshold in the three nucleon system is much less explored as compared to the two nucleon system. The database for the $pd \rightarrow {}^3\text{He}\eta$ reaction [1, 2, 3, 4, 5] has improved recently, however, for the reaction $pd \rightarrow dp\eta$ close to threshold there exist only data measured with the SPESIII spectrometer at SATURNE [6] for excess energies of $Q = 1.1$ and 3.3 MeV and by the PROMICE/WASA collaboration [7, 8] at higher energies for $Q \geq 14$ MeV. Unfortunately, the uncertainty of the excess energy of $\Delta Q = \pm 0.6$ MeV [6] of the SPESIII data points is very large when taking into account the rapid rise of the cross section near the threshold.

The aim of the present experiment was determination of the $dp \rightarrow dp\eta$ cross sections near threshold in order to study the interaction between the particles in the final state. The energy dependence of the total cross section is expected to be very sensitive to the $d - \eta$ interaction. The measurement was performed for three deuteron beam momenta above the $dp \rightarrow dp\eta$ threshold namely: 3177.4, 3189.4 and 3202.4 MeV/c and one momentum below the threshold equal to 3163.4 MeV/c. The measurement below the threshold was used for the background subtraction under the eta peak in the missing mass spectra. Application of the stochastic cooling to the COSY deuteron beam guarantees a high quality of the beam with the momentum smearing on the level of $\Delta p/p \approx 10^{-4}$. However, the absolute beam momentum determined on the basis of the accelerator frequency is known with an accuracy of $\Delta p/p \approx 10^{-3}$ only. Therefore, for a more precise beam momentum determination, which is crucial in the present near threshold measurements, we used the distribution of the center of mass momenta of the ${}^3\text{He}$ ions from the $dp \rightarrow {}^3\text{He}\eta$ reaction. The resulting correction to the nominal beam momentum was equal to -1.6 ± 0.4 MeV/c corresponding to an uncertainty of the excess energy for the $dp \rightarrow dp\eta$ reaction of ± 0.1 MeV.

Protons from the $dp \rightarrow dp\eta$ reaction were identified using the Time Of Flight (TOF) measurement on the path of 9.3 m between the scintillator hodoscope S1 and S3. Fig. 1 shows the TOF dependence on the magnetic rigidity with clearly separated protons, deuterons and ${}^3\text{He}$. Due to the setting of the triggering electronics, only the tail of the pion TOF distribution was registered as can be seen in the figure. Deuterons originating from the $dp \rightarrow dp\eta$ reaction have been measured using a drift chamber with hexagonal cells (D4 [9]). Dependence of the TOF on the magnetic rigidity for particles registered with the D4 drift chamber is shown in the right panel of Fig. 1. After the reconstruction of the protons and deuterons four-momentum vectors the η mesons have been identified via the missing mass technique. Corresponding spectra are shown in the left panel of Fig. 2. The determined $dp \rightarrow dp\eta$ total cross sections are shown in Fig. 2 together with the data measured at SATURNE and at WASA. The data confirm a strong effect of the interaction in the $dp\eta$ meson final state. The enhancement of the near-threshold cross sections with respect to the phase-space behavior indicates a strong interaction between the final state particles. We expect that further

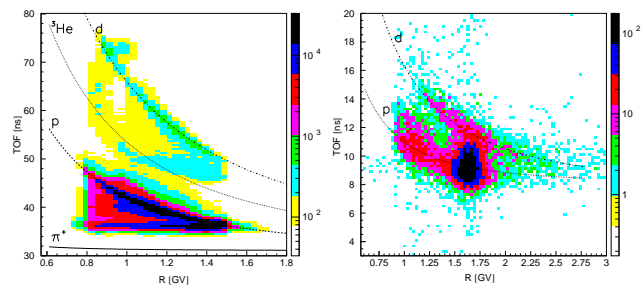


Fig. 1: TOF versus magnetic rigidity for particles registered in the drift chambers D1, D2 (left panel) and for particles detected in the D4 chamber (right panel).

analysis of the collected experimental data will allow to reduce substantially the relatively large statistical uncertainties of the preliminary data points reported here.

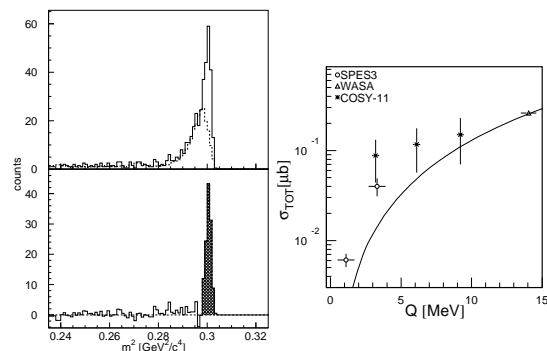


Fig. 2: Left panel: The missing mass spectrum for the $dp \rightarrow dp\eta$ reaction at a beam momentum of 3189.4 MeV/c. In the upper figure the background is marked by the dashed line. The lower figure shows the missing mass distribution obtained after the subtraction of the background. On the right panel the dependence of total cross section on the excess energy is shown. The line indicates three body phase-space normalized to the PROMICE/WASA data point [8]. Open circles show data from reference[6], and stars denote preliminary results determined by the COSY-11 group.

References:

- [1] B. Mayer et al., Phys. Rev. C **53**, 2068 (1996).
- [2] M. Betigeri et al., Phys. Lett. B **472** 267 (2000).
- [3] R. Bilger et al., Phys. Rev. C **65** 44608 (2002).
- [4] H.-H. Adam et al., Int. J. of Mod. Phys. **A20** 643 (2004).
- [5] J. Smyrski et al., Acta Phys. Slovaca **56** 213 (2006).
- [6] F. Hibou et al., Eur. Phys. J. **A7** 537 (2000).
- [7] J. Złomańczuk et al., Physica Scripta **T104** 84 (2003).
- [8] R. Bilger et al., Phys. Rev. C **69** 014003 (2004).
- [9] J. Smyrski et al., Nucl. Instr. & Meth. **A541** 574 (2005).

* Institute of Physics, Jagiellonian University, 30-059 Cracow, Poland

The physics of the η' meson receives an increasing interest in view of the forthcoming measurements planned e.g. at the COSY, DAΦNE-2 and MAMI-C facilities where the η' will be produced in hadron-hadron, e^+e^- , and γ -hadron reactions, respectively. Therefore, the precise determination of the natural width of the η' meson ($\Gamma_{\eta'}$) will have an impact on the physics results which will be derived from future measurements of detector setups like: WASA-at-COSY [1] and KLOE [2].

Among previous experiments the one performed by the NIMROD collaboration extracted the width of the η' meson with the smallest error: $\Gamma_{\eta'} = 0.28 \pm 0.1 \text{ MeV}/c^2$ [3]. Based on many years of experience gained with the COSY-11 apparatus and thorough simulations we have established that at the COSY-11 facility, combined with the excellent features of the COSY proton beam, the natural width of η' can be determined with at least five times better precision. This will be due to an about three times better experimental resolution, larger statistics, larger signal to background ratio, and finally due to a simultaneous use of two independent methods for the derivation of the width of the η' meson. The $\Gamma_{\eta'}$ will be derived directly from the missing mass distribution of the $pp \rightarrow ppX$ reaction and also from the shape of the excitation function.

In May 2006 the COSY Programme Advisory Committee has recommended the realisation of a corresponding proposal [5] and the measurement of the $pp \rightarrow pp\eta'$ reaction was conducted by the COSY-11 collaboration in October 2006. In the experiment five discrete values of beam momentum were used: 3211, 3213, 3214, 3218 and 3224 MeV/c, where the threshold beam momentum is equal to 3208.3 MeV/c. In order to improve the experimental resolution of the four-momentum determination of the registered particles and in order to decrease the spread of the momentum of the beam protons reacting with the target two major changes have been applied to the COSY-11 setup. Namely, the spatial resolution of the measurement of the particle track coordinates in the drift chambers was improved by increasing the supply voltage up to the maximum allowed value and also the dimensions of the target in the direction perpendicular to the COSY beam was decreased from 9 to ≈ 1 mm (rectangular 9×1 mm instead of circular target).

In order to control the systematical uncertainties each of the crucial parameters (like target dimensions or beam momentum spread) were monitored by at least two independent methods [5].

The received mean luminosity equals to $1.4 \cdot 10^{30} \text{ s}^{-1} \text{ cm}^{-2}$ resulting in an integrated luminosity of 1.3 pb^{-1} . This is smaller than the expected 3.6 pb^{-1} used for the estimations in the proposal [5] because of a reduction in the beam time (almost 5 days breakdown in COSY operation) and because of a 30% smaller luminosity.

An online analysis has revealed a signal originating from the production of the η' meson at each of the investigated beam momenta (see Fig. 1). The obtained width of the η' peak in the missing mass spectra (FWHM) equals to approximately $0.5 \text{ MeV}/c^2$. Thus, already online spectra show that the achieved mass resolution is at least three times better than reached at the best of the previous measurements. Although

such a resolution is already comparable with the expected value of the width of the η' meson, it is still broader than expected but we are confident to improve it in the off-line analysis.

Probably, the broadening was due to changes of the beam optics which caused variations of the beam momentum value at the interaction region on the 10^{-4} level. In order to enable an off-line correction of these variations we have monitored various parameters which could influence the beam conditions like current in the COSY dipoles, temperature of the cooling water of the magnets, air temperature, humidity and barometric pressure inside COSY tunnel. Independently it will be possible to correct the variation of the beam momentum based on the distribution of the elastically scattered protons measured simultaneously with the $pp \rightarrow pp\eta'$ reaction.

The off-line analysis of the data is in progress.

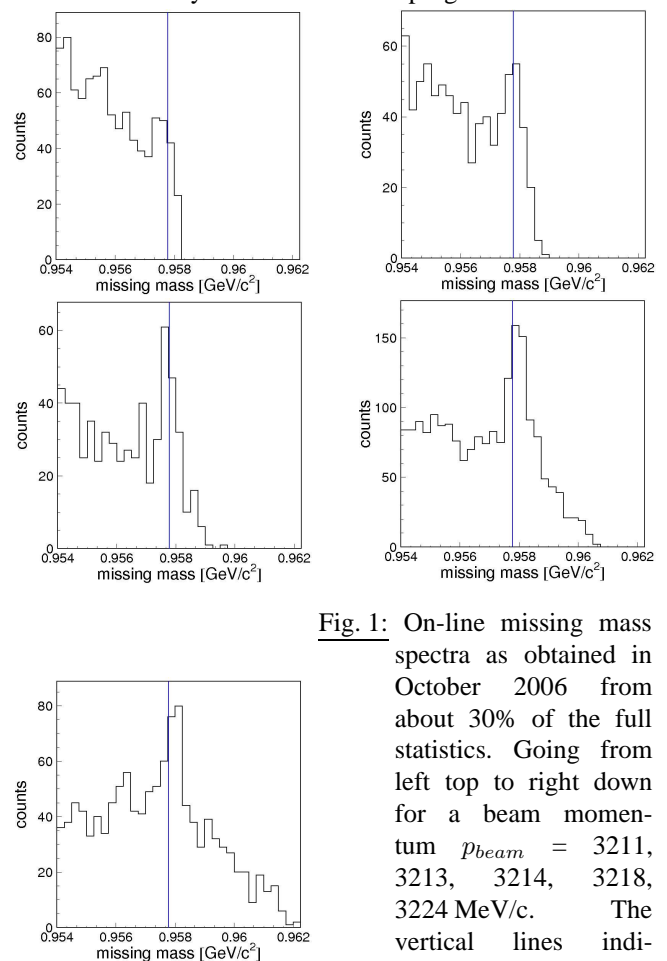


Fig. 1: On-line missing mass spectra as obtained in October 2006 from about 30% of the full statistics. Going from left top to right down for a beam momentum $p_{beam} = 3211, 3213, 3214, 3218, 3224 \text{ MeV}/c$. The vertical lines indicate the value of the mass of the η' meson ($m_{\eta'} = 957.78 \text{ MeV}/c^2$)

References:

- [1] H.-H. Adam, *et. al.* e-Print Archive **nucl-ex/0411038**.
- [2] F. Ambrosino *et. al.*, e-Print Archive **hep-ex/0603056**.
- [3] D. M. Binnie *et. al.*, Phys. Lett. **B83** 141 (1979).
- [4] E. Czerwiński, D. Grzonka, P. Moskal, A. Täschner, IKP Annual Report 2006;
- [5] E. Czerwiński, D. Grzonka, P. Moskal, COSY Proposal **No. 162** (2006) available at: <http://www.fz-juelich.de/ikp/publications/PAC31/proposaletaprimewidth.pdf>

* Jagiellonian University, Cracow, Poland

The COSY-11 collaboration has taken data during three weeks measurement of the $pp \rightarrow pp\eta'$ reaction in September 2003. That experiment has been performed at $Q = 15.5$ MeV, the same excess energy at which the differential distributions of the invariant masses for two-particles subsystems for the $pp \rightarrow pp\eta$ reaction had been established [1]. The determination of analogous distributions for the $pp\eta'$ system could bring to light the still unknown interaction between the η' meson and the proton. It could also be helpful in disentangling ambiguities in the interpretation of the distribution of the two-particle invariant masses in the low energy $pp\eta$ system.

The experiment performed using the COSY-11 detection setup, was based on the registration of two outgoing positively charged ejectiles. Then, we selected only these events with two reconstructed tracks, which corresponded to the $pp \rightarrow ppX$ reaction. In further analysis, the mass of the unobserved meson have been identified using the missing mass technique. The missing mass resolution depends on the accuracy of the momentum determination which in the case of the reconstruction technique used by the COSY-11 group relies on the knowledge of the position of the center of the interaction region. Therefore, the possible changes of the position at which the proton beam crosses the target could have significantly influence the momentum reconstruction and in consequence could worsen the determination of the mass of an undetected particle.

The center of the beam and target overlap can be determined from the distribution of the momentum of the elastically scattered protons. Hence, we applied an analysis of proton-proton elastic scattering for controlling the conditions of the beam-target interaction region. The distribution of the perpendicular versus parallel (to the beam direction) momentum components of the elastically scattered protons is presented in the figure 1. The mean value of the distance between the

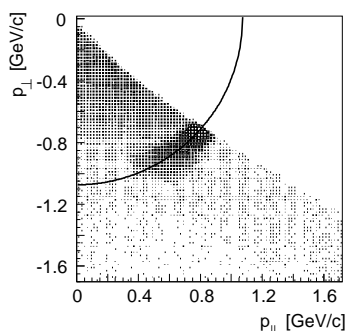


Fig. 1: The distribution of perpendicular p_{\perp} versus parallel p_{\parallel} momentum component for the $pp \rightarrow pp$ elastic scattering determined at the beam momentum of 3.257 GeV/c. The solid line corresponds to kinematical ellipse.

kinematical ellipse and the experimental points may be used as a measure of the deviation of the center of the interaction region from its nominal position assumed in the analysis [2]. Figure 2(left) presents a relation between the mean distance from the kinematical ellipse and the position of the center of the reactions. In the figure the center of the reaction points (beamshift) was expressed with respect to its nominal value. As can be seen in this figure the real position differs by about 0.4 cm from the nominal one.

In order to study possible variations of the position of the center of the reaction points during the experiment we have divided the whole sample of data into groups corresponding to 13 hours of measurement and calculated the mean distance from the ellipse for each group separately. Right panel of figure 2 shows the obtained result which indicates that the beam and target conditions were stable during the course of the experiment. Fluctuations seen in figure 2(right) originates from the statistical errors of the determination of the mean value of the distance to the ellipse. The variations are at the level of 10^{-3} , and as can be inferred from figure 2(left), they correspond to shifts of the center of the interactions by less than 0.01 mm.

The duration of a one measurement cycle was 10 minutes and so the energy losses and straggling of the beam circulating through the target could lead to the changes of the beam orbit. Therefore, we have also checked the behaviour of the beam-target overlap during the COSY cycle. To this end we have grouped the data according to the time counted from the beginning of the cycle. In this case variations of the mean distance to the kinematical ellipse were also found to be negligible. In the figure 3 we present the preliminary miss-

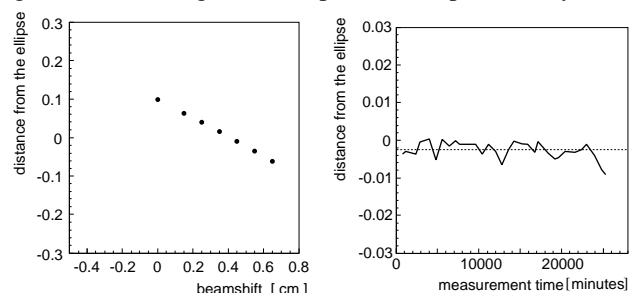


Fig. 2: **Left panel:** The distance between the expected ellipse and the center of the experimental distribution on the $(p_{\perp}, p_{\parallel})$ plot versus a beamshift parameter. **Right panel:** The deviation of the distance from the kinematical ellipse as a function of the time of measurement. The mean value of the distance from ellipse has been plotted for each 13 hours intervals.

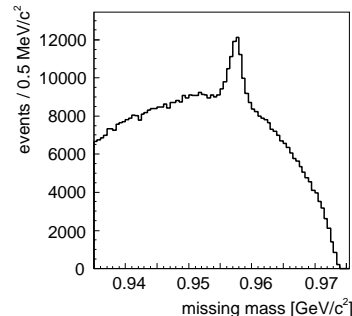


Fig. 3: Experimental missing mass spectrum for the $pp \rightarrow ppX$ reaction determined at the beam momentum of 3.257 GeV/c. In the figure a clear signal with about 15000 events corresponding to the $pp \rightarrow pp\eta'$ reaction is visible.

References:

- [1] P. Moskal et al., Phys. Rev. **C 69**, 025203 (2004)
- [2] P. Moskal, e-Print Archive: hep-ph/0408162

^a Institute of Physics, Jagellonian University, Poland

In August 2004 –for the first time– using the COSY-11 [1] facility we have conducted a measurement of the η' meson production in the proton-neutron collision [2]. The aim of the experiment is the determination of the total cross section of the $pn \rightarrow pn\eta'$ reaction near the kinematical threshold. The comparison of the $pp \rightarrow pp\eta'$ and $pn \rightarrow pn\eta'$ total cross sections will allow to learn about the production of the η' meson in different isospin channels and to investigate aspects of the gluonium component of this meson.

The experimental precision of the missing mass determination of the $pn \rightarrow pn\eta'$ reaction rely on the accuracy of the reconstruction of the momentum of protons and neutrons. For each proton, which gave a signal in the drift chamber, the momentum vector can be determined. First the trajectories of the particles are reconstructed, and then knowing the magnetic field of the dipole, the momentum vector is derived. In this report we give an account on the time-space calibration of drift chambers and timing calibration of the neutral particle detector.

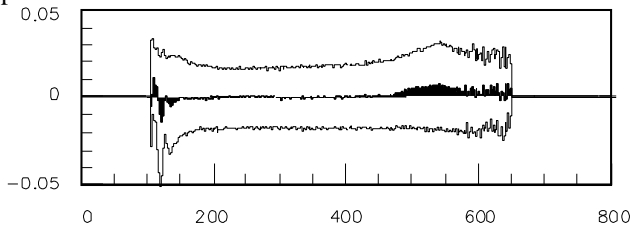


Fig. 1: Example of the spectrum used for the drift chamber calibration. Shaded area presents mean values of ΔX (in cm) as a function of the drift time (in ns). Upper and lower histograms indicate a band of one standard deviation of the ΔX distribution.

Due to changes of the pressure, temperature and humidity of the air inside the COSY tunnel, the drift chamber calibration has to be performed for time frames not longer than few hours. The calibration is derived in an iterative way. First, distances of the particle's trajectory to the wires are derived from the working calibration, and to the obtained points a straight line is fitted. Next, the deviation ΔX between the fitted and measured distances of the particle's trajectory to the wire is calculated. An example of a mean value of ΔX as a function of the drift time is shown in the Fig.1. Afterwards the relation between the drift time and distance from the wire is corrected by the determined mean value of ΔX . The procedure is repeated until corrections become negligible.

The neutral particle detector delivers information about the time at which the registered neutron or gamma quanta induced correspondingly a hadronic or electromagnetic reaction.

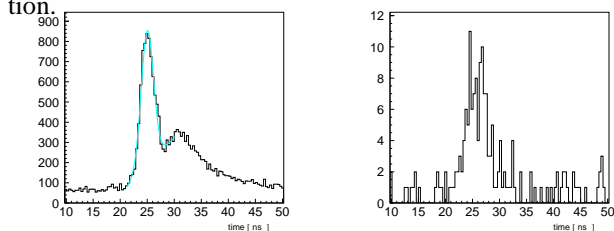


Fig. 2: Time-of-flight determined between the target and the neutron detector. Details are described in the text.

This information together with the time of the reaction allows

to calculate the time-of-flight between the target and the neutron detector and to determine the absolute momentum of registered particles, provided that it could have been identified. The time calibration of the neutron detector proceeds in two steps. First the relative timing between modules of the neutron detector are established from experimental distributions of time differences between neighbouring modules. In the next step a general time offset of the neutron counter with respect to another (S1) detector has to be established. For this purpose the $pd \rightarrow pd\pi^0\pi^0$ reaction is used. The meson π^0 decays in the target into two gamma quanta. Thus, the calibration is based on the measurement of the proton, deuteron in drift chambers and scintillators (S1 and S3), and gamma quanta in the neutral particle detector. Knowing the distance between the target and a module in the neutral particle detector which gave the signal as a first one, one can adjust the general time offset between this detector and the S1 counter. The time of the reaction in the target can be calculated from the times when proton and deuteron crossed the S1 scintillator and from their reconstructed momenta and trajectories. Figure 2(left) presents the time-of-flight distribution –for neutral particles– measured between the target and the neutral particle detector. The spectrum was obtained under the condition that in coincidence with a signal in the neutral particle detector two charged particles were registered in the drift chambers. A clear signal originating from the gamma rays is seen over a broad enhancement from neutrons. This histogram shows that discrimination between signals originating from neutrons and gamma quanta can be done by a cut on the time of flight. An analogous spectrum with an additional requirement that the registered charged particles correspond to proton and deuteron ($pd \rightarrow pdX$) is shown in the right panel of figure 2. As expected, in this spectrum only a signal from the gamma quanta is seen.

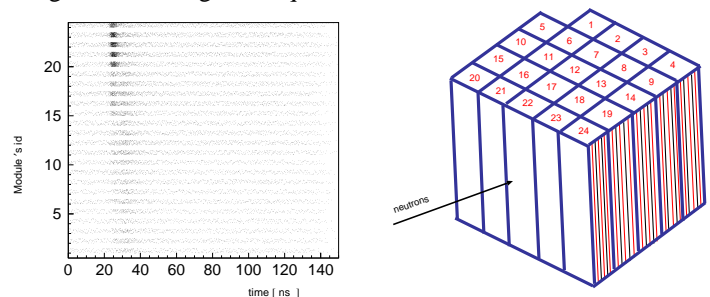


Fig. 3: (left) Time-of-flight determined between the target and the neutral particle detector as a function of module's number. (right) Configuration of the detection units

Figure 3 shows, as expected from the known absorption coefficients [3], that the gamma quanta are predominantly registered in the first row of the detector whereas interactions points of neutrons are distributed more homogeneously. As a next step in the analysis of the $pn \rightarrow pn\eta'$ reaction a calibration of the spectator detector will be conducted.

References:

- [1] S. Brauksiepe et al., Nucl. Inst. & Meth. **A 376** 396 (1996).
- [2] P. Moskal et al., COSY Proposal **No. 133** (2003).
- [3] K. Hagiwara et al., Phys. Rev. **D 66** 010001 (2002).

Measurement of the $pn \rightarrow d\eta'$ reaction at COSY-11.

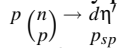
B. Rejdych¹, J. Przerwa¹, P. Moskal¹ for the COSY-11 collaboration

One of the main interest of the COSY-11 collaboration are investigations of the η' meson production in nucleon-nucleon collisions which aim at the explanation of the reaction mechanism and unknown interaction between the η' meson and the proton.

In the previous experiments we have determined the close-to-threshold excitation function for the $pp \rightarrow pp\eta'$ reaction, [1] but it was not possible to judge about mechanism responsible for the η' meson production from this reaction channel only. Therefore, we investigated the η' meson production in proton-neutron scattering conducting in August 2004 measurement of the $pn \rightarrow pn\eta'$ reaction [2]. At present the analysis of the data and simulations are in progress [3].

In February 2006 we have extended our study of the production of the η' meson in the NN collisions to a pure isospin zero state of the interacting nucleons. We have measured the excitation function of the $pn \rightarrow d\eta'$ reaction [4] using deuteron target and proton beam with a momentum of 3.365 GeV/c. The identification of the $pn \rightarrow d\eta'$ reaction is based on the measurement of the four-momentum vectors of the outgoing deuteron and the spectator proton p_{sp} . The meson η' is identified via the missing mass technique.

The reaction may be symbolically presented as:



where p_{sp} denotes the proton from the deuteron regarded as a spectator which does not interact with the bombarding particle, carrying the Fermi momentum possessed at the moment of the collision.

Such measurement was possible at the COSY-11 facility using the spectator detector and the deuteron chamber (denoted as Si_{spec} and $D4$ in fig.1), which were installed formerly to study the $pd \rightarrow pd\eta$ [5] and $pn \rightarrow pn\eta'$ [3] reactions.

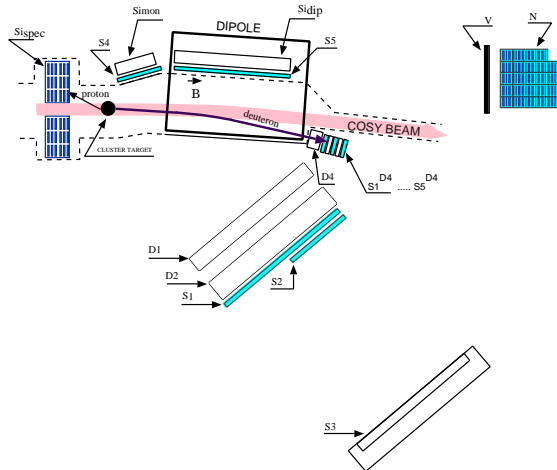


Fig. 1: Schematic view of COSY-11 detection setup. D1, D2, and D4 denote the drift chambers; S1, S2, S3, S4, S5, $S1^{D4}$... $S5^{D4}$ and V stand for the scintillation detectors; N is the neutron detector and Si_{mon} , Si_{spec} and Si_{dip} are silicon strip detectors to detect elastically scattered protons, spectator protons and negatively charged particles, respectively.

In order to reduce the trigger counting rate, which based on the registration of one particle would be a factor of 200 too large to be accepted by our data acquisition system, we installed five scintillation detectors (shown in fig.1 as $S1^{D4}$... $S5^{D4}$).

In the off-line analysis the energy loss in these five detectors will be used for the separation of deuterons from protons and pions. The momentum of deuterons will be established by the reconstruction of their trajectory in the magnetic field of the COSY dipole. The determination will be based on the known reaction point and reconstruction of the deuteron track from signals registered by the D4 drift chambers. In the case of the spectator protons two layers of the spectator detector permit to measure the kinetic energy of proton from 0,5 to 9 MeV and to distinguish them from the fast particles which cross both detection layers whereas slow protons are stopped in the first layer.

The luminosity will be established from the number of the quasi-free proton-proton elastic scattering events measured simultaneously with the main investigated reaction. During the on-line analysis the integrated luminosity was roughly established to be $500nb^{-1}$. Assuming that the ratio of the cross section $pn \rightarrow d\eta'$ and $pp \rightarrow pp\eta'$ will be on the same order as already established ratio [6] for the $pn \rightarrow d\eta$ and $pp \rightarrow pp\eta$ reactions we expect to identify about 1000 $pn \rightarrow d\eta'$ events in the whole data sample. Presently the off-line analysis is in progress.

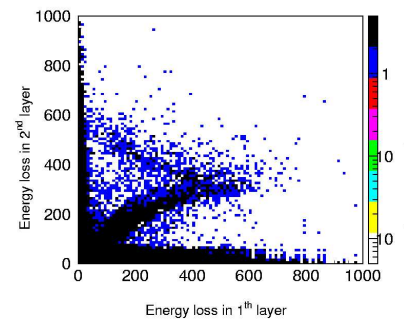


Fig. 2: Energy losses in the first layer versus the second layer as measured at COSY-11 with a deuteron target and a proton beam with momentum of 3.365 GeV/c.

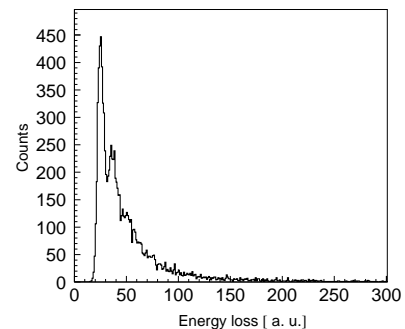


Fig. 3: An on-line spectrum of the energy loss as measured using scintillator detector $S5^{D4}$

References:

- [1] P. Moskal e-Print Archive: hep-ph/0408162.
- [2] P. Moskal et al., COSY Proposal **No. 133** (2003).
- [3] J. Przerwa, IKP, FZ-Jülich, Ann. Rep. 2006.
- [4] P. Moskal et al., COSY Proposal **No. 155** (2005).
- [5] C. Piskor-Ignatowicz, IKP, FZ-Jülich, Ann. Rep. 2006.
- [6] H. Calen et al., Phys. Rev. **C 58**, 2667 (1998).

¹ Institute of Physics, Jagellonian University, Poland

At present little is known about the strength of the hyperon–nucleon interaction at low energies (parameterized by the scattering length) and even less about its spin dependence. Most of the data are available for the Λ -p system but also here the experimentally extracted low energy parameters of s-wave scattering, the scattering length a and the effective range r , have large uncertainties. Furthermore, a clear separation of the spin singlet and triplet channels is not possible as long as no polarized target/beam system is used. A detailed analysis of the world data set for elastic Λp scattering gave $a_s = -1.8^{+2.3}_{-4.2}$ fm and $a_t = -1.6^{+1.1}_{-0.8}$ fm [1] for the spin singlet and spin triplet scattering lengths, respectively, where the errors are strongly correlated.

The reaction $pp \rightarrow K^+ p \Lambda$ at low excess energies has been investigated by the COSY-11 collaboration [2] to determine the low energy parameters of the ΛN interaction. An average value of -2 ± 0.2 fm for the ΛN scattering length was extracted in an analysis that utilizes the effective range expansion which, however, is only applicable for systems where the scattering length is significantly larger than the effective range. In addition, using this procedure one encounters strong correlations between the effective range parameters a and r that can only be disentangled by including other data, e.g. ΛN elastic cross sections, into the analysis [2].

A new method to determine the Λp scattering lengths was proposed in Ref. [3]. It allows the extraction of the YN scattering lengths from the production data directly with a theoretical uncertainty of at most 0.3 fm.

In Ref. [3] it was also shown that already a measurement of a single spin asymmetry in $\bar{p}p \rightarrow YNK$ allows to isolate the spin triplet contribution from the final YN state, since the Pauli Principle strongly limits the number of structures possible for the initial state. It was especially shown that the asymmetry :

$$\frac{d^2\sigma(\uparrow)}{dm'^2 dt} - \frac{d^2\sigma(\downarrow)}{dm'^2 dt}$$

gets contributions from the spin triplet final state only, as long as the kaon in the final state is emitted at 90° in the center of mass system (cms) and the outgoing YN is in an S -wave.

In order to extract the spin triplet scattering length of the $p\Lambda$ system, the $\bar{p}p \rightarrow K^+ p \Lambda$ reaction was studied with the COSY-11 installation at a beam momentum of 2.457 GeV/c, corresponding to an excess energy of 40 MeV. The acceptance of the COSY-11 detection system covers the full azimuthal angular range of the kaon emission angle with a rather flat distribution around 90° (cms) which is the relevant region for this investigation.

A proton beam polarisation of about 80 % was achieved which was checked by measurements with the EDDA detector and monitored with the COSY-11 polarimeter system. The spin direction was flipped after each 20 minutes measurement cycle to reduce systematic uncertainties.

The reaction channel $\bar{p}p \rightarrow K^+ p \Lambda$ can be well separated with the standard missing mass technique used at COSY-11. The four momenta of two charged particles were measured by momentum reconstruction using the drift chamber tracks and the missing mass was calculated. In fig.1 a distribution of the invariant mass of one charged particle versus the missing

mass is given. The data sample results from cuts on the invariant mass of the first charged particle to be a proton and a cut on the emission angle of the second charged particle to be within $-0.2 < \cos \Theta_{cm} < 0.2$. A clear enhancement in the expected region indicated by the cross point of the lines for the K^+ and Λ masses is seen.

The data are presently under evaluation.

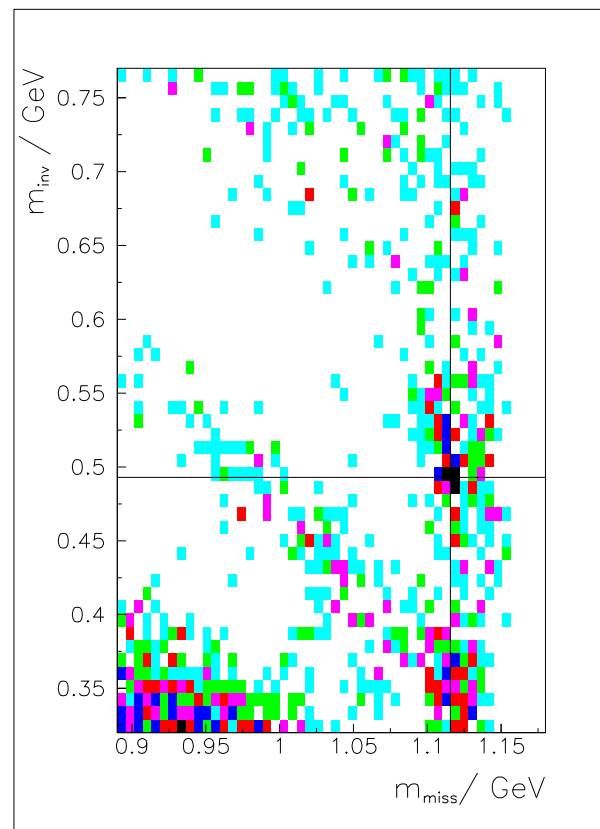


Fig. 1: Invariant mass of a charged particle measured with COSY-11 versus calculated missing mass. The lines indicate the K^+ and Λ masses.

References:

- [1] G. Alexander et al., Phys. Rev. 173 (1968) 1452.
- [2] J. T. Balewski *et al.*, Eur. Phys. J. A 2, (1998) 99.
- [3] A. Gasparyan et al., Phys. Rev. C 69 (2004) 034006.

In October 2006 COSY-11 took data in order to determine the width of the η' meson[1]. For this high precision measurement of the reaction $pp \rightarrow pp\eta'$ the installed cluster-jet target had to be modified in order to reduce the size of the cluster jet down to around 1 mm perpendicular to the direction of the COSY beam without changing the target thickness.

In figure 1 the principle of operation of a Münster type cluster jet target is shown. Purified hydrogen gas is cooled down to temperatures of around 25 K at a pressure of around 20 bar. This supersaturated gas passes a narrow laval nozzle with minimum diameter of $16 \mu\text{m}$ and expands into vacuum. At this point a small percentage of the gas molecules start to condensate and form nanoparticles called clusters.

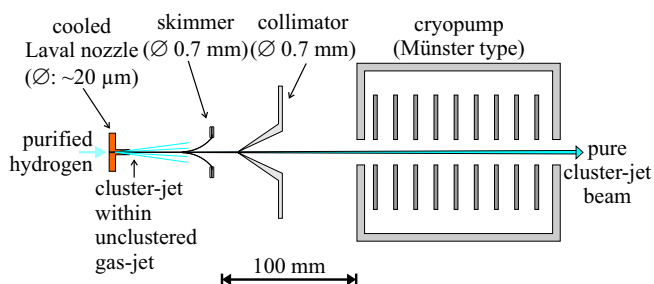


Fig. 1: Production of cluster-jets in Münster type cluster-jet targets.

In order to separate the gas from the cluster-jet beam an conical shaped aperture called skimmer is used. The size and shape of the cluster-jet beam is afterwards defined by a second skimmer called collimator. In the case of the COSY-11 experiment skimmer and collimator have a round hole with a diameter of 0.7 mm. Behind the collimator the differential pumping scheme is completed with a Münster type cryopump which connects the vacuum chambers of the cluster source with the scattering chamber of COSY.

Behind the collimator the cluster-jet beam expands undisturbed by pure geometry resulting in a conical shaped cluster-jet beam with a round cross section. At the interaction point between the COSY beam and the cluster-jet beam the cluster-jet has a diameter of around 9 mm.

Up to now the most precise measurement of the width of the η' meson was performed by the NIMROD collaboration who published a value of $\Gamma_{\eta'} = 0.28 \pm 0.10 \text{ MeV}$ [2]. The COSY-11 measurement intends to improve the precision by a factor of five leading to an uncertainty of 0.02 MeV. In order to accomplish this goal the momentum resolution of the experiment has to be improved by reducing the transversal width of the cluster jet down to around 1 mm. For this we developed a new collimator with a slit shaped opening instead of a round one. This required a new manufacturing technique since a slit of around 0.7 by 0.07 mm had to be cut into the stainless steel cone of the collimator (Fig. 2). In cooperation with the Laser Center of the Fachhochschule Münster situated in Steinfurt this collimator was fabricated using a laser cutting technique. The new collimator was tested successfully with the cluster-jet target in Münster where it was possible to measure the profile of the cluster jet. Extrapolation of the measured width

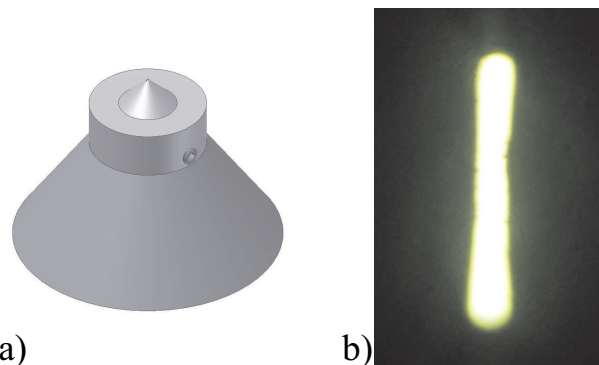


Fig. 2: a) Technical drawing of the new collimator with slit shaped opening. It consists of two parts in order to have the opportunity to adjust the alignment of the slit when mounted in COSY-11. b) Photo of the slit in the new collimator taken with a transmitted light microscope. The dimensions of the slit are around 0.7 by 0.07 mm.

down to the geometries at COSY-11 led to the expected values of around 1 mm. During the measurement at COSY-11 we used a special wire device [3] in order to measure the size of the cluster beam. The analysis of the data measured by this device is still in progress.

The first analysis of the COSY-11 data taken in this beam time indicates that the expected improvement of the momentum resolution was reached. As expected the target density was not affected by the reduction of the target size perpendicular to the COSY beam. The reduced cross section of the beam led to an improvement of the vacuum conditions at the interaction point by a factor of around 10 leading to a significant reduction of background events. The improvement of the vacuum also led to a substantial increase in the life time of the COSY beam. Normally the duration of the flat top is around 10 minutes whereas with the new collimator it was extended to 1 hour.

These working conditions are of high interest for future experiments like PANDA where the use of a cluster-jet target is discussed. An increase in beam lifetime at a constant target thickness is essential for an experiment like PANDA where an antiproton beam is used which is much more difficult to generate compared to a proton beam.

References:

- [1] E. Czerwiński, D. Grzonka, and P. Moskal, A precise measurement of the total width of the η' meson, Proposal 155, COSY-PAC 30 (2006)
- [2] D. M. Binnie et al., Phys. Lett. 83B, 141 (1979)
- [3] E. Czerwiński et al., Wire device for the measurement of the dimensions of the COSY-11 cluster-jet target, this report

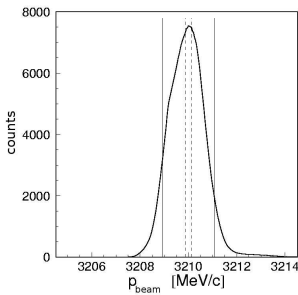
¹ Institut für Kernphysik, Universität Münster, 48149 Münster, Germany

² Institut für Kernphysik, Forschungszentrum Jülich, 52428 Jülich, Germany

* supported by Jülich FFE

In October 2006 the COSY-11 collaboration performed a direct measurement of the total width of the η' meson ($\Gamma_{\eta'}$). The value of $\Gamma_{\eta'}$ will be derived from the missing mass distribution of the $pp \rightarrow ppX$ reaction and from the shape of the excitation function of the total cross section determined near the kinematical threshold for the $pp \rightarrow pp\eta'$ process. In the experiment a proton beam of COSY and a cluster target were used. The systematical error of the extraction of $\Gamma_{\eta'}$ will depend on the accuracy of the determination the missing mass resolution. This depends predominantly on the momentum spread of the COSY beam (Fig. 1) and on the accuracy of the four-momentum determination of the registered protons. In the case of the experimental technique used by the

Fig. 1: Beam momentum distribution calculated from the Schotky frequency spectrum measured during the COSY-11 run in 2004. The dashed and solid lines show limits deduced from the target dimensions of 1 mm and 9 mm, respectively. The estimations was based on the know value of dispersion of the COSY beam at the position of the COSY-11 target.



COSY-11 collaboration, both mentioned factors, depend on the dimensions of the target. Therefore it is crucial to monitor precisely the spacial size of the target perpendicular to the COSY beam. To this end we used two independent methods. One of the techniques was based on the determination

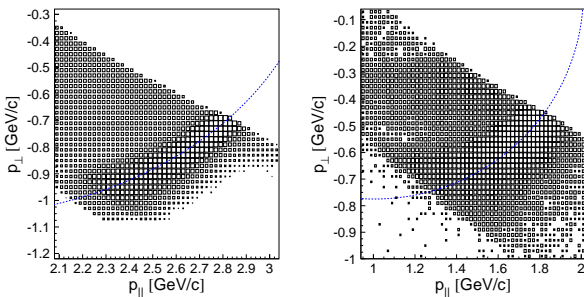


Fig. 2: Distribution of elastically scattered protons. The number of entries per bin is shown in logarithmic scale. (left) This experiment: $\approx 1\text{mm}$ target width, $p_{beam} = 3211 \text{ MeV/c}$ (right) One of the previous experiments: 9mm target width, $p_{beam} = 2010 \text{ MeV/c}$ [3]

of the momentum distribution of elastically scattered protons (Fig. 2), and the second method relied on the measurement of the pressure of the gas in the last chamber of the cluster-jet dump. The pressure was measured as a function of the position of wires moving with the constant velocity through the cluster beam. These wires were rotated around the axis perpendicular to the beam of hydrogen clusters. In case that one or more wires crossed the cluster beam the clusters hitting a wire were stopped causing a decrease of the vacuum pressure in the last stage of the cluster dump. The wire device (Fig. 3) was located above the reaction point (Fig. 4) making it possible to monitor the target dimensions without disturb-

ing the measurement of the $pp \rightarrow pp\eta'$ reaction. From the knowledge about the dimensions of the wire device it is possible to calculate the target dimensions from the measurement of the pressure change as function of the position of the device. Fig. 5 shows an example of the pressure measurement as function of time using a constant angular velocity of the device. The extraction of target dimensions is in progress. We expect to achieve an accuracy of about 0.2 mm.



Fig. 3: Photograph of the wire device for precision measurement of the cluster target dimensions. The rotation axis of the device is mounted perpendicular to the cluster jet.

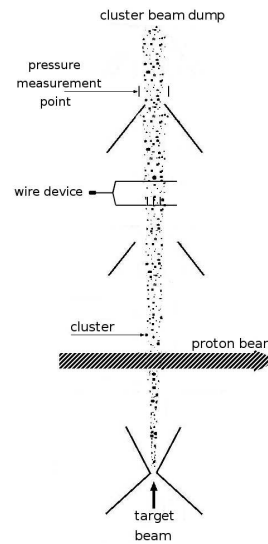


Fig. 4: Schematic view of the target dimensions measurement.

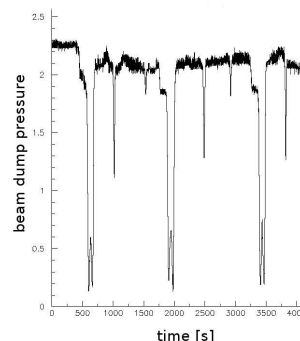


Fig. 5: Experimental data form a target scan using wire device.

References:

- [1] D. M. Binnie *et. al.*, Phys. Lett. **B83** 141 (1979);
- [2] E. Czerwiński, D. Grzonka, P. Moskal, <http://www.fz-juelich.de/ikp/publications/PAC31/proposaletaprimewidth.pdf>
- [3] R. Czyżykiewicz, PhD thesis, Jagiellonian U. (2007).

* Jagiellonian University, Cracow, Poland
University of Münster, Germany

Study of the $p + {}^6\text{Li} \rightarrow \eta + {}^7\text{Be}$ reaction close to threshold

GEM Collaboration

The physics motivation of the study of the $p + {}^6\text{Li} \rightarrow \eta + {}^7\text{Be}$ reaction is to learn more on the interactions of η -meson with nucleons and nuclei. This motivation was presented already earlier in the GEM proposals [1, 2]. There are theoretical assumptions of the existence of strong η -nucleus bound states, so called η -mesic nuclei [3–5]. The other aspects that can be also investigated in studying of η -nucleus final state interactions is the behavior of the $N^*(1535)$ resonance in nuclear matter. The best method of investigations of $p + {}^6\text{Li} \rightarrow \eta + {}^7\text{Be}$ reaction is the detection of the heavy recoiling nuclei. Near the threshold these particles will be emitted in a small forward cone. The magnetic spectrometer Big Karl (BK) is a good tool for these measurements. The detection system, mounted at the Big Karl exit inside of a huge vacuum chamber contains the a $\Delta E - E$ system of organic scintillators and a position sensitive detector, which allows to reconstruction of three momentum vector of the emitted particle. As a position sensitive detector, a set of two multi wire avalanche chambers (MWAC) was used. These detectors are position sensitive in both horizontal (X) and vertical (Y) directions. This allowed to measure the momentum of reaction products as well as their directions. These detectors were followed by the $\Delta E - E$ and time-of-flight scintillators system. The MWAC is a double-grid avalanche low pressure gas counter.

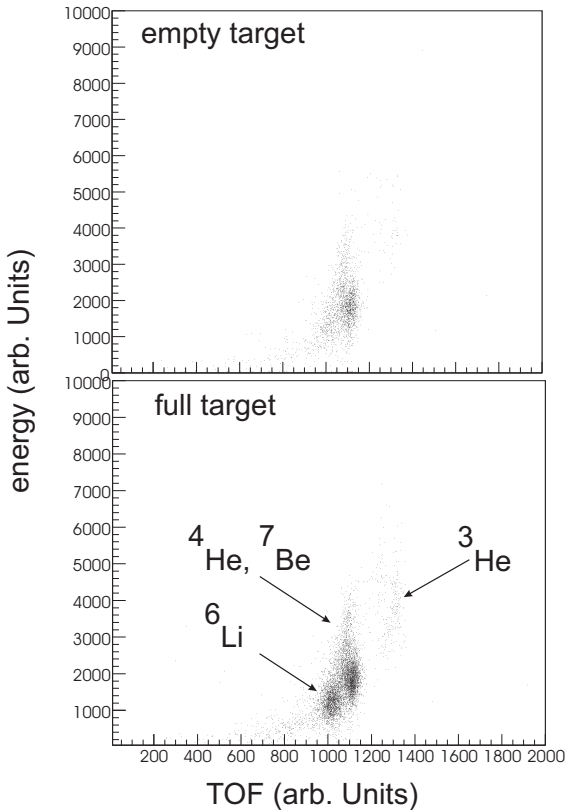


Fig. 1: Energy deposited in the scintillators as function of the time-of-flight.

The only measurement of this reaction was performed by Scomparin et al. [6] at a beam energy of 1322 MeV/c. They detected the two photons from the η decay. A total of 8 events was found leading to a mean cross section of 5.6 ± 3.8 nb/sr, when s-wave production is assumed. We performed the experiment at a beam momentum of 1310 MeV/c. From this measurement we estimate the cross section to be in the order of magnitude of 2 nb/sr.

In Fig. 1 the deposited energy is shown as function of the time-of-flight for an empty target frame and the full target. For both diagrams the same cuts were applied. Separated groups can be identified. Unfortunately the events with ${}^7\text{Be}$ -ions have the same loci as the much more abandoned α -particles. For the events of this group missing mass spec-

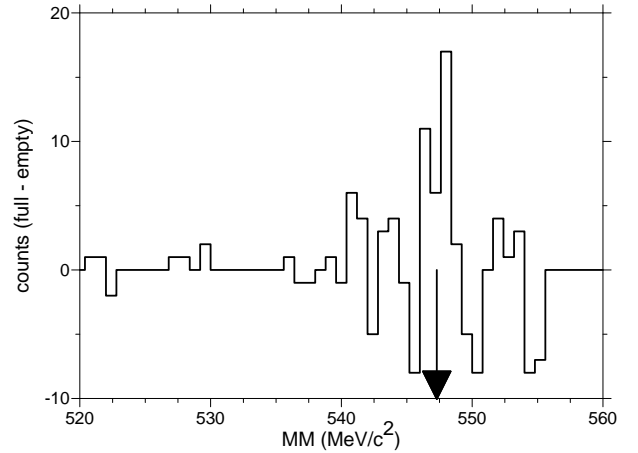


Fig. 2: Preliminary missing mass spectrum. Shown is the difference between the empty target run and the spectrum employing a ${}^6\text{Li}$ target. The arrow indicates the η -mass.

tra were computed. Then the difference of both was derived which is shown in Fig. 2. There is an enhancement around the η -mass. Now the differences between two body kinematics and multi body kinematics will be applied to distinguish the events from the reaction of interest from reactions of the type $p + {}^6\text{Li} \rightarrow {}^7\text{Be} + X^0$ with $X^0 = 2\pi, 3\pi$ or 4π .

References:

- [1] H. Machner et al., COSY Proposal 88 (1999).
- [2] H. Machner et al., COSY Beam Request 88,1 (1999).
- [3] R.S. Bhalerao, L.C. Liu, Phys. Rev. Lett. **54**(1985)865.
- [4] Q. Haider, L.C. Liu, Phys. Lett. **B 172** (1986)257.
- [5] S. S.A. Rakityanski et al., Phys. Rev. **C 53**(1996) R2043.
- [6] E. Scomparin et al., J. Phys. **G 19** (1993) L51

An η -mesic nucleus ($\eta \otimes A$) is a bound system of an η -meson and a nucleus. The η -mesic nuclei, which are solely the result of strong interactions unlike the pionic atoms, are a new kind of atomic nuclei and their research has fundamental significance in studying in-medium properties of hadrons, in particular, medium modification of meson masses. The experimental confirmation of the existence of such an η -bound system will lead to new possibilities of studying the interaction between a nucleus and the short lived η meson. This system should be produced in a reaction

$$p + A \rightarrow {}^3\text{He} + \eta \otimes (A - 2), \quad (1)$$

where all beam momentum is carried away by the ${}^3\text{He}$ and the η as well as the $A - 2$ spectator nucleons are at rest in the laboratory system. The beam momentum for such a situation of recoil free kinematics is also known as magic momentum. The ${}^3\text{He}$ ion was detected by the magnetic spectrograph BIG KARL thus allowing to identify the η -mesic nucleus via missing mass technique. A huge background from nuclear fragmentation is expected to superimpose the small signal from the mesic nuclei.

The optimal choice of a target would be an odd-odd nucleus. In such a case the residual nucleus will be even-even, thus reducing the probability for nuclear excitation. The only two possibilities would be ${}^6\text{Li}$ and ${}^{14}\text{N}$. These are, however, rather light systems and might be without binding. In the actual experiment we have therefore chosen ${}^{27}\text{Al}$ as target nucleus. This is heavier but only odd-even. The beam momentum was chosen to magic kinematics.

In Fig. 1 we show missing mass spectra as calculated from the ${}^3\text{He}$ detected under zero degree in the magnetic spectrograph for two different settings. The shape is almost governed by the acceptance. Hence, the momentum spectrum is flat. In order to reduce the physical background a second detector was applied. This is a large acceptance plastic scintillator detector "ENSTAR" with state-of-art fibre optics readout. It has been designed and built at Bhabha Atomic Research Centre (BARC) in Mumbai, India. One expects the following chain of reactions to occur:

$$\eta + N \rightleftharpoons N^*(1535) \rightleftharpoons \pi + N. \quad (2)$$

In the case of two charged particles in the exit channel they can be detected with ENSTAR (see Ref. [1]).

Fig. 2 shows a cross section of through the ENSTAR. It consists of three layers. Each layer consists of scintillators with shapes indicated in the figure. Since the ${}^3\text{He}$ ion carries all the beam momentum away, the intermediate N^* is at rest and its decay particles move back to back to each other. Such a case is indicated in the figure. The red painted scintillators will be hit by a proton moving down, which is stopped in the middle layer, and a pion moving up, which passes to all three layers.

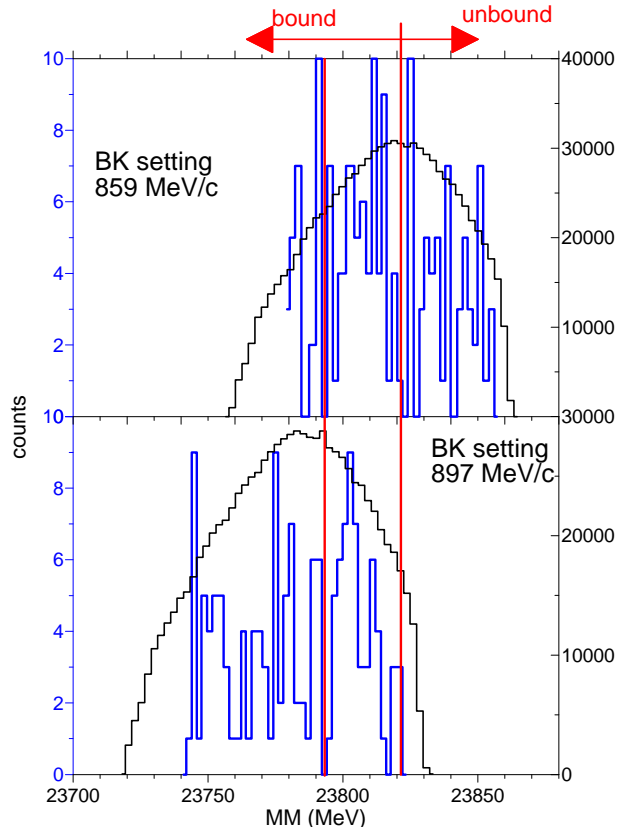


Fig. 1: Preliminary missing mass spectrum including the system ${}^{25}\text{Mg} \otimes \eta$ for two different settings of the magnetic spectrograph BIG KARL. The black histograms (right ordinates) show the missing mass distribution for only ${}^3\text{He}$'s selected with beam momentum. The blue histograms (left ordinates) show the events after selecting the triple coincidence as discussed in the text. The solid lines indicate the binding and excitation of ≈ 28 MeV.

In the analysis we now require a triple coincidence: A ${}^3\text{He}$ in the magnetic spectrograph and two hits of the discussed type in ENSTAR. The real reaction studied is

$$p + {}^{27}\text{Al} \rightarrow {}^3\text{He} + \pi^- + p + X \quad (3)$$

with the constraints on momenta. This results in the spectra also shown in Fig. 1. In addition a background contribution was subtracted.

Note that the count rate is reduced from 30000 per channel to approximately five counts! Also the limiting missing mass for binding is indicated. The lower missing mass spectrum shows a structure ranging up to ≈ 28 MeV excitation energy. However, its width ($\Gamma \approx 7.6$ MeV) is much smaller than the result of a recent calculation [2] which is $\Gamma \approx 36$ MeV. If this is true then the whole strength observed is due to an η -bound state. However, a different setting of the spectrograph allows the detection of events from the unbound region. This event rate is only slightly smaller than in the binding range indicating that the binding probability, if not even

First test measurement of the deuteron-proton breakup has been performed with the use of Germanium Wall detector and polarized deuteron beam. The beam time was devoted primarily to beam tuning and background studies, as well as to confirming the feasibility of the assumed goals (statistical accuracies). This project follows a series of successful experiments at KVI [1-4] and aims at supplementing their results with data in a very interesting region of forward angles of the two breakup protons. Precise results on cross sections and analyzing powers of the $^1\text{H}(\vec{d},\text{pp})\text{n}$ breakup reaction will extend the data base, necessary for testing modern theoretical models of the interaction dynamics in the few-nucleon system.

One of the most important outcomes of the very preliminary data analysis are the particle identification ($\Delta E - E$) spectra. Outside the angular range of the beam-like background, a clear separation between the loci of protons and deuterons is observed. Also the elastic protons are quite well separated from the breakup continuum - see fig. 1. This feature enables to obtain a clear and unambiguous selection of the reaction channel and assures low level of systematic uncertainties.

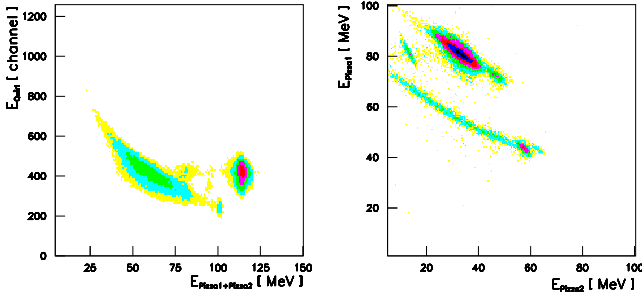


Fig. 1: Examples of the $\Delta E - E$ particle identification spectra. *Left panel:* for Quirl (in channels) vs. Pizza1+Pizza2 energy. *Right panel:* for Pizza1 vs. Pizza2 energies. The energies are only roughly calibrated. One can distinguish the proton branch (lower), followed by the elastic proton spot, and the deuteron loci - with the rest-overs of the beam deuterons and accidental events.

Using the particle identification information together with the kinematical constraints leads to a very clean selection of the elastic $^1\text{H}(\text{d},\text{dp})$ scattering channel. Those events are used for testing the geometrical properties of the detection system, for fine tuning of the energy calibration of all detector elements, for absolute normalization of the breakup cross sections and for the beam polarization determination. The last aspect of the above list is shortly outlined in the following. Taking the ratio of rates of the elastic d-p scattering events obtained with the polarized (N_P) and unpolarized (N_0) beam and plotting its dependence on the azimuthal angle φ (for a selected polar angle θ), one should obtain an oscillating pattern described by the formula:

$$\frac{N_P}{N_0} \equiv f(\varphi) = 1 + P_z \cdot g(\varphi) + P_{zz} \cdot h(\varphi),$$

with P_z and P_{zz} denoting the vector and tensor beam polarizations. The dependency on φ as well as the corresponding analyzing powers at the chosen angle θ are represented by the functions $g(\varphi)$ and $h(\varphi)$:

$$g(\varphi) \equiv iT_{11}(\theta)\sqrt{3}\cos\varphi,$$

$$h(\varphi) \equiv -T_{22}(\theta)\frac{\sqrt{3}}{2}\cos 2\varphi - T_{20}(\theta)\frac{\sqrt{2}}{4}.$$

Adopting theoretical values of the analyzing powers iT_{11} , T_{20} and T_{22} allows to determine the beam polarizations from a fit of the measured $f(\varphi)$ distribution with P_z and P_{zz} as free parameters. Two examples are shown in fig. 2, left panels. We used two nominally pure beam polarization states: vector polarized, with the ideal value of $P_z = -\frac{2}{3}$, and tensor polarized, with $P_{zz} = +1$. One can observe that even with a crude data treatment the method is working correctly. The results (values from the fit shown in panels) from 10 hours run data sample are $P_z = -0.50 \pm 0.01$, $P_{zz} = 0.18 \pm 0.04$ for the first and $P_z = 0.10 \pm 0.02$, $P_{zz} = 0.71 \pm 0.08$ for the second state, respectively, and therefore indicate that the polarization setting efficiency is around 70-75%.

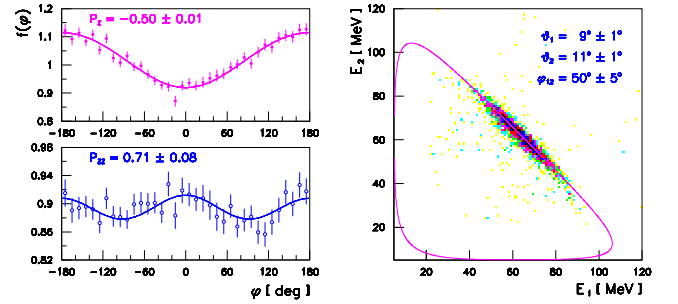


Fig. 2: *Left panels:* beam polarization determination with the elastic scattering events. The obtained polarization values are shown in the panels. *Right panel:* breakup kinematical spectrum of two-proton coincidences for the angular configuration specified in the panel.

Selection of the breakup events as proton-proton coincidences is exemplified in fig. 2, right panel. The chosen kinematical configuration is indicated in the figure. One concludes that also this reaction channel can be selected very cleanly, without much background. Quantitative estimation of the rate confirms that the assumptions used in the proposal are fulfilled and that the final statistical accuracy for cross sections and analyzing powers should be obtained in the next data taking run.

References:

- [1] St. Kistryn et al., Phys. Rev. **C 68**, 054004 (2003)
- [2] St. Kistryn et al., Phys. Rev. **C 72**, 044006 (2005)
- [3] A. Biegun et al., Acta Phys. Pol. **B 37**, 213 (2006)
- [4] St. Kistryn et al., Phys. Lett. **B 641**, 23 (2006)

A high resolution study of the $p + p \rightarrow K^+ + X$ reaction has been performed at COSY using BIG KARL spectrometer. Previous investigations of inclusive kaon production in pp collisions at SATURNE II [1] show strong final state enhancement of the missing mass spectra at Λp and Σ nucleon threshold. Data with much higher missing mass resolution and improved statistical accuracy provide a precise determination of the Λp final state interaction (FSI), constraints on $\Sigma^0 p$ and $\Sigma^+ n$ FSI and energy dependent structures near the Σ -nucleon threshold. The experiment gives also the opportunity for high resolution search of the lowest mass, narrow, strangeness -1 dibaryons predicted by bag model calculations [2, 3]

The reaction $p + p \rightarrow K^+ + X$ was studied in the missing mass range 2.054 - 2.18 GeV, at two incoming beam momenta of 2.735 and 2.87 GeV/c and at a few central momenta of the Big Karl magnetic spectrometer. Measured particles were identified using dE/dx and time-of-flight information from focal plane detectors [4]. The background of fast pions was suppressed from kaons using two silica aerogel threshold Čerenkov counters with aerogel refractive index of $n=1.05$. An example of Čerenkov detector ADC spectrum for pions and protons at 960 MeV/c momentum is presented in Fig.1.

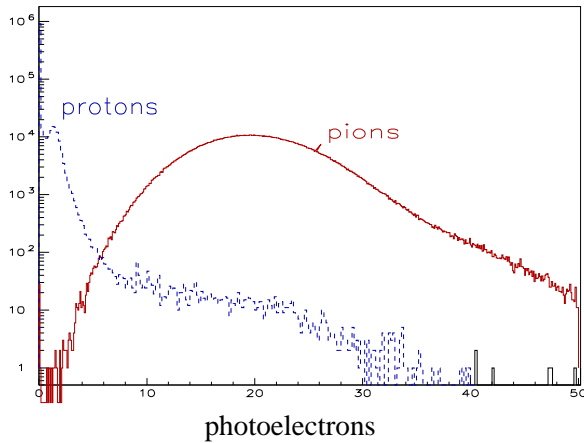


Fig. 1: ADC Čerenkov counter spectrum of the pions and protons at 960 MeV/c momentum.

Very high pion suppression factor of 10^5 and low misidentification of particles with velocity below Čerenkov threshold (protons, kaons) was achieved as is seen in Fig. 2.

A preliminary missing mass distribution of the $p + p \rightarrow K^+ + X$ below Σ nucleon production threshold is presented in Fig. 3. No evidence for strange dibaryons in the mass range of 2.08 - 2.11 GeV was found. At present the detailed studies of the fraction of kaons decaying on the way through the Big Karl magnetic spectrometer are performed. The particle path length in the magnetic spectrometer is investigated using simulations with code TURTLE and experimental measurements of proton and pion time-of-flight.

References:

[1] R. Siebert et al., Nucl. Phys. A567 (1994) 819.

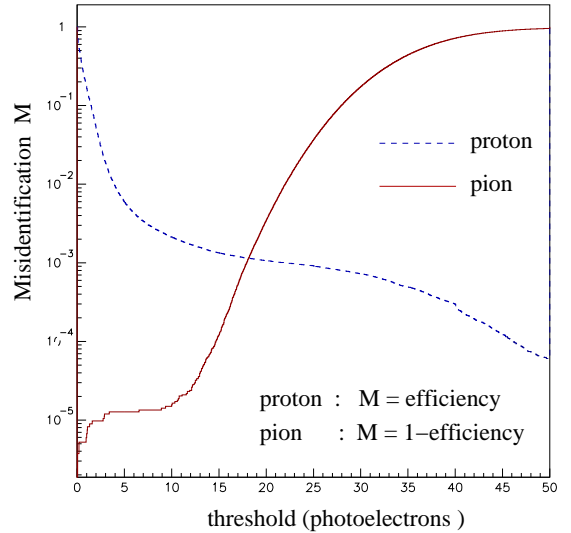


Fig. 2: Suppression of pions and misidentification of protons at 960 MeV/c momentum from silica aerogel Čerenkov counter.

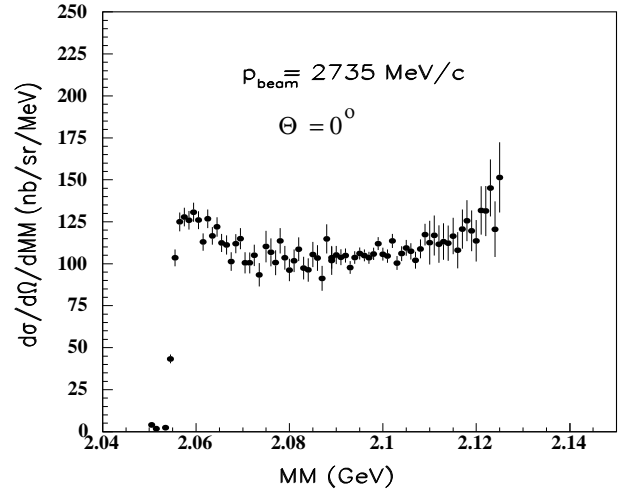


Fig. 3: Missing mass spectrum of the $p + p \rightarrow K^+ + X$ reaction at proton beam energy 1953 MeV and the scattering angle 0° . The data are preliminary.

[2] A.T.M. Aerts and C.B. Dover, Phys. Lett. 146B (1984) 95.
 [3] A.T.M. Aerts and C.B. Dover, Nucl. Phys. B253 (1985) 116.
 [4] J. Bojowald et al., Nucl. Instr and Meth. A487 (2002) 314.

We investigate the K^+K^- interactions in the reaction $pd \rightarrow {}^3\text{He}K^+K^-$ and estimate possible contributions from the $a_0(980)$ and $f_0(980)$ mesons. The a_0 and f_0 resonances may give some contributions to the $pd \rightarrow {}^3\text{He}K^+K^-$ cross section. In this case one can write the invariant K^+K^- mass distribution as

$$\frac{d\sigma_{pd \rightarrow {}^3\text{He}K^+K^-}}{dM} = \frac{d\sigma_{\text{BG}}}{dM} + \frac{d\sigma_{\phi}}{dM} + \frac{d\sigma_{a_0}}{dM} + \frac{d\sigma_{f_0}}{dM}. \quad (1)$$

The first term describes the non-resonant K^+K^- production with a constant interaction amplitude near threshold. The $K^- {}^3\text{He}$ FSI effects can be neglected since their influence on the K^+K^- distribution is very small, see Ref. [1]. The $\phi(1020)$ -meson contribution $d\sigma_{\phi}/dM$ has also been considered in the same paper. The last two terms reflect the contributions from the $a_0(980)$ and $f_0(980)$ resonances. Each of them can be written as a product of the total a_0 - or f_0 -production cross section σ_{a_0} (σ_{f_0}) as a function of the invariant mass M of the $K\bar{K}$ system and the Flatté mass distribution. Using Eq. (1) we calculate the K^+K^- mass distributions with parameters of Set a_0 [Crystal Barrel] [3] and Set a_0 [E852] [4] for the $a_0(980)$ resonance contribution as well as Set f_0 [BES][5] and Set f_0 [E791][6] for the $f_0(980)$. We then compare the shape of the calculated spectra with that of the measured relative energy $T(K^+K^-)$ distribution at the excess energy $Q = 41$ MeV [2]. The solution without a_0 and f_0 resonances is in best agreement with the data with $\chi^2_{\text{min}} = 11.5$. The different curves in Fig. 1 represent the relative contributions of the $a_0(980)$ or $f_0(980)$ meson versus the fraction of the $\phi(1020)$ meson obtained at $\chi^2 = \chi^2_{\text{min}} + 1, \chi^2_{\text{min}} + 2$ and $\chi^2_{\text{min}} + 3$. Note that it is important to take into account the effects of the experimental mass resolution. We conclude that the $a_0(980)$ contribution might reach 20–25% within a $\chi^2_{\text{min}} + 3$ limit while that from the f_0 does not exceed $\sim 10\%$ of the total $pd \rightarrow {}^3\text{He}K^+K^-$ cross section at $Q = 41$ MeV.

We are grateful to Hartmut Machner, Hans Ströher and Colin Wilkin for helpful discussions. This work was supported by DFG 436 RUS 113/787 and RFBR grant 06-02-04013 and the Russian Federal Agency of Atomic Energy.

References:

- [1] V.Yu. Grishina, M. Büscher and L.A.Kondratyuk, Phys. Rev. C (2007) in print, arXiv:nucl-th/0608072.
- [2] F. Bellemann *et al.* Phys. Rev. C **75** (2007) 015204.
- [3] A. Abele *et al.*, Phys. Rev. D**57**, (1998) 3860.
- [4] S. Teige *et al.*, Phys. Rev. D**59**, (2001) 012001.
- [5] M. Ablikim *et al.*, Phys. Lett. B**607**, (2005) 243.
- [6] M. Aitala *et al.*, Phys. Rev. Lett.**86**, (2001) 765.

^aInstitute for Nuclear Research, 60th October Anniversary Prospect 7A, 117312 Moscow, Russia

^bInstitute for Theoretical and Experimental Physics, B. Chermushkinskaya 25, 117218 Moscow, Russia

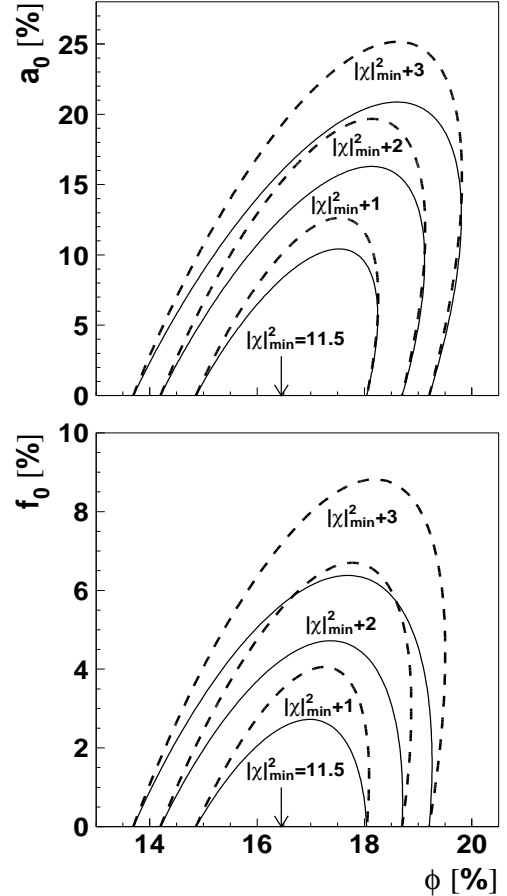


Fig. 1: Result of our fit to the experimental K^+K^- mass distribution for the $pd \rightarrow {}^3\text{He}K^+K^-$ reaction at an excess energy of 41 MeV. The $\chi^2 = \chi^2_{\text{min}} + 1, \chi^2_{\text{min}} + 2, \chi^2_{\text{min}} + 3$ contour lines are obtained for relative contributions of $a_0(980)$ or $f_0(980)$ as a function of the $\phi(1020)$ -meson fraction. In the upper figure the solid and dashed lines were calculated using the Flatté distributions for the a_0 meson with the parameters of Set a_0 [Crystal Barrel] and Set a_0 [E852], respectively. In the lower figure the solid and dashed contour lines correspond to the contribution of the f_0 meson with the Flatté parameters of Set f_0 [BES] and Set f_0 [E791].

The apparatus of PISA project (described in details in ref. [1]) has been applied for investigation of reactions induced by 2.5 GeV protons on the gold target. Whereas light charged particles, (i.e. hydrogen and helium ions) as well as lightest intermediate mass fragments (IMF's) were detected and identified by telescopes consisted of semiconductor silicon detectors, other detection method had to be used for heavier IMF's (C - Al nuclei). As can be seen in fig. 1, the low energy carbon ions were stopped in the thin ΔE silicon detector leading to low energy cut of the spectra. Thus, low energy threshold Bragg curve detectors were used to allow for observing the maximum of the double differential cross section distributions. This enabled us to extract with reasonable accuracy the total production cross sections by fitting the Maxwell-like distributions of isotropically emitting moving source to the experimental cross sections.

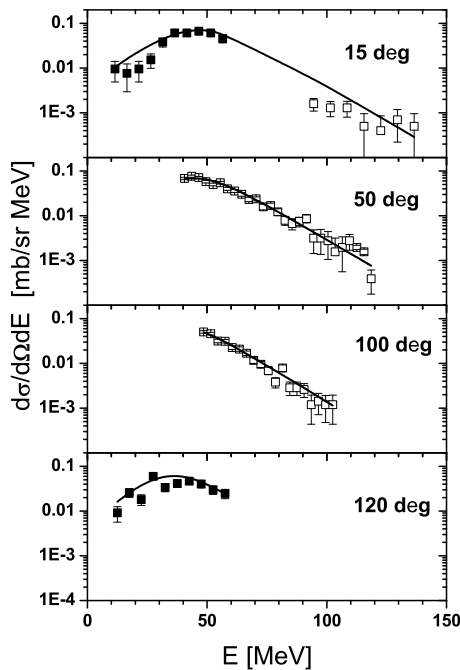


Fig. 1: Experimental differential cross sections $d\sigma/d\Omega dE$ obtained for Au(p,C)X reaction at $T_p=2.5$ GeV from silicon telescopes (open squares) and from Bragg curve detectors (full squares), which were positioned only at 15° and 120° . Solid line shows results of the fit of contribution from isotropically emitting, moving source.

The Bragg curve detectors placed at 15° and 120° were applied to measure the spectra for elementally identified heavier IMF's - from $Z = 4$ to $Z = 13$. Examples of the experimental spectra (full squares) and the phenomenological model distributions (lines) are presented in fig. 2 for oxygen, neon, and aluminium ejectiles (lower, intermediate, and upper part of the figure). As can be seen the maximum of the spectra can be observed what puts rather strong constraints on the fitted parameters and thus leads to good accuracy of the extracted total production cross sections.

The dependence of the obtained total production cross section on the ejectile charge is shown in fig. 3. The logarithmic

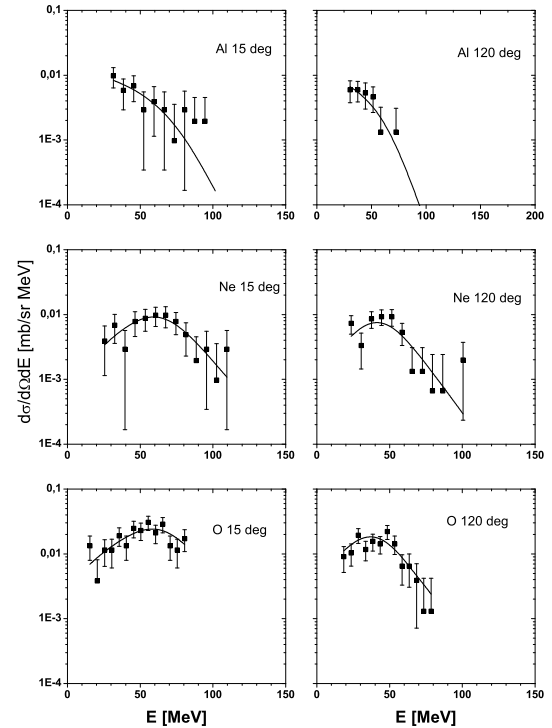


Fig. 2: Experimental (full squares) and fitted (solid lines) spectra for selected ejectiles measured by PISA collaboration for Au+p reaction at $T_p=2.5$ GeV.

mic scale was used for both axes to illustrate that the charge dependence of the cross sections may be approximated by power law formula: $\sigma \sim Z^{-\tau}$. The fit to full range of ejectiles ($1 \leq Z \leq 13$) gives $\tau = 3.07 \pm 0.18$, whereas the fit constrained to IMF's only ($3 \leq Z \leq 13$) leads to $\tau = 2.47 \pm 0.21$.

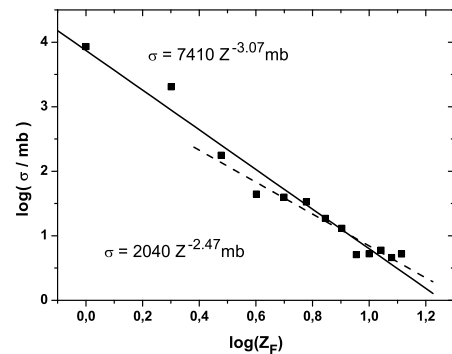


Fig. 3: Experimental total production cross section as a function of the atomic number Z of ejectiles (squares). The lines present results of the fit of the $\sigma \sim Z^{-\tau}$ formula.

We acknowledge the support of the European Community-Research Infrastructure Activity under FP6 "Structuring the European Research Area" programme (CARE, contract number RII3-CT-2003-506395).

References:

- [1] R.Barna, V. Bollini, A. Bubak et al., Nucl. Instr. and Methods in Phys. Research A **519**, 610 (2004)

Do Unpolarized Electrons Affect the Polarization of a Stored Proton Beam?

D. Oellers, L. Barion, P. Lenisa, F. Rathmann, R. Schleichert, E. Steffens and H. Ströher
for the PAX and ANKE-Collaborations

The PAX Collaboration aims to produce polarized antiprotons in order to access the transversity distribution of the nucleon by a measurement of Drell-Yan events [1]. So far, spin dependent attenuation of a stored (anti-)proton beam (spin filtering) is the only experimentally tested method to produce a polarized antiproton beam. Presently, there exist two competing theoretical scenarios: one[2, 3] with substantial spin filtering of (anti-)protons by atomic electrons, while the second one[4, 5] suggests an almost exact self-cancellation of the electron contribution to spin filtering. The existing experimental data from FILTEX [6] allow neither an unambiguous discrimination between the two scenarios nor do they give a direct constraint on the role of the spin-flip scattering in spin filtering, discussed by Walcher et al. [7]. In order to clarify this issue, the depolarization of a proton beam stored at COSY with injection energy $T_p = 45$ MeV by the electrons in a ^4He target should be studied, as in effect inverse to the polarization buildup by polarized atomic electrons as predicted by Meyer and Horowitz. Here, we discuss the experimental setup and the Monte Carlo simulations that were carried out in order to prepare the investigation.

The basic idea of the planned experiment is the following supposition: If polarized electrons polarize an unpolarized proton beam, then unpolarized electrons should depolarize a polarized proton beam (H.O.Meyer). Therefore, the observation of the electron induced depolarization of a stored proton beam allows to discriminate between the two theoretical scenarios. The cross section, as predicted by Meyer and Horowitz, drops dramatically with increasing energy. Therefore, it is planned to work with a stored proton beam at COSY-injection energy of $T_p = 45$ MeV. As a suitable

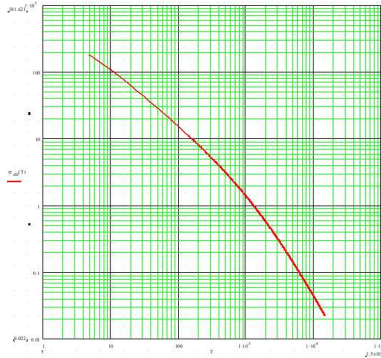


Fig. 1: Cross Section of e-p spin transfer as predicted from Meyer and Horowitz [2, 3].

electron target, ^4He atoms are chosen, which are injected into the storage cell at the ANKE target point. The ^4He nucleus itself has spin 0 and cannot contribute to spin filtering. On the other hand, the p - ^4He scattering at 45 MeV has an analyzing power of > 0.8 , leading to a large Figure Of Merit ($\text{FOM} = A_y^2 * \frac{d\sigma}{d\Omega}$). This allows us, together with a dedicated detection system, to precisely measure the beam polarization. The detection system is capable to determine the complete kinematics of the reaction. The existing Silicon Tracking Telescopes with three layers of double sided micro-

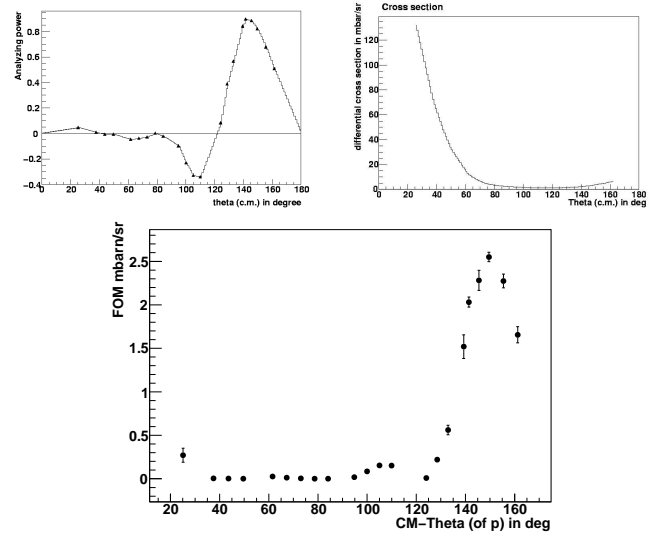


Fig. 2: Analyzing power, differential cross section and Figure Of Merit of p - ^4He elastic scattering at $T_p = 45$ MeV.

structured Silicon of $69\mu\text{m}$, $300\mu\text{m}$ and $5100\mu\text{m}$ thickness each provides for the detection of the recoil proton. As the FOM peaks at 145°_{Lab} , each layer is shifted by 1.7cm in downstream direction. One additional layer of $300\mu\text{m}$ silicon is utilized to detect the α -particle. This setup is placed on each side of the target in order to measure the left-right asymmetries. During one cycle there are always two contri-

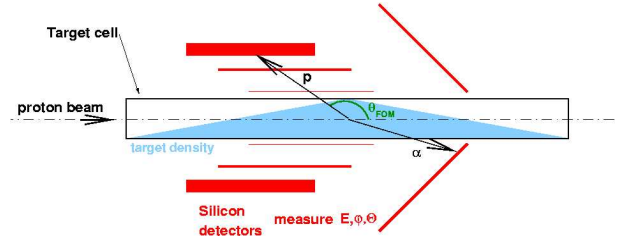


Fig. 3: Setup of silicon detectors placed around a storage cell.

butions to the depolarization of the beam. Firstly, the effect of the target τ_p^{MH} , which should be studied and secondly, the effect of depolarizing the resonances of COSY τ_p^{COSY} , which enters into the polarization lifetime. The total polarization lifetime is calculated as

$$\frac{1}{\tau_p^{total}} = \frac{1}{\tau_p^{MH}} + \frac{1}{\tau_p^{COSY}} \quad (1)$$

Since only the total polarization lifetime can be measured directly, a dedicated cycle is needed (see Fig. 4). While during T1 and T3 the total polarization lifetime will be measured, no data will be available during T2, because the target is switched off during this time. From the difference in polarization between the end of T1 and the beginning of T3 the

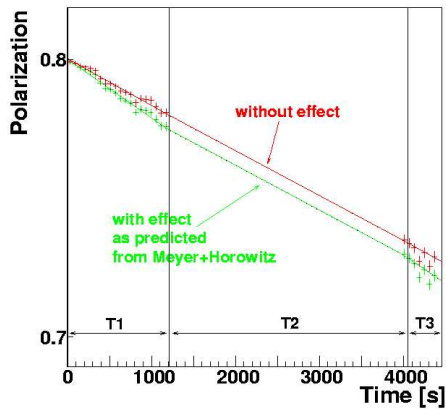


Fig. 4: Setup of COSY cycle to distinguish the depolarization caused by COSY from the one caused by the target electrons.

polarization lifetime of COSY is accessible. By using Equation (1) the polarization lifetime caused by the target can be extracted.

The experiment should be carried out with $2 \cdot 10^{10}$ polarized protons ($p_{init} > 0.7$) and a target thickness of $2 \cdot 10^{14}$ $^4\text{He}/\text{cm}^{-2}$. With a four week measurement the effect can be determined with a significance of 4 to 5 σ . Prerequisites are i) a lifetime of the COSY beam of 600s/4000s (with/without target) and ii) a polarization lifetime $\tau_p^{COSY} > 10000$ s.

References:

- [1] Technical Proposal for Antiproton Proton Scattering Experiments with Polarization, <http://www.fz-juelich.de/ikp/pax/>
- [2] H.O. Meyer, Phys. Rev. E **50**, 1485 (1994).
- [3] C.J. Horowitz and H.O. Meyer, Phys. Rev. Lett. **72**, 3981 (1994).
- [4] A.I. Milstein and V.M. Strakhovenko, Phys. Rev. E **72**, 066503 (2005).
- [5] N.N. Nikolaev and F.F. Pavlov, Buildup of the polarization of stored protons and antiprotons: FILTEX result arXiv:hep-ex:0601184.
- [6] F. Rathmann, Phys Rev. Lett. **71**, 1379 (1993).
- [7] Walcher et al., private communication.

A Polarized Target for Spin Filtering Tests at COSY and AD

A. Nass^a, M. Capiluppi^b, H. Kleines^c, P. Lenisa^b, F. Rathmann^c, J. Sarkadi^c, E. Steffens^a and H. Ströher^c

A technical proposal for spin-physics experiments with polarized antiprotons has been submitted by the PAX collaboration [1]. It suggests to study the interaction of polarized antiprotons with polarized protons and deuterons in an internal storage-cell gas target. The antiprotons are polarized through spin-dependent scattering on a polarized hydrogen gas target in a separate antiproton polarizer ring (APR). The polarizing process is based on spin dependent scattering of the orbiting antiprotons from the polarized target atoms (Spin Filtering). This technique was tested with a proton beam at TSR in Heidelberg in 1993 and a polarization buildup was observed [2]. There, however the polarization effect by the polarized electrons and the polarized nuclei could not be disentangled. Theoretical investigations were leading to two different descriptions with [3] and without [4] spin-transfer from polarized electrons.

To clarify the contribution by the polarized electrons and to test the technique, experiments with protons at COSY (Jülich) [5] and with antiprotons at AD (CERN) [6] are being prepared. A first depolarization measurement [7] is planned with the existing setup at ANKE. Later, a low- β section [8] will be implemented at COSY for the installation of a polarized target. As target, the former HERMES target (see fig. 1) will be used which was removed from the HERMES experiment end of 2005 and transferred to Jülich. It consists of an polarized atomic beam source (ABS) and a so-called Breit-Rabi-polarimeter (BRP).

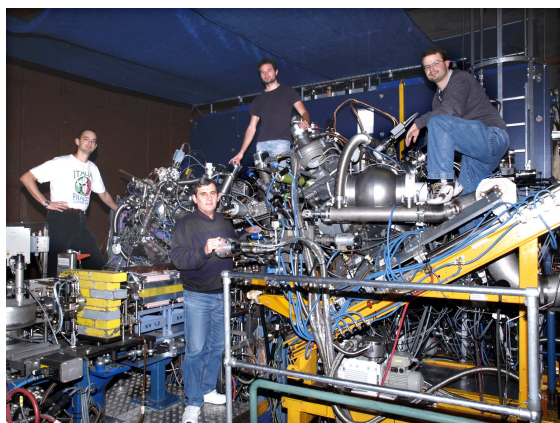


Fig. 1: The HERMES target section at HERA (DESY, Hamburg)

Because of limited space the ABS and the BRP cannot be implemented at COSY as well as at AD with the earlier support. In 2006 the ABS was completely dismantled and a new support was designed and produced in the Erlangen mechanical workshop. A vertically movable platform was installed in the basement of the IKP building (Jülich) using part of an earlier installation. In fall, the ABS vacuum chambers and the pumping system were mounted on the support (see fig. 2). By the end of 2006 the mechanical parts were finished. The next steps

are the cabling and the installation of the Slow Control system to monitor and interlock the vacuum system. The BRP support and a chamber for ABS beam studies and measurements with the target cell were designed and their manufacturing has been started in the FZ-Jülich mechanical workshops and will be finished in early 2007.



Fig. 2: The reassembled ABS mounted on the new support.

References:

- [1] *Antiproton-Proton Scattering Experiments with Polarization*, Technical Proposal for the HESR at FAIR, Jülich (2006), Spokespersons: P. Lenisa and F. Rathmann, and references therein. Available from www.fz-juelich.de/ikp/pax.
- [2] F. Rathmann et al., Phys. Rev. Lett. 72, 1379 (1993).
- [3] C.J. Horowitz and H.O. Meyer, Phys. Rev. Lett. 72, 3981 (1994).
- [4] A.I. Milstein and V.M. Strakhovenko, Phys. Rev. E 72, 066503 (2005).
- [5] *Spin Filtering studies at COSY*, Letter of Intent for COSY, Jülich (2006), www.fz-juelich.de/ikp/pax.
- [6] *Measurement of the Spin-Dependence of the $p\bar{p}$ -Interaction at the AD-Ring*, Letter of Intent for the AD at CERN, Jülich (2006), www.fz-juelich.de/ikp/pax.
- [7] D. Oellers, Contribution to the present report.
- [8] A. Garishvili, Contribution to the present report.

^a Phys. Institut der Universität Erlangen Nürnberg, Germany

^b Istituto Nazionale di Fisica Nucleare, Ferrara, Italy

^c Forschungszentrum Jülich, IKP, Jülich, Germany

Detector concept development for the spin-filtering experiment at COSY

M. Contalbrigo^a, N. Lomidze^b, G. Macharashvili^{b,c}, M. Tabidze^b for the PAX Collaboration

The main objective of recently proposed spin-filtering experiments at COSY [1] and AD-CERN [2] relate to physics of the polarization build-up in a stored proton (antiproton) beams. Two scenarios of stored beam polarization passing through polarized internal target exist. Understanding to which one is really work is crucial to progress towards the goal to produce stored antiproton beam. The polarized antiproton beam is the main necessary component to realize the PAX project [3].

The simulation study has been carried out in order to design and optimize a common detector to measure the polarization observables in pp and $\bar{p}p$ elastic scattering. The detector has to be optimized to detect the scattered particles in the energy range $40 < T_{p(\bar{p})} < 500 \text{ MeV}$. For the detector performance estimate we used Geant3 and Geant4 packages. To generate events according to the differential cross section we used the flat p.d.f. for the variable $\cos\vartheta_{cm}$. It reproduces SAID [4] predicted $d\sigma/d\vartheta$ at 40 MeV beam energy with good approximation. For some special purposes we used the SAID generated spectrum.

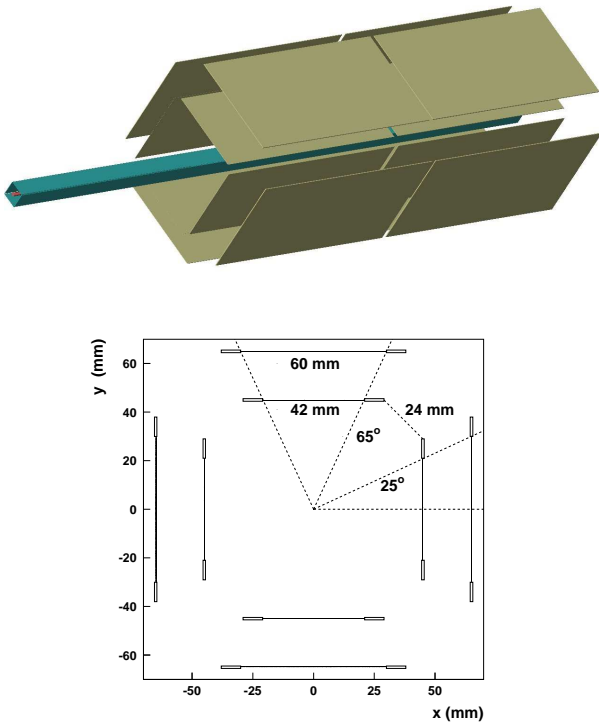


Fig. 1: (*Top panel*) The two-layer silicon detector geometry used by the simulation code. Each layer consists of four adjacent modules. The target cell of 40 cm length is shown. (*Bottom panel*) xy -view of the detector (rotated for convenience).

For simulation we used the detector set-up shown in Fig. 1. The detector covers the scattering angle range $10^\circ < \vartheta_{lab} < 45^\circ$. The target cell of $10 \times 10 \text{ mm}^2$ section and 40 cm length is made of teflon foil with thickness of $10 \mu\text{m}$. The detector is made of four sets of two-layer silicon strip modules, as shown in Fig. 1. The first layer plane is located at a distance of 40 mm away from the beam axis and the second one at 60 mm . The first layer modules have a dimensions of active area $42 \times 60 \text{ mm}$

and the second layer modules $60 \times 60 \text{ mm}$, respectively [5]. The outer layer is staggered by $+11 \text{ mm}$ along the beam to match better the elastic scattering geometry. The gaps of 24 mm are foreseen between the inner modules in the x, y -plane (see Fig. 1) to keep a free space for the target communications, supporting mechanics, and connections. At the event generation stage we used the layers consisting of 7 adjacent modules with 4 mm gap inactive area between the modules. However, at the analysis stage the acceptable detector configuration varied depending on particular task.

We considered two classes of "reconstructed" events:

- (A) two hits per track were detected. The interaction vertex is defined as a cross-point of forward and recoil tracks. The requirement is efficient for large-angle scattering events, with high energies for forward and recoil particles;
- (B) two hits of the forward track and one hit in the first layer for recoil particles were detected, i.e. the low energy recoil particle stopped in first layer. The interaction vertex is defined as the intersection between forward particle and the beam line.

Although only two silicon layers are used, the elastic event is overconstrained when the recoil stops in both (A) and (B) -type events.

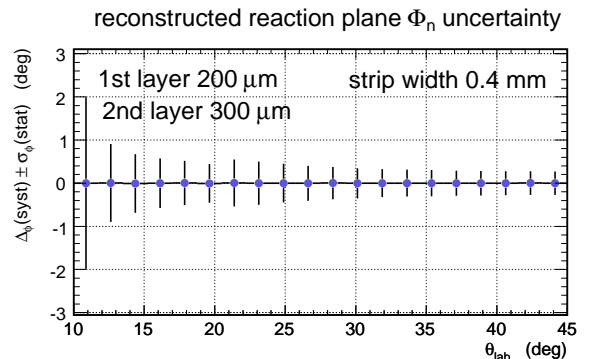


Fig. 2: The reconstructed reaction plane normal uncertainty. The multiple scattering and the energy losses are accounted. The detector resolution (x, y strip widths) is assumed to be both equal to 0.4 mm . Cut on χ^2 has not been applied.

Most important reaction parameters (kinematically independent) are ϕ_n - the reaction plane normal, and ϑ - the scattering angle. Reliable and precise reconstruction of these parameters in each event makes possible to measure any spin observable using the beam and the target of appropriate directions of polarization. The reaction plane reconstruction algorithm has been developed in order to define the expected uncertainties caused by the multiple scattering and the energy losses. The reaction plane is reconstructed using 3D-coordinates of 4 (or 3) hits (A and B -type events). The plane is built with a severe constraints, to be parallel to the beam axis (z), and minimum distance to z axis to be less than the beam radius. The reconstruction algorithm is based on

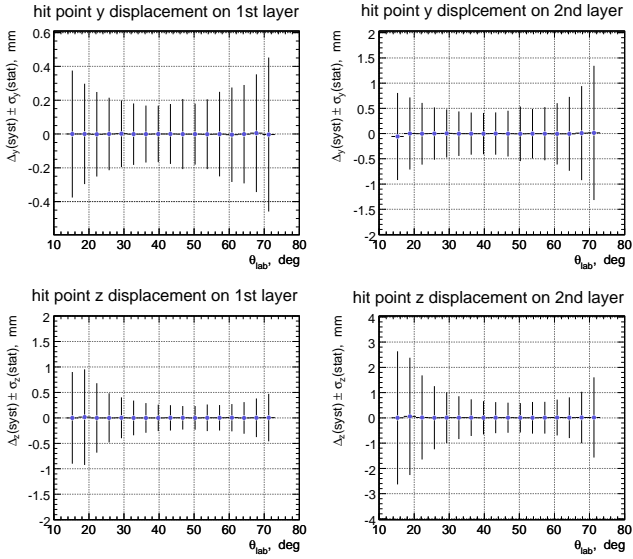


Fig. 3: Silicon hit y and z coordinate displacement due to multiple scattering for 1st and 2nd layers (the thickness of 1st layer is equal to $100 \mu\text{m}$.)

the *orthogonal regression method* providing a parameter characterizing 'goodness of fit' (χ^2).

The local displacement of each track in 1st and 2nd layers due to multiple scattering is shown in Fig. 3. ϑ_{lab} corresponds to the track lab angle, for the scattered protons up to 45° and for the recoil - above 45° . The displacement values depend not only on the deflection but also on the hit angle, e.g. σ_z increases at small scattering angles (long tracks and small hit angles) and at large angles (low energies).

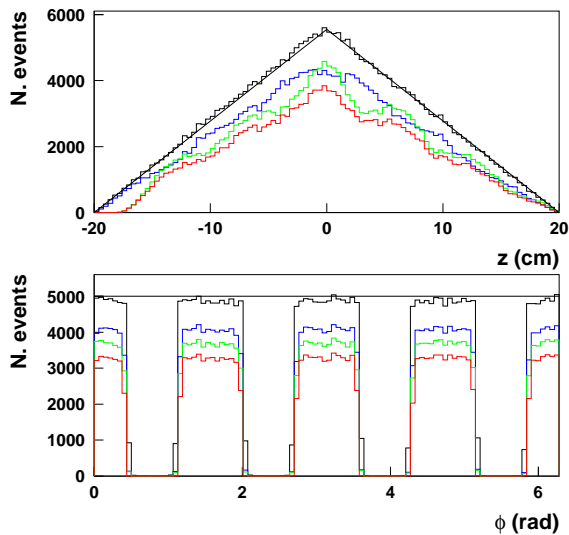


Fig. 4: Geometrical acceptance of the silicon detector at 40 MeV beam energy: accepted events as a function of z coordinate (Top) and ϕ angle (Bottom).

Fig. 4 shows the geometrical acceptance of the detector. The black lines shows events with at least one hit into the silicon. The blue (green) lines shows events where the forward (recoil) track is reconstructed. The red lines shows events where both tracks are reconstructed: the modulation is due to the 4 mm gaps between silicon active areas.

Fig. 5 shows the event distribution of reconstructed event as a function of the scattering angle and the typical deposit energy into the silicon layers. On top-left panel,

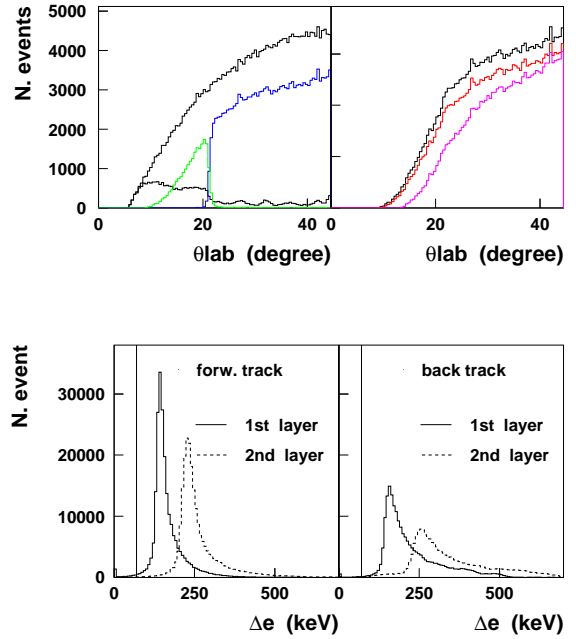


Fig. 5: **Top panel:** Event distribution as a function of the laboratory scattering angle. **Bottom panel:** Energy deposited into the silicon layers by forward (Left) and recoil (Right) particle.

the black lines shows the events with at least one silicon hit. The blue lines shows the events (class A) with 2 silicon hits per reconstructed track. The green lines shows events (class B) where the recoil track, stopped in the first silicon layer, was reconstructed using the energy information. The dashed black lines shows events with no reconstructed track (lost). On top-right panel, the black lines shows the reconstructed events (class A and B). The red lines shows the reconstructed events when the upstream recoil telescopes is disregarded. The green lines shows the reconstructed events when in addition the two downstream forward telescopes are disregarded and only the central 4-modules detector is used. On bottom panel the energy deposition of forward and recoil particle into the two silicon layers is plotted. The signals are all above the detection threshold, of the order of 70 keV.

In case we consider the central part of the detector (4 adjacent modules), the geometrical acceptance equals to 25%. If we assume an expected luminosity of $10^{29} \text{cm}^{-2} \text{s}^{-1} = 100 \text{mb}^{-1} \text{s}^{-1}$, a total cross section for pp scattering $\sigma_{tot} = 70 \text{mb}$, a dead-time correction factor equal to 0.9, a detection efficiency equal to 80%, a reconstruction efficiency equal to 70%, and a trigger efficiency equal to 70%, the estimated event rate is about 600s^{-1} .

References:

- [1] *Spin-Filtering Studies at COSY*, 2006
- [2] *Measurement of the Spin-Dependence of the $\bar{p}p$ Interaction at the AD-Ring*, 2005
- [3] PAX Proposal, [arXiv:hep-ex/0505054](https://arxiv.org/abs/hep-ex/0505054)
- [4] <http://gwdac.phys.gwu.edu>
- [5] A. Mussgiller, Ph.D. thesis, Univ. of Cologne, 2006

^a INFN, Ferrara, Italy

^b Tbilisi State University, Tbilisi, Georgia

^c JINR, Dubna, Russia

High statistics measurement of the $K\beta$ transition in pionic deuterium

D. F. Anagnostopoulos^a, F. Amaro^b, P. Bühler^c, D. Covita^b, D. Gotta, A. Hirtl^c, A. Gruber^c, P. Indelicato^d, E.-O. Le Bigot^d, M. Nekipelov, J. M. F. dos Santos^b, S. Schlessler^d, P. Schmid^c, Th. Strauch, L. M. Simons^e, J. F. C. A. Veloso^b, J. Zmeskal^c

The high statistics measurement of pionic deuterium (PSI experiment R-06.03) constitutes a natural completion of experiment R-98.01 set up at the Paul Scherrer Institut (PSI), Switzerland, which resulted in a new precision determination of the hadronic shift ϵ_{1s} and width Γ_{1s} of the pionic hydrogen ground state [1, 2].

The hadronic shift in pionic deuterium, when determined to a comparable precision than in pionic hydrogen will provide a constraint for the isoscalar and isovector scattering length a^+ and a^- and allow for the determination of the low-energy constant f_1 [3]. Furthermore, the hadronic width is directly related to pion production at threshold. The production reaction $pp \rightarrow d\pi^+$ is connected to absorption $d\pi^+ \rightarrow pp$ by detailed balance, which in the case of charge symmetry is equal to $d\pi^- \rightarrow nn$. These processes will become calculable at the percent level within the framework of Chiral Perturbation Theory in the near future. The most precise experimental values for the strong-interaction shift ϵ_{1s} and width Γ_{1s} in pionic deuterium are reported to be [4]

$$\epsilon_{1s} = -2468 \pm 55 \text{ meV} (\pm 2.2\%) \quad (1)$$

$$\Gamma_{1s} = 1193 \pm 129 \text{ meV} (\pm 11\%). \quad (2)$$

The πD measurement was performed in July and August 2006 at the $\pi E5$ channel of the ring cyclotron of the Paul Scherrer Institut (PSI) which provides a high intensity low energy pion beam. The experimental set-up consists of the cyclotron trap II, a cryogenic target, a reflection-type crystal spectrometer equipped with spherically bent crystals and a large-area CCD array for position-sensitive X-ray detection.

Nearly 10000 πD events have been detected (Fig.1) which have been measured at the three different target densities equivalent to 3.5, 10 and 28 bar to be sensitive to effects like molecular formation ($\pi^- d + D_2 \rightarrow [(\pi dd)d]ee$) during the atomic cascade. If radiative de-excitation occurs from such molecular states small line shifts may falsify the extracted hadronic shift. In that case the pure hadronic value must be obtained from extrapolation to density zero.

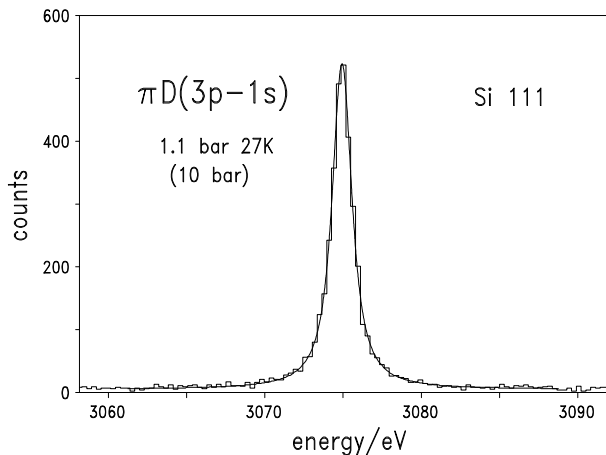


Fig. 1: The spectrum of $K\beta$ transition in pionic deuterium measured with a Si Bragg crystal in first order at a target density equivalent to 10 bar.

The energy calibration is performed with precisely measured $K\alpha$ fluorescence radiation of gallium (Fig.2). The gallium target was placed in the gas cell, which contained the deuterium. The X radiation was excited by means of an X-ray tube.

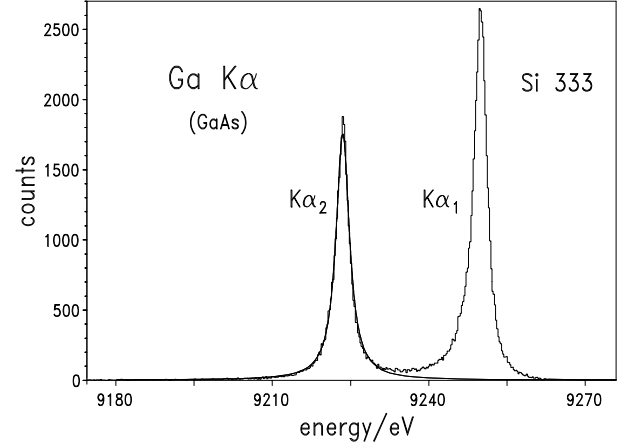


Fig. 2: Gallium $K\alpha$ transition measured in third order used for the energy calibration of the crystal spectrometer.

Preanalysis of the taken data shows, that it will be possible to decrease the uncertainty of the hadronic shift ϵ_{1s} to about 0.5% and of the hadronic width Γ_{1s} to 4% or better.

References:

- [1] <http://pihydrogen.web.psi.ch>.
- [2] Annual report IKP, 2005, jül-4212.
- [3] U. G. Meissner, U. Raha, and A. Rusetski, Phys. Lett. B 639 (2006) 478.
- [4] P. Hauser et al., Phys. Rev. C 58 (1998)R1869.

^a Dept. of Mat. Sci., Univ. Ioannina, Greece

^b Dept. of Phys., Univ. Coimbra, Portugal

^c SMI, Österr. Akademie d. Wiss., Vienna

^d Lab. Kastler-Brossel, Univ. P. et M. Curie, Paris

^e PSI, Switzerland

2 Theoretical Physics

Novel evaluation of the two-pion contribution to the nucleon isovector form-factors

M. Belushkin (Bonn), H.-W. Hammer (Bonn), and Ulf-G. Meißner (Bonn & FZJ)

We calculate the two-pion continuum contribution to the nucleon isovector spectral functions drawing upon the new high statistics measurements of the pion form factor by the CMD-2, KLOE, and SND collaborations [1]. The general structure of the spectral functions remains unchanged, but the magnitude increases by about 10%. Using the updated spectral functions, we calculate the contribution of the two-pion continuum to the nucleon isovector form factors and radii. We compare the isovector radii with simple rho-pole models and illustrate their strong underestimation in such approaches. Moreover, we give a convenient parametrization of the result for use in future form factor analyses.

References:

- [1] M. A. Belushkin, H. W. Hammer and U.-G. Meißner, Phys. Lett. B **633** (2006) 507 [arXiv:hep-ph/0510382].

Improved analysis of J/ψ decays into a vector meson and two pseudoscalars

T. A. Lähde (Bonn) and Ulf-G. Meißner (Bonn & FZJ)

Recently, the BES collaboration has published an extensive partial wave analysis of experimental data on $J/\psi \rightarrow \phi\pi^+\pi^-$, $J/\psi \rightarrow \omega\pi^+\pi^-$, $J/\psi \rightarrow \phi K^+K^-$ and $J/\psi \rightarrow \omega K^+K^-$. These new results are analyzed in [1], with full account of detection efficiencies, in the framework of a chiral unitary description with coupled-channel final state interactions between $\pi\pi$ and $K\bar{K}$ pairs. The emission of a dimeson pair is described in terms of the strange and nonstrange scalar form factors of the pion and the kaon, which include the final state interaction and are constrained by unitarity and by matching to the next-to-leading-order chiral expressions. This procedure allows for a calculation of the S-wave component of the dimeson spectrum including the $f_0(980)$ resonance, and for an estimation of the low-energy constants of chiral perturbation theory, in particular the large N_c suppressed constants L_4^r and L_6^r . The decays in question are also sensitive to physics associated with OZI violation in the 0^{++} channel. It is found that the S-wave contributions to $\phi\pi^+\pi^-$, ϕK^+K^- and $\omega\pi^+\pi^-$ given by the BES partial-wave analysis may be very well fitted up to a dimeson center-of-mass energy of 1.2 GeV, for a large and positive value of L_4^r and a value of L_6^r compatible with zero. An accurate determination of the amount of OZI violation in the $J/\psi \rightarrow \phi\pi^+\pi^-$ decay is achieved, and the S-wave contribution to ωK^+K^- near threshold is predicted.

References:

- [1] T. A. Lähde and U.-G. Meißner, Phys. Rev. D **74** (2006) 034021 [arXiv:hep-ph/0606133].

Chiral corrections to the Roper mass

B. Borasoy (Bonn), P. C. Bruns (Bonn), Ulf-G. Meißner (Bonn & FZJ), and R. Lewis (Regina)

We analyze the quark mass dependence of the Roper mass to one-loop order in relativistic baryon chiral perturbation theory. The loop integrals are evaluated using infrared regularization which preserves chiral symmetry and establishes a chiral counting scheme. The derived chiral expansion of the Roper mass may prove useful for chiral extrapolations of lattice data. For couplings of natural size the quark mass dependence of the Roper mass is similar to the one of the nucleon.

References:

- [1] B. Borasoy, P. C. Bruns, U.-G. Meißner and R. Lewis, Phys. Lett. B **641** (2006) 294 [arXiv:hep-lat/0608001].

On the chiral effective meson-baryon Lagrangian at third order

M. Frink (Bonn) and Ulf-G. Meißner (Bonn & FZJ)

We show that the recently constructed complete and “minimal” third order meson-baryon effective chiral Lagrangian can be further reduced from 84 to 78 independent operators.

References:

- [1] M. Frink and U.-G. Meißner, Eur. Phys. J. A **29** (2006) 255 [arXiv:hep-ph/0609256].

K^-p scattering length from scattering experiments

B. Borasoy (Bonn), Ulf-G. Meißner (Bonn & FZJ), R. Nißler (Bonn)

The strong K^-p scattering length is extracted within chiral SU(3) unitary approaches from a very large variety of fits to low-energy K^-p scattering data [1]. Very good overall agreement with available scattering data is obtained and the resulting scattering length is compared with the new accurate kaonic hydrogen data from DEAR. The pole structures of the obtained fits to experiment are critically examined.

References:

- [1] B. Borasoy, U.-G. Meißner and R. Nißler, Phys. Rev. C **74** (2006) 055201 [arXiv:hep-ph/0606108].

On the extraction of the quark mass ratio $(m_d - m_u)/m_s$ from $\Gamma(\eta' \rightarrow \pi^0 \pi^+ \pi^-)/\Gamma(\eta' \rightarrow \eta \pi^+ \pi^-)$

B. Borasoy (Bonn), Ulf-G. Meißner (Bonn & FZJ), R. Nisler (Bonn)

The claim that the light quark mass ratio $(m_d - m_u)/m_s$ can be extracted from the decay width ratio $\Gamma(\eta' \rightarrow \pi^0 \pi^+ \pi^-)/\Gamma(\eta' \rightarrow \eta \pi^+ \pi^-)$ is critically investigated within a U(3) chiral unitary framework [1]. The influence of the recent VES data on the $\eta' \rightarrow \eta \pi^+ \pi^-$ decay is also discussed.

References:

- [1] B. Borasoy, U.-G. Meißner and R. Nisler, Phys. Lett. B **643** (2006) 41 [arXiv:hep-ph/0609010].

T-odd correlations in radiative K_{l3}^+ decays and chiral perturbation theory

E. H. Müller (Bonn), B. Kubis (Bonn), Ulf-G. Meißner (Bonn & FZJ)

The charged kaon decay channel $K_{l3\gamma}^+$ allows for studies of direct CP violation, possibly due to non-standard mechanisms, with the help of T-odd correlation variables. In order to be able to extract a CP-violating signal from experiment, it is necessary to understand all possible standard model phases that also produce T-odd asymmetries. We complement earlier studies by considering strong interaction phases in hadronic structure functions that appear at higher orders in chiral perturbation theory, and compare our findings to other potential sources of asymmetries [1].

References:

- [1] E. H. Müller, B. Kubis and U.-G. Meißner, Eur. Phys. J. C **48** (2006) 427 [arXiv:hep-ph/0607151].

$B_{s,d} \rightarrow \gamma\gamma$ decay in the model with one universal extra dimension

G. Devidze (Tbilisi), A. Liparteliani (Tbilisi), and Ulf-G. Meißner (Bonn & FZJ)

We estimate the beyond the Standard Model (SM) contribution to the $B_{s,d} \rightarrow \gamma\gamma$ double radiative decay in the framework of the model with one universal extra dimension. This contribution gives a $\sim 3(6)\%$ enhancement of the branching ratio calculated in the SM for $B_{s(d)} \rightarrow \gamma\gamma$ [1].

References:

- [1] G. Devidze, A. Liparteliani and U.-G. Meißner, Phys. Lett. B **634** (2006) 59 [arXiv:hep-ph/0510022].

The Triton and three-nucleon force in nuclear lattice simulations

B. Borasoy (Bonn), H. Krebs (Bonn) , D. Lee (North Carolina), and Ulf-G. Meißner (Bonn & FZJ)

We study the triton and three-nucleon force at lowest chiral order in pionless effective field theory both in the Hamiltonian and Euclidean nuclear lattice formalism [1]. In the case of the Euclidean lattice formalism, we derive the exact few-body worldline amplitudes corresponding to the standard many-body lattice action. This will be useful for setting low-energy coefficients in future nuclear lattice simulations. We work in the Wigner SU(4)-symmetric limit where the S-wave scattering lengths 1S_0 and 3S_1 are equal. By comparing with continuum results, we demonstrate for the first time that the nuclear lattice formalism can be used to study few-body nucleon systems.

References:

- [1] B. Borasoy, H. Krebs, D. Lee and U.-G. Meißner, Nucl. Phys. A **768** (2006) 179 [arXiv:nucl-th/0510047].

Testing the nature of the $\Lambda(1520)$ resonance in proton-induced production

L. Roca (Murcia) , C. Hanhart, E. Oset (Valencia), and Ulf-G. Meißner (Bonn & FZJ)

The $\Lambda(1520)$ resonance has been recently studied in a unitarized coupled channel formalism with $\pi\Sigma(1385)$, $K\Xi(1530)$, $\bar{K}N$ and $\pi\Sigma$ as constituents blocks. We provide a theoretical study of the predictions of this model in physical observables of the $pp \rightarrow pK^+K^-p$ and $pp \rightarrow pK^+\pi^0\pi^0\Lambda$ reactions [1]. In particular, we show that the ratio between the $\pi^0\pi^0\Lambda$ and K^-p mass distributions can provide valuable information on the ratio of the couplings of the $\Lambda(1520)$ resonance to $\pi\Sigma(1385)$ and $\bar{K}N$ that the theory predicts. Calculations are done for energies which are accessible in an experimental facility like COSY at Jülich or the developing CSR facility at Lanzhou.

References:

- [1] L. Roca, C. Hanhart, E. Oset and U.-G. Meißner, Eur. Phys. J. A **27** (2006) 373 [arXiv:nucl-th/0602016].

The reaction $\pi N \rightarrow \pi\pi N$ in a meson-exchange approach

S. Schneider, S. Krewald, and Ulf-G. Meißner (Bonn & FZJ)

A resonance model for two-pion production in the pion-nucleon reaction is developed that includes information obtained in the analysis of pion-nucleon scattering in a meson-exchange model [1]. The baryonic resonances $\Delta(1232)$, $N^*(1440)$, $N^*(1520)$, $N^*(1535)$, and $N^*(1650)$ are included. The model reproduces the total cross sections up to kinetic energies of the incident pion of 350 MeV and obtains the shapes of the differential cross sections in reasonable agreement with the data.

References:

- [1] S. Schneider, S. Krewald and U.-G. Meißner, Eur. Phys. J. A **28** (2006) 107 [arXiv:nucl-th/0603040].

Omega-phi mixing in chiral perturbation theory

A. Kucurkarlan (Canakkale) and Ulf-G. Meißner (Bonn & FZJ)

We investigate omega-phi meson mixing to leading order in chiral perturbation theory utilizing the antisymmetric tensor field formulation [1]. We update the quark mass ratio R from rho-omega mixing, $R = 42 \pm 4$.

References:

- [1] A. Kucurkarlan and U.-G. Meißner, Mod. Phys. Lett. A **21** (2006) 1423 [arXiv:hep-ph/0603061].

The nucleon axial-vector coupling beyond one loop

V. Bernard (Strasbourg) and Ulf-G. Meißner (Bonn & FZJ)

We analyze the nucleon axial-vector coupling to two loops in chiral perturbation theory [1]. We show that chiral extrapolations based on this representation require lattice data with pion masses below 300 MeV.

References:

- [1] V. Bernard and U.-G. Meißner, Phys. Lett. B **639** (2006) 278 [arXiv:hep-lat/0605010].

Isospin-breaking corrections in the pion-deuteron scattering length

Ulf-G. Meißner (Bonn & FZJ), U. Raha (Bonn), and A. Rusetsky (Bonn)

It is shown that isospin-breaking corrections to the pion-deuteron scattering length can be very large, because of the vanishing of the isospin-symmetric contribution to this scattering length at leading order in chiral perturbation theory [1]. We further demonstrate that these corrections can explain the bulk of the discrepancy between the recent experimental data on pionic hydrogen and pionic deuterium. We also give the first determination of the electromagnetic low-energy constant f_1 .

References:

- [1] U.-G. Meißner, U. Raha and A. Rusetsky, Phys. Lett. B **639** (2006) 478 [arXiv:nucl-th/0512035].

Kaon-nucleon scattering lengths from kaonic deuterium experiments

Ulf-G. Meißner (Bonn & FZJ), U. Raha (Bonn), and A. Rusetsky (Bonn)

The extraction of the S-wave kaon-nucleon scattering lengths a_0 and a_1 from a combined analysis of existing kaonic hydrogen and synthetic deuterium data has been carried out within the framework of a low-energy effective field theory. It turns out that with the present DEAR central values for the kaonic hydrogen ground-state energy and width, a solution for a_0 and a_1 exists only in a restricted domain of input values for the kaon-deuteron scattering length. Consequently, measuring this scattering length imposes stringent constraints on the theoretical description of the kaon-deuteron interactions at low energies.

References:

- [1] U.-G. Meißner, U. Raha and A. Rusetsky, Eur. Phys. J. C **47** (2006) 473 [arXiv:nucl-th/0603029].

Resonances and final state interactions in the reaction $pp \rightarrow pK^+\Lambda$

A. Sibirtsev (Bonn), J. Haidenbauer, H.-W. Hammer (Bonn), and S. Krewald

A study of the strangeness production reaction $pp \rightarrow pK^+\Lambda$ for excess energies of $\epsilon \leq 150$ MeV, accessible at high-luminosity accelerator facilities like COSY, is presented. Methods to analyze the Dalitz plot distribution and angular spectra in the Jackson and helicity frames are worked out and suitable observables for extracting information on low lying resonances that couple to the $K\Lambda$ system and for determining the Λp effective-range parameters from the final state interaction are identified and discussed. Furthermore, the chances for identifying the reaction mechanism of strangeness production are investigated. The results are published in Ref. [1].

References:

- [1] A. Sibirtsev, J. Haidenbauer, H. W. Hammer and S. Krewald, Eur. Phys. J. A **27**, 269 (2006) [arXiv:nucl-th/0512059].

Aspects of ϕ -meson production in proton-proton collisions

A. Sibirtsev (Bonn), J. Haidenbauer, and U.-G. Meißner (Bonn & FZJ)

We analyze near-threshold cross section data for the reaction $pp \rightarrow pp\phi$ published by the DISTO Collaboration and recent, still preliminary results presented by the ANKE Collaboration. We formulate a procedure to evaluate the OZI ratio at low energies by taking into account corrections from the kinematics and the final-state interaction. Combining the new data with the few measurements available at higher energies we give a limit for the OZI rule violation. We also demonstrate and discuss the effect of a possible contribution from a five-quark baryonic resonance coupled to the ϕp system on the $pp \rightarrow pp\phi$ cross section and the ϕp and pp invariant mass spectra. The results are published in Ref. [1].

References:

- [1] A. Sibirtsev, J. Haidenbauer and U.-G. Meißner, Eur. Phys. J. A **27**, 263 (2006) [arXiv:nucl-th/0512055].

Near threshold $p\bar{p}$ enhancement in B and J/Ψ decay

J. Haidenbauer, Ulf-G. Meißner (Bonn & FZJ), A. Sibirtsev (Bonn)

The near-threshold enhancement in the $p\bar{p}$ invariant mass spectrum from the $B^+ \rightarrow K^+ p\bar{p}$ decay reported recently by the BaBar Collaboration is studied within the Jülich $N\bar{N}$ model. We illustrate that the invariant mass dependence of the $p\bar{p}$ spectrum close to the threshold can be reproduced by the final state interactions. This explanation is in line with our previous analysis of the $p\bar{p}$ invariant mass spectrum from the $J/\Psi \rightarrow \gamma p\bar{p}$ decay measured by the BES Collaboration. We also comment on a structure found recently in the $\pi^+ \pi^- \eta'$ mass spectrum of the radiative J/Ψ decay by the BES Collaboration. In particular we argue that one should be rather cautious in bringing this structure in connection with the enhancement found in the $p\bar{p}$ invariant mass spectrum or with the existence of $N\bar{N}$ bound states. The results are published in Ref. [1].

References:

- [1] J. Haidenbauer, U.-G. Meißner and A. Sibirtsev, Phys. Rev. D **74**, 017501 (2006) [arXiv:hep-ph/0605127].

Comment on 'Mass and $K\Lambda$ coupling of the $N^*(1535)$ '

A. Sibirtsev (Bonn), J. Haidenbauer, Ulf-G. Meißner (Bonn & FZJ)

We comment on a recent paper by B.C. Liu and B.S. Zou [1] where it was argued that the coupling of the $N^*(1535)$ to $K\Lambda$ is even larger than its coupling to the ηN channel. Specifically, we point out that recently measured Dalitz plot distributions for $pp \rightarrow pK^+\Lambda$ provide clear evidence for the importance of $(p\Lambda)$ final-state interactions in this reaction and, at the same time, exclude a decisive role of the $N^*(1535)$ resonance, in contradiction to claims made by Liu and Zou. The results are published in Ref. [2].

References:

- [1] B.C. Liu and B.S. Zou, Phys. Rev. Lett. **96**, 042002 (2006).
- [2] A. Sibirtsev, J. Haidenbauer and U.-G. Meißner, Phys. Rev. Lett. **98**, 049903 (2007).

On the strong energy dependence of the $e^+e^- \leftrightarrow p\bar{p}$ amplitude near threshold

J. Haidenbauer, H.-W. Hammer (Bonn), Ulf-G. Meißner (Bonn & FZJ), A. Sibirtsev (Bonn)

We study the energy dependence of the $e^+e^- \rightarrow p\bar{p}$ cross section close to the two-nucleon threshold, recently reported by the BaBar collaboration. Our analysis also includes the $\bar{p}p \rightarrow e^+e^-$ data collected by PS170 collaboration and the $e^+e^- \rightarrow N\bar{N}$ data from the FENICE collaboration. We show that the near-threshold enhancement in the $e^+e^- \rightarrow p\bar{p}$ cross section can be explained by the final-state interaction between proton and antiproton in the 3S_1 partial wave, utilizing the Jülich nucleon-antinucleon model. As a consequence, the strong dependence of the proton electromagnetic form factors on the momentum transfer close to the two-nucleon threshold is then likewise driven by this final-state interaction effect. This result is in line with our previous studies of the near-threshold enhancement of the $p\bar{p}$ invariant mass spectrum seen in the $J/\Psi \rightarrow \gamma p\bar{p}$ decay by the BES collaboration and in the $B^+ \rightarrow p\bar{p}K^+$ decay by the BaBar collaboration. The results are published in Ref. [1].

References:

- [1] J. Haidenbauer, H. W. Hammer, U.-G. Meißner and A. Sibirtsev, Phys. Lett. B **643**, 29 (2006) [arXiv:hep-ph/0606064].

Phenomenology of the Λ/Σ^0 production ratio in pp collisions

A. Sibirtsev (Bonn), J. Haidenbauer, H.-W. Hammer (Bonn) and U.-G. Meißner (Bonn & FZJ)

We show that the recently measured asymmetry in helicity-angle spectra of the Λ -hyperons, produced in the reaction $pp \rightarrow K^+ \Lambda p$ reaction, and the energy dependence of the total $pp \rightarrow K^+ \Lambda p$ cross section can be explained consistently by the same Λp final-state interaction. Assuming that there is no final-state interaction in the $\Sigma^0 p$ channel, as suggested by the available data, we can also reproduce the energy dependence of the Λ/Σ^0 production ratio and, in particular, the rather large ratio observed near the reaction thresholds. The nominal ratio of the Λ and Σ^0 production amplitudes squared, i.e. when disregarding the final-state interaction, turns out to be about 3, which is in line with hyperon production data from proton and nuclear targets available at high energies. The results are published in Ref. [1].

References:

- [1] A. Sibirtsev, J. Haidenbauer, H. W. Hammer and U.-G. Meißner, Eur. Phys. J. A **29**, 363 (2006) [arXiv:hep-ph/0608098].

Kaon-Deuteron Scattering at Low Energies

A. Sibirtsev (Bonn), J. Haidenbauer, S. Krewald and Ulf-G. Meißner (Bonn & FZJ)

We review the experimental information on the K^+d reaction for K^+ -meson momenta below 800 MeV/c. The data are analysed within the single scattering impulse approximation – utilizing the Jülich kaon-nucleon model – that allows to take into account effects due to the Fermi motion of the nucleons in the deuteron and the final three-body kinematics for the break-up and charge exchange reaction. We discuss the consistency between the data available for the $K^+d \rightarrow K^+np$, $K^+d \rightarrow K^0pp$ and $K^+d \rightarrow K^+d$ reactions and the calculations based on the spectator model formalism. The results are published in Ref. [1].

References:

- [1] A. Sibirtsev, J. Haidenbauer, S. Krewald and U.-G. Meißner, J. Phys. G **32**, R395 (2006) [arXiv:nucl-th/0608028].

Processes with high transferred momenta can give unique information on the short-range structure of nuclei if the reaction mechanisms are well established. Except in the Δ -isobar region of $0.4 - 0.6$ GeV, the unpolarized cross section $d\sigma/d\Omega(pd \rightarrow dp)_{\theta_{cm}=180^\circ}$ can be explained semi-quantitatively within the one-nucleon-exchange (ONE) mechanism with the Paris NN-potential up to large nucleon momenta in the deuteron, $k \approx 1$ GeV/c. A similar result was found for the inclusive disintegration of the deuteron on nuclear targets. However, for both reactions the experimental values of the tensor analyzing power T_{20} disagree strongly with the ONE calculations already for $k > 0.3$ GeV/c. This might be due to more complicated mechanisms, such as Δ -isobar excitation.

Isospin considerations reduce the Δ -mechanism in the $pd \rightarrow \{pp\}_s n$ cross section by a factor of nine compared to $pd \rightarrow dp$ [1]. Here $\{pp\}_s$ denotes a 1S_0 final pp pair. Though the ONE amplitude does not suffer the isospin suppression, it has a node at $k \sim 0.4$ GeV/c arising from the NN-repulsive core [1]. The comparison of the two reactions might therefore allow one to get a clearer picture of the relative importance of the ONE and Δ -contributions.

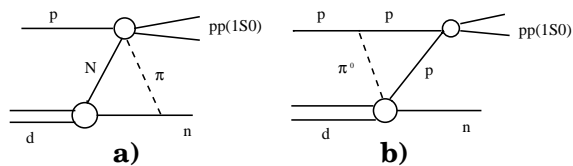


Fig. 1: The one-pion-exchange (OPE) mechanisms considered for the $pd \rightarrow \{pp\}_s n$ reaction: (a) OPE-I; (b) OPE-II.

The unpolarized $pd \rightarrow \{pp\}_s n$ differential cross section has been measured at $0.6 - 1.9$ GeV for neutron c.m. angles $\theta_{cm} \approx 180^\circ$ [2]. Events were selected with an excitation energy $E_{pp} < 3$ MeV, corresponding to the 1S_0 diproton state. An analysis of these data was performed in Ref. [3] within a model originally suggested to describe the $pd \rightarrow dp$ reaction. This included the ONE, single pN scattering, and the excitation of the Δ -isobar. This showed that for a wide range of commonly used NN potentials the contribution of the ONE mechanism is actually quite small. Only for a soft NN potential, such as the CD Bonn, and with distortion taken into account in the initial and final states, can a qualitative agreement with data be achieved [3]. Harder NN -potentials, *e.g.* the Paris, generate intense high-momentum components in the NN wave functions. These lead to very large ONE contributions that are in strong disagreement with the $pd \rightarrow \{pp\}_s n$ data [2]. This is the most interesting result of the analysis.

In a new approach [4], the $pd \rightarrow \{pp\}_s n$ reaction is related to the $\pi^0 d \rightarrow pn$ and $pN \rightarrow \{pp\}_s \pi$ subprocesses using two different one-pion-exchange (OPE) diagrams

(Fig. 1). Reasonable agreement could be obtained with the data below 1 GeV within either of these models. The similarity of the energy dependence of the $pd \rightarrow \{pp\}_s n$ and $pd \rightarrow dp$ cross sections, and the small ratio of about 1.5% in the production of $\{pp\}_s$ and deuteron final states, follow naturally within the OPE models.

The agreement obtained for the OPE-II model points to an important contribution below 1 GeV from the Δ -isobar, which enters *via* the $\pi^0 d \rightarrow pn$ subprocess. On the other hand, it suggests that the ONE mechanism is relatively unimportant. To a large extent, these conclusions are compatible with the results of the previous analysis of this reaction [3]. Using the $pp \rightarrow \{pp\}_s \pi^0$ data at 0.8 GeV [5] within the OPE-I model, agreement with the experimental results [2] can be achieved by assuming a baryon (or Reggeon) exchange mechanism for the $pN \rightarrow \{pp\}_s \pi$ reaction. To test these predictions requires the measurement of the ratio of π^- and π^0 production in the $pN \rightarrow \{pp\}_s \pi$ reaction.

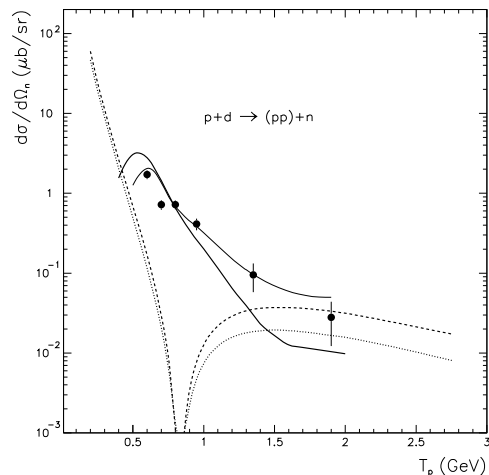


Fig. 2: Differential cross section for the $pd \rightarrow \{pp\}_s n$ reaction [2]. The full thick curve shows the OPE-II results. The ONE predictions [3] with the CD Bonn potential are shown by the dashed (Born approximation) and dotted (with distortions) curves. The coherent sum of the OPE-II and the ONE is shown by the thin full line.

^a Joint Institute for Nuclear Research, Dubna, Russia

^b Physics & Astronomy Dept., UCL, London, UK

References:

- [1] O. Imambekov and Yu.N. Uzikov, *Yad. Fiz.* **52** (1990) 1362.
- [2] V.I. Komarov *et al.*, *Phys. Lett. B* **553** (2003) 179.
- [3] J. Haidenbauer and Yu.N. Uzikov, *Phys. Lett. B* **562** (2003) 227.
- [4] Yu.N. Uzikov, J. Haidenbauer, and C. Wilkin, *Phys. Rev. C* **75** (2007) 014008 [arXiv:nucl-th/0611006].
- [5] S. Dymov *et al.*, *Phys. Lett. B* **635** (2006) 270.

Insights on scalar mesons from their radiative decays

Yu. Kalashnikova (ITEP), A. Kudryavtsev (ITEP), A. V. Nefediev (ITEP), J. Haidenbauer, C. Hanhart

We estimate the rates for radiative transitions of the lightest scalar mesons $f_0(980)$ and $a_0(980)$ to the vector mesons ρ and ω . We argue that measurements of the radiative decays of those scalar mesons can provide important new information on their structure. The results are published in [1].

References:

- [1] Yu. Kalashnikova, A. E. Kudryavtsev, A. V. Nefediev, J. Haidenbauer and C. Hanhart, Phys. Rev. C **73**, 045203 (2006) [arXiv:nucl-th/0512028].

Hyperon-nucleon interactions – a chiral effective field theory approach

H. Polinder, J. Haidenbauer, Ulf-G. Meißner (Bonn & FZJ)

We have constructed the leading order (LO) hyperon-nucleon (YN) potential in a chiral effective field theory (EFT) approach based on a modified Weinberg power counting. The potential consists of one-pseudoscalar-meson exchanges and non-derivative four-baryon contact terms. The YN interactions are related via $SU(3)$ symmetry, the nucleon-nucleon (NN) interaction is not considered explicitly since it can not be described with a LO EFT. We solve a regularized Lippmann-Schwinger equation and show that a good description of the available YN scattering data is possible with five free parameters. The potential can be used as further input for hypernucleus and hypernuclear matter calculations. Preliminary hypertriton calculations yielded the correct hypertriton binding energy. The results are published in Ref. [1].

References:

- [1] H. Polinder, J. Haidenbauer and U.-G. Meißner, Nucl. Phys. A **779**, 244 (2006) [arXiv:nucl-th/0605050].

On the sign of the $\pi\rho\omega$ coupling constant

K. Nakayama, Yongseok Oh (Athens), J. Haidenbauer, T.-S. H. Lee (Argonne)

It is shown that the relative sign between the $NN\omega$ and $\pi\rho\omega$ coupling constants can be determined most sensitively from ω production processes in NN collisions. Recent data on these reactions clearly favor the sign of the $\pi\rho\omega$ coupling constant which is opposite to that inferred from studies of the photoproduction reaction in combination with the vector meson dominance assumption and used by many authors. Implication of this finding in the description of other reactions is discussed. The results are available at [1].

References:

- [1] K. Nakayama, Y. Oh, J. Haidenbauer and T. S. Lee, arXiv:nucl-th/0611101.

Unitarity cutting rules for the nucleus excitation and topological cross sections in hard production off nuclei from nonlinear k_t -factorization

N.N. Nikolaev and W. Schäfer (INP Cracow)

At the partonic level, a typical final state in small- x deep inelastic scattering off nuclei and hard proton-nucleus collisions can be characterized by the multiplicity of color-excited nucleons. Within reggeon field theory, each color-excited nucleon is associated with the unitarity cut of the pomeron exchanged between the projectile and nucleus. We derive the unitarity rules for the multiplicity of excited nucleons, alias cut pomerons, alias topological cross sections, for typical hard dijet production processes. We demonstrate how the coupled-channel non-Abelian intranuclear evolution of color dipoles, inherent to pQCD, gives rise to the reggeon field theory diagrams for final states in terms of the uncut, and two kinds of cut, pomerons. Upon the proper identification of the uncut and cut pomeron exchanges, the topological cross sections for dijet production follow in a straightforward way from the earlier derived nonlinear k_t -factorization quadratures for the inclusive dijet cross sections. The concept of a coherent (collective) nuclear glue proves extremely useful for the formulation of reggeon field theory vertices of multipomeron - cut and uncut - couplings to particles and between themselves. A departure of our unitarity cutting rules from the ones suggested by the pre-QCD Abramovsky-Kancheli-Gribov rules, stems from the coupled-channel features of intranuclear pQCD. We propose a multiplicity re-summation as a tool for the isolation of topological cross sections for single-jet production. The results are published in Ref. [1].

References:

- [1] N. N. Nikolaev and W. Schäfer, Phys. Rev. D **74** (2006) 074021

Quenching of Leading Jets and Particles: the p_t Dependent Landau-Pomeranchuk-Migdal effect from Nonlinear k_t -Factorization

N.N. Nikolaev, W. Schäfer

We report the first derivation of the Landau-Pomeranchuk-Migdal effect for leading jets at fixed values of the transverse momentum p_t in the beam fragmentation region of hadron-nucleus collisions from RHIC (Relativistic Heavy Ion Collider) to LHC (Large Hadron Collider). The major novelty of this work is a derivation of the missing virtual radiative pQCD correction to these processes - the real-emission radiative corrections are already available in the literature. We manifestly implement the unitarity relation, which in the simplest form requires that upon summing over the virtual and real-emission corrections the total number of scattered quarks must exactly equal unity. For the free-nucleon target, the leading jet spectrum is shown to satisfy the familiar linear Balitsky-Fadin-Kuraev-Lipatov leading $\log(1/x)$ (LL-1/ x) evolution. For nuclear targets, the nonlinear k_t -factorization for the LL-1/ x evolution of the leading jet spectrum is shown to exactly match the equally nonlinear LL-1/ x evolution of the collective nuclear glue - there emerges a unique linear k_t -factorization relation between the two nonlinear evolving nuclear observables. We argue that within the standard dilute uncorrelated nucleonic gas treatment of heavy nuclei, in the finite energy range from RHIC to LHC, the leading jet spectrum can be evolved in the LL-1/ x Balitsky-Kovchegov approximation. We comment on the extension of these results to, and their possible reggeon field theory interpretation for, mid-rapidity jets at LHC. The results have been published in [1].

References:

- [1] N. N. Nikolaev and W. Schäfer, Phys. Rev. D **74** (2006) 014023

Glue in the pomeron from nonlinear k_{\perp} -factorization

N.N. Nikolaev, W. Schäfer, B.G. Zakharov (Landau Inst., Moscow), V.R. Zoller (ITEP, Moscow)

We derive the nonlinear k_{\perp} -factorization for the spectrum of jets in high-mass diffractive deep inelastic scattering as a function of three hard scales - the virtuality of the photon Q^2 , the transverse momentum of the jet and the saturation scale Q_A . In contrast to all other hard reactions studied so far, we encounter a clash between the two definitions of the glue in the pomeron – from the inclusive spectrum of leading quarks and the small- β evolution of the diffractive cross section. This clash casts a further shadow on customary applications of the familiar collinear factorization to a pQCD analysis of diffractive deep inelastic scattering. The results are published in Ref. [1].

References:

- [1] N. N. Nikolaev, W. Schäfer, B. G. Zakharov and V. R. Zoller, JETP Lett. **83** (2006) 192

Investigations of Subthreshold resonances with the Trojan Horse Method [1]

G. Baur, S. Typel (GSI, Darmstadt)

In the Trojan horse method a two-body reaction $A + x \rightarrow C + c$ that is relevant for nuclear astrophysics is studied experimentally by a reaction $A + a \rightarrow C + c + b$ where a is composed predominantly of clusters x and b . The continuous transition from negative energies E_{Ax} of the $A + x$ system to positive energies E_{Ax} is studied in a coupled channels model. It is pointed out that the Trojan horse method is a suitable tool to investigate subthreshold resonances.

References:

- [1] G.Baur and S. Typel, nucl-th/0604057

High-energy direct reactions with exotic nuclei and low-energy nuclear astrophysics [1]

G. Baur, S. Typel (GSI, Darmstadt)

A mini-review of indirect methods in nuclear astrophysics is given, with special emphasis on Coulomb dissociation and the Trojan horse method. Recent work on Coulomb dissociation and an effective-range theory of low-lying electromagnetic strength of halo nuclei is presented. Coulomb dissociation of a halo nucleus bound by a zero-range potential is proposed as a homework problem .

References:

[1] G.Baur and S. Typel, nucl-th/0601004

Electromagnetic strength of one- and two-neutron halo nuclei [1]

G. Baur, S. Typel*

Intermediate energy Coulomb excitation and dissociation is a useful tool for nuclear structure and astrophysics studies. Low-lying strength in nuclei far from stability was discovered by this method. The effective range theory for low-lying strength in one-neutron halo nuclei is summarized and extended to two-neutron halo nuclei. In the two-neutron case, the first neutron is excited by the photon into the continuum, the second neutron is ejected into the continuum by a shake off process. This is of special interest in view of recent rather accurate experimental results on the low-lying electric dipole strength in ^{11}Li .

References:

[1] G.Baur and S. Typel, nucl-th/0610082

* GSI, Darmstadt.

Transverse momentum distribution of vector mesons produced in ultraperipheral relativistic heavy ion collisions [1]

K.Hencken (Basel), G. Baur, and D.Trautmann (Basel)

We study the transverse momentum distribution of vector mesons produced in ultraperipheral relativistic heavy ion collisions (UPCs). In UPCs there is no strong interaction between the nuclei and the vector mesons are produced in photon-nucleus collisions where the (quasireal) photon is emitted from the other nucleus. Exchanging the role of both ions leads to interference effects. A detailed study of the transverse momentum distribution which is determined by the transverse momentum of the emitted photon, the production process on the target and the interference effect is done. We study the total unrestricted cross section and those, where an additional electromagnetic excitation of one or both of the ions takes place in addition to the vector meson production, in the latter case small impact parameters are emphasized.

References:

- [1] Kai Hencken, Gerhard Baur and Dirk Trautmann,
Phys. Rev. Lett. 96(2006)012303

How accurate are the ponium breakup calculations?[1]

D.Trautmann (Basel), T.Heim (Basel), K.Hencken (Basel), and G. Baur

For the analysis of the experiment DIRAC very precise calculations of electromagnetic excitation and ionization cross sections for ponium in the target material are required. Our calculations incorporate a fully quantum mechanical treatment of the electromagnetic transitions in ponium and target-elastic(coherent) as well as target-inelastic (incoherent) scattering processes within the framework of Dirac-Hartree-Fock theory. Higher order contributions have been calculated in the Glauber approximation.

References:

- [1] Workshop on exotic hadronic atoms, deeply bound kaonic nuclear states and antihydrogen, ECT* June 19-24, 2006 hep-ph/0610201 , p.20

* Institut für Physik, Universität Basel, Schweiz

Scalar Casimir effect between Dirichlet spheres or a plate and a sphere

A. Bulgac (Seattle), P. Magierski (Warsaw), A. Wirzba (FZJ)

We present a simple formalism for the evaluation of the Casimir energy for two spheres and a sphere and a plane, in case of a scalar fluctuating field, valid at any separations. We compare the exact results with various approximation schemes and establish when such schemes become useful. The formalism can be easily extended to any number of spheres and/or planes in three or arbitrary dimensions, with a variety of boundary conditions or non-overlapping potentials/non-ideal reflectors. The results are published in Ref. [1].

References:

- [1] A. Bulgac, P. Magierski and A. Wirzba, Phys. Rev. D **73**, 025007 (2006) [arXiv:hep-th/0511056].

Neutron-proton mass difference in nuclear matter

Ulf-G. Meißner, A.M. Rakhimov (Tashkent), A. Wirzba, U.T. Yakhshiev (Tashkent & FZJ)

Isospin-breaking effects in nuclear matter are studied in the framework of a medium-modified Skyrme model. The proposed effective Lagrangian incorporates both the medium influence of the surrounding nuclear environment on the single nucleon properties and an explicit isospin-breaking effect in the mesonic sector. The approach predicts that the neutron-proton mass difference decreases in isospin-symmetric nuclear matter but by a very small amount only. The results can be found in Ref. [1].

References:

- [1] U.-G. Meißner, A.M. Rakhimov, A. Wirzba, U.T. Yakhshiev, FZJ-IKP-TH-2006-29, arXiv:nucl-th/0611066.

Periodic orbits in scattering from elastic voids

N. Søndergaard (Lund), P. Cvitanović (Atlanta), A. Wirzba (FZJ)

The scattering determinant for the scattering of waves from several obstacles is considered in the case of elastic solids with voids. The multi-scattering determinant displays contributions from periodic ray-splitting orbits. A discussion of the weights of such orbits is presented in Ref. [1].

References:

- [1] N. Søndergaard, P. Cvitanović and A. Wirzba, AIP Conf. Proc. (USA) **834**, 175 (2006) [arXiv:nlin.CD/0603043].

A force from nothing onto nothing: Casimir effect between bubbles in the Fermi sea

A. Wirzba (FZJ)

We report in Ref. [1] on a new force that acts on cavities (literally empty regions of space) when they are immersed in a background of non-interacting fermionic matter fields. The interaction follows from the obstructions to the (quantum mechanical) motions of the fermions in the Fermi sea caused by the presence of bubbles or other (heavy) particles immersed in the latter, as, for example, nuclei in the neutron sea in the inner crust of a neutron star. This effect resembles the traditional Casimir effect, which describes the attraction between two parallel metallic mirrors in vacuum. Here, however, the fluctuating (bosonic) electromagnetic fields are replaced by fermionic matter fields. Furthermore, the Casimir energy is inferred from the geometry-dependent part of the density of states, and its sign is not fixed, but oscillates according to the relative arrangement and distances of the cavities. In fact, with the help of Krein's trace formula, the quantum field theory calculation is mapped onto a quantum mechanical billiard problem of a point-particle scattered off a finite number of non-overlapping spheres or disks; i.e. classically hyperbolic (or even chaotic) scattering systems. This topic is relevant to the physics of neutron stars (nuclei or quark bubbles embedded in a neutron gas), to dilute Bose-Einstein-condensate bubbles inside the background of a Fermi-Dirac condensate, to buckyballs in liquid mercury and to superconducting droplets in a Fermi liquid.

References:

- [1] A. Wirzba, NATO Sci. Ser. II: Mathematics, Physics and Chemistry **213**, 229 (2006).

Casimir interaction between normal or superfluid grains in the Fermi sea

A. Wirzba (FZJ), A. Bulgac (Seattle), P. Magierski (Warsaw)

There exists an effective interaction of Casimir-type between obstacles (grains) in the Fermi sea that can be traced back to the obstructions of the sea-fermions caused by the presence of bubbles or heavy particles in the Fermi sea, such as nuclei in the neutron sea in the inner crust of a neutron star or superfluid grains in a normal Fermi liquid. It is shown that the fermionic Casimir problem for a system of spherical cavities can be solved exactly, since the calculation can be mapped onto a quantum mechanical billiard problem of a point-particle scattered off a finite number of non-overlapping spheres or discs. Finally, the map method is generalized to other Casimir systems, especially to the case of a fluctuating massless scalar field between two spheres or a sphere and a plate under Dirichlet boundary conditions [1].

References:

- [1] A. Wirzba, A. Bulgac and P. Magierski, *J. Phys. A: Math. Gen.* **39**, 6815 (2006) [arXiv:quant-ph/0511057].

Hyperon-nucleon interactions in effective field theory

H. Polinder

We have constructed the leading order hyperon-nucleon potential in a chiral Effective Field Theory approach. The chiral potential consists of one-pseudoscalar-meson exchanges and non-derivative four-baryon contact terms. The hyperon-nucleon interactions are derived using $SU(3)$ symmetry, the nucleon-nucleon interaction is not considered explicitly since it can not be described well with a leading order chiral Effective Field Theory. We solve a regularized Lippmann-Schwinger equation and show that a good description of the available hyperon-nucleon scattering data is possible with five free parameters. The chiral potential can be used as further input for hypernucleus and hypernuclear matter calculations. Preliminary hypertriton calculations yielded the correct hypertriton binding energy. This work has been published in Ref. [1].

References:

- [1] H. Polinder, arXiv:nucl-th/0612042.

Three-nucleon force effects in the analyzing powers of the d(pol.) p breakup at 130 MeV

A. Biegun, E. Stephan (Silesia U.), S. Kistryn, K. Bodek, I. Ciepal (Jagiellonian U.), A. Deltuva (Lisbon U.),
E. Epelbaum (Jefferson Lab), W. Glöckle (Ruhr U., Bochum), J. Golak (Jagiellonian U.),
N. Kalantar-Nayestanaki (Groningen, KVI), H. Kamada (Kyushu Inst. Tech.), M. Kis (Groningen, KVI),
B. Klos (Silesia U.), A. Kozela (Cracow, INP), J. Kuros-Zolnierczuk (Jagiellonian U.),
M. Mahjour-Shafiei (Groningen, KVI), U.-G. Meißner (Jülich, Forschungszentrum), A. Micherdzinska (Silesia U.),
A. Nogga (Jülich, Forschungszentrum), P.U. Sauer (Hannover U.), R. Skibinski, R. Sworst, H. Witala,
J. Zejma (Jagiellonian U.), W. Zipper (Silesia U.)

A measurement of the analyzing powers for the $^1\text{H}(d, pp)n$ breakup reaction at 130 MeV polarized deuteron beam energy was carried out at KVI Groningen. The experimental setup covered a large fraction of the phase space. Obtained tensor analyzing powers T_{22} for selected kinematical configurations have been compared to theoretical predictions based on various approaches: the rigorous Faddeev calculations using the realistic nucleon-nucleon potentials with and without three nucleon force (3NF) models, predictions of the chiral perturbation theory, and coupled channel calculations with the explicit degrees of freedom. In the presented configurations the results of all predictions are very close to one another and there are no significant 3NF influences. Not all of the data can be satisfactorily reproduced by the theoretical calculations. The results are published in [1].

References:

- [1] A. Biegun *et al.*, Acta Phys. Polon. B **37**, 213 (2006).

Compton Scattering on ^3He

D. Choudhury (Ohio U.), D.R. Phillips (Ohio U.), A. Nogga(Jülich, Forschungszentrum)

We present first calculations for Compton scattering on ^3He . The objective of the calculation is an extraction of the neutron polarizabilities. The results are published in [1].

References:

- [1] D. Choudhury, D. R. Phillips and A. Nogga, arXiv:nucl-th/0611032.

More on the infrared renormalization group limit cycle in QCD

E. Epelbaum (FZJ & Bonn), H.-W. Hammer (Bonn), Ulf-G. Meißner (Bonn & FZJ), A. Nogga

We present a detailed study of the recently conjectured infrared renormalization group limit cycle in QCD using chiral effective field theory [1]. It was conjectured that small increases in the up and down quark masses can move QCD to the critical trajectory for an infrared limit cycle in the three-nucleon system. At the critical quark masses, the binding energies of the deuteron and its spin-singlet partner are tuned to zero and the triton has infinitely many excited states with an accumulation point at the three-nucleon threshold. We exemplify three parameter sets where this effect occurs at next-to-leading order in the chiral counting. For one of them, we study the structure of the three-nucleon system in detail using both chiral and contact effective field theories. Furthermore, we investigate the matching of the chiral and contact theories in the critical region and calculate the influence of the limit cycle on three-nucleon scattering observables. The results are published in Ref. [1].

References:

- [1] E. Epelbaum, H. W. Hammer, U.-G. Meißner and A. Nogga, *Eur. Phys. J. C* **48** (2006) 169 [arXiv:hep-ph/0602225].

Lorentz boosted nucleon-nucleon potential applied to the ^3He -polarized(e-polarized, e' p)pn and ^3He -polarized(e-polarized, e' n)pp processes

J. Golak, R. Skibinski, H. Witala (Jagiellonian U.), W. Glöckle (Ruhr U., Bochum),
A. Nogga (Jülich, Forschungszentrum), H. Kamada (Kyushu Inst. Tech.)

We formulate an approximate relativistic framework for an analysis of the $^3\text{He}(e, e' p)pn$ and $^3\text{He}(e, e' n)pp$ reactions. Restricting the rescattering series to one term linear in the two-nucleon (2N) t-matrix we incorporate various relativistic features when calculating a nuclear current matrix element. These relativistic ingredients encompass the relativistic ^3He wave function based on the concept of the Lorentz boosted nucleon-nucleon potential together with the boosted 2N t-matrix, relativistic kinematics and relativistic single-nucleon current operator. This allows us to estimate the magnitude of relativistic effects not included in the standard nonrelativistic approach. The results are published in [1].

References:

- [1] J. Golak, R. Skibinski, H. Witala, W. Glöckle, A. Nogga and H. Kamada, arXiv:nucl-th/0605049.

Cross sections and tensor analyzing powers A_{yy} of the reaction ${}^1\text{H}(\text{d}, \text{pp})\text{n}$ in 'symmetric constant relative energy' geometries at $E_d = 19$ MeV.

J. Ley, C. Duweke, R. Emmerich, A. Imig, H. Paetz gen. Schieck (Cologne U.), J. Golak, H. Witala (Jagiellonian U.), E. Epelbaum (Jefferson Lab), A. Delgado, A.C. Fonseca (Lisbon U., CFNUL), W. Glöckle (Ruhr U. Bochum), U.-G. Meißner (Jülich, Forschungszentrum), A. Nogga (Jülich, Forschungszentrum), P.U. Sauer (Hannover U.)

We measured the cross sections and tensor analyzing powers of the ${}^1\text{H}(\text{d}, \text{pp})\text{n}$ breakup reaction at $E_d = 19$ MeV in four symmetric constant relative energy (SCRE) configurations. The data are compared with theoretical predictions from four different approaches: the first based on high-precision (semi)phenomenological potentials alone or, the second, combined with model three-nucleon forces, and the third based on chiral forces up to next-to-next-to-leading order (NNLO) in the chiral expansion. In these cases the Coulomb interaction is not included. In addition, a fourth approach consists in a comparison with predictions based on CD Bonn including the excitation and the Coulomb force. In all cases the measured cross sections are significantly below the theoretical values, whereas the magnitudes of the tensor analyzing powers agree within the error bars in three of the four cases. The apparent discrepancies in the breakup cross sections are similar to the known differences for the space-star breakup. This adds to the data base of unsolved low-energy discrepancies (puzzles). The results are published in [1].

References:

- [1] J. Ley *et al.*, Phys. Rev. C **73**, 064001 (2006).

Measurement of the ${}^2\text{H}(n,\gamma){}^3\text{H}$ reaction cross section between 10 and 550 keV

Y. Nagai (Osaka U.), T. Kobayashi (Tokyo Inst. Tech.), T. Shima (Osaka U.), T. Kikuchi,
K. Takaoka (Tokyo Inst. Tech.), M. Igashira (Tokyo Inst. Tech.), J. Golak, R. Skibinski,
H. Witala (Jagiellonian U.), A. Nogga (Jülich, Forschungszentrum), W. Glöckle (Bochum U.),
H. Kamada (Tokyo Inst. Tech.)

We have measured for the first time the cross section of the ${}^2\text{H}(n,\gamma){}^3\text{H}$ reaction at an energy relevant to big-bang nucleosynthesis by employing a prompt discrete γ -ray detection method. The outgoing photons have been detected by means of anti-Compton NaI(Tl) spectrometers with a large signal-to-noise ratio. The resulting cross sections are 2.23 ± 0.34 , 1.99 ± 0.25 , and $3.76 \pm 0.41 \mu\text{b}$ at $E_n = 30.5$, 54.2, and 531 keV, respectively. At $E_n = 30.5$ keV the cross section differs from the value reported previously by a factor of 2. Based on the present data the reaction rate has been obtained for temperatures in the range 107-1010 K. The astrophysical impact of the present result is discussed. The obtained cross sections are compared with a theoretical calculation based on the Faddeev approach, which includes meson exchange currents as well as a three-nucleon force. The results are published in [1].

References:

- [1] Y. Nagai *et al.*, Phys. Rev. C **74**, 025804 (2006).

New data for total ${}^3\text{He}(\gamma, \text{p})\text{D}$ and ${}^3\text{He}(\gamma, \text{pp})\text{n}$ cross sections compared to current theory

S. Naito, Y. Nagai, T. Shima, H. Makii, K. Mishima (Osaka U.), K. Tamura (Tokyo Inst. Tech.),
H. Toyokawa (AIST, Tsukuba), H. Ohgaki (AIST, Tsukuba), J. Golak, R. Skibinski, H. Witala (Jagiellonian U.),
W. Glöckle (Ruhr U., Bochum), A. Nogga (Jülich, Forschungszentrum), H. Kamada (Tokyo Inst. Tech.)

A simultaneous measurement of the cross sections of the ${}^3\text{He}(\gamma, \text{p})\text{D}$ and ${}^3\text{He}(\gamma, \text{pp})\text{n}$ reactions has been performed for the first time using monoenergetic pulsed γ -rays at $E_\gamma = 10.2$ and 16.0 MeV. Charged fragments from the reactions were detected with an efficiency of 100% using a 4π time projection chamber containing ${}^3\text{He}$ gas as an active target. The incident γ -ray flux was measured by a γ -ray detector. Both the track and energy loss signals of charged fragments were obtained in an off-line analysis and used to clearly identify the reaction channel. Thus, the (γ, p) and (γ, pp) cross sections have been determined with small uncertainty. A comparison of the new data to current theory based on the AV18+Urbana IX nuclear forces including π - and ρ -like meson exchange currents shows a severe discrepancy at 10.2 MeV, while at 16.0 MeV data and theory agree within about 12%. Three-nucleon force effects are small, but in general shift the theory in the correct direction. The results are published in [1].

References:

- [1] S. Naito *et al.*, Phys. Rev. C **73**, 034003 (2006).

Realistic few-body physics in the $dd \rightarrow \alpha \pi^0$ reaction

A. Nogga (Jülich, Forschungszentrum) , A.C. Fonseca (Lisbon U., CFNUL) , A. Gårdestig (South Carolina U.) ,
C. Hanhart (Jülich, Forschungszentrum) , C.J. Horowitz (Indiana U.) , G.A. Miller (Washington U., Seattle) ,
J.A. Niskanen (Helsinki U.) , U. van Kolck (Arizona U.)

We use realistic two- and three-nucleon interactions in a hybrid chiral-perturbation-theory calculation of the charge-symmetry-breaking reaction $dd \rightarrow \alpha \pi_0$ to show that a cross section of the experimentally measured size can be obtained using LO and NNLO pion-production operators. This result supports the validity of our power counting scheme and demonstrates the necessity of using an accurate treatment of ISI and FSI. It also becomes evident that a full calculation requires the use of consistent chiral nuclear forces to overcome the visible model dependence of our result. The results are published in [1].

References:

- [1] A. Nogga *et al.*, Phys. Lett. B **639**, 465 (2006) [arXiv:nucl-th/0602003].

Application of chiral nuclear forces to light nuclei

A. Nogga(Jülich, Forschungszentrum)

In these proceedings, we discuss the current status of nuclear bound state predictions based on chiral nuclear interactions. Results of ordinary s- and p-shell nuclei and light hypernuclei are shown. The results are published in [1].

References:

- [1] A. Nogga, arXiv:nucl-th/0611081.

A First estimation of chiral four-nucleon force effects in ${}^4\text{He}$

D. Rozpedzik, J. Golak, R. Skibinski, H. Witala (Jagiellonian U.) , W. Glöckle (Ruhr U., Bochum) ,
E. Epelbaum (Jülich, Forschungszentrum) , A. Nogga (Jülich, Forschungszentrum) ,
H. Kamada (Kyushu Inst. Tech.)

We estimate four-nucleon force effects between different ${}^4\text{He}$ wave functions by calculating the expectation values of four-nucleon potentials which were recently derived within the framework of chiral effective field theory. We find that the four-nucleon force is attractive for the wave functions with a totally symmetric momentum part. The additional binding energy provided by the long-ranged part of the four-nucleon force is of the order of a few hundred keV. The results are published in [1].

References:

- [1] D. Rozpedzik *et al.*, Acta Phys. Polon. B **37**, 2889 (2006) [arXiv:nucl-th/0606017].

Nucleon-deuteron capture with chiral potentials

R. Skibinski, J. Golak, H. Witala (Jagiellonian U.), W. Glöckle (Ruhr U., Bochum),
A. Nogga (Jülich, Forschungszentrum), E. Epelbaum (Jülich, Forschungszentrum)

Present day chiral nucleon nucleon potentials up to next-to-next-to-next- to leading order and three nucleon forces at next-to-next-to leading order are used to analyze nucleon deuteron radiative capture at deuteron laboratory energies below $E_d \approx 100$ MeV. The differential cross section and the deuteron analyzing powers $A_y(d)$ and A_{yy} are presented and compared to data. The theoretical predictions are obtained in the momentum-space Faddeev approach using the nuclear electromagnetic current operator with exchange currents introduced via the Siegert theorem. The chiral forces provide the same quality of data description as a combination of the twonucleon AV18 and the three-nucleon Urbana IX interactions. However, the different parametrizations of the chiral potentials lead to broad bands of predictions. The results are published in [1].

References:

- [1] R. Skibinski, J. Golak, H. Witala, W. Glöckle, A. Nogga and E. Epelbaum, Acta Phys. Polon. B **37**, 2905 (2006) [arXiv:nucl-th/0606021].

Testing nuclear forces by polarization transfer coefficients in $d(\text{polarized-p, polarized-p})d$ and $d(\text{polarized-p, polarized-d})p$ reactions $E_{p,lab} = 22.7$ MeV

H. Witala, J. Golak, R. Skibinski (Jagiellonian U.), W. Glöckle (Ruhr U., Bochum),
A. Nogga (Jülich, Forschungszentrum), E. Epelbaum (Jefferson Lab), H. Kamada (Kyushu Inst. Tech.),
A. Kievsky, M. Viviani (INFN, Pisa)

The proton to proton polarization transfer coefficients $K_x^{x'}$, $K_y^{y'}$, and $K_z^{x'}$, and the proton to deuteron polarization transfer coefficients $K_x^{x'}$, $K_y^{y'}$, $K_z^{x'}$, $K_x^{y'z'}$, $K_y^{z'z'}$, $K_z^{y'z'}$, $K_y^{x'z'}$, and $K_y^{x'y'y'}$ were measured in $d(\vec{p}, \vec{p})d$ and $d(\vec{p}, \vec{d})p$ reactions, respectively, at $E_{lab,p} = 22.7$ MeV. The data were compared to predictions of modern nuclear forces obtained by solving the three-nucleon Faddeev equations in momentum space. Realistic (semi)phenomenological nucleon-nucleon potentials combined with model three-nucleon forces and modern chiral nuclear forces were used. The AV18, CD Bonn, and Nijm I and II nucleon-nucleon interactions were applied alone or combined with the Tucson-Melbourne 99 three-nucleon force, adjusted separately for each potential to reproduce the triton binding energy. For the AV18 potential, the Urbana IX three-nucleon force was also used. In addition, chiral NN potentials in the next-to-leading order and chiral two- and three-nucleon forces in the next-to-next-to-leading order were applied. Only when three-nucleon forces are included does a satisfactory description of all data result. For the chiral approach, the restriction to the forces in the next-to-leading order is insufficient. Only when going over to the next-to-next-to-leading order does one get a satisfactory description of the data, similar to the one obtained with the (semi)phenomenological forces. The results are published in [1].

References:

- [1] H. Witala *et al.*, Phys. Rev. C **73**, 044004 (2006) [arXiv:nucl-th/0601075].

Density matrix functional theory that includes pairing correlations

S. Krewald, V. B. Soubbotin (St. Petersburg), V. I. Tselyaev (St. Petersburg), and X. Vinas (Madrid)

The extension of density functional theory (DFT) to include pairing correlations without formal violation of the particle-number conservation condition is described. This version of the theory can be considered as a foundation of the application of existing DFT plus pairing approaches to atoms, molecules, ultracooled and magnetically trapped atomic Fermi gases, and atomic nuclei where the number of particles is conserved exactly. The connection with Hartree-Fock-Bogoliubov (HFB) theory is discussed, and the method of quasilocal reduction of the nonlocal theory is also described. This quasilocal reduction allows equations of motion to be obtained which are much simpler for numerical solution than the equations corresponding to the nonlocal case. Our theory is applied to the study of some even Sn isotopes, and the results are compared with those obtained in the standard HFB theory and with the experimental ones.

References:

- [1] S. Krewald, V. B. Soubbotin, V. I. Tselyaev and X. Vinas, Phys. Rev. C **74**, 064310 (2006).

Gauge-invariant approach to meson photoproduction including the final-state interaction

H. Haberzettl (Washington), K. Nakayama (Athens, USA), S. Krewald

A fully gauge-invariant (pseudoscalar) meson photoproduction amplitude off a nucleon including the final-state interaction is derived. The approach based on a comprehensive field-theoretical formalism developed earlier by one of the authors replaces certain dynamical features of the full interaction current by phenomenological auxiliary contact currents. A procedure is outlined that allows for a systematic improvement of this approximation. The feasibility of the approach is illustrated by applying it to both the neutral and charged pion photoproductions.

References:

- [1] H. Haberzettl, K. Nakayama and S. Krewald, Phys. Rev. C **74**, 045202 (2006) [arXiv:nucl-th/0605059].

Dispersive and absorptive corrections to the pion deuteron scattering length

V. Lensky, V. Baru (Moscow), J. Haidenbauer, C. Hanhart,
A. E. Kudryavtsev (Moscow) and U.-G. Meißner (FZJ & Bonn)

We present a parameter-free calculation of the dispersive and absorptive contributions to the pion–deuteron scattering length based on chiral perturbation theory. We show that once all diagrams contributing to leading order to this process are included, their net effect provides a small correction to the real part of the pion–deuteron scattering length. At the same time the sizable imaginary part of the pion–deuteron scattering length is reproduced accurately. The results are published in Ref. [1].

References:

- [1] V. Lensky, V. Baru, J. Haidenbauer, C. Hanhart, A. E. Kudryavtsev and U.-G. Meißner, arXiv:nucl-th/0608042; Phys. Lett. B, in print.

Towards a field theoretic understanding of $NN \rightarrow NN\pi$,

V. Lensky, V. Baru (Moscow), J. Haidenbauer, C. Hanhart,
A. E. Kudryavtsev (Moscow) and U.-G. Meißner (FZJ & Bonn)

We study the production amplitude for the reaction $NN \rightarrow NN\pi$ up to next-to-leading order in chiral perturbation theory using a counting scheme that takes into account the large scale introduced by the initial momentum. In particular we investigate a subtlety that arises once the leading loop contributions are convoluted with the NN wavefunctions as demanded by the non-perturbative nature of the NN interaction. We show how to properly identify the irreducible contribution of loop diagrams in such type of reaction. The net effect of the inclusion of all next-to-leading order loops is to enhance the leading rescattering amplitude by a factor of $4/3$, bringing its contribution to the cross section for $pp \rightarrow d\pi^+$ close to the experimental value. The results are published in Ref. [1].

References:

- [1] V. Lensky, V. Baru, J. Haidenbauer, C. Hanhart, A. E. Kudryavtsev and U.-G. Meißner, Eur. Phys. J. A **27** (2006) 37 [arXiv:nucl-th/0511054].

3 Accelerator Division

The High-Energy Storage Ring (HESR) [1] of the future International Facility for Antiproton and Ion Research (FAIR) at GSI in Darmstadt is planned as an anti-proton cooler ring in the momentum range from 1.5 to 15 GeV/c. An important and challenging feature of the new facility is the combination of phase space cooled beams with internal targets. The required beam parameters and intensities are prepared in two operation modes: the high luminosity mode with beam intensities up to 10^{11} anti-protons, and the high resolution mode with 10^{10} anti-protons cooled down to a relative momentum spread of only a few 10^{-5} . Consequently, powerful phase space cooling is needed, taking advantage of high-energy electron cooling and high-bandwidth stochastic cooling. A detailed numerical and analytical approach to the Fokker-Planck equation for longitudinal filter cooling including an internal target has been carried out to demonstrate the stochastic cooling capability [2]. The great benefit of the stochastic cooling system is that it can be adjusted in all phase planes independently to achieve the requested beam spot and the high momentum resolution at the internal target within reasonable cooling down times for both HESR modes even in the presence of intra-beam scattering.

Experimental stochastic cooling studies with the internal ANKE target [3] to test the model predictions for longitudinal cooling were carried out at the cooler synchrotron COSY. The routinely operating longitudinal stochastic cooling system applies the optical notch filter method in the frequency band I from 1-1.8 GHz [4].

Longitudinal stochastic cooling to reduce the momentum spread in the beam and to increase its longitudinal density can be utilized by two methods [5]. The first method (*Palmer cooling*) uses the fact that the momentum deviation of a particle can be measured directly by a position sensitive pickup located at a point in the ring with high position dispersion. The signal at the output of the pickup averaged over the betatron motion is then proportional to the product $D \cdot \delta$ where D is the dispersion and δ is the relative momentum deviation of a particle. This correction signal is amplified and sent to the kicker operated in sum mode to provide the necessary momentum or energy correction. In the second method (*Filter cooling*) a pickup in sum mode measures the beam current and the discrimination of particles with different momentum deviations is obtained by inserting a notch filter in the signal path before it drives a kicker in sum mode. The advantage of the filter cooling method, preferred for the HESR design, is that it uses a sum mode pickup which is much more sensitive especially for a smaller number of particles as compared to a pickup that measures the beam position. Moreover, due to filtering after the preamplifier the signal-to-noise ratio is much higher even for a low particle number in the ring. A fact that really helps when the cooling system has to be adjusted for an optimized operation. A further benefit of filter cooling is that the center frequency of the filter can be adjusted to optimize the cooling in the presence of an internal target. A flexibility that is demonstrated below. A disadvantage in filter cooling comes from the notch filter construction. The signal delivered by the pickup is at first equally divided into two paths. One path is delayed by the revolution time

corresponding to the nominal beam momentum. Then both signals are subtracted and the resulting signal is amplified and fed to the kicker. Thus a particle sees two correcting kicks at the kicker. The first one when it passes from pickup to kicker and the other one after one turn when it is back at the kicker. Consequently, the undesired mixing from pickup to kicker is larger as compared to the Palmer cooling method where only the undesired mixing on the way from pickup to kicker is relevant. This may lead to a severe restriction in the practical cooling bandwidth when the filter cooling system is applied to a beam with a large initial momentum spread. A fact that is illustrated in more detail below. The filter cooling method can only be practical if the longitudinal Schottky bands are well separated in the cooling bandwidth.

In longitudinal cooling the time evolution of the beam distribution $\Psi(\delta, t)$ is found from (numerically) solving a *Fokker-Planck equation (FPE)* [5]

$$\frac{\partial}{\partial t} \Psi(\delta, t) = - \frac{\partial}{\partial \delta} \Phi(\delta, t) \quad (1)$$

with the flux

$$\Phi(\delta, t) = F(\delta) \Psi(\delta, t) - D(\delta, t) \frac{\partial}{\partial \delta} \Psi(\delta, t) \quad (2)$$

where δ is the relative momentum deviation of a particle. The flux $\Phi(\delta, t)$ is determined by two terms. The *drift term* $F(\delta)$ describes the coherent cooling effect by the self interaction of a single particle with its own momentum deviation. The second term describes the incoherent beam heating by diffusion and its strength is determined by the *diffusion coefficient* $D(\delta, t)$. Diffusion always leads to a broadening of the beam distribution.

Both drift and diffusion coefficient are determined by the system layout and were calculated in [6] for a specific design of the cooling system at TARN. Later corrections and improvements were given independently by two of the authors (H. St. and T. K.) where it is assumed that pickup and kicker structures are designed as quarterwave loop couplers with electronic transfer functions as given in [7]. The signal path contains a notch filter. This filter exhibits a phase change of 180 degrees in the middle of each Schottky band and the magnitude is symmetric around each revolution harmonic with a sharp drop at the center. The complete theory including the target beam interaction will be published in detail separately [8]. A brief sketch of the main quantities entering the drift and diffusion terms are now given. Under the assumption of small momentum deviations and neglecting beam feedback the drift term for cooling is approximately given by

$$F(\delta) \propto \eta_{tot} \cdot \delta \cdot G_A \cdot \tilde{Z}_P \cdot \tilde{Z}_K \cdot \sum_{n=n_1}^{n_2} n \sin(2\theta + n\pi(2r\eta_{PK} + \eta_{tot})\delta + 2\pi n f_0 \Delta T_D) \cdot \sin^2(\theta) \quad (3)$$

where the sum runs over all harmonics n in the cooling bandwidth $W = (n_2 - n_1) f_0$. The revolution frequency is f_0 , the ratio distance from pickup to kicker to the ring length is r and an additional delay in the signal path is denoted by

ΔT_D . The additional delay is used to maximize the cooling effect over the whole cooling bandwidth. The frequency slip factor from pickup to kicker is η_{PK} and the total slip factor for the whole ring is η_{tot} . The momentum and thus frequency dependent phase θ determines the pickup and kicker magnitude response by $\sin^2(\theta)$.

It can be seen that to first order the drift term at each harmonic is proportional to the relative momentum deviation, i.e. the larger the momentum deviation is the larger the correction will be. The correction increases with gain G_A and the product of pickup and kicker sensitivities $\tilde{Z}_p \cdot \tilde{Z}_k$. The total frequency slip factor η_{tot} must be chosen such that there is no band overlap in the whole cooling bandwidth. The undesired mixing however can partly diminish the cooling and is represented at each harmonic by the contribution of the first sin-term in eq. (3). Too much undesired mixing can be avoided if the upper frequency limit of the cooling system is restricted to

$$f_{max} < \frac{f_0}{2 \cdot |2r\eta_{PK} + \eta_{tot}| \cdot |\delta|}. \quad (4)$$

Note that both frequency slip factors determine this limit due to the fact that two kicks form the correction in correlator filter cooling as discussed here. On contrary, the undesired mixing in Palmer cooling is only determined by η_{PK} . The same result is also found in the work presented in [9] where stochastic cooling of rare isotopes is discussed.

The condition according to eq. (4) is very well met in the case of COSY. Here both frequency slip factors are equal, $\eta_{PK} = \eta_{tot} = 1/\gamma^2 - 1/\gamma_{tr}^2$. With the measured values $f_0 \approx 1.6 \text{ MHz}$, $\eta = -0.1$, $\delta = 2\delta_{rms} = 6 \cdot 10^{-4}$ and $r = 0.5$ the upper frequency limit should not exceed about 7 GHz. In COSY the upper limit of the cooling system is 3 GHz. In the case of HESR the restriction is much more severe since the revolution frequency is about a factor of three smaller. This problem can be overcome by a proper choice of the pickup to kicker distance (small ratio r) and a proper choice of the lattice layout leading to small frequency slip factors. Or special filters may be applied in the initial phase of cooling [10] to reduce the momentum tails.

The diffusion coefficient is a sum of Schottky noise heating D_S and thermal noise D_{th} in the electronic system:

$$\text{Schottky noise: } D_S(\delta, t) \propto G_A^2 \cdot \delta^2 \cdot \Psi(\delta, t)$$

$$\text{Thermal noise: } D_{th}(\delta, t) \propto G_A^2 \cdot T \cdot \delta^2$$

Note that both quantities are proportional to the squared amplifier gain and Schottky noise additionally depends on the beam distribution. Obviously thermal noise is proportional to the system temperature T .

In the presence of an internal target at a location with zero position and angle dispersion both, the drift term and the diffusion coefficient will be modified. It is assumed that the target beam interaction [11] leads to a mean energy loss per turn ϵ resulting in a shift of the whole beam distribution towards lower energies. This effect is taken into account in the FPE as an additional constant drift term $F_T \propto f_0 \cdot \epsilon$.

The longitudinal emittance growth due to energy straggling is given by the mean square relative momentum deviation per target traversal δ_{loss}^2 so that the diffusion term due to the target beam interaction is $D_T = f_0 \cdot \delta_{loss}^2$ for the case of an

unbunched beam [11]. Thus diffusion due to the target beam interaction leads to a linear increase of the squared relative momentum spread. Both quantities, mean energy loss per turn and mean square relative momentum deviation per turn can be determined experimentally when cooling is switched off. The measured values are then used in the FPE to describe beam cooling in the presence of the target beam interaction.

The cooling experiments were carried out at beam momentum $3.2 \text{ GeV}/c$ with about 10^{10} stored protons. The frequency slip factor was measured and resulted in $\eta = -0.1$, i.e. the machine was operated above transition, $\gamma > \gamma_{tr}$. Longitudinal cooling was carried out with band I ranging from 1 to 1.8 GHz. Particle distributions were measured in the frequency range of the harmonic number 1500 with the band II system and can be converted to momentum distributions using the relation $\Delta f / f_0 = \eta \cdot \Delta p / p_0$. The frequency distributions were measured every 2.5 min or 5 min in flat top with a duration of about 30 min.

First the target beam interaction was investigated in order to determine the mean energy loss per turn ϵ and the mean square relative momentum deviation per turn δ_{loss}^2 . The results are shown in the figures 1 and 2. In figure 1 the measured center of the frequency distributions are shown from which the revolution frequency of the protons can be derived by dividing the values by the harmonic number 1500. At time zero this gives $f_0 \approx 1.568 \text{ MHz}$.

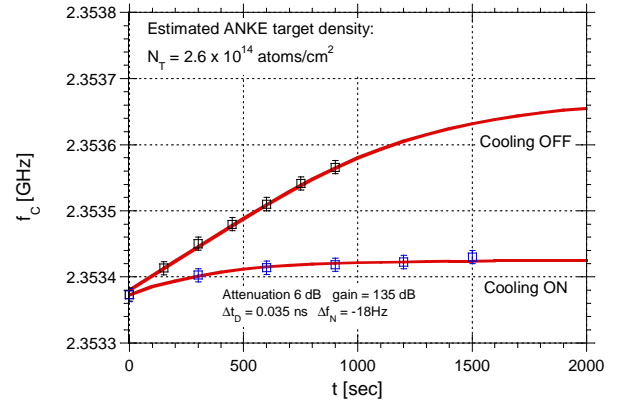


Fig. 1: The measured center frequency at harmonic 1500 (blue symbols: cooling ON, black symbols: cooling OFF) in comparison with the model predictions (red curves).

The measured data (black symbols) in figure 1 show the expected behavior that the beam distributions are shifted linearly towards lower energies due to the beam target interaction. Note that due to the negative frequency slip factor this corresponds to a linear increase in frequency. Thus the revolution frequency of the protons increases with increasing energy loss. From the slope of the data in figure 1 the mean energy loss per turn was determined to $\epsilon = -1.8 \cdot 10^{-3} \text{ eV/turn}$. The relative momentum spread in figure 2 shows only a small increase.

From the linear increase of δ_{rms}^2 the mean square relative momentum deviation per turn $\delta_{loss}^2 = 2 \cdot 10^{-17} / \text{turn}$ was derived. The indicated error bars result from three consecutive measurements and reflect the uncertainties due to the finite frequency resolution of the spectrum analyzer. The values for ϵ and δ_{loss}^2 have been then used in the FPE

when cooling is switched off to determine the beam distributions versus time.

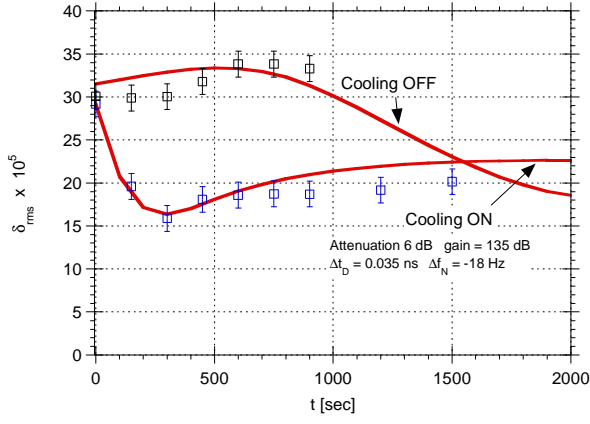


Fig. 2: The measured relative momentum spread at harmonic 1500 (blue symbols: cooling ON, black symbols: cooling OFF) in comparison with the model predictions (red curves). The linear increase of the squared momentum spread determines the mean square relative momentum deviation per turn when cooling is switched off.

A Gaussian initial distribution in the calculations was assumed. The results are shown in figure 1 and 2 as red curves. As can be seen the model deviates from the linear behavior at about 600 s which is due to particle losses when the shifted distributions reach the momentum acceptance of the machine. This becomes clearly visible when the measured frequency distributions are compared with the distributions predicted by the model as is depicted in figures 3 to 5. The measurement as well as the model prediction show a cut off in the distributions at about 2.3537 GHz which corresponds to the negative relative momentum acceptance limit $\delta_{acc} = -1.4 \cdot 10^{-3}$. It is seen that this value is reached after about 600 s. Particle losses are increasing then with time as indicated by the increase in the slope at the high frequency side of the distributions.

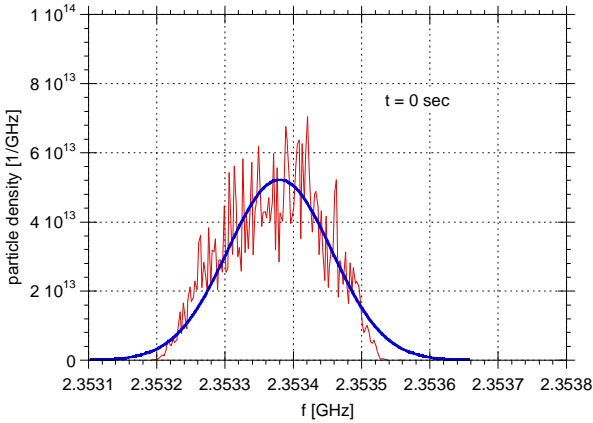


Fig. 3: The measured initial frequency distribution at harmonic 1500 (red) in comparison with the model prediction (blue).

Also in these figures one observes that the main effect of the target beam interaction is an increase in the center frequency, i.e. a decrease in the mean momentum of the beam. The beam width only slightly changes during the measuring time.

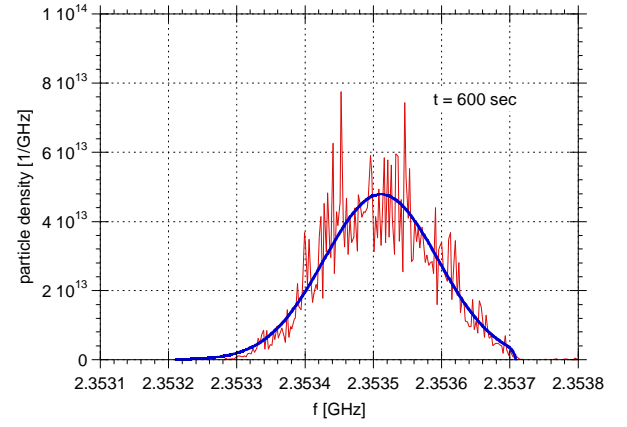


Fig. 4: The measured frequency distribution at $t = 600$ s (red) in comparison with the model prediction (blue).

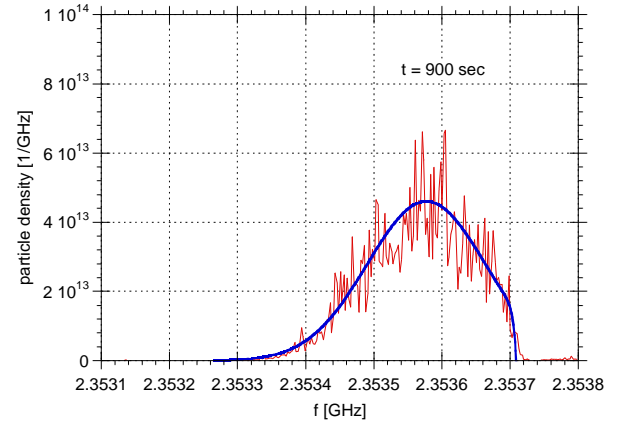


Fig. 5: The measured frequency distribution at $t = 900$ s (red) in comparison with the model prediction (blue).

An estimate of the ANKE target thickness can now be made with the measured values for mean energy loss and momentum acceptance. According to the Bethe-Bloch formula the restricted energy loss ε in units MeV [12]

$$\varepsilon = -0.307 \frac{N_T}{N_A} \frac{1}{\beta^2} \left[\frac{1}{2} \ln \left(\frac{2m_e c^2 \beta^2 \gamma^2 T_{acc}}{I^2} \right) - \frac{\beta^2}{2} \left(1 + \frac{T_{acc}}{T_{Max}} \right) \right]$$

is proportional to the target thickness N_T measured in atoms per cm^2 . A gaseous hydrogen target with $I = 19.2$ eV is assumed. The usual kinematic factors are β and γ and T_{max} is the maximum energy that can be transferred in a collision. The mass of the target electrons is m_e and $N_A = 6.023 \cdot 10^{23}$. The energy loss is restricted due to the finite acceptance to $T_{acc} = \delta_{acc} T_0 (\gamma + 1) / \gamma$ where T_0 is the kinetic energy of the proton beam. Inserting the measured values yields an ANKE target thickness $N_T \approx 3 \cdot 10^{14}$ atoms/cm². The measured value for the mean square relative momentum deviation per turn $\delta_{loss}^2 = 2 \cdot 10^{-17}$ /turn is consistent with the value that is derived from the formula as given in [11]. Note that the rest gas scattering that has been measured too in this experiment is not subtracted here for this estimation of the target thickness. Also, no systematic error study has been carried out so far.

After determining the parameters of the beam target interaction stochastic cooling was switched on. The system delay was adjusted for cooling by means of BTF

measurements and the notch filter was set 18 Hz below the center frequency of the distribution at harmonic one. In momentum space this means that the filter was set above the mean momentum of the protons. Measurements for different attenuations of the electronic gain of the cooling system were then carried out. Since the absolute gain and delay of the cooling system was not known the gain and delay in the calculations were once adjusted to reproduce all measured beam distributions. As an example the following figures show the results for the attenuation set to 6 dB which corresponds to a model gain and an additional delay of 135 dB and $\Delta T_D = 0.035\text{ ns}$, respectively. Figure 1 shows the center frequency measured at harmonic number 1500 (blue data points) in comparison with the model prediction. The figure clearly shows the cooling effect. The mean energy loss is nearly compensated by cooling. The time development of the relative momentum spread during cooling and ANKE target on (blue data points) is fairly well predicted by the model as shown in figure 2. Initially the momentum spread drops down and increases until an equilibrium value $\delta_{rms} = 2.3 \cdot 10^{-4}$ between target beam interaction and cooling is attained after about 1000 s . Again the cooling effect is clearly visible when the data with cooling on and off are compared. Figure 6 presents a comparison of the measured distribution with the model prediction after 900 s of cooling.

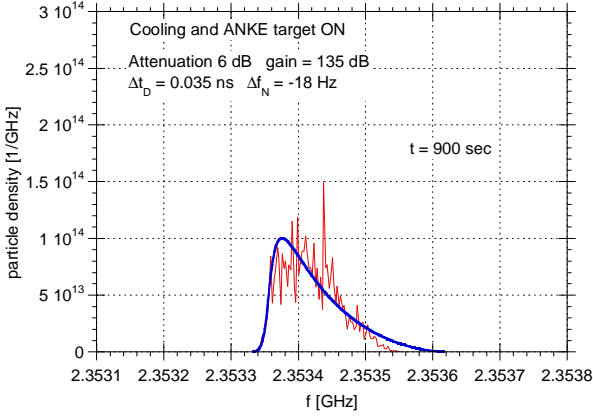


Fig. 6: Comparison of the measured frequency distribution at harmonic 1500 (red) in comparison with the model prediction (blue) after 900 s of cooling.

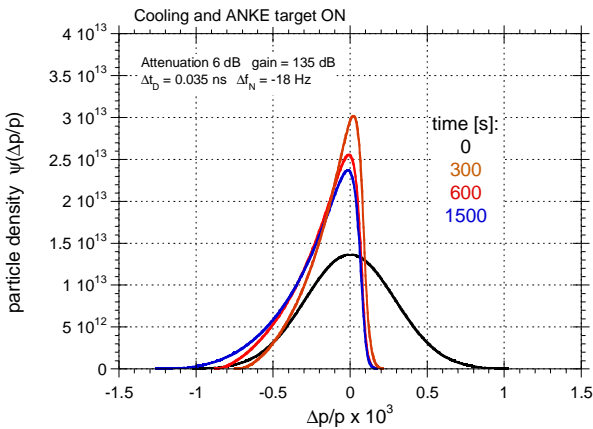


Fig. 7: Calculated momentum distributions for different times during cooling with the ANKE target on.

Momentum distributions at different times during cooling when the ANKE target is on are shown in figure 7. As can be seen the distributions are asymmetric with respect to

zero as a result from the mean energy loss. The conclusion is that it is in general not sufficient to describe the beam distribution only by its second moment. All higher moments are necessary.

If the mean energy loss is compensated cooling achieves an equilibrium value $\delta_{rms} = 6 \cdot 10^{-5}$, which is about a factor of four smaller than without compensation, see figure 8.

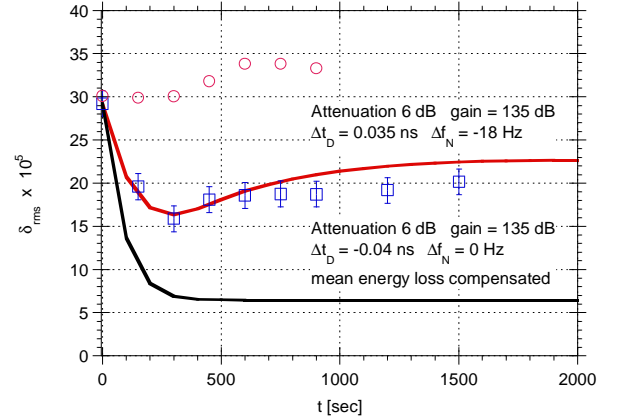


Fig. 8: Same as in figure 2 but the mean energy loss is now compensated resulting in a significantly reduced equilibrium rms relative momentum spread.

The beam distributions are now symmetric and nearly Gaussian as shown in figure 9. In the case of a compensated mean energy loss and a negligible undesired mixing from pickup to kicker the equilibrium relative momentum spread can be determined by the formula [8]

$$\delta_{eq,rms} = \frac{4}{5} \left(\frac{3}{32} \cdot \frac{N f_0^2}{|\eta| W f_C} \delta_{loss}^2 \right)^{1/3} \quad (5)$$

where W is the bandwidth of the cooling system and f_C is the center frequency. This formula also applies if the bandwidth covers not an octave. Note that the equilibrium value does not depend on the initial relative momentum spread. It should be pointed out that if the undesired mixing is significant and/or the mean energy loss is not compensated this formula likely delivers results which are more than a factor of four away from the results found from a solution of the FPE.

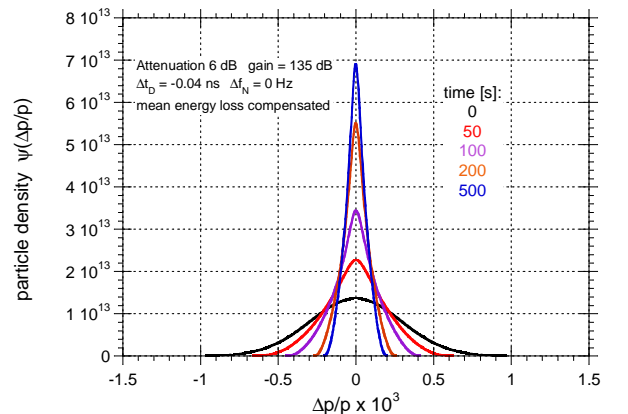


Fig. 9: Predicted momentum distribution during cooling and ANKE target with $N_T \approx 3 \cdot 10^{14}\text{ atoms/cm}^2$ target thickness when the mean energy loss in the target is compensated.

The stochastic filter cooling model developed for the investigation of stochastic cooling at the HESR receives a

remarkable good agreement with the experimental results at COSY. The beam target interaction is well described by the model through the quantities mean energy loss and mean square relative momentum deviation per turn. Both quantities can be measured. Once the main parameters are known the model can be used to predict the cooling properties under different conditions, e.g. if the target thickness is increased, different beam energy, etc.. The good agreement of the model with the experimental results at COSY gives a save confidence that the model will also fairly well predict the cooling properties in the case of the planned HESR at the FAIR facility. However more investigation are needed concerning the undesired mixing that is here much more severe as at COSY. Also methods to compensate the mean energy loss have to be studied. One method to compensate the mean energy loss by a barrier bucket cavity will be investigated theoretically and will be soon tested at COSY. In general, COSY turns out to be a well dedicated machine for beam dynamic models to be tested in view of HESR. In addition new sensitive pickup and kicker structures [13, 14] developed for the HESR stochastic cooling system can be well studied at COSY.

Acknowledgement

The authors acknowledge valuable and stimulating discussions with D. Möhl (CERN), L. Thorndahl (CERN) and F. Nolden (GSI).

References:

- [1] HESR, “*Baseline Technical Report*”, <http://www.fz-juelich.de/ikp/hesr/2-11-HESR.pdf>
- [2] H. Stockhorst, D. Prasuhn, R. Maier, B. Lorentz and T. Katayama, “*Stochastic Cooling for the HESR at the GSI-FAIR Complex*”, Proc. EPAC 2006, Edinburgh, Scotland, 26-30 June 2006, p. 231
- [3] Annual Report 2005, Jül-4212, Forschungszentrum Jülich
- [4] P. Brittner, H.U. Hacker, R. Maier, U. Pfister, D. Prasuhn, H. Singer, W. Spiess, R. Stassen, H. Stockhorst, A. Zumloh, “*The stochastic cooling system for COSY*”, proceedings of EPAC92, Berlin
- [5] D. Möhl et al., Phys. Rep. Vol. 58, No.2, Feb. 1980
- [6] T. Katayama and N. Tokuda, Part. Acc., 1987, Vol. 21, pp. 99-120
- [7] G. Lambertson, “*Dynamic Devices – Pickup and Kickers*”, in AIP Conf. Proc. 153, p. 1413
- [8] H. Stockhorst and T. Katayama, to be published
- [9] F. Nolden, I. Nesmiyan, C. Peschke, Nucl. Instr. and Meth. A 564 (2006), 87-93
- [10] L. Thorndahl, private communication
- [11] F. Hinterberger, “*Beam-Target Interaction and Intrabeam Scattering in the HESR Ring*”, 2006, Jül-4206, ISSN 0944-2952
- [12] <http://pdg.lbl.gov/2000/passagerpp.pdf>
- [13] R. Stassen, P. Brittner, H. Singer, G. Schug, “*Printed loop coupler for the HESR stochastic cooling system*”, this Annual Report
- [14] R. Stassen, P. Brittner, R. Greven, H. Heimbach, H. singer, G. Schug, L. Thorndahl, “*Ring-Slot coupler for the HESR stochastic cooling system*”, this Annual Report

¹ Tokyo

Experiments on Proton Beam Ordering by Electron Cooling

A. Kobets¹, I. Meshkov¹, A. Sidirin¹, A. Smirnov¹
J. Dietrich², R. Maier², D. Prasuhn², H.J. Stein²

The idea of utilization of an ion beam crystalline state for nuclear physics experiments has a large interest now. The achievement of very low ion temperature in the beam rest frame may open new possibilities in accelerator physics. First off all it is related to a precise mass measurements based on the very small momentum spread of the beam in the ordered state. Another possible application of the ordered beam has the aim to increase the luminosity in an electron-ion collider using the ion beam at relatively high linear density and very small transverse dimensions. In the frames of the FAIR project the utilization of ordered ion beams can be discussed for electron-ion collisions at the New Experimental Storage Ring (NESR).

Experiments on proton beam ordering, named crystallization, that have been started in August 2005 [1, 2] were continued. Two COSY runs dedicated to electron cooling development were performed at COSY in 2006 by the electron cooling collaboration IKP FZJ and Dzhelpev Lab. of Nuclear Problems JINR, Dubna. During the 1st run the average pressure in COSY was at the level of $\sim 5 \cdot 10^{-8}$ mbar due to a leak in section 2. The leak had been fixed before the 2nd run. The vacuum was then about $5 \cdot 10^{-9}$ mbar. Special measures were taken for improvement of the experiment conditions.

A feedback system for suppression of the ripples of the 35 kV high voltage power supply was installed yielding a reduction of the ripples amplitude by a factor of two. The reference signal was taken directly from the gun cathode potential through a capacitor.

The integrated Schottky noise power ($P_{Schottky}$), directly determined with the spectrum analyser HP89410A, was taken as a measure for the proton number at low intensity. $P_{Schottky}$ was calibrated before using the beam current transformer (I_{BCT}) and the H^0 flux intensity $F(H^0)$. The procedure was as following:

1st step – measurement of $F(H^0)$ vs I_{BCT} . A good linear dependence was obtained (Fig. 1a).

2nd step – measurement of $P_{Schottky}$ vs $F(H^0)$ (Fig. 1b).

The background noise, to be subtracted from the primarily measured $P_{Schottky}$ between two markers, was measured in the frequency ranges of 2, 1, 0.5, 0.2 and 0.1 kHz.

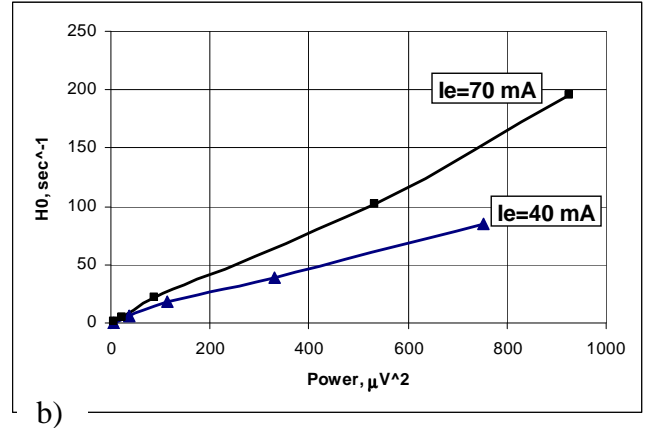
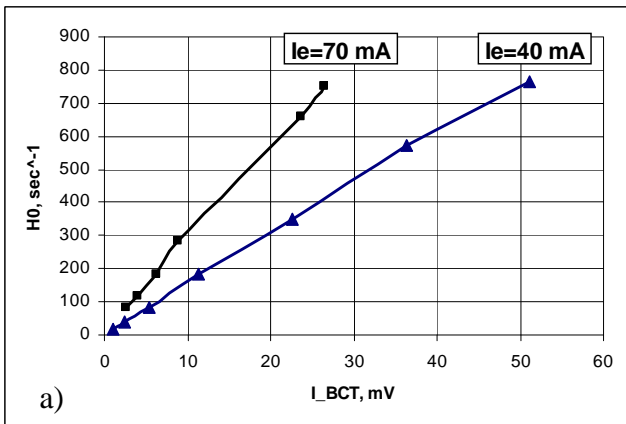


Fig. 1: Calibration of proton beam intensity monitoring. Upper part: $F(H^0)$ vs I_{BCT} , lower part: $F(H^0)$ vs $P_{Schottky}$.

The Schottky signal was measured on the 18th harmonics of proton revolution frequency of 488.2 kHz with “The Schottky PU” through an amplifier of 72 db and 84 db gain and a resonant circuit that gave a gain of about 30 db. The analysis of the Schottky noise spectrum was performed with HP89410A in “averaging” mode operation. Typical measurement of one spectrum at lowest proton beam intensity required averaging of 10 – 20 times. It lasted about 2-3 min. The recorded spectra were extracted in digital form, squared and fitted with a Gaussian function (Fig. 2). The 1σ momentum spread was calculated from the FWHM width Δf with the following formula:

$$\frac{\Delta p}{p} = \frac{I}{\eta_{\omega} 2\sqrt{2} \cdot \ln 2} \cdot \frac{\Delta f}{f_0}$$

Here $\eta_{\omega} = 0.65$ is the off-momentum factor and f_0 the 18th harmonics of the revolution frequency.

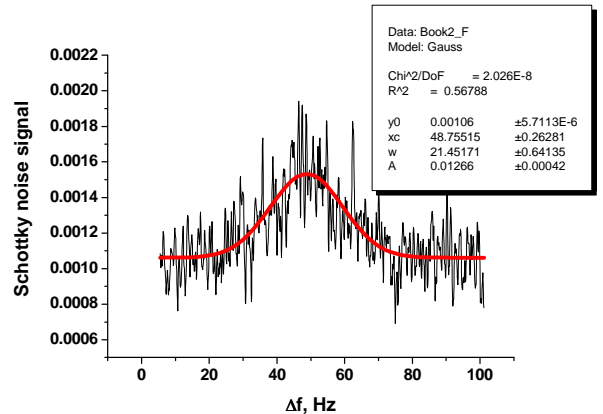


Fig. 2: Typical Schottky spectrum fitted with Gaussian function, proton number $5.4 \cdot 10^5$, $\Delta p/p = 1.5 \cdot 10^{-6}$. $\Delta f = f - f_{18}$, where f – frequency at HP89410A analyser, $f_{18} = 8.787$ MHz – the 18th harmonics of the revolution frequency.

The Schottky spectrum of proton beam was measured at injection energy (45 MeV) at different electron current values for decreasing proton numbers in the beam. After

injection the proton number was reduced by the horizontal scraper that decreased the ring aperture leading to a faster beam loss. After reaching a certain proton number (measured via the Schottky noise power) the scraper was taken out and the averaging procedure of the spectrum measurement was started.

The minimum value of the momentum spread was reached at a proton number below $1 \cdot 10^6$ but it did not decrease below $1.3 \cdot 10^{-6}$ (Fig. 3 and Fig.4). It should be noted that this result was not sensitive on the application of the HVPS feedback.

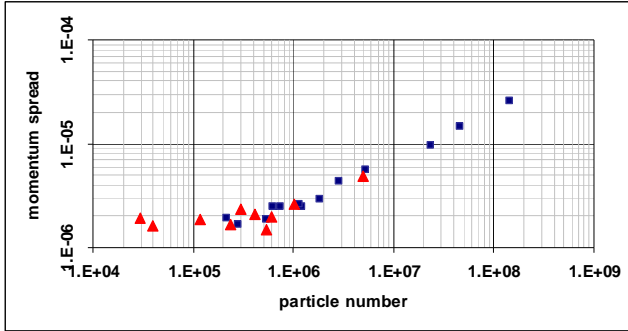


Fig. 3: Proton beam momentum spread vs particle number: squares - feedback OFF, triangles – feedback ON. Electron current 70 mA.

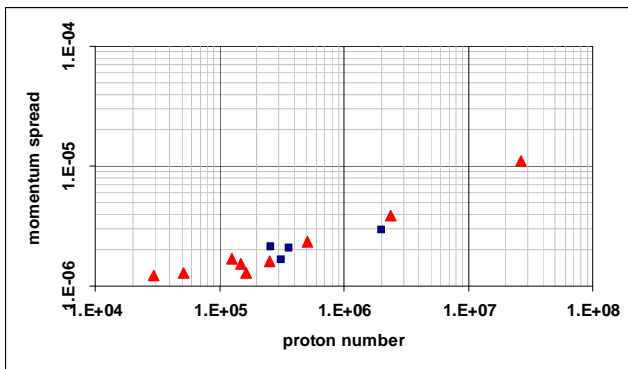


Fig. 4: Proton beam momentum spread vs particle number: squares - feedback OFF, triangles – feedback ON. Electron current 40 mA.

It was proposed to use an artificial transverse heating of the protons in the ring under electron cooling to reduce intrabeam scattering (IBS) in the longitudinal degree of freedom. For this purpose a white noise voltage in the frequency range of 100 kHz - 5 MHz was applied to the stripline PU electrodes (exciter for tune measurements). The experiment has shown that application of the noise voltage excites a parasitic signal on the revolution frequency at “The Schottky PU”. Due to this reason this heating technique was cancelled.

In the experiments on proton beam ordering a momentum spread at the level of $1.3 \cdot 10^{-6}$ at $3 \cdot 10^4$ protons was achieved. An influence of the lower HVPS ripple was not detected. The ordered state which should appear as a sudden reduction of the momentum spread at a critical proton number could not be observed. Only a constant momentum spread at low proton numbers was seen. Additional heating effects such as scattering on residual gas or magnetic field ripples in the COSY bending magnets might be a reason for this result.

Acknowledgement:

We thank the COSY staff for successful operation of COSY. Special thanks to I. Mohos for technical support during experiments with the HV feedback system and the development of the resonant Schottky pickup electronics.

References:

- [1] I.N. Meshkov et al., IKP internal report 2005.
- [2] J. Dietrich et al., Electron cooling of proton beam in COSY and S-LSR, Proceedings Russian Particle Accelerator Conference RUPAC06, Novosibirsk, 2006.

¹ JINR Dubna, DLNP, 141980 Dubna

² Forschungszentrum Jülich, IKP, D-52425 Jülich

Loss Phenomena of Electron Cooled Ion Beams

A. Kobets¹, I. Meshkov¹, A. Sidirin¹, A. Smirnov¹
 J. Dietrich², R. Maier², D. Prasuhn², H.J. Stein²

The achievable intensity of electron cooled ion beams at COSY is restricted by two main beam loss phenomena.

(i) Initial losses occurring during the 5 to 10 s long cooling process after stripping injection into COSY.

(ii) Additional losses occurring after the ion beam is well cooled due to self-excitation of coherent betatron oscillations visible in the Fourier spectrum of the transverse Schottky signal at the machine tune frequencies.

These coherent oscillation can be damped by the feedback system operational since 2003. At COSY the lifetime of the stabilized cooled beam is typically of the order of 1000 seconds. This relatively poor value is most probably caused by large angle Coulomb scattering at the residual gas atoms in the ring [1].

As long as the feedback is active the initial losses are obviously of incoherent nature since no betatron oscillations are seen during the cooling period. Our interpretation for these losses has always been the fact that after the stripping injection the ion beam is filling the whole ring acceptance and therefore is larger than the electron beam diameter. The nonlinear electric field outside the electron beam containing higher multipoles may excite nonlinear resonances and in this way cause beam loss. Immediately after injection multiple scattering at the acceptance limit is also contributing to the loss. This is demonstrated by Fig. 1. In the first cycle both losses are active until the cooling process is finished and the ion beam is finally well inside the electron beam. In the second cycle where the electron beam is switched on only 24 s after injection the action of both effects are clearly separated.

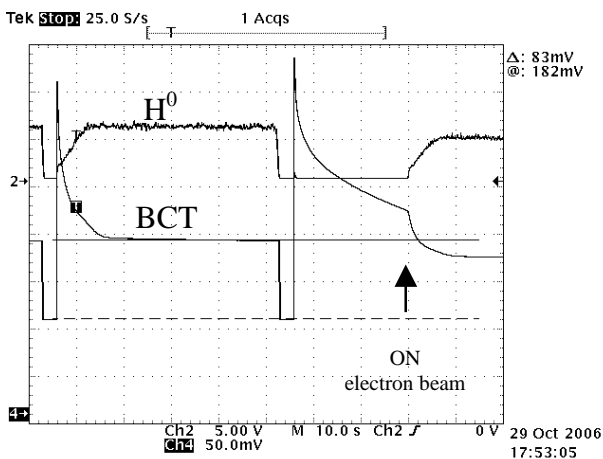


Fig. 1: Incoherent initial losses after injection before the 45 MeV proton beam is well cooled. The lower curve (BCT) is the proton current, the upper one the H^0 count rate. In the second cycle the electron beam is switched on later after injection into COSY. The cooled beam is stabilized by horizontal and vertical feedback, therefore no coherent oscillations at all (the same in Fig.2 and Fig. 3).

To study the influence of the electron beam on a proton beam inside and outside the electron beam we made the following experiment. After the proton beam was well cooled and stabilized by feedback, the electron beam energy was detuned by 1kV and set back to the proper

cooling energy after 10 s. As shown in Fig. 2 there was, as presumed, no effect on the proton beam. The re-cooling needed about 2 s without any change in proton current or H^0 rate.

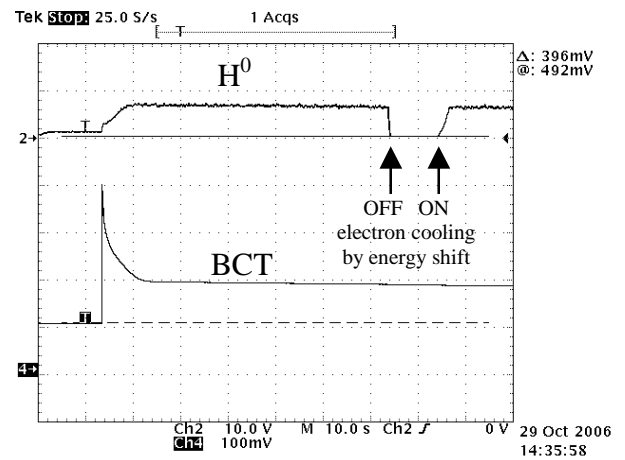


Fig. 2: Cooled proton beam inside the electron beam. Detuning the electron energy by 1 keV and setting it back to the proper cooling energy showed no influence on the proton current.

In a second step the electron beam was switched off and vertically steered such that the cooled proton beam was located near the edge of the electron beam. Fig. 3 shows the result after the electron beam was switched on again. Due to the smaller overlap the H^0 rate was lower and after 8 s the proton current started to decrease, a clear demonstration for the loss mechanism of protons outside the electron beam.

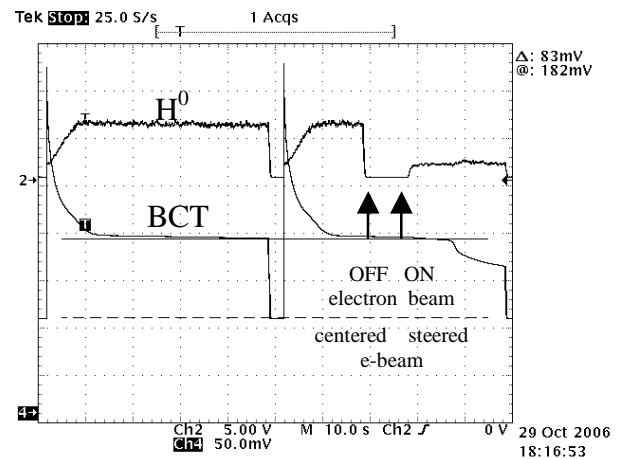


Fig. 3: Simulation of “initial losses” by positioning a cooled proton beam at the edge of the (1 inch, 170 mA) electron beam.

References:

[1] J. Dietrich et al., IKP Annual Report 2004.

¹ JINR Dubna, DLNP, 141980 Dubna

² Forschungszentrum Jülich, IKP, D-52425 Jülich

Proposed 2 MeV Electron Cooler for COSY-Juelich

J. Dietrich, V. V. Parkhomchuk¹

Electron cooling at COSY is applied at low energies, at present mainly at injection energy, to prepare low-emittance beams to be used after acceleration and extraction for internal and external experiments. Stochastic cooling, covering the momentum range from 1.5 GeV/c up to the maximum momentum, is used to compensate energy loss and emittance growth at internal experiments. Requests for future COSY experiments as WASA – a detection system from CELSIUS accelerator of The Svedberg Laboratory (TSL) at Uppsala with a pellet target [1] - are higher luminosities ($> 10^{32} \text{ cm}^{-2} \text{ s}^{-1}$). There are two possible ways i) increasing the band width of the stochastic cooling system and/or ii) electron cooling up to maximum momentum. For operations with thick internal targets, the combination of stochastic and fast (magnetized) electron cooling is the preferred solution. At COSY the combination of two cooling techniques-stochastic and electron cooling at the same beam energy could be studied and the advantages of both methods are unified. The electron cooling-cooling of the beam core and stochastic cooling-cooling the beam tails. Realisation of such a cooling system will be an important step toward creation of a novel experimental technique aiming to reduce significantly parasitic effects related to halo in accelerated beams – a step to “backgroundless” detection systems. Future experiments with the 2 MeV electron cooler at COSY with an inner target and stochastic cooling can open the way for made the intensive cooling on high energy at more simple and cheaper manner.

For electron cooling up to maximum momentum of COSY an electron cooler up to 2 MeV electron energy has to be developed together with the Budker Institute in Novosibirsk [2,3]. The basic parameters and requirements are listed in Table 1. The most important restrictions are given by the available space at the COSY ring itself. The height is limited by the building up to 7 m, the length of the cooler in beam direction by the existing electron cooler and the ring itself to 3 m. The acceleration of polarized beams at COSY must to be taken into account. Space for compensating magnets must be foreseen to achieve conservation of polarisation.

Table 1: Basic Parameters and Requirements.

COSY 2 MeV Electron Cooler	Parameter
Energy Range	0.025 ... 2 MeV
High Voltage Stability	$< 10^{-4}$
Electron Current	0.1 ... 3 A
Electron Beam Diameter	10 ... 30 mm
Cooling Length	3 m
Toroid Radius	1.5 m
Variable Magnetic Field (cooling section solenoid)	0.5 ... 2 kG
Vacuum at Cooler	$10^{-8} \dots 10^{-9}$ mbar
Available Overall Length	7 m
Maximum Height	7 m
COSY Beam Axis above Ground	1.8 m

Calculations are performed with the trubs.exe code [2], in which the cooling force is approximated by the well known Parkhomchuk formula [4]. The effect of intra beam

scattering is included by the simple model of relaxation distribution velocity. The increase of the angle spread due to scattering of an internal target is also taken into account. The simulation was made with following parameters: cooler length 3 m, beta function in the cooling section 13 m, electron beam radius 0.5 cm, electron beam current 2 A, magnetic field 2 kG, initial normalized emittance $10^{-6} \pi$ m rad, 2 GeV proton beam energy and number of protons $2 \cdot 10^{10}$ (5 mA).

As it is seen in Fig. 1, the ion beam emittance is effectively decreased during 10 s. The reached equilibrium emittance is a result of balance between intra-beam scattering and electron cooling.

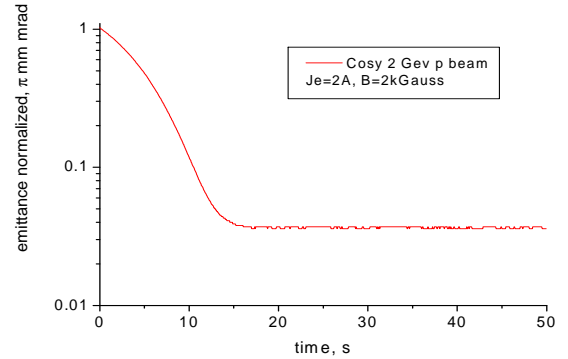


Fig. 1: Normalized beam emittance versus time at electron cooling of 2 GeV proton beam (without target, parameters see text).

The proposed electron cooler consists of a high voltage vessel with electrostatic acceleration and deceleration columns, two bending toroids and cooling drift section. The preliminary scheme of the cooler is shown in Fig. 2 [2]. The basic features of the design are i) the longitudinal magnet field from the electron gun to the collector, in which the electron beam is embedded, ii) the collector and electron gun placed at the common high voltage terminal and iii) the power for magnet field coils at accelerating and decelerating column is generated by turbines operated on SF₆ gas under pressure. The gas flux which drives the turbines is also used for cooling the magnetic coils and for keeping the temperature inside the vessel constant.

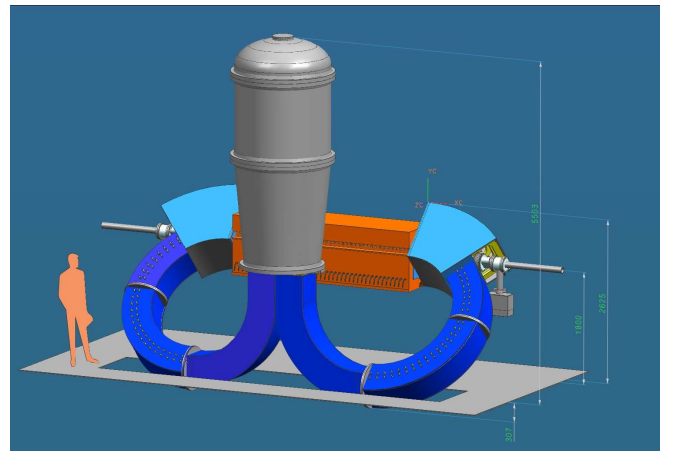


Fig. 2: Layout of the proposed 2 MeV electron cooler for COSY.

The high voltage system consists of the vessel, the accelerating and decelerating column, high voltage sections and high voltage head with gun and collector. For the vessel and column the main parameters of the industrial accelerator ELV-8 which works on 2.5 MV are taken [5]. The vessel geometry is identical to the vessel of the ELV-8. The vessel withstands pressures up to 10 bars. The diameter of the high voltage sections amounts to 80 cm. At the ELV-8 accelerator SF₆ gas is used as insulation gas. The ELV-8 has no magnetic coils inside. The electron current is equal to 0.05 A. The beam power is 100 kW. Budker Institute has experience in recuperation of high voltage beams with an energy of 1 MeV and a current of 1A [6]. The high voltage sections for the 2 MeV electron cooler (Fig. 3) contains: high voltage power supply, coils for the magnet field along acceleration and deceleration columns, power source and control units for measurement and control of parameters for each section. Each section has two high voltage power units on 30 kV. Using of two power units allow to decrease the voltage for insulation from 60 kV to 30 kV. The whole 2 MV column consists of 34 sections. The electric field between the sections will be 30 kV/cm. The pressured SF₆ gas can be used for protection from sparking [7]. To suppress sparking a SF₆ gas pressure of about two bars is sufficient. Special measures must be taken to prevent destructions from sparks. Accelerating rings are surrounded by collar rings.

The simplest system of powering the high voltage sections and power supply for the magnetic field is a mechanical electric generator. The most popular system consists of a electric engine on ground potential and an insulation shaft (plastic) which transfers power to an electric generator on high voltage potential. In the present case too many generators (>35) along the acceleration column and to the high voltage terminal would be necessary. The twisting moment of the shaft for the first generator would be 35 times larger than for the last one. Vibrations of the whole system could be an other disadvantage. Therefore turbo engines with integrated electric generators (maximum electric power of 0.5 kW) at each section are proposed. A compressor at ground potential will pump SF₆ gas from the vessel, compress it to 4-5 bar and feed it to a thermo exchange chamber and gas filter. Pressurized gas is directed with plastic tubes along the high voltage column. At each section the pressurized gas is used to drive a turbo generator for production of the electric power (Fig. 3) and after this the gas is used for cooling and regulating the temperature constant.

References:

- [1] J. Zabierowski et al., The CELCIUS/WASA Detector Facility, *Physica Scripta* T99, (2002) 159.
- [2] V. V. Parkhomchuk, Electron Cooling for COSY, Internal Report (2005).
- [3] V. B. Reva et al., Budker INP proposals for HESR and COSY electron cooler system, *AIP Conf. Proc.* 821 (2006) 308. J. Dietrich et al., *AIP Conf. Proc.* 821 (2006) 299.
- [4] V. V. Parkhomchuk, *Nucl. Instr. Meth. A* 441, (2000) 9.

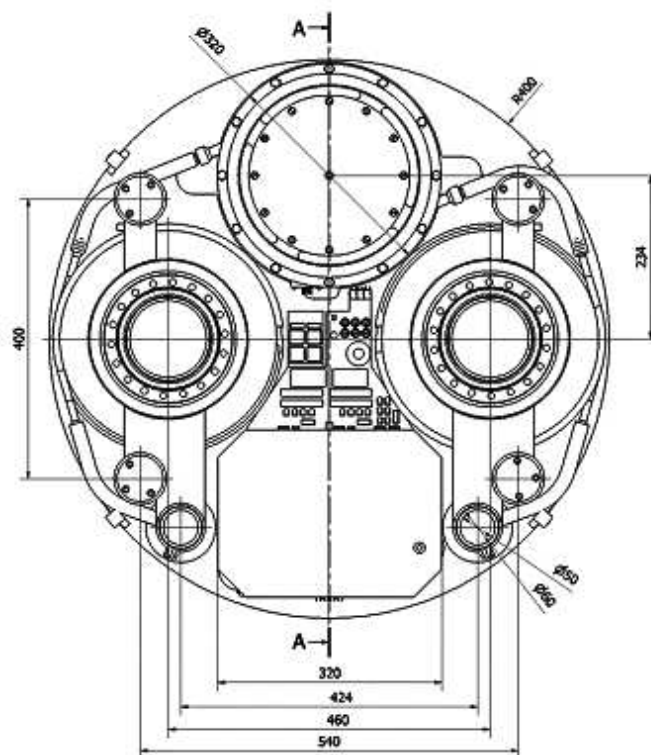
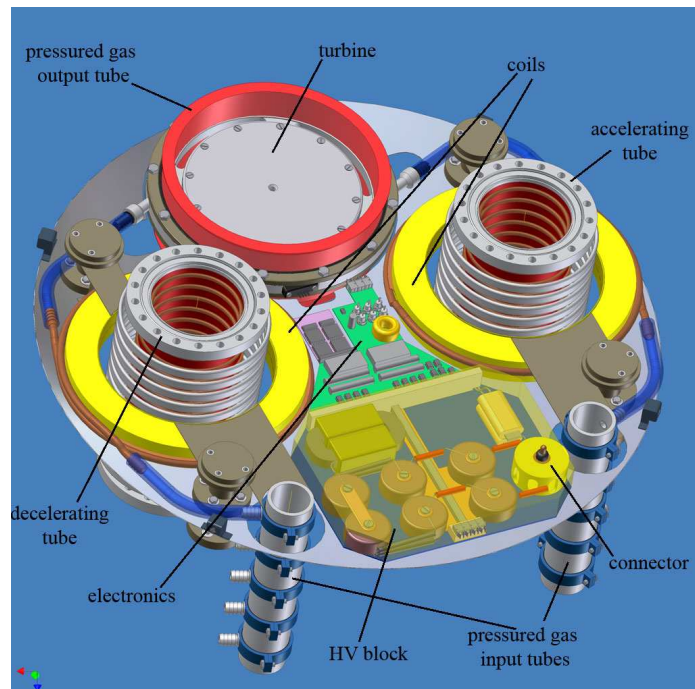


Fig. 3: Layout of a complete high voltage section.

- [5] Y. I. Golubenko et al., Accelerators of ELV-Type: Status, Development, Applications, Budker INP 97-7, Novosibirsk (1997).
- [6] R. Salimov et al., *Nucl. Instr. Meth A* 391, (1997) 138.
- [7] I. M. Bortnik, Physical properties and electric strength of sulfur hexafluoride (SF₆), Energoatomizdat, Russia (1988).

¹ BINP, Novosibirsk

Study of a Pulsed Hydrogen Dissociator for the COSY Polarized Ion Source

A.S. Belov, O. Felden, R. Gebel, A. Kieven, P. von Rossen, N. Rotert

The intensity of polarized atomic hydrogen and deuterium beams of the COSY polarized ion source has been measured to be of $7.5 \cdot 10^{16} \text{ s}^{-1}$ [1]. The development of a new hydrogen dissociator has been started with the goal to increase the intensity of the polarized atomic beam [2]. The new dissociator was supposed to operate at higher hydrogen gas pressure and higher RF discharge power, similar to the short pulse dissociator of the INR, Moscow source [3] and the IUCF polarized ion source [4], but with a significantly extended rf discharge pulse duration of about 25 ms. Several changes have been made in the design of the present dissociator in comparison with the previous quasi-dc design. The volume of the dissociator tube has been decreased to $\sim 20 \text{ cm}^3$ by shortening the dissociator tube and placing the gas valves in the vicinity of the dissociator tube. An rf generator with an amplifier producing rf power up to 4000 W was used to feed the rf discharge. A precooling channel has been added in addition to the cooled nozzle with the goal to cool down the hot hydrogen gas produced in the rf discharge due to the increased power and to reduce the influence of plasma penetrating from the discharge area to the nozzle stage. The precooler walls were cooled down to 100 K using a flexible thermal contact from the cryogenerator's 1st stage to the aluminum block of the precooler stage was arranged using a bundle of aluminum foils.

The dissociator nozzle's diameter was 2.5 mm. A new skimmer with an orifice of 6 mm in diameter has been installed 35 mm downstream of the nozzle exit.

The density of the atomic hydrogen beam was measured with a time-of-flight mass spectrometer (TOF-MS) which was installed 54 cm downstream the skimmer. The velocities of atoms and molecules were measured with the time-of-flight method using an apparatus having a chopper wheel with two slits and a quadrupole mass spectrometer installed 88 cm downstream of the chopper wheel [2].

The velocity distributions, collected under different

settings, were fitted with the function

$$f(v) = A \cdot v^2 \cdot \exp\left(\frac{(v-U)^2}{2kT_1}\right).$$

U is the drift velocity of the atoms in a beam and T_1 is a parameter, with the dimension of a temperature, describing the width of the velocity distribution.

The measurements showed that the parameters of the atomic hydrogen beam produced with the high power rf discharge dissociator were influenced by plasma penetration to the nozzle stage of the dissociator tube. The plasma penetration was found to depend on the rf discharge power, the hydrogen gas flux, the position of the rf coil relative to the nozzle and also on the amount of oxygen injected into the dissociator tube. Figure 1 shows the dependence of the most probable velocity for hydrogen atoms versus gas flux for the precooler channel made of a pyrex glass tube with an internal diameter of 9 mm when the plasma penetration was not eliminated. The rf power was increased with increasing gas flux in order to have high ($\sim 80\%$) relative part of hydrogen atoms in the hydrogen beam produced. Figure 2 shows the respective dependence for parameter T_1 . There is a step like increase of the most probable velocity from $2 \cdot 10^5 \text{ cm/s}$ up to $2.8 \cdot 10^5 \text{ cm/s}$ and of the temperature from about 15 K up to 43 K values at high gas flux. This step like velocity and temperature rise was found to occur due to the plasma penetration from the rf discharge area to the nozzle. This effect is shown in fig. 3. It is obvious that the observed increase of the most probable velocity and of the temperature reduces the atomic beam quality. Therefore, a study has been performed to overcome the problem.

It was found that it is possible to eliminate the plasma penetration by proper tuning of the rf generator and the rf coil position relative to the nozzle, minimizing the oxygen flux and decreasing the diameter of the precooling channel.

Figures 4 and 5 show the dependence of the most probable

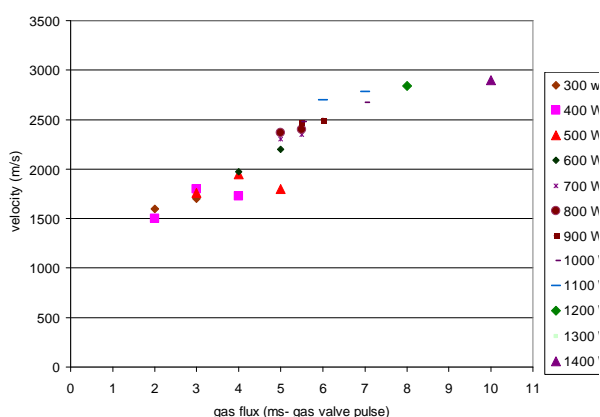


Fig. 1: Most probable velocity vs. gas flux for the dissociator when plasma penetration has not been eliminated.

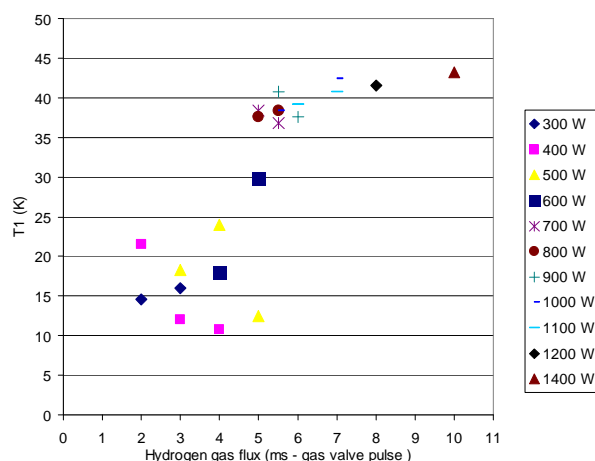


Fig. 2: Parameter T_1 vs. gas flux for dissociator when plasma penetration has not been eliminated.

velocity and the parameter T_1 when plasma penetration has been eliminated and applying the rf power up to the highest level. The plasma penetration has been eliminated due to several changes. In particular, the internal diameter of the pyrex precooling channel was reduced to 6 mm. Also, the rf coil has been moved 30 mm from its initial position near the precooling channel toward center of the dissociator tube. As a result, the most probable velocity and the parameter T_1 became a monotonic function of gas flux in spite of rf power level up to 3000 W. For the highest gas flux and rf power level the most probable velocity value reaches $2.1 \cdot 10^5$ cm/s and a temperature of 17.8 K.

Figure 6 shows results for the density of the atomic hydrogen beam obtained with the TOF-MS. The density of the atomic hydrogen beam obtained for the highest hydrogen gas flux and rf power of 3000 W exceeds 2.2 times that of the previous design of the dissociator.

A respective increase in polarized atomic hydrogen beam intensity is expected after the installation of permanent sextupole magnets in the apparatus. Taking the results of the actual velocity distribution measurements into account, new parameters for the sextupole magnets configuration will be chosen on the basis of trajectory calculation for the atoms.

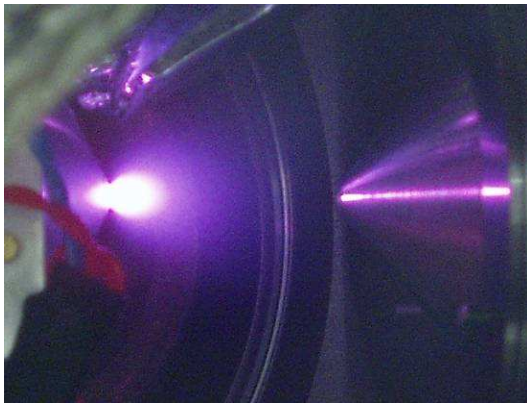


Fig. 3: Plasma penetration through the nozzle. The distance between nozzle and skimmer is 35 mm.

References:

- [1] Belov, A.S. et al.; Velocity measurements of the pulsed atomic hydrogen beam of the COSY polarized ion source; IKP Annual Report 2004
- [2] Belov, A.S. et al.; Summary of the results of the first test of a new Dissociator for the COSY polarized ion source; IKP Annual Report 2005
- [3] Belov A.S., Esin S.K., Kubalov S.A., Kuzik V.E., Stepanov A.A., Yakushev V.P, "Pulsed highintensity source of polarized protons", Nuclear Instruments and Methods in Physics Research, A255, (1987) 442-459.
- [4] Derenchuk, V.P., Belov, A.S., "A multi-milliamper polarized and unpolarized negative source for IUCF", In proceedings of the 2001 Particle Accelerator Conference, Chicago, USA, (2001) 2093-2095.

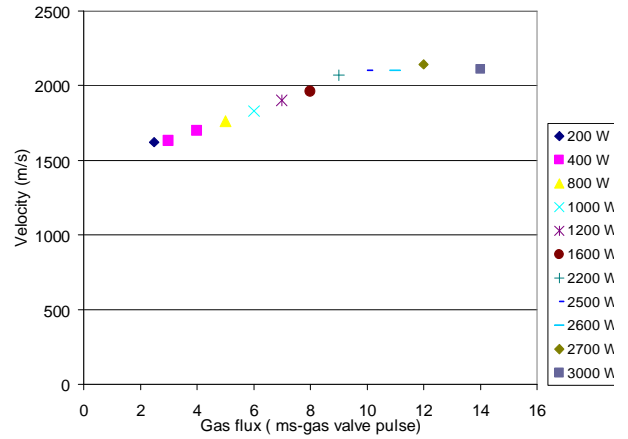


Fig. 4: Most probable velocity vs. gas flux.

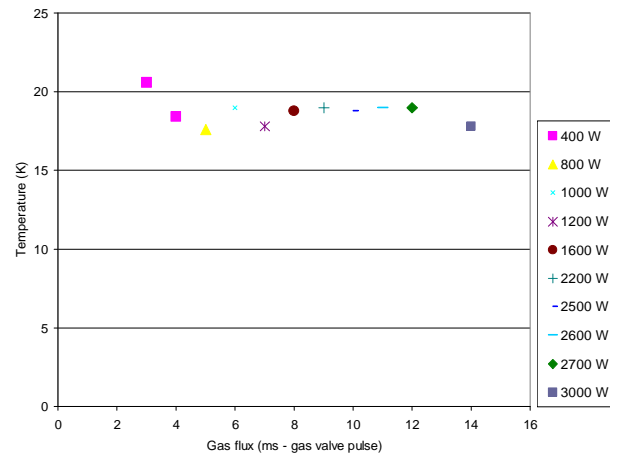


Fig. 5: Parameter beam temperature T_1 vs. gas flux.

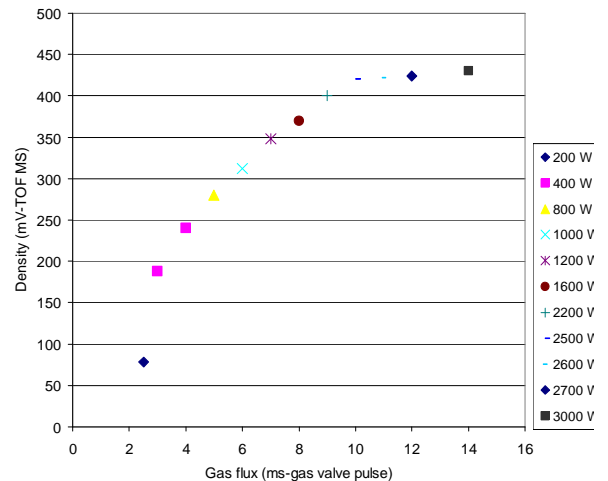


Fig. 6: Atomic hydrogen beam density vs. gas flux.

Cyclotron operation

In 2006 the injector cyclotron did provide beams for 5062 hours for the accelerator facility COSY. In that year in December the injector passed 108,851 hours of operation since it started delivering beams as COSY injector in 1989 after a major refurbishment. The time distribution over the years is shown in fig. 1. The operation of the cyclotron in 2006 was interrupted for about 500 hours due to a failure of the adjustable air line tube of the central conductor of the rf system. Besides serving COSY as injector the cyclotron was used in providing irradiations at the internal and external target stations for external users, e.g. the Institute for Nuclear Chemistry (INC).

Recent studies at the polarized ion sources

The atomic beam stage of the polarized ion source has been further investigated with the intent to increase the density of the nuclear polarized atomic beam. The achieved improvement is described in a more specific contribution to this annual report [1-3]. The very fruitful collaboration with the Institute for Nuclear Research (INR Troitsk, Russia) has been continued. The optimization studies have been partly funded by the European Community under the contract acronym HP-NIS (High Performance Negative Ion Sources). The installation of the lambda-shift polarimeter at the first beam line section started in spring 2006.

Improvement of cyclotron components

A vacuum leak at a welded flange was finally found and successfully fixed in the beginning of the year [4]. The polishing of critical surfaces, the installation of new vulcanized vacuum seals, where accessible, resulted in the recovery of the intolerable state of the vacuum system, which has reduced the performance for beam delivery of the injector in the second half of 2005. The pressure dependence of the intensity close to the extraction radius is depicted in figure 3. The beam losses reached a critical level of over 50% in November 2005. Shortly after the recovery from the shutdown the system has reached a pressure in the low 10^{-7} mbar regime. After a few weeks the average pressure in the chamber decreased to values below $1 \cdot 10^{-7}$ mbar. The improved beam transmission through the cyclotron is depicted in fig. 2, here for the case of unpolarized deuterons.

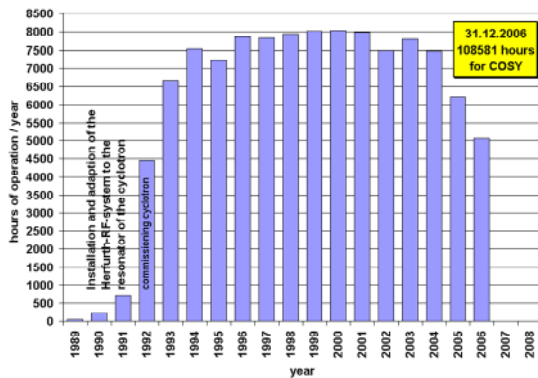


Fig. 1: Operation of the Cyclotron as the injector for COSY. At the end of 2006 the operating time of the cyclotron rf reached 108,851 hours.

During the year several components of the cyclotron have been replaced successfully. The efforts are briefly summarized and depicted in fig. 4 to 8.

Dee tip connector

In order to minimize unwanted field contributions from the Dee tips in the zone of the first acceleration the connector to the central point of the cyclotron has been modified. The new set-up is schematically depicted in fig. 4.

Septum

A long term activity is the improvement of the extraction septum for the operation with deuteron beams at high momentum. Due to depositions on the isolator the usability of the septum is limited in case of operation at high voltages above 30 kV. An example is shown in fig. 5. The differential pumping system of the linear actuators has been replaced successfully.

Replacement of tuning condensator

The water cooled condensators with their motor driven positioning has been replaced successfully. A new construction has been installed.

Repair of the adjustable air line

During the summer shutdown the damages at the linear tuning element of the central tuner became obvious during maintenance. Severe burn-out, scratches and broken contact springs made it necessary to overhaul the linear tuner completely. After refurbishment of the parts the operation has been continued delayed and with reduced working range for the frequency. The set-up of the matching hardware is shown in fig. 6-8.

The complete functionality will be available again after the successful repair, planned for summer 2007.



Fig. 2: Beam transmission through the cyclotron as the demonstration for the improved situation in 2006.

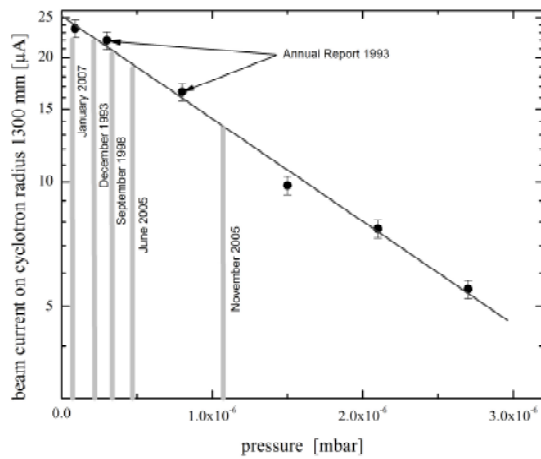


Fig. 3: A semi-log plot of the beam intensity close to the extraction radius as a function of the measured pressure. The exponential fit includes all points and shows the limit for unrestricted pumping speed.

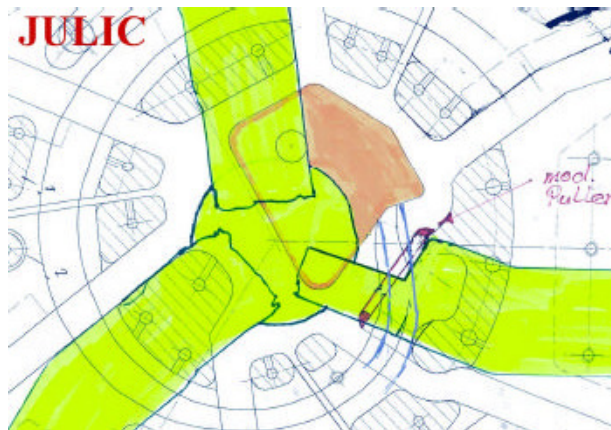


Fig. 4: The schematic view of the new dee tip.

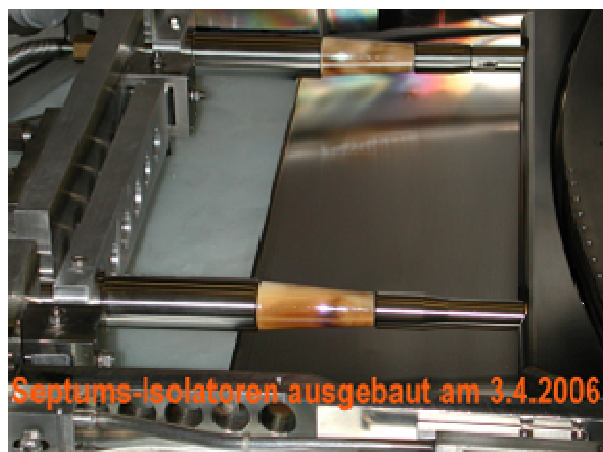


Fig. 5: Septum situation in summer 2006.

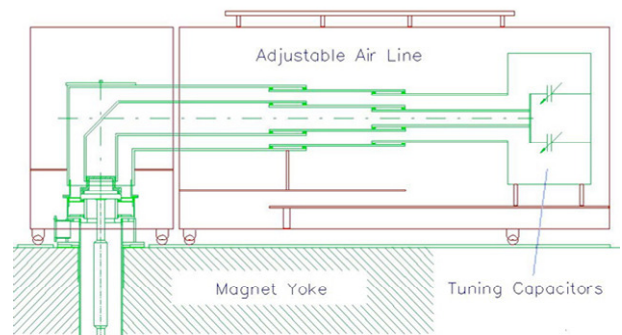


Fig. 6: The schematic view of the matching hardware on the top of the cyclotron magnet's yoke.

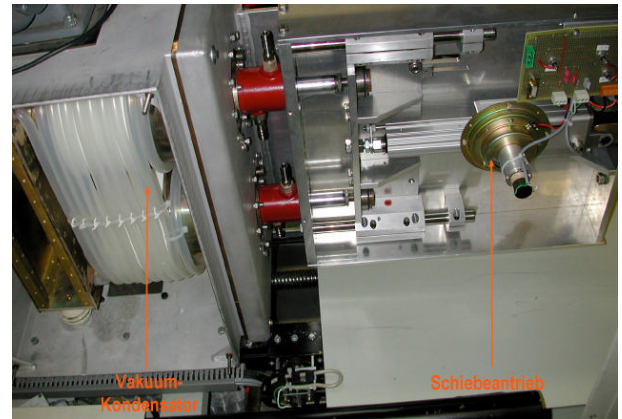


Fig. 7: The tuning capacitors have been replaced in the winter shutdown period 2006.

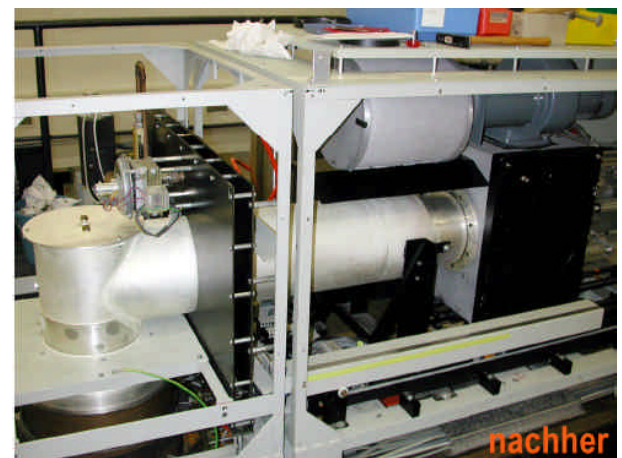


Fig. 8: The air line has been improved in summer 2006.

References

- [1] Belov, A.S. et al.; Velocity measurements of the pulsed atomic hydrogen beam of the COSY polarized ion source; IKP Annual Report 2004
- [2] Belov, A.S. et al.; Summary of the results of the first test of a new Dissociator for the COSY polarized ion source; IKP Annual Report 2005
- [3] Belov, A.S. et al.; Study of a Pulsed Hydrogen Dissociator for the COSY Polarized Ion Source; IKP Annual Report 2006
- [4] Brings, R. et al.; Operation of the injector cyclotron and the ion sources; IKP Annual Report 2005.

Substitute of Power Supplies and Improving of Water Cooling Circuits

P. Birx, H. Borsch, R. Hecker, K. Kruck, A. Richert, D. Ruhrig, J. Schmitz, H. Schneider

This report shows changes and improvements concerning power supplies and water cooling circuits at COSY. More than 20 years Bruker power converters reliably supplied the magnets of the Ion source beam line. But a lot of water hoses inside of the converts became porous. Little water ran out, some power stages failed and rust appeared everywhere. A repair was not efficient anymore. Hence these supplies have been replaced by air-cooled devices from Bruker, Danfysik and Rohrer.

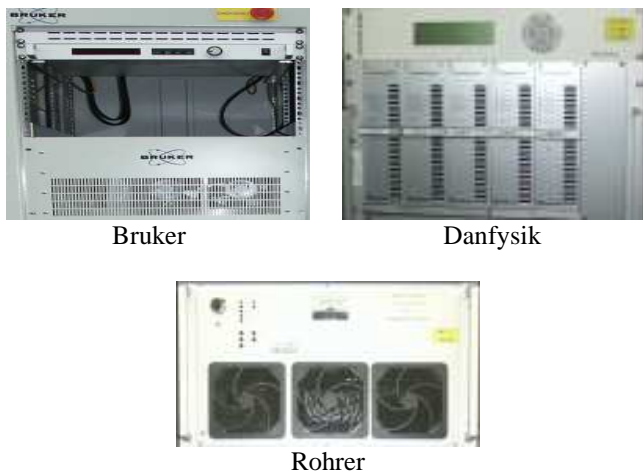


Fig. 1: New converters for magnets of the Ion source beam line.

The water connections of the compressors from the vacuum cryogenic pumps of the cyclotron have been switched from the domestic tap water to a closed water cooling circuit with heat exchanger. In advance another three water junction points have been installed for temporary needed loads as well. Thus the yearly operating costs of these devices are reduced by a factor of 10!



Fig. 2: Water distribution station

Overflow- (6.5bar) and safety- (8.5bar) valve at the Injector water cooling circuit of the Cyclotron are now exactly adjusted to each other. Closing of any outlet does not switch off the main pump anymore.

The reactive power compensation plant had to be repaired. In stormy weather twigs were blown into the outside facility. There they caused several interruptions by short circuits and the thyristor-bridge broke down. The new bridge did not fit to the existing electronic. So the control

part had to be renewed as well. In addition all components standing outside were maintained and painted newly. All connecting screws are well insulated now.

On output stages of COSY ring quadrupole power supplies all porous hoses have been replaced by stronger tubes. Now the reliability is better than 98%. Before this action on average a chopper broke down once a month. Each fault caused two hours beam time loss at least.



Fig. 3: Defect hoses, very often with little holes or porous.



Fig. 4: Blue tubes in figure 3 replaced by more durable ones (red).

The installation of the WASA detector system inside the COSY-accelerator ring which took place in 2006 had not only large implications for the future physics program but also mandated the development of a concept to satisfy the aspects of radiation safety with respect to shielding [1]. Any intended change had to be reported to the regulating authorities to obtain their approval. Additionally, an appropriate radiation surveillance and monitoring was implemented for the large number of persons from different companies, FZJ-institutes and collaborating experimentalists from German and foreign universities who were involved during construction and testing. The overall dose of these persons during the installation of WASA is below 1mSv. Because those persons were working on various projects at COSY or in other controlled areas in the research centre this number cannot be given as an upper limit. The number of persons under radiation protection survey at the IKP rose by 5% to 150. The number of persons allowed to enter the inner hall of COSY while beam is on went up by about 10% to 112. During the first runs of the WASA detector in August/September dose rate measurements have been done at selected locations (red dots) around the WASA detector setup as shown in figure 1. For the measurements a portable neutron-dose meter REM 500 and a γ -dose meter TOL-F have been used.

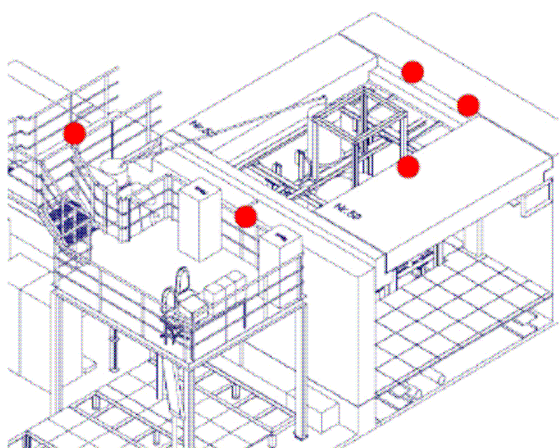


Fig. 1: Technical view on the WASA experimental setup with its shielding. The locations for dose rate measurements are marked in red.

The measured dose rates were in the expected range derived from calculations [1] and compared well with the numbers taken at the door next to the detector with the permanently installed neutron monitor NMTK 34. The maximum dose rate is by a factor 1.2 slightly above the dose rate at the door measured with NMTK 34 which is shown in fig 2. Because of the unstable operation of the WASA pellet target only a few measurements could be done. To reaffirm the measured dose rates around the WASA detector setup these measurements will be redone under proper and stable conditions.

It is envisioned to repeat these measurements during the upcoming runs of WASA Experiments in order to fix the numbers on a more quantitative level.

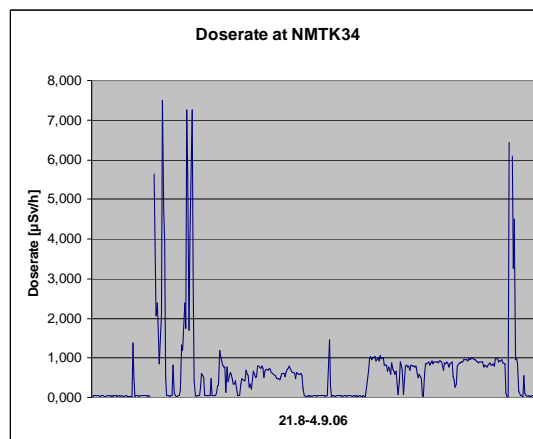


Fig. 2: Dose rates measured with NMTK 34 at the door next to WASA detector during the first run between 21.8.06 to 4.9.06.

In 2003 we started to upgrade our radiation survey and personal safety system (PSA). The Safety System is based on programmable logic systems (PLS). After Siemens announced that the support of the S5-System, which was the PLS in use, runs out we switched over to the S7-System.

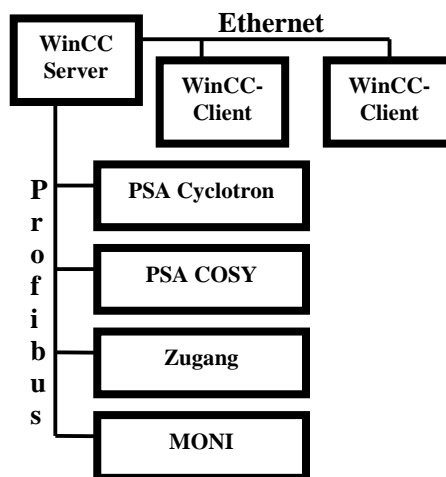


Fig. 3: Overview of the personal safety and radiation survey systems

In early 2004 we first replaced the old S5-System (PSA-COSY) running at COSY by an S7-400. In October 2004 we changed the next S5-System (“Zugang”) controlling the access to the inner hall during beam operation [2, 4].

At last there was only one S5-PLS (MONI) left, measuring the beam-losses by checking the radiation levels outside of COSY. In the event of exceeding the limits stipulated by the authorities the beam is switched off immediately. Meanwhile, this system was replaced by a S7-400 system, too. By means of watchdog functions the machines check each other. In case one should fail the COSY-beam is stopped immediately by sliding in beam-stoppers. The systems are interconnected via the profibus (fig.3), a standardized communication protocol.

All important data from the different Systems, e.g. number of people inside the inner hall, actual dose levels or position of beam-stoppers are collected by a WinCC-Server and displayed on clients in the operating room of the cyclotron

as well as in the COSY control room [3]. Warnings are given by the safety system in case of exceeding any limits, malfunctions or stopping the beam. The data are also written to files or printed on paper automatically.

References:

- [1] Radiation Protection, Annual report 2005
- [2] Radiation Protection, Annual report 2001
- [3] Status Survey System at COSY, Annual Report 2002
- [4] Radiation Protection, Annual report 2003

4 Preparations for FAIR

The High-Energy Storage Ring (HESR) of the Future international Facility for Antiproton and Ion Research (FAIR) at GSI in Darmstadt is planned to be an antiproton storage ring in the momentum range of 1.5 to 15 GeV/c [1]. Dense internal hydrogen pellet targets will be utilized to reach maximum luminosities of up to $2 \cdot 10^{32} \text{ cm}^{-2} \text{ s}^{-1}$. Luminosity estimates are presented for additional target materials from deuterium to gold [2].

The antiproton production rate is specified to be $\dot{N}_{\bar{p}} = 2 \cdot 10^7 / \text{s}$. If the total production rate is equal to the beam loss rate, the maximum luminosity reads $L_{\text{max}} = \dot{N}_{\bar{p}} / \sigma_{\text{total}}$, with σ_{total} the total cross section for beam-target interaction. The relative beam loss is then given by the expression $(\tau_{\text{loss}}^{-1}) = n_t \sigma_{\text{total}} f_0$, where n_t denotes the target thickness, and f_0 the reference particle's revolution frequency. Three dominating contributions of the beam-target interaction have been identified: Hadronic interaction, single Coulomb scattering and energy straggling [3,4].

The hadronic cross section for the interaction of antiprotons with for nuclear targets is estimated by [5]

$$\sigma_{\bar{p}p} = 100 \text{ mb} \equiv \pi(r_p)^2, \sigma_{\bar{p}A} = \pi(R_A + r_p)^2, R_A = r_0 A^{1/3}$$

$$r_0 = 1.2 \text{ fm}, r_p = 0.9 \text{ fm}$$

In Table 1 hadronic cross sections for different target materials are summarized, taking 100 mb for hydrogen targets at 1.5 GeV/c beam momentum as a reference. The total hadronic cross section changes with the beam momentum. $\sigma_{\text{hadronic}} = 100, 60$ to 50 mb for hydrogen targets at $1.5, 9,$ and 15 GeV/c, respectively. The cross sections for nuclear targets at higher beam momenta is scaled accordingly [6].

Table 1: Estimation of hadronic cross section at 1.5 GeV/c

	Cluster-Jet / Pellet						Solid					
Target ZA	H 1,1	D 1,2	N 7,14	Ne 10,20	Ar 18,40	Kr 36,84	Xe 54,131	C 6,12	Al 13,27	Ni 28,58	Ag 47,108	Au 79,197
Cross Section /b	0.1	0.2	0.45	0.54	0.79	1.19	1.54	0.42	0.64	0.97	1.37	1.95

Fig. 1 summarizes relative beam loss rates and maximum luminosities for nuclear targets. A longitudinal ring acceptance of $\Delta p_{\text{max}}/p = \pm 10^{-3}$ is assumed. The transverse normalized rms emittance is $\varepsilon = 1 \text{ mm-mrad}$.

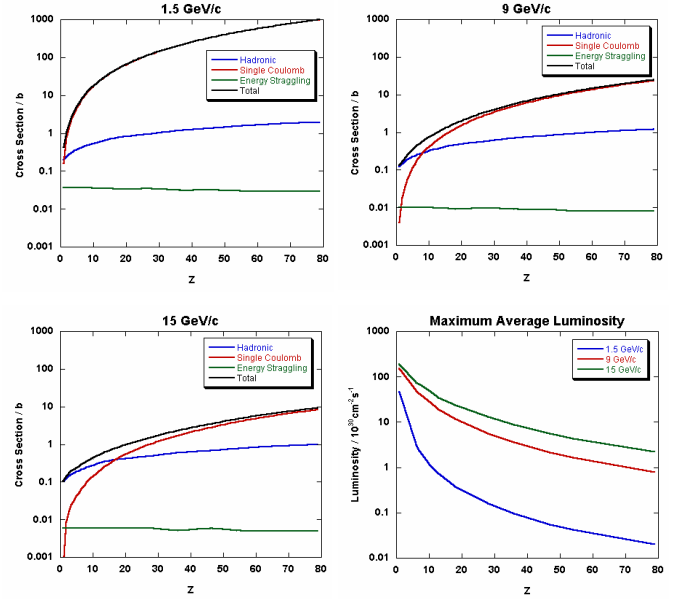


Fig. 1: Beam loss cross section due to beam-target interaction vs. atomic number Z for three different beam momenta (plot 1-3). Maximum average luminosity vs. atomic number Z for three different beam momenta (plot 4).

For the specified antiproton production rate maximum average luminosities of $5 \cdot 10^{31}, 4 \cdot 10^{29}$ to $4 \cdot 10^{28} \text{ cm}^{-2} \cdot \text{s}^{-1}$ (deuterium, argon to gold) are reached at 1.5 GeV/c beam momentum. The minimum effective target thickness to realize those luminosities is ranging from $1 \cdot 10^{15}, 9 \cdot 10^{12}$ to $5 \cdot 10^{11} \text{ cm}^{-2}$ assuming the maximum number of circulating particles in the HESR.

For maximum beam momentum of 15 GeV/c the maximum average luminosities are increasing by more than one order of magnitude to $1.9 \cdot 10^{32}, 2.4 \cdot 10^{31}$ to $2.2 \cdot 10^{30} \text{ cm}^{-2} \cdot \text{s}^{-1}$ (deuterium, argon to gold). In this case the minimum effective target thickness is ranging from $3.6 \cdot 10^{15}, 4.6 \cdot 10^{14}$ to $4.1 \cdot 10^{13} \text{ cm}^{-2}$ for 10^{11} circulating antiprotons.

References:

- [1] FAIR Baseline Technical Report, Volume 2: Accelerator and Science Infrastructure (2006).
- [2] A. Lehrach, Maximum Luminosity with Nuclear Targets in HESR, plenary talk at the XIX. PANDA Collaboration Meeting, GSI Darmstadt, Dec. 2006.
- [3] F. Hinterberger, Beam-Target Interaction and Intra-beam Scattering in the HESR Ring: Emittance, Momentum Resolution and Luminosity, Jül-Report No. 4206, ISSN 0944-2952 (2006).
- [4] A. Lehrach et al., Nucl. Instr. Meth. A 561, 289 (2006).
- [5] A. Gillitzer, private communication.
- [6] see <http://pdg.lbl.gov/>

¹ Institut für Kernphysik, Forschungszentrum Jülich

Ring-Slot Coupler for the HESR Stochastic Cooling System

R. Stassen, P. Brittner, R. Greven, H. Heimbach, H. Singer, G. Schug, L. Thorndahl

Animated by the octagonal lambda/4 structure [2], we analysed a slot coupler with the same HESR aperture of 89 mm. The structure consists of AlMg4,5Mn rings with 8 shorted electrodes (Fig. 1). The total image current passes the surrounding uninterrupted gap formed by two adjacent rings (Fig. 2). We obtain the desired octave bandwidth (2-4 GHz) due to the heavy loading by the eight 50-Ohm coaxial lines.

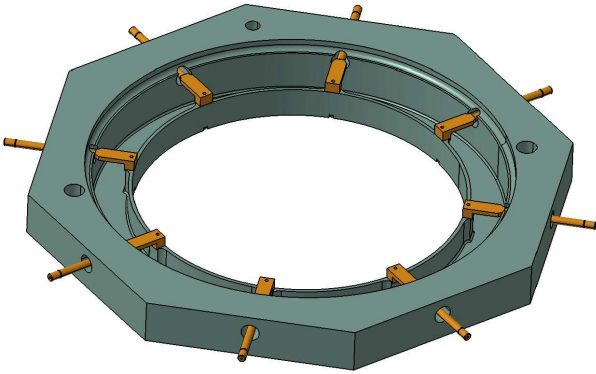


Fig. 1: slot coupler design

The HFSS [4] simulations gives a more than two times higher longitudinal coupling impedance per unit length than comparable lambda/4 structures [1]. The results of the MWS [3] simulation including a 30mm inner conductor which will substitutes the beam during the first RF-tests agree very well with the HFSS simulation. The coupling between one of the 8 coaxial pickup ports and the beam simulating central coax line amounts to 21 +/- 1.5 dB over the whole frequency range.

The modular design of this structure allows an easy increase of the number of rings. Two following octagonal rings are centred together by circumferential steps of 3mm length and fits of the diameter within 0.05mm; pivots provide the angular fits. In order to compare the slot coupler with the lambda/4 structure, a group of 8 rings is under fabrication at our central workshop.

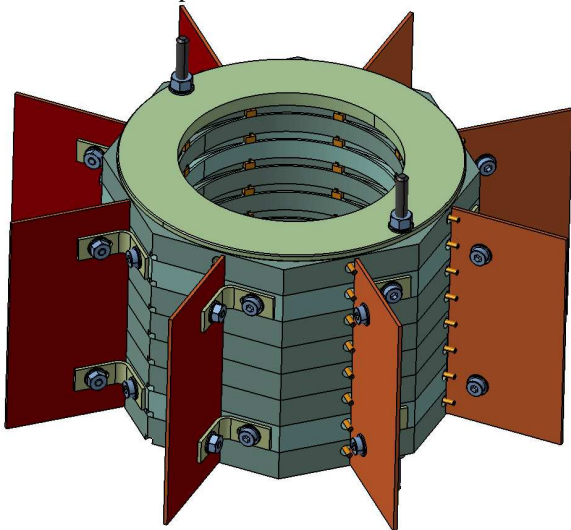
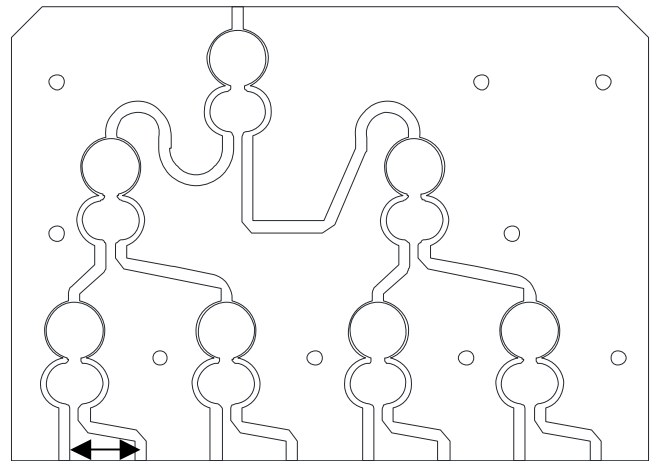


Fig. 2: Test structure with 8 rings including mounting plates for combiner boards

A similar combiner board as the simple transforming

network used for the lambda/4 coupler [2] can not be used in this case because of great influence of neighbouring low-impedance electrodes. A good decoupling can be reached by using Wilkinson couplers instead of impedance transforming networks.

The combiner boards will be mounted in a rectangular position (Fig. 3) during the first tests, while in the final version the layout of the Wilkinson coupler boards will be changed to fit on a flat board directly mounted at one face of the octagons of the rings. This will give us a very compact and robust design. The good separation of the beam-area and the possibly out gassing polymer material of the combiner boards qualified this structure for heavy ion cooling with higher vacuum requirements as well.



12.5mm

Fig. 3: Wilkinson combiner board; decoupling resistors are not shown

The design includes high-power resistors and heat flow estimation and uses the same board at the kicker structure. After the first RF tests, the calculated improvements of longitudinal sensitivity (around several dB) by enlargement of the ring cavities and reduction to 4 coupling lines will experimentally verified.

References:

- [1] L. Thorndahl, Fixed 90mm Full-Aperture Structures with TM₁₀-Mode propagation for Stochastic Cooling in HESR, 2006
- [2] R. Stassen, Pickup structures for HESR stochastic cooling system, EPAC2006, Edinburgh, UK
- [3] MicroWaveStudio, CST GmbH, Darmstadt, <http://www.cst.de>
- [4] HighFrequencyStructureSimulator, Ansoft Corporation, USA, <http://www.ansoft.com>

The design of the High-Energy Storage Ring (HESR) of the future international Facility for Antiproton and Ion Research (FAIR) [1] at the GSI in Darmstadt includes electron and stochastic cooling. Simulations have shown that the bandwidth of a 2-4 GHz stochastic cooling system is sufficient to achieve the requested beam quality at the internal target [2]. New 2-4 GHz pickup structures have been developed and tested mainly for transversal operation. The printed loop boards have been constructed as a part of a universal modular octagonal structure. Different modes of signal combinations outside the vacuum envelopes will allow to pick up different transversal beam positions as a part e.g. of a core or a halo cooling system.

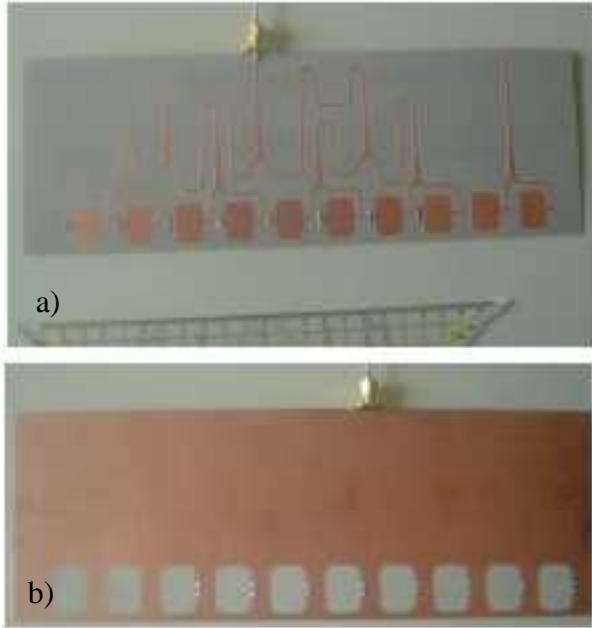


Fig.1: Printed loop couplers (the grid of the ruler is 1cm) including the combiners: a) combiner side, b) beam side

The $\lambda/4$ loops of the 2-4GHz system are part of the combiner boards. This simplified the whole structure and minimized the fabrication costs. Top and bottom side of the first $\lambda/4$ -loop test-board are shown in Fig. 1. The low aperture in the HESR and the possibility to gain sensitivity by combining different electrode rows supersede the necessity of moving electrode bars. The base material for the $\lambda/4$ loops is the temperature compensated TMM3 [3] with a low permittivity of $\epsilon_r=3.27$. A microstrip ring resonator built at this material has been cooled down to 77K. The resonator frequency changed by less than 1.4% . Thus no significant parameter change between cold pickup and warm kicker operation is expected.

A first check at the vacuum test stand has shown that the material is well compatible with the vacuum conditions of the HESR.

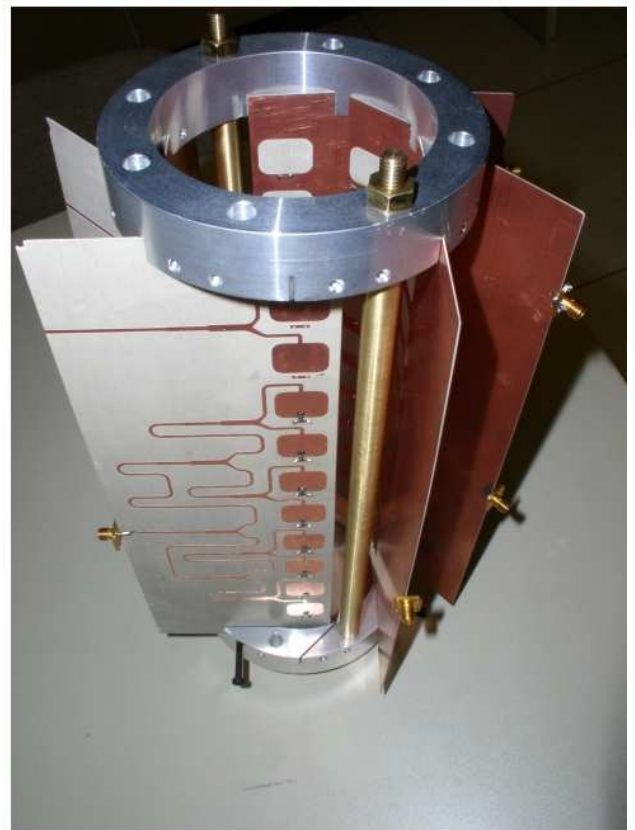


Fig. 2: Octagonal pickup structure, equipped with 6 $\lambda/4$ -electrode rows

The couplers have been tested in an air-filled microstrip test bench to compare the sensitivity of the new simpler coupler to that of the COSY band 2 electrodes. The width of the COSY loops is the same as that of the printed loops. Even the number of combined loops is the same, thus a direct comparison is possible. Fig. 3 shows the cooling pickup structure of COSY [4] which was adapted from the CERN AC structure [5].



Fig. 3: COSY cooling structure and test bench. The length in the beam direction reaches about 0.25m (8 electrodes).

The results of the measurements are presented in Fig. 4. Although the printed loops have been optimized for a frequency range of 2-4 GHz the measurements shows that these loops have the same transversal sensitivity as the COSY loops and can be used even at a larger frequency band.

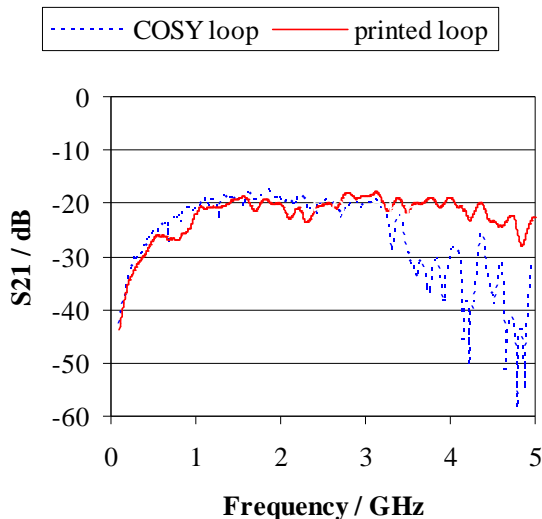


Fig. 4: Comparison of COSY-loop and printed-loop structures using the test bench of Fig. 3.

The transversal sensitivity of the octagonal structure has been measured using a 30mm inner conductor with a coaxial transition to 50 Ohm as a beam replacement. The signal of a vertical beam displacement was gained by following three steps:

- addition of the powers of each board pair adjacent to their middle boards,
- combining these signals with that of the corresponding adjacent middle board,
- subtraction of the signals of both groups of three boards.

The difference signal of a 7mm displacement was about 10dB higher than the one of a centred inner conductor over the whole frequency range (2-4GHz).

In a next step we will compare the corresponding transverse sensitivity to that of a stack of ring-slot couplers [6].

References:

- [1] W.F. Henning, An International Accelerator Facility for Research with Ions and Antiprotons, proceedings of EPAC04, Lucerne, Switzerland
- [2] H. Stockhorst, B. Lorentz, R. Maier, D. Prasuhn, T. Katayama, Stochastic cooling for the HESR at the GSI-FAIR complex, EPAC2006, Edinburgh, UK
- [3] TMM3, temperature stable microwave laminate ($\epsilon_r=3.27$), Rogers Corporation.
- [4] P. Brittner, H.U. Hacker, R. Maier, U. Pfister, D. Prasuhn, H. Singer, W. Spiess, R. Stassen, H. Stockhorst, A. Zumloh, The stochastic cooling system for COSY, proceedings of EPAC92, Berlin
- [5] B. Autin, G. Carron, F. Caspers, S. Milner, L. Thorndahl, S. van der Meer, ACOL stochastic cooling systems, proceedings of PAC87, Washington, USA, 1987
- [6] R. Stassen, P. Brittner, R. Greven, H. Heimbach, H. singer, G. Schug, L. Thorndahl, Ring-Slot coupler for the HESR stochastic cooling system, this report

Investigation of the Operation Regimes with the Moscow-Jülich Pellet Target*

A. Boukharov^a, M. Büscher^b, V. Balanutsa^c, V. Chernetsky^c, A. Demekhin^c, P. Fedorets^{b,c}, A. Gerasimov^c, L. Gusev^c, I. Maryshev^a, S. Podchasky^c, A. Semenov^a

The tests with the Pellet Target in 2006 focused on the investigation of cooling regimes of the cryogenic gases which are used for the production of thin cryogenic jets. According to our previous studies, the size and velocity variations of the droplets before the first sluice critically depend on the temperature and velocity stability of the jet when emanating from the nozzle. Excellent droplet stability in turn is crucial for a minimal velocity spread and a narrow angular distribution of the pellets at the sluice outlet and at the interaction point with the accelerator beam. The tests have been performed with jet diameters of 10–20 μm . In order to work with such small diameters of jets, the droplet generator and the temperature-measurement system in the condenser and in the droplet generator have been modified.

Temperature monitoring inside the cryostat has been realized with a set of specially calibrated sensors *TG-120-SD* from *Lake Shore Cryotronics* which are shown in Fig.1.

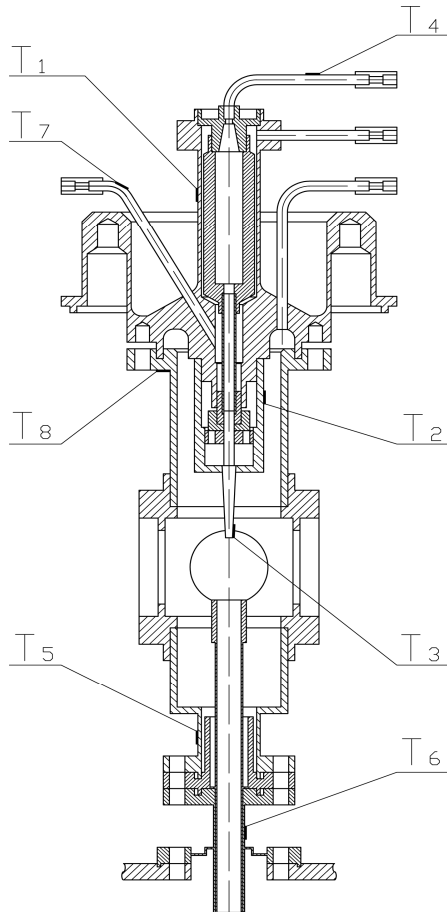


Fig 1: Positions of the temperature sensors at the condenser and the triple point chamber

Liquefaction of the cryogenic gas in the condenser has been controlled by sensor T_1 . The control of temperature in the droplet generator has been achieved with

sensors T_2 and T_3 located directly on the droplet generator. The input gas temperature of the condenser has been controlled with T_4 , fixed on the input tube. The temperature of the cold He gas for cooling in the condenser has been monitored by T_7 . The cold evaporated He gas was used during the tests for liquefaction of N_2 and H_2 . For liquefaction of Ar evaporated nitrogen has been utilized. The control of the upper and lower parts of the triple point chamber was realized with T_5 and T_8 . The sluice temperature was obtained from T_6 , installed on the bottom of the triple point chamber. The sensor information has been read and digitized by block Thermometers 208 from *Lake Shore Cryotronics* and a PC. The accuracy of the temperature measurements was ± 0.3 K. The software performs the data analysis and produces plots of temperature distributions. During the tests, the dependence of the temperature gradient in the condenser and in the droplet generator from the expense and temperature of the cold evaporated He coming into the condenser has been studied.

A stroboscope CT-MPEI and a *Pro.imaging PixelFly* digital video-camera have been used to control the droplet-production process. The stroboscope illuminated the jet and droplets with short light impulses (duration around 1 μs). The stroboscope has been triggered by a signal with a frequency which was synchronous with the frequency of the signal in the droplet generator. The digital camera has been applied for detection of the processes taking place during the droplet formation.

After analysis of the temperature data, the cooling parameters providing minimal temperature gradients have been defined. The monodisperse jet decay from N_2 and H_2 has been detected at the minimal temperature gradient. The photos of decays and their parameters are presented in Fig.2 and in Table 1.

Table 1: Parameters of the jets from Fig. 2.

	N_2	H_2
TPC temperature (K)	74	17
TPC pressure (mbar)	300	130
Nozzle frequency f (kHz)	14	24
Jet diameter D_0 (μm)	17	12
Jet velocity v_{jet} (m/s)	1.4	1.5

Figure 2 shows the breakup of N_2 and H_2 jets in the triple-point chamber (TPC) of our drop generator for parameters as given in Table 1. The photos exhibit the first observation of satellite-free and mono-disperse drop production from cryogenic liquids.

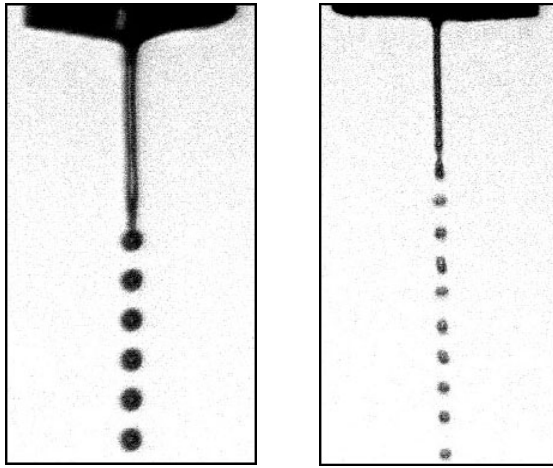


Fig. 2: Satellite-free and mono-disperse disintegration of N_2 (left) and H_2 (right) jets.

Besides of tests with nitrogen and hydrogen, tests for production of Argon jets have been performed with the same experimental facility. The Ar enters the condenser through a specially constructed gas line. This allowed us to avoid premature freezing of the Ar. For Ar liquefaction cold evaporated nitrogen from the nitrogen bath was used instead of the cold He gas. Thin jets of liquid Ar have been observed, see Fig.3 and Table 2.

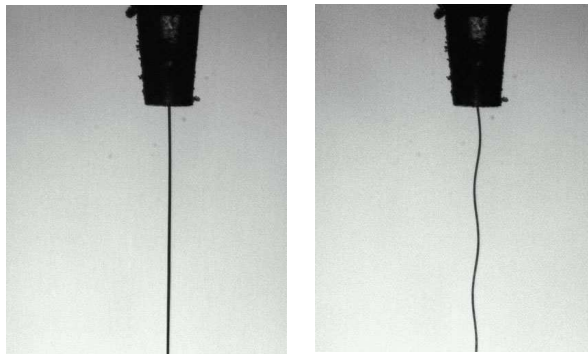


Fig. 3: Jets from Ar in the triple point chamber at different pressure values.
 TPC pressure = 300 mbar (left)
 TPC pressure = 700 mbar (right)

The analysis of the data shows, that as lower pressure in the triple point chamber, the more stable are the jet.

Table 2: Parameters of the jets from Fig. 3.

	Ar	Ar
TPC temperature (K)	83	83
TPC pressure (mbar)	300	700
Jet diameter D_0 (μm)	12	12

^a MPEI, Moscow

^b IKP FZJ

^c ITEP, Moscow

*Supported by grants EU-000419, RFFI03-02-04013, RFFI02-02-16349, DFG-436RUS-113/733.

A. Lehrach¹ for the HESR consortium and PAX collaboration

The HESR at FAIR is being designed to accelerate and store unpolarized antiprotons in the momentum range from 1.5 to 15 GeV/c [1]. Two experimental collaborations (ASSIA [2] and PAX [3]) expressed interest in spin physics experiments utilizing the HESR. This would require the generation of polarized protons in a state-of-the-art polarized ion-source and advanced techniques to produce polarized antiprotons [4]. Additional equipment has to be implemented at several machines of the acceleration chain to measure and preserve the beam's polarization. Required modifications and extensions of the accelerator layout are discussed and luminosity estimates presented [5].

The proposed extension of the FAIR accelerator scheme for polarized beams can be found in [5,6,7]. Unpolarized antiproton beams will be injected from RESR into the Cooler Synchrotron Ring CSR at roughly 3.8 GeV/c (3 GeV), decelerated down to 730 MeV/c (250 MeV) and electron cooled. Then the beam is transferred into a dedicated antiproton polarizer ring APR, where the polarization build-up takes place. The polarized antiproton beam is then transferred back to the CSR. Polarized protons can be delivered by a standard polarized proton source, the planned 70 MeV Linac and the existing SIS18. Both polarized beams can then be provided for fixed target or colliding beam experiments in CSR and HESR.

Polarized antiprotons can be produced in a large acceptance Antiproton Polarizer Ring APR by spin-dependent interaction in a pure hydrogen gas target. Spin-filtering has been established experimentally at the Test Storage Ring TSR (MPI Heidelberg) in 1992 [8]. Presently the main parameters for the APR are: beam energy of 250 MeV, and maximum ring acceptance of 250 mm-mrad [9]. A solenoidal Siberian snake has to be added to provide a longitudinal invariant spin axis at the interaction point to enforce the polarization build-up.

Since the CSR ring will be very similar to COSY, the same techniques to overcome depolarizing resonances can be applied. For a ramping rate of 1 GeV/c per second adiabatic spin flips can be excited by vertical orbit bumps of 1 mrad or a 0.5% partial snake at all five imperfection resonances. A super-periodicity for the magnet structure of one is expected due to symmetry breaking modifications in the interaction region and strong magnetic fields of the electron cooling system, leading to eleven intrinsic resonances. For a normalized emittance of 1 mm-mrad the maximum resonance strength is approximately 10^{-3} and the COSY tune-jump system would be suitable for the CSR. For the collider options the CSR will be equipped with a Siberian snake.

The SIS18 magnet structure consists of 12 super-periods. Only one intrinsic resonance has to be crossed up to 2 GeV. Its resonance strength is below 10^{-3} for a normalized emittance of 1 mm-mrad. In this case tune-jumping can be applied. For the high-intensity mode of SIS18 vertical emittances of up to 20 mm-mrad (normalized) are discussed [1]. The resonance strength would roughly be five times stronger and tune-jumping would become complicated due to increased jump width and speed. In addition four imperfection resonances have to be overcome. Since the specified ramping rate of SIS18 is larger than 1 GeV/c per 0.05s, at least a 3% partial snake is required. A small beam

emittance for efficient tune-jumping and a lower acceleration rate to reduce the snake strength would be beneficial for polarized beam acceleration in SIS18.

In the momentum range of the HESR 25 imperfection resonances and 50 intrinsic resonances have to be crossed. In addition 50 depolarizing coupling resonances are expected, due to strong solenoids in the electron cooler and target section. The strength of the resonances is ranging from 10^{-2} to 10^{-5} for the expected beam parameter with a normalized emittance of 1 mm-mrad. To guarantee low polarization losses during acceleration, a Siberian snake scheme has been specified [6,7].

In a first stage experiments with polarized antiproton beam and polarized hydrogen gas targets are planned. For the specified antiproton production rate maximum luminosities with polarized internal targets of 0.6 to $4.2 \cdot 10^{31}$ cm⁻²·s⁻¹ (1.5 to 15 GeV/c) are possible [5], depending on the beam momentum.

The PAX collaboration proposed an asymmetric collider concept [6], where the polarized beam in the CSR with maximum momentum of 3.5 GeV/c collides with a polarized beam of up to 15 GeV/c in HESR. The limits for luminosities are determined by the antiproton production rate, cooling force of electron cooling, intra-beam scattering, space charge at injection, and beam-beam parameter. Estimates indicate that maximum values above 10^{31} cm⁻²·s⁻¹ are challenging [5]. A symmetric collider scheme (both beams colliding at 15 GeV/c in the HESR) is also proposed [7].

References:

- [1] FAIR Baseline Technical Report, Volume 2: Accelerator and Science Infrastructure (2006).
- [2] Letter-of-Intent, ASSIA collaboration (2004).
- [3] Letter-of-Intent, PAX collaboration (2004).
- [4] F. Rathmann et al., Phys. Rev. Lett. 93, 224801 (2004).
- [5] A. Lehrach, Proc. of 17th International Spin Physics Symposium SPIN2006, Kyoto.
- [6] Technical Proposal, PAX collaboration (2006).
- [7] F. Bradamante et al., arXiv.org: physics/0511252.
- [8] F. Rathmann et al., Phys. Rev. Lett. 71, 1379 (1993).
- [9] A. Garishvili et al., Proc. of 10th European Particle Accelerator Conference EPAC2006, Edinburgh.

¹ Institut für Kernphysik, Forschungszentrum Jülich

In the framework of the FAIR [1] project, the PAX collaboration has suggested new experiments using polarized antiprotons [2]. The central physics issue is now to study the polarization build-up by spin filtering of antiprotons via multiple passage through an internal polarized gas target. The goals for spin-filtering experiments with protons at COSY are to test our understanding of the spin-filtering processes and to commission the setup for the experiments with antiprotons at the Antiproton Decelerator (CERN). Spin-filtering experiments with antiprotons at the AD will allow us to determine the total spin-dependent transversal and longitudinal cross sections.

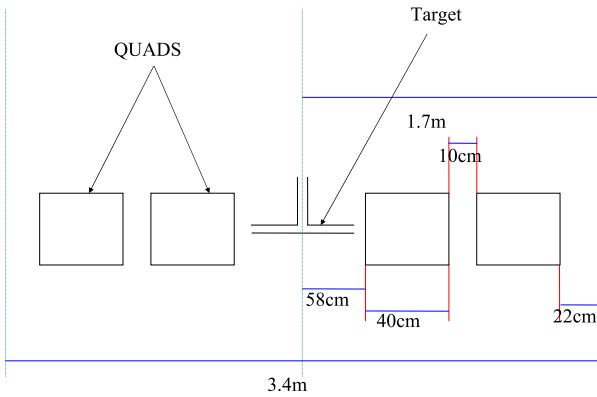


Fig. 1: The low beta section at COSY.

The COSY ring has an acceptance of 30π mm mrad and magnetic rigidity of 12.34 Tm which implies a maximum momentum of 3.7 GeV/c for the stored protons. After cooling, the beam has an emittance of 3π mm mrad. The lowest beta function reachable with the present lattice settings is about 2 m. The spin-filtering tests request the use of a small cross section storage cell to produce a high-density polarized target. For this reason a new low beta section has to be implemented in the ring at TP1. The total available space at that position is 3.4 m.

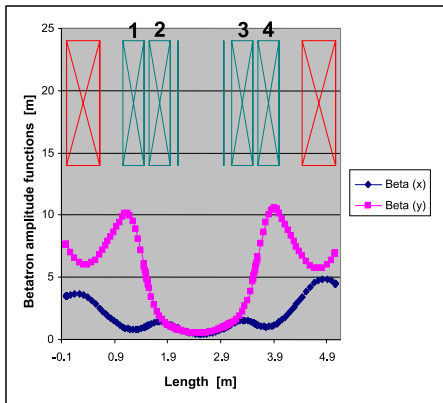


Fig. 2: Distribution of the beta functions along the low beta section. Red magnets are existing COSY quads, green new low beta quads.

The scheme of the new low beta section is presented in Figure 1. The section is composed of two superconducting quadrupole magnets on each side of the target with a length of 40 cm. Drift space between the magnets is 10 cm. For the target, 116 cm space is reserved.

The betatron amplitude function (beta function) in the low-beta section has been calculated by fixing the original input lattice parameters ($\alpha_x, \alpha_y, \beta_x$ and β_y) at the beginning of the available space and matching them to the original input parameters at the end of the available space. The highest focusing strength for corresponding quadrupoles is 5.5 m^{-2} . The minimum beta functions at the center of the target are $\beta_x=0.436 \text{ m}$ and $\beta_y=0.497 \text{ m}$.

The maxima of the beta functions in the low-beta section are around 10m, which will allow to inject in the target cell also an uncooled beam (Figure 3).

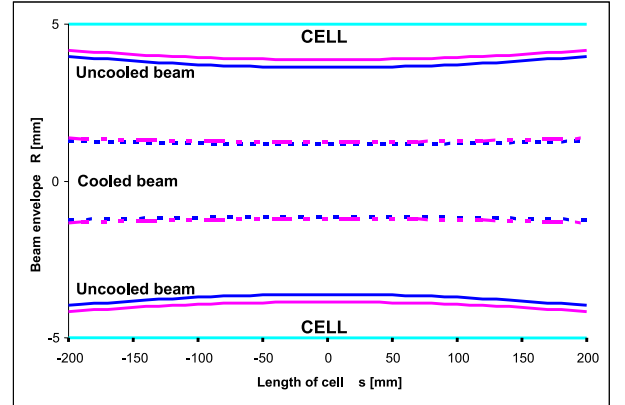


Fig. 3: Beam envelope at the cell. Dark blue lines are R_x , red lines R_y . Solid lines are uncooled beam, and dashed lines cooled beam. Blue lines show the size of the cell (10 mm).

At COSY, thanks to the ring telescopic mode in the straight sections, it will be possible to turn on and off the low-beta section during the running by compensating the phase advance with the regular COSY quadrupoles.

The AD ring at Cern presents a magnetic rigidity of 12.07 Tm which implies maximum momentum of 3.57 GeV/c. The horizontal acceptance of the machine 220π mm mrad and the vertical 190π mm mrad. At the lowest energy (50 MeV) the beam emittance in both planes goes down to around 5π mm mrad. The present beta functions are higher than 2 m, therefore a new low-beta section has to be installed here as well. The available space for the low-beta section is 5.67 m. provided that one of the existing AD quadrupoles at the center of the straight section at the AD. A preliminary design of the low-beta section at the AD is shown at Figure 4.

At the AD an additional SuperConducing quadrupole (identical to the others) is requested on each side of the target. In the design the space foreseen of the target is longer than at COSY (1.67 m). The gap between the additional and the quadrupoles used at COSY is 40 cm.

The distribution of the low beta function has been calculated in an analogous way as in COSY and is shown in Figure 5.

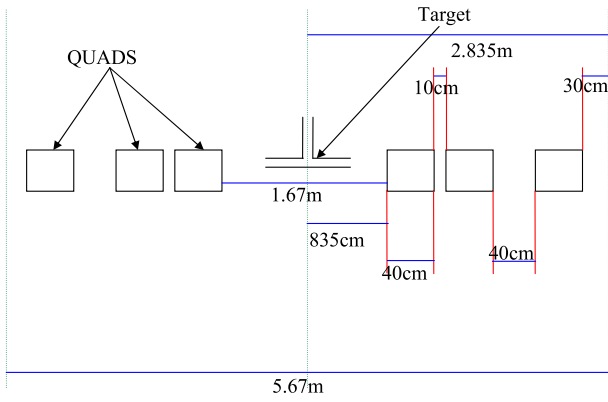


Fig. 4: The low beta section at the AD.

The highest focusing strength for corresponding quadrupoles is 4.84 m^{-2} . The minimum beta functions at the center of the target are $\beta_x=0.37\text{m}$ and $\beta_y=0.55\text{m}$. The maximum beta function in the low-beta section is around 12.5m.

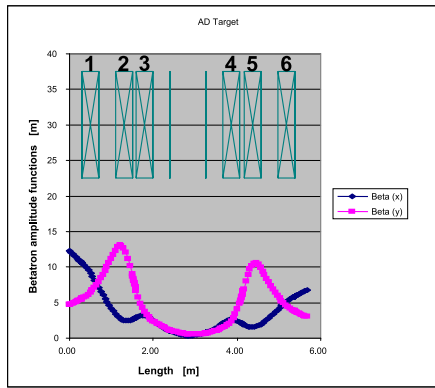


Fig. 5: The distribution of beta functions at low beta section at the AD.

As it can be deduced from Figure 6, the uncooled beam cannot be injected through the target cell. For this reason, at the AD, we have to open the cell by about 2cm, before beam will be cooled.

At the AD the low beta section has to be turned on during the whole deceleration cycle.

In total, the low-beta section will require the production of six new superconducting quadrupoles. The gradient of the magnet g is given by:

$$g = \frac{B_p}{R_1} \quad (1)$$

where B_p is pole tip field and R_1 is the inner radius of current. The requirement for R_1 is:

$$R_1 = d_1 + d_2 + d_3 \quad (2)$$

where d_1 is the beam envelope (beam radius, determined from optics calculation) plus 10 mm safety margin for closed orbit deviation, d_2 is the space for the vacuum chamber, which is 2 mm, and d_3 is the required gap between vacuum chamber and the inner radius of current (5 mm). The beam envelope is

$$R = \sqrt{\varepsilon \times \beta} \quad (3)$$

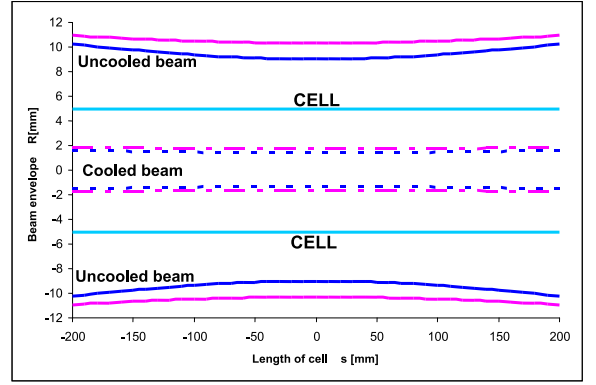


Fig. 6: Beam envelope at the cell. Dark blue lines are R_x , red lines R_y . Solid lines are uncooled beam, and dashed lines cooled beam. Blue lines show the size of the cell (10 mm).

where β is the betatron amplitude function, ε is the beam emittance.

With the calculated maximum beta function in the target region of 12.5 m, R_1 should be 67 mm. Field calculations for a quadrupole magnet design yield for this R_1 a pole tip field $B_p=5.6 \text{ T}$. The focusing strength of the magnet is

$$K = \frac{g}{B_p} \quad (4)$$

where B_p is the magnetic rigidity and K is the gradient. With given pole tip field the required focusing strength can be reached.

In more details, our studies can be found in the talk [3].

References:

- [1] Conceptual Design Report for an International Facility for Antiproton and Ion Research, <http://www.gsi.de/GSI-future/cdr>.
- [2] PAX Technical Proposal, <http://www.fz-juelich.de/ikp/pax>.
- [3] A. Garishvili, CANU meeting, 2006, available from <http://www.fz-juelich.de/ikp/pax>.

^a Institut für Kernphysik, Forschungszentrum Jülich, Jülich, Germany

^b Institute of High Energy Physics, Tbilisi State University, Tbilisi, Georgia

^c Physikalisches Institut, Universität Erlangen-Nürnberg, Erlangen, Germany

^d Istituto Nazionale di Fisica Nucleare, Ferrara, Italy

The PAX collaboration recently suggested to study the polarization build-up in an antiproton beam at the AD-ring of CERN at energies in the range of 50 – 200 MeV [1]. The polarization build-up by spin filtering of stored antiprotons by multiple passage through a polarized internal hydrogen gas target gives a direct access to the spin dependence of the $\bar{p}p$ total cross section.

An important subject is the development of a detector system that allows one to efficiently determine the polarizations of beam and target. Such a system based on silicon microstrip detectors has recently been developed at IKP [2].

A simulation study has been carried out in order to estimate the \bar{p} interaction with silicon detector layers of different thickness, where experimental data are scarce. The physics processes simulation package, included in GEANT4, contains the chiral invariant phase-space decay model (CHIPS) [3] which makes possible to simulate \bar{p} annihilation in different materials. The model, recently added to the GEANT4 hadronic physics package, is well tested for $p\bar{p}$ annihilation using two-particle final state branchings.

The distribution of the number of the secondary particles produced in \bar{p} annihilation is shown in Fig. 1(a). The distribution of the sum of the kinetic energies of all these secondaries, i.e. the energy which can potentially be deposited in a medium, is shown in Fig.1(b).

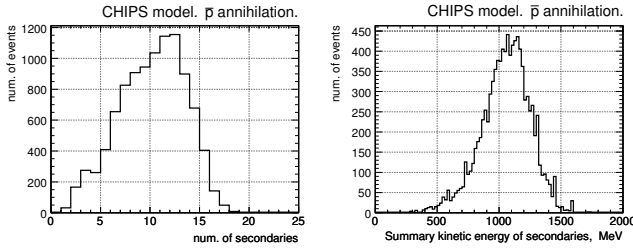


Fig. 1: (a) Number of secondaries in \bar{p} annihilation; (b) Sum of kinetic energies of secondaries.

Antiprotons of fixed kinetic energy (in the range $0.1 < E_k < 50 \text{ MeV}$) were directed to the detector containing three silicon layers of 70, 300, and 5000 μm thickness. These three layers are stacked perpendicularly to the antiproton beam axis with a distance from the 1st layer to the 2nd layer of 15 mm, and a distance of 20 mm from the 2nd to the 3rd layer. The deposited energy in a layer is determined from the sum of the deposited energies of all secondaries in a $1 \times 1 \text{ mm}^2$ area. The corresponding spectra of the deposited energies in case of antiproton annihilations are shown in Fig. 2(a)-(d).

The main part of the deposited energy is produced by various ions (from deuterons up to ^{28}Si) generated in the \bar{p} annihilation process. If antiprotons pass the detector layer, the energy deposition does not differ from that for protons. The energy dependence of the antiproton range in silicon is shown in Fig. 3.

In case of antiproton annihilation the deposited energy is almost independent on the kinetic energy of the antiproton. It depends mainly on the thickness of the layer and the annihilation depth. In thin layers most of the ionizing secondaries leave the sensitive volume. The slight difference of the spec-

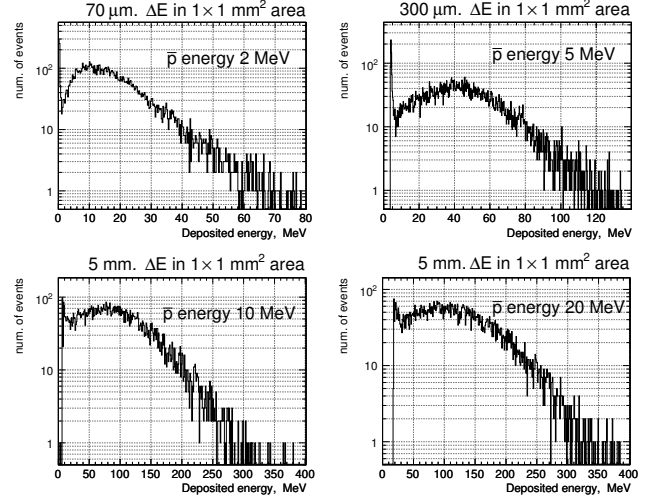


Fig. 2: Spectra of the deposited energy for silicon layers of (a) 70 μm , (b) 300 μm , (c) 5 mm (10 MeV), and (d) 5 mm (20 MeV) thickness.

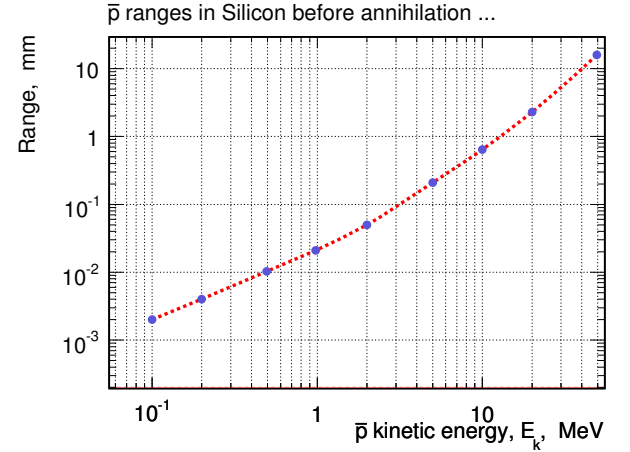


Fig. 3: Energy dependence of the antiproton range in silicon.

tra for the 5 mm layer (see Fig. 3(c) and (d)) at different energies is also caused by different depths of the annihilation point. The mean values of annihilation depths are 0.6 mm for (c) and 2.4 mm for (d), respectively. In order to detect antiprotons by the annihilation signal, we can use degraders in front of silicon detector to reduce the \bar{p} kinetic energy to a proper value.

References:

- [1] PAX Collaboration. Measurement of the spin-dependence of the $\bar{p}p$ interaction at the AD-ring. Jülich, 2005. <http://www.fz-juelich.de/ikp/pax/>
- [2] A. Kacharava *et al.*, *Spin Physics from COSY to FAIR*. 2005. <http://www.fz-juelich.de/ikp/anke/>
- [3] J.P. Wellish., **ePrint: nucl-th/0306006**

^a Tbilisi State University, Tbilisi, Georgia, and JINR, Dubna, Russia

5 Technical Developments

The technology of Gas Electron Multiplier(GEM) invented by F. Sauli [1] attracts big interest during the last years and starts to be widely used in present experiments and developed for the future projects [2, 3]. Investigations of GEM have been performed since they are considered as potential candidates for application in future tracking devices of the ANKE and WASA experiments. The main component is a polymer foil metallized on both sides which is pierced by a regular pattern of holes. Upon application of high voltage across the foil the high electric field inside the holes permits gas multiplication. Several GEM stages can be coupled together to give sufficient gain for single-electron detection. Amplified charges are collected on pad or strip structures for position determination. The advantage of GEM amplification stages is a fast response and high-rate capability since the signal is mainly due to the fast electron component.

We have combined a $10 \times 10 \text{ cm}^2$ GEM foil with $70 \mu\text{m}$ holes and a pitch of $140 \mu\text{m}$ obtained from 3M company with a plane multiwire drift chamber. The GEM foil replaces one of the two cathodes foils between which the anode wires are positioned. On the outer side of the GEM foil there is a 35 mm drift space which is closed by the drift electrode. Electrons liberated in the drift space are captured by the electric field in the holes of the GEM-foil and electron clusters after amplification are then transferred in the drift chamber where further amplification takes place.

A similar idea but without GEM preamplifier was exploited in the PHENIX experiment [4] where tracking and the pion-electron discrimination in the momenta region between 200 MeV/c and 2.5 GeV/c was realized by multiple measurement of the particles ionization losses in a special drift volume of the wire chamber.

GEM gives an additional gain in the overall amplification which is helpful to detect single electron ionization clusters. The possibility to share the overall charge amplification between GEM and the wire chamber gives a flexibility to optimize the electric field in the drift region from the point of view of electron diffusion and charge transfer efficiency. Additional drift chambers below and above the GEM drift chamber together with scintillation counters serve as an external tracker and trigger for cosmic muons. For the readout of the drift chamber signals CMP16 amplifier-discriminator boards were used together with a F1 TDC.

The GEM drift chamber was operated using different gas mixtures and electrical potentials, see Tab.1

Table 1

Gas mixture	Voltage across GEM	Drift field
$80\%Ar + 20\%C_2H_6$	380 V	220 V/cm
$85\%CF_4 + 15\%C_2H_6$	480 V	505 and 591 V/cm
$70\%Ar + 30\%CO_2$	450 V	386 and 529 V/cm
$80\%CO_2 + 20\%C_2H_6$	500 V	500 V/cm

A typical drift time spectrum for one wire obtained with a gas mixture $80\%Ar + 20\%C_2H_6$ is shown on the fig.1. A time spectrum from the drift gap as well as a peak corresponding to particles which cross the cell of the drift chamber are clearly visible. The mixture $80\%CO_2 + 20\%C_2H_6$ was found

optimal for cluster counting due to smaller drift velocity and good quenching properties. Multiple hits time distributions were registered with a TDC F1 (up to 7 hits per trigger) which validate the feasibility of the method. Further investigation with higher multihit and faster electronics are foreseen.

A triple GEM prototype out of the same type of GEM foils was built in order to test the design and measure the gas amplification. An amplification of about 3×10^6 was measured in a gas mixture $80\%Ar + 20\%C_2H_6$ at GEM high voltage $\approx 360 \text{ V}$ by measuring the current in the detector while exposing it with a γ source ^{55}Fe .

The basic applications of detector based on GEM are high rate trackers and Time Projection Chambers.

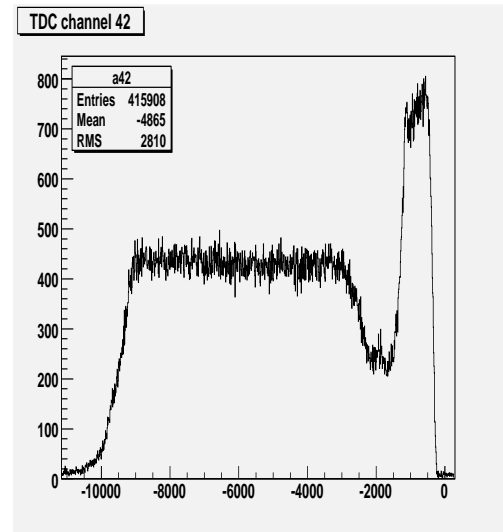


Fig. 1: A typical drift time spectrum for one anode wire, $80\%Ar + 20\%C_2H_6$, GEM H.V. = 380 V, $E_{dr} = 220 \text{ V/cm}$

References:

- [1] F. Sauli, Nucl. Instr. and Meth. A386 (1997) 531
- [2] B. Ketzer, Nucl. Instr. and Meth. A494 (2002) 142
- [3] TESLA Technical Design Report, DESY-01-011, ECFA 2001-209 (2001)
- [4] B. Libby et al., Nucl. Instr. and Meth. A367 (1995) 244

¹ Institut für Kern Physik, Forschungszentrum Jülich, Germany

² Joint Institute for Nuclear Research, Dubna, Russia

³ Institute of Physics, Jagellonian University, Cracow, Poland

⁴ Institute of Nuclear Physics, Polish Academy of Science, Cracow, Poland

Development of a Large-Volume Si(Li) Compton Polarimeter

D. Protić¹⁾, Th. Stöhlker²⁾, T. Krings¹⁾, I. Mohos¹⁾, U. Spillmann²⁾

Recent developments of large-volume Si(Li) orthogonal-strip detectors [1] have attracted particular attention for applications in the field of x-ray polarimetry [2] and Compton imaging [3]. For photon energies below 140 keV a Compton polarimeter based on a large-volume two-dimensional Si(Li) strip detector should clearly outperform similar systems utilizing germanium or cadmium telluride. Therefore, a powerful Si(Li) Compton polarimeter has been constructed for x-ray spectroscopy and polarization studies on highly-charged heavy ions at GSI-Darmstadt. The polarimeter consists out of a large-volume double-sided Si(Li) strip detector (2 x 32 strips) mounted in a cryostat attached on a commercial dewar and 2 x 32 preamplifiers in a housing placed near the detector. Whereas the cryostat, the detector holder, preamplifiers and their housing have already been manufactured and tested, the Si(Li) detector itself is still being prepared. Whereas the cryostat, the detector holder, preamplifiers and their housing have already been manufactured and tested (Fig. 1 and Fig. 2), the Si(Li) detector itself is still being prepared [4].

A 15 mm thick diode having 4" in diameter is being in Li-drift process. The thickness of the already Li-compensated region amounts to 11.5 mm. At this stage an excessive reverse current prevents applying of higher bias voltages so that the Li-drift process is slowed down [4]. In the meantime the cause of the excessive reverse current was identified. After removing of an outer part of the diode we expect better reverse current and the completion of the Li-compensation process.

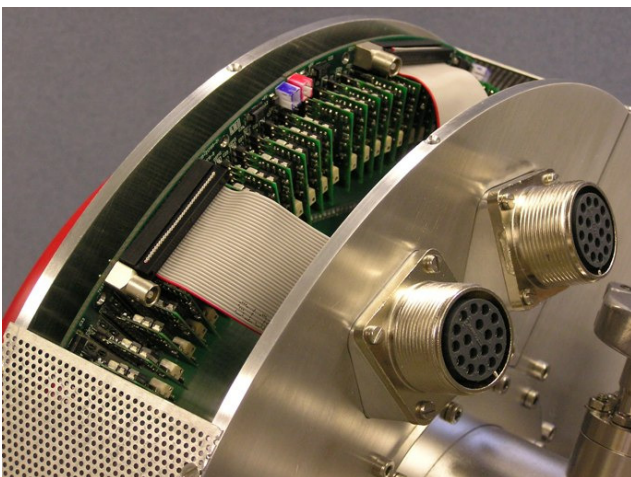


Figure 1: View of the Si(Li) polarimeter with open cryostat cap. In the center part of the cryostat there are the mounted detector-dummy and the PCBs.

For the beginning a just finished 9.4 mm thick Si(Li) detector will be soon mounted into the cryostat. Both contacts, the boron-implanted p⁺-contact and the thin Li-

diffused n-contact, received the same strip structure (orthogonally oriented) consisting of 32 strips on an area of 64 mm x 64 mm, surrounded by a ~8 mm wide guard-ring. The same position-sensitive structure is destined also for the 15 mm thick detector.

Any orientation of the polarimeter will be possible due to the special dewar (commercially available) that prevents the loss of liquid nitrogen at any position. Low capacitance feedthroughs will be applied to achieve a good energy resolution. Using proved preamplifiers supplied by MTA-ITA-LAI-Budapest (Hungary) an energy resolution below 2 keV will be possible.

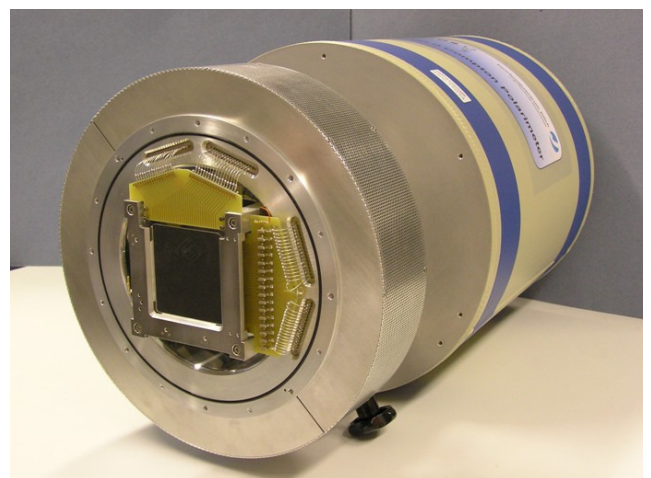


Figure 2: View of a part of the PCBs with the charge-sensitive preamplifiers.

References:

- [1] D. Protić, E. L. Hull, T. Krings and K. Vetter, "Large-Volume Si(Li) Orthogonal-Strip Detectors for Compton-Effect-Based Instruments", *IEEE Trans. Nucl. Sci.*, vol. 52, pp. 3181-3185, Dec. 2005.
- [2] Th. Stöhlker, U. Spillmann, D. Banas et al., "A 2D Position-Sensitive Germanium Detector for Spectroscopy and Polarimetry of High-Energetic X-rays", accepted for publication, *Journal of Physics*, 2006.
- [3] K. Vetter, M. Burks, C. Cork et al., "High-Sensitivity Compton Imaging with Position-Sensitive Si and Ge Detectors", presented at *IEEE Nucl. Sci. Symp.*, San Diego, Nov. 2006.
- [4] D. Protić, Th. Stöhlker, et al., "Large-Volume Si(Li) Compton Polarimeter", presented at *IEEE Nucl. Sci. Symp.*, San Diego, Nov. 2006.

1) FZ Jülich

2) GSI Darmstadt

Position-Sensitive Si(Li) Transmission Detectors for the EXL-Experiments at GSI-Darmstadt

D. Protić ¹⁾, T. Krings ¹⁾, S. Niessen ¹⁾, P. Egelhof ²⁾, E. C. Pollacco ³⁾, M. Müller-Veggian ⁴⁾

A large target-recoil detector will be constructed for the future EXL-experiments (EXotic nuclei studied in LIght-ion induced reactions) at the NESR storage ring of the future FAIR project at GSI-Darmstadt [1]. As a part of the recoil detector, position-sensitive Si(Li) transmission detectors (5 to 9 mm thick) are intended for construction of ΔE -E charged-particle telescopes. Si(Li) detectors of transmission type has been an important aspect concerning the total-energy measurement for target recoils transversing the silicon ΔE -E telescopes and stopped in inorganic scintillators placed behind the telescopes.

Two ~6.5 mm thick Si(Li) transmission detectors equipped with 8 pads on the implanted p+-contact have been prepared for the test measurements at ESR (GSI-Darmstadt). To relieve the efforts for the first experiments a telescope configuration and position-sensitive structure very similar to that of the MUST2 experiment (SACLAY, ORSAY and GANIL) have been applied [2], but with UHV-capable components.

The schematic view of the Si(Li) transmission detector is presented in Fig. 1. The Si(Li) detector in the UHV-compatible housing is shown in Fig. 2.

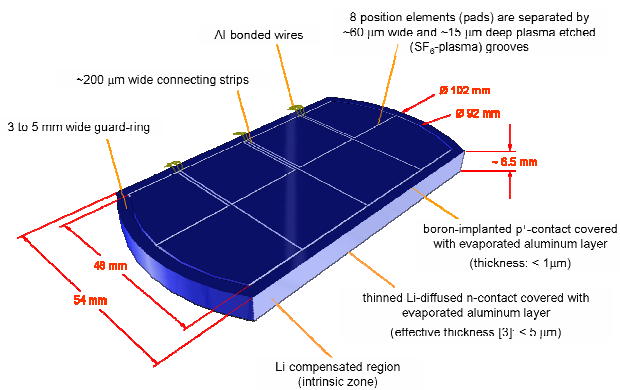


Figure 1: Schematic view of the Si(Li) transmission detector.

The results of the test measurements in the laboratory confirm that the predetermined specifications, listed in Table 1, have been fulfilled.

Some of these results were presented at IEEE Nucl. Sci. Symp., San Diego, Nov. 2006. Test measurements in UHV environment will be performed inside the ESR-ring at GSI-Darmstadt.

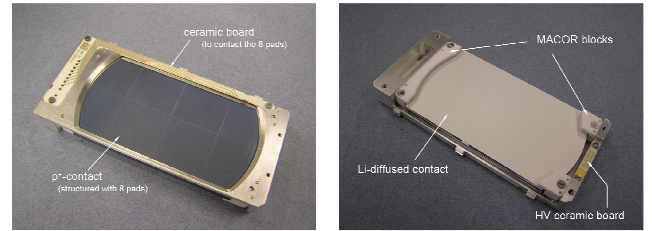


Figure 2: The Si(Li) detector in the UHV-compatible housing.

• transmission type Si(Li) detector	
➤ ~ 6.5 mm thick	
• 8 pads on the boron-implanted contact	
➤ the same structure as for the Si(Li) detectors for the MUST2-setup	
• thin Li-diffused contact	
➤ effective thickness below 5 μm	
➤ without position-sensitive structure	
• operating bias:	≥ 700 V
• energy resolution [FWHM] for 5.8 MeV α-particles:	< 50 keV
• reverse current / pad:	< 250 nA
• resistance pad - neighbourhood:	> 1 MΩ
T = 273 K	
• housing / frame:	
➤ design is identical to the MUST2-design	
➤ all components have to be UHV-compatible	

Table 1: Predetermined specifications of the Si(Li) detectors.

References:

- [1] www.gsi.de
- [2] E. C. Pollacco et al., to be published in Nucl. Instr. Meth.
- [3] D. Protić and T. Krings, "Development of transmission Si(Li) detectors", IEEE Trans. Nucl. Sci., vol. 50, pp. 1008-1012, August 2003.

- 1) FZ Jülich
- 2) GSI Darmstadt
- 3) CEA Saclay
- 4) FH Aachen, Abteilung Jülich

The activities of the IKP Electronics Laboratory can be assigned to mainly the following three topics:

Electronics and Data Acquisition for experiments

For the straw chamber project at TOF the ongoing development of pre-amplifiers and signal conversion circuitry has been continued. Adapter boards and system crates for the ASD8 bases readout system were finally developed and produced. Connection units consisting of 0,5mm thick coaxial cables, connecting the pre-amplifiers and the ASD8 circuitry were produced for appr. 1000 channels. The development of a vacuum and light tight printed circuit board carrying 3000 high density feedthrough contacts is ongoing.

For the spectator detector at ANKE extensive support was given to the ADC development at ZEL. Because of permanent failures in the low-voltage, high-current ($\pm 5V$, 2A), low-cost(!) power supplies due to manufacturing faults all existing units were re-worked. Additional units will consist of more reliable power supplies which are under test.

The atomic beam source (ABS) setup for the polarized internal target was (PIT) rebuilt within the ANKE experiment and tested. A new gas inlet system was designed, built, and tested, this comprised design of logic circuits, modifications of the user interface and of the control program inside the PLCs. For positioning of the target cell a xy-table was designed and tested. The vacuum system interlock of the Lamb shift polarimeter was successfully tested. For process visualization a new embedded controller was taken into operation, running WinCC under Windows XP. The existing application was adapted to the new environment and extensively tested.

The interlock system needed to protect detectors at ANKE and in laboratory setups against damage in case of vacuum leakage was extended by HPT vacuum gauges which were implemented into the Profibus gateway.

For the atomic beam source (ABS) setup to be built at the PAX detector the electrical specifications of the whole system were developed, power and signal distributor boxes and the process visualization system were designed.

For the ATRAP-II experiment additional pre-amplifiers were produced and tested. Power supplies were modified, and the whole system was installed at CERN.

In 2006 the WASA experiment consumed most of our laboratory resources. Active and passive splitter boxes for 1900 detector channels, including crates containing the splitter boxes and the necessary power supplies, were developed, produced, and successfully tested. The same applies for the summing amplifiers which were developed with the help of I.Mohos. The splitter boxes fulfil all the requirements concerning crosstalk and impedance matching. The cables needed to connect the detector channels to the readout electronics were procured and produced, or modified if the existing cables met the requirements at the new detector location. The handling of materials procurement for electronic components and the readout system, which was developed and build mainly at ZEL, was done by our laboratory. Various control and display units for the gas mixing system of the straw detectors at WASA were designed and built. Moreover, we assisted the development of amplifiers and discriminators for the detector part MDC and FPC.

The pionic hydrogen experiment at PSI was dismantled and the detector part of the crystal spectrometer was rebuilt in Jülich.

Within a collaboration with the Atomic Energy Authority Nuclear Research Center in Cairo/Egypt the cyclotron there will get a new Simatic S7 based vacuum control system. For this purpose various signal distributors for the S7 control units were designed and built here and installed and taken into operation on-site.

For the detector laboratory a liquid level control device for temperature controlled water baths was developed and built. It is based on a conductance measurement using AC to prevent electrolytic effects.

COSY diagnostics

Maintenance was provided for the multi-wire chambers for beam diagnostics in the extraction beamlines and for the viewer cameras. This also included repair of broken components, e.g. power supplies.

Computer network

After planning and measurements the installation of wireless LAN access points in the institute, COSY, and cyclotron buildings still awaits completion. For the installation in building 09.6 (COSY office building with accommodation facility) new WLAN components were tested. Frequent support was granted to ensure continuous operation of the existing networks.

Miscellaneous

Like every year substantial support was given with regard to short term maintenance and repair or replacement of electronics. In some cases the urgent demand didn't allow a time consuming outside repair procedure, in other cases the manufacturer doesn't even exist anymore, but the electronics can not be replaced easily, or the manufacturer was unable to perform the repair.

Prototypes and small series of cables or electronics, for which an outside production would not have been reasonable, were delegated to infrastructure facilities or done here, mainly by trainees and student auxiliary workers.

The standard data acquisition systems at several COSY experiments were taken care of to assure stable operation during several beamtimes.

In addition, some members of our laboratory supported experiments by taking over shifts at beamtimes, mainly at COSY-11.

Regarding S7 systems continuous support was given to the radiation safety division and to the cyclotron group.

Part time supervision of a diploma students of the FH Aachen was provided in the field of process automation.

A revision of the IKP webpages is under way, some of the pages have been replaced already.

A Councils

A.1 Hadron Physics Program Advisory Council

Prof. R. Beck	Universität Bonn	
Prof. J.-P. Blaizot	CEA Saclay, FR	
Prof. D.F. Geesaman	Argonne National Laboratory, U.S.A.	
Dr. P. Gianotti	Laboratori Nazionali di Frascati, I	
Prof. M. Harakeh	KVI Groningen, NL	
Prof. E. Jaeschke	Humboldt Universität Berlin	
Prof. K. Königsmann	Albert-Ludwigs-Universität Freiburg	
Prof. R. Kulesa	Uniwersytet Jagiellonski Cracow, PL	
Prof. St. Paul	TU München	Chairperson
Prof. K. Peters	GSI Darmstadt	
Prof. U. Wiedner	Universität Bochum	
Prof. U.-J. Wiese	Universität Bern	

A.2 COSY Program Advisory Committee

Prof. D. Barber	DESY, DE	
Prof. J. Bijnens	Lund University, SE	
Prof. H. Freiesleben	TU Dresden, DE	
Prof. B. Friman	GSI Darmstadt, DE	
Prof. N. Herrmann	Universität Heidelberg, DE	
Prof. T. Johansson	Uppsala Universitet, SE	
Prof. H. Löhner	KVI Groningen, NL	
Prof. A. Magiera	Jagellonian University Cracow, PL	
Prof. W. Meyer	Universität Bochum, DE	
Prof. W.T.H. van Oers	University of Manitoba, CA	Chairperson
Prof. E. Oset	Universitat de Valencia, ES	
Prof. C. Schaerf	INFN Roma II, IT	

B Publications 2006

1. Experiment

1. M. Abd El-Samad, R. Bilger, K.-Th. Brinkmann, H. Clement, M. Dietrich, E. Doroshkevich, S. Dshemuchadse, A. Erhardt, W. Eyrich, A. Filippi, H. Freiesleben, M. Fritsch, R. Geyer, A. Gillitzer, J. Hauffe, D. Hesselbarth, R. Jaekel, B. Jakob, L. Karsch, K. Kilian, H. Koch, J. Kress, E. Kuhlmann, S. Marcello, S. Marwinski, R. Meier, K. Möller, H.P. Morsch, L. Naumann, E. Roderburg, P. Schönmeier, M. Schulte-Wissermann, W. Schröder, M. Steinke, F. Stinzing, G.Y. Sun, J. Waechter, G.J. Wagner, M. Wagner, U. Weidlich, A. Wilms, S. Wirth, G. Zhang, P. Zupranski (COSY-TOF collaboration)
Single-pion production in pp collisions at 0.95 GeV/c (I)
European Physical Journal A **30** (2006) 443.
2. M. Abd El-Samad, R. Bilger, A. Böhm, K.-Th. Brinkmann, H. Clement, S. Dshemuchadse, b, W. Eyrich, A. Erhardt, C. Fanara, A. Filippi, H. Freiesleben, M. Fritsch, R. Geyer, J. Hauffe, A. Hassan, P. Herrmann, D. Hesselbarth, B. Jakob, K. Kilian, H. Koch, J. Kress, E. Kuhlmann, S. Marcello, S. Marwinski, A. Metzger, P. Michel, K. Möller, H.P. Morsch, L. Naumann, E. Roderburg, A. Schamlott, P. Schönmeier, M. Schulte-Wissermann, W. Schröder, M. Steinke, F. Stinzing, G.Y. Sun, J. Wächter, G.J. Wagner, M. Wagner, A. Wilms, S. Wirth, U. Zielinski (COSY-TOF collaboration)
Hyperon production in the channel $pp \rightarrow K^+ \Lambda p$ near the reaction threshold
Physics Letters B **632** (2006) 27.
3. S. Abdel-Samad, K. Kilian, J. Ritman, M. Abdel-Bary
Cryogenic Target With Very Thin 'Gold Finger' Heat Pipe
Nuclear Instruments and Methods A **556** (2006) 20.
4. M. Abdel-Bary, K.-Th. Brinkmann, H. Clement, E. Doroshkevich, S. Dshemuchadse, A. Erhardt, W. Eyrich, H. Freiesleben, A. Gillitzer, R. Jäkel, L. Karsch, K. Kilian, E. Kuhlmann, K. Möller, H.P. Morsch, L. Naumann, N. Paul, C. Pizzolotto, J. Ritman, E. Roderburg, P. Schönmeier, W. Schröder, M. Schulte-Wissermann, G. Y. Sun, A. Teufel, A. Ucar, G.J. Wagner, M. Wagner, P. Wintz, P. Wüstner, P. Zupranski (COSY-TOF collaboration)
Study of spectator tagging in the reaction $np \rightarrow pp\pi^-$ with a deuteron beam
European Physical Journal A **29** (2006) 353.
5. M. Bashkanov, D. Bogoslawsky, H. Calen, F. Cappellaro, H. Clement, L. Demiroers, C. Ekström, K. Fransson, J. Greiff, L. Gustafsson, B. Höistad, G. Ivanov, M. Jacewicz, E. Jiganov, T. Johansson, O. Khakimova, M.M. Kaskulov, S. Keleta, I. Koch, F. Kren, S. Kullander, A. Kupsc, A. Kuznetsov, P. Marciniewski, R. Meier, B. Morosov, W. Oelert, C. Pauly, Y. Petukhov, A. Povtorejko, R.J.M.Y. Ruber, W. Scobel, T. Skorodko, B. Shwartz, V. Sopov, J. Stepaniak, V. Tchernyshev, P. Thörngren-Engblom, V. Tikhomirov, A. Turowiecki, G.J. Wagner, M. Wolke, A. Yamamoto, J. Zabierowski, J. Zlomanczuk
Exclusive measurements of $pd \rightarrow {}^3\text{He} \pi\pi$: The ABC effect revisited
Physics Letters B **637** (2006) 223
6. W. Bertl, R. Engfer, E.A. Hermes, G. Kurz, T. Kozlowski, J. Kuth, G. Otter, F. Rosenbaum, N.M. Ryskulov, A. van der Schaaf, P. Wintz, I. Zychor
A search for μ -e conversion in muonic gold
European Physical Journal C **47** (2006) 337.
7. V. Bollini, A. Bubak, A. Budzanowski, J. Cugnon, D. Filges, F. Goldenbaum, A. Heczko, H. Hodde, L. Jarczyk, B. Kamys, M. Kistryn, St. Kistryn, St. Kliczewski, A. Kowalczyk, P. Kulesa, H. Machner, A. Magiera, W. Migdal, K. Nünighoff, N. Paul, B. Piskor-Ignatowicz, K. Pysz, Z. Rudy, R. Siudak, M. Wojciechowski, E. Kozik
Light charged particle and intermediate mass fragment cross sections in GeV proton induced reactions-the PISA experiment
Nuclear Instruments and Methods A **562** (2006) 733.
8. D. Chiladze, A. Kacharava, F. Rathmann, C. Wilkin, S. Barsov, J. Carbonell, S. Dymov, R. Engels, P.D. Eversheim, R. Gebel, V. Glagolev, K. Grigoriev, D. Gusev, M. Hartmann, F. Hinterberger, V. Hejny, A. Khoukaz, I. Keshelashvili, H.R. Koch, V. Komarov, P. Kulesa, A. Kulikov, A. Lehrach, B. Lorentz, G. Macharashvili, R. Maier, Y. Maeda, R. Menke, T. Mersmann, S. Merzliakov, M. Mikirtychiants, S. Mikirtychiants, A. Mussgiller, M. Nioradze, H. Ohm, D. Prasuhn, H. Rohdjess, R. Schleichert, H. Seyfarth, E. Steffens, H.J. Stein, H. Ströher, S. Trusov, K. Ulbrich, Yu. Uzikov, A. Wronska, S. Yaschenko
Determination of Deuteron Beam Polarization at COSY
Physics Review ST-AB **9** (2006) 050101.
9. D. Chiladze, J. Carbonell, S. Dymov, V. Glagolev, M. Hartmann, V. Hejny, A. Kacharava, I. Keshelashvili, A. Khoukaz, H.R. Koch, V. Komarov, P. Kulesa, A. Kulikov, G. Macharashvili, Y. Maeda, T. Mersmann, S. Merzliakov, S. Mikirtychiants,

- A. Mussgiller, M. Nioradze, H. Ohm, F. Rathmann, R. Schleichert, H.J. Stein, H. Ströher, Yu. Uzikov, S. Yaschenko, C. Wilkin
Vector and tensor analysing powers in deuteron-proton breakup reactions at intermediate energies
Physics Letters B **637** (2006) 170.
10. S.Dymov, M. Büscher, D. Gusev, M. Hartmann, V. Hejny, A. Kacharava, A. Khoukaz, V. Komarov, P. Kulesa, A. Kulikov, V. Kurbatov, N. Lang, G. Macharashvili, T. Mersmann, S. Merzliakov, S. Mikirtychiants, A. Mussgiller, D. Prasuhn, F. Rathmann, R. Schleichert, H. Ströher, Yu. Uzikov, C. Wilkin, S. Yaschenko
Production of the 1S_0 diproton in the $pp \rightarrow (pp)\pi^0$ reaction at 0.8 GeV
Physics Letters B **635** (2006) 270.
11. A. Dzyuba, V. Kleber, M. Büscher, V.P. Chernyshev, S. Dymov, P. Fedorets, V. Grishina, C. Hanhart, M. Hartmann, V. Hejny, L. Kondratyuk, V. Koptev, P. Kulesa, Y. Maeda, T. Mersmann, S. Mikirtychiants, M. Nekipelov, D. Prasuhn, R. Schleichert, A. Sibirtsev, H.J. Stein, H. Ströher, I. Zychor
Scalar-isovector $K\bar{K}$ production close to threshold
European Physical Journal A, **29** (2006), 245
12. P. Fedorets, M. Büscher, V.P. Chernyshev, S. Dymov, V.Yu. Grishina, C. Hanhart, M. Hartmann, V. Hejny, V. Kleber, H.R. Koch, L.A. Kondratyuk, V. Koptev, A.E. Kudryavtsev, P. Kulesa, S. Merzliakov, S. Mikirtychiants, M. Nekipelov, H. Ohm, R. Schleichert, H. Ströher, V.E. Tarasov, K.-H. Watzlawik, I. Zychor
Evidence of a_0^+ (980)-resonance production in the reaction $pp \rightarrow d\pi^+\eta$
Physics of Atomic Nuclei **69** (2006) 306.
13. A. Gadea, S.M. Lenzi, S. Lunardi, N. Mrginean, A.P. Zuker, G. de Angelis, M. Axiotis, T. Martinez, D.R. Napoli, E. Farnea, R. Menegazzo, P. Pavan, C.A. Ur, D. Bazzacco, R. Venturelli, P. Kleinheinz, P. Bednarczyk, D. Curien, O. Dorvaux, J. Nyberg, H. Grawe, M. Górska, M. Palacz, K. Lagergren, L. Milechina, J. Ekman, D. Rudolph, C. Andreoiu, M.A. Bentley, W. Gelletly, B. Rubio, A. Algora, E. Nacher, L. Caballero, M. Trotta, M. Morszyski
Observation of ^{54}Ni : Cross-Conjugate Symmetry in $f_{7/2}$ Mirror Energy Differences
Physical Review Letters **97** (2006) 152501.
14. M. Hartmann, Y. Maeda, I. Keshelashvili, H.R. Koch, S. Mikirtychiants, S. Barsov, W. Borgs, M. Büscher, V.I. Dimitrov, S. Dymov, V. Hejny, V. Kleber, V. Koptev, P. Kulesa, T. Mersmann, S. Merzliakov, A. Mussgiller, M. Nekipelov, M. Nioradze, H. Ohm, K. Pysz, R. Schleichert, H.J. Stein, H. Ströher, K.-H. Watzlawik, P. Wüstner
The Near-threshold production of ϕ mesons in pp collisions
Physical Review Letters **96** (2006) 242301.
15. C.M. Herbach, D. Hilscher, U. Jahnke, V.G. Tishchenko, J. Galin, A. Letourneau, A. Peghaire, D. Filges, F. Goldenbaum, L. Pienkowski, W.U. Schröder, J. Töke
Charged Particle Evaporation and pre-Equilibrium Emission in 1.2 GeV Proton-Induced Spallation Reactions
Nuclear Physics A **765** (2006) 426.
16. P. Indelicato, E.-O. Le Bigot, M. Trassinelli, D. Gotta, M. Hennebach, N. Nelms, Chr. David, L.M. Simons
Characterization of a charge-coupled device array for Bragg spectroscopy
Review of Scientific Instruments **77** (2006) 043107.
17. H. Kleines, J. Sarkadi, K. Zwill, R. Engels, K. Grigoryev, M. Mikirtychiants, M. Nekipelov, F. Rathmann, H. Seyfarth, P. Kravtsov, A. Vasilyev
The control system of the polarized internal target of ANKE at COSY
Nuclear Instruments and Methods A **560** (2006) 503.
18. H. Machner, D.G. Aschman, K. Baruth-Ram, J. Carter, A.A. Cowley, F. Goldenbaum, B.M. Nangu, J.V. Pilcher, E. Sideras-Haddad, J.P.F. Sellschop, F.D. Smit, B. Spoelstra, D. Steyn
Isotopic production cross sections in proton-nucleus collisions at 200 MeV
Physical Review C **73** (2006) 044606.
19. Y. Maeda, M. Hartmann, I. Keshelashvili, S. Barsov, M. Büscher, A. Dzyuba, S. Dymov, V. Hejny, A. Kacharava, V. Kleber, H.R. Koch, V. Koptev, P. Kulesa, T. Mersmann, S. Mikirtychiants, A. Mussgiller, M. Nekipelov, H. Ohm, R. Schleichert, H.J. Stein, H. Ströher, Yu. Valdau, K.-H. Watzlawik, C. Wilkin, P. Wüstner
Precision measurement of the quasi-free $pn \rightarrow d\phi$ reaction close to threshold
Physical Review Letters **97** (2006) 142301.

20. P. Moskal, H.-H. Adam, A. Budzanowski, R. Czyzykiewicz, D. Grzonka, M. Janusz, L. Jarczyk, T. Johansson, B. Kamys, P. Klaja, A. Khoukaz, K. Kilian, J. Majewski, W. Oelert, C. Piskor-Ignatowicz, J. Przerwa, J. Ritman, T. Rozek, T. Sefzick, M. Siemaszko, J. Smyrski, A. Täschner, J. Wessels, P. Winter, M. Wolke, P. Wüstner, Z. Zhang, W. Zipper
A method to disentangle single- and multi-meson production in missing mass spectra from quasi-free $pn \rightarrow pn X$ reactions
Journal of Physics G **32** (2006) 629.
21. R.Ortega, D. d’Enterria, G. Martinez, D. Baiborodin, H. Delagrangé, J. Diaz, F. Fernandez, H. Loehner, T. Matulewicz, R.W. Ostendorf, S. Schadmand, Y. Schutz, P. Tlusty, R. Turrisi, V. Wagner, H.W. Wilschut, N. Yahlali
Constraints on the Time-Scale of Nuclear Breakup from Thermal Hard-Photon Emission
European Physical Journal A **28** (2006) 161.
22. H. Rohdjeß, D. Albers, J. Bisplinghoff, R. Bollmann, K. Büßer, O. Diehl, F. Dohrmann, H.-P. Engelhardt, P. D. Ever-
sheim, J. Greiff, A. Gross, R. Groß-Hardt, F. Hinterberger, M. Igelbrink, R. Langkau, R. Maier, F. Mosel, M. Müller, M.
Münstermann, D. Prasuhn, P. von Rossen, H. Scheid, N. Schirm, F. Schwandt, W. Scobel, H.J. Trelle, A. Wellinghausen,
W. Wiedmann, K. Woller, R. Ziegler
Radiation damage of polypropylene fiber targets in storage rings
Nuclear Instruments and Methods B **243** (2006) 127.
23. T. Rozek, D. Grzonka, H.-H. Adam, A. Budzanowski, R. Czyzykiewicz, M. Janusz, L. Jarczyk, B. Kamys, A. Khoukaz, K.
Kilian, P. Klaja, P. Kowina, P. Moskal, W. Oelert, C. Piskor-Ignatowicz, J. Przerwa, J. Ritman, T. Sefzick, M. Siemaszko,
J. Smyrski, A. Taschner, P. Winter, M. Wolke, P. Wustner, Z. Zhang, W. Zipper
Threshold hyperon production in proton-proton collisions at COSY-11
Physics Letters B **643** (2006) 251.
24. S. Tashenov, Th. Stöhlker, D. Banas, K. Beckert, P. Beller, H.F. Beyer, F. Bosch, S. Fritzsche, A. Gumberidze, S. Hagmann,
C. Kozhuharov, T. Krings, D. Liesen, F. Nolden, D. Protic, D. Sierpowski, U. Spillmann, U. Steck, A. Surzhykov
First Measurement of the Linear Polarization of Radiative Electron Capture Transitions
Physical Review Letters **97** (2006) 223202.
25. P. Winter, M. Wolke, H.-H. Adam, A. Budzanowski, R. Czyzykiewicz, D. Grzonka, M. Janusz, L. Jarczyk, B. Kamys, A.
Khoukaz, K. Kilian, P. Klaja, P. Moskal, W. Oelert, C. Piskor-Ignatowicz, J. Przerwa, J. Ritman, T. Rozek, T. Sefzick, M.
Siemaszko, J. Smyrski, A. Täschner, P. Wüstner, Z. Zhang, W. Zipper
Kaon pair production close to threshold
Physics Letters B **635** (2006) 23.
26. I. Zychor, V. Koptev, M. Büscher, A. Dzyuba, I. Keshelashvili, V. Kleber, H.-R. Koch, S. Krewald, Y. Maeda, S. Mikir-
tichyants, M. Nekipelov, H. Ströher, C. Wilkin
Evidence for an excited hyperon state in $pp \rightarrow p K^+ Y^{*0}$
Physical Review Letters **96** (2006) 012002.

2. Theory

27. M.A. Belushkin, H.W. Hammer, U.-G. Meißner
Novel evaluation of the two-pion contribution to the nucleon isovector form factors
Physics Letters B **633** (2006) 507
28. V. Bernard, U.-G. Meißner
The nucleon axial-vector coupling beyond one loop
Physics Letters B **639** (2006) 278.
29. B. Borasoy, P.C. Bruns, U.-G. Meißner, R. Lewis
Chiral corrections to the Roper mass
Physics Letters B **641** (2006) 294.
30. B. Borasoy, H. Krebs, D. Lee, U.-G. Meißner
The triton and three-nucleon force in nuclear lattice simulations
Nuclear Physics A **768** (2006) 179.
31. B. Borasoy, U.-G. Meißner, R. Nissler
 $K^- p$ scattering length from scattering experiment
Physical Review C **74** (2006) 055201.

32. B. Borasoy, R. Nissler, U.-G. Meißner
On the extraction of the quark mass ratio $(m_d - m_u)/m_s$ from $\gamma(\eta' \rightarrow \pi^0\pi^+\pi^-)/\gamma(\eta' \rightarrow \eta\pi^+\pi^-)$
Physics Letters B **643** (2006) 41.
33. A. Bulgac, P. Magierski, A. Wirzba
Scalar Casimir effect between Dirichlet spheres or a plate and a sphere
Physical Review D **73** (2006) 025007.
34. G. Devidze, A. Liparteliani, U.-G. Meißner
 $B_{s,d} \rightarrow \gamma\gamma$ decay in the model with one universal extra dimension
Physics Letters B **634** (2006) 59.
35. E. Epelbaum, W. Hammer, U.-G. Meißner, A. Nogga
More on the infrared renormalization group limit cycle in QCD
European Physical Journal C **48** (2006) 169.
36. M. Frink, U.-G. Meißner
On the chiral effective meson-baryon Lagrangian at third order
European Physical Journal A **29** (2006) 255.
37. F. Grümmer, J. Speth
Landau-Migdal theory of interacting Fermi systems: A framework for effective theories in nuclear structure physics
Journal of Physics G **32** (2006) R193.
38. H. Haberzettl, K. Nakayama, S. Krewald
Gauge-invariant approach to meson photoproduction including the final-state interaction
Physical Review C **74** (2006) 045202.
39. J. Haidenbauer, H.W. Hammer, A. Sibirtsev, U.-G. Meißner
On the strong energy dependence of the $e^+e^- \leftrightarrow p\bar{p}$ amplitude near threshold
Physics Letters B **643** (2006) 29.
40. J. Haidenbauer, A. Sibirtsev, U.-G. Meißner
Near threshold $p\bar{p}$ enhancement in B and J/Ψ decay
Physical Review D **74** (2006) 017501.
41. K. Hencken, G. Baur, D. Trautmann
Transverse momentum distribution of vector mesons produced in ultraperipheral heavy ion collisions
Physical Review Letters **96** (2006) 012303.
42. Yu.S. Kalashnikova, A.E. Kudryavtsev, A.V. Nefediev, J. Haidenbauer, C. Hanhart
Insights on scalar mesons from their radiative decays
Physical Review C **73** (2006) 045203.
43. H. Krebs, B. Borasoy
Renormalization of two-loop diagrams in scalar lattice field theory
Nuclear Physics B **748** (2006) 1.
44. S. Krewald, V.B. Soubbotin, V.I. Tselyaev, X. Vinas
Density matrix functional theory that includes pairing correlations
Physical Review C **74** (2006) 064310.
45. A. Kucukarslan, U.-G. Meißner
Omega-phi mixing in chiral perturbation theory
Modern Physics Letters A **21** (2006) 1423.
46. V. Lensky, V. Baru, J. Haidenbauer, C. Hanhart, A.E. Kudryavtsev, U.-G. Meißner
Towards a field theoretic understanding of $NN \rightarrow NN\pi$
European Physical Journal A **27** (2006) 37.
47. A. Lähde, U.-G. Meißner
Improved Analysis of J/Ψ Decays into a Vector Meson and Two Pseudoscalars
Physical Review D **74** (2006) 034021.

48. J. Ley, C. Düweke, R. Emmerich, A. Imig, H. Paetz gen. Schieck, J. Golak, H. Witala, E. Epelbaum, A. Deluva, A.C. Fonseca, W. Glöckle, U.-G. Meißner, A. Nogga, P.U. Sauer
Cross sections and tensor analyzing powers A_{yy} of the reaction $^1\text{H}(d, \vec{pp})n$ in 'symmetric constant relative energy' geometries at $E_d=19$ MeV
Physical Review C **73** (2006) 064001.
49. H. Machner, J. Niskanen
Charge independence studied in $NN \rightarrow d\pi$ reactions
Nuclear Physics A **776** (2006) 172.
50. U.-G. Meißner, U. Raha, A. Rusetsky
Isospin-breaking corrections in the pion-deuteron scattering length
Physics Letters B **639** (2006) 478.
51. U.-G. Meißner, U. Raha, A. Rusetsky
Kaon-nucleon scattering lengths from kaonic deuterium experiments
European Physical Journal C **47** (2006) 473.
52. E.H. Müller, B. Kubis, U.-G. Meißner
T-odd correlations in radiative K_{e3}^+ decays and chiral perturbation theory
European Physical Journal C **48** (2006) 427.
53. Y. Nagai, T. Kobayashi, T. Shima, T. Kikuchi, K. Takaoka, M. Igashira, J. Golak, R. Skibinski, H. Witala, A. Nogga, W. Glöckle, H. Kamada
Measurement of the $^2\text{H}(n, \gamma)^3\text{H}$ reaction cross section between 10 and 550 keV
Physical Review C **74** (2006) 025804.
54. S. Naito, Y. Nagai, T. Shima, H. Makii, K. Mishima, K. Tamura, H. Toyokawa, H. Ohgaki, J. Golak, R. Skibinski, H. Witala, W. Glöckle, A. Nogga, H. Kamada
New data for total $^3\text{He}(\gamma, p)D$ and $^3\text{He}(\gamma, pp)n$ cross sections compared to current theory
Physical Review C **73** (2006) 034003.
55. N.N. Nikolaev, W. Schäfer
Unitarity cutting rules for the nucleus excitation and topological cross sections in hard production off nuclei from nonlinear $k(T)$ -factorization
Physical Review D **74** (2006) 074021.
56. N.N. Nikolaev, W. Schäfer
Quenching of leading jets and particles: The $p(T)$ dependent Landau-Pomeranchuk-Migdal effect from nonlinear $k(T)$ factorization
Physical Review D **74** (2006) 014023.
57. N.N. Nikolaev, W. Schäfer, B.G. Zakharov and V.R. Zoller
Glue in the pomeron from nonlinear $k(T)$ -factorization
JETP Letters **83** (2006) 192.
58. A. Nogga, C. Fonseca, A. Gardestig, C. Hanhart, C.J. Horowitz, G.A. Miller, J.A. Niskanen, U. van Kolck
Realistic few-body physics in the $dd \rightarrow \alpha\pi^0$ reaction
Physics Letters B **639** (2006) 465.
59. A. Nogga, C. Hanhart
Can one extract the π -neutron scattering length from π -deuteron scattering?
Physics Letters B **634** (2006) 210.
60. A. Nogga, P. Navratil, B.R. Barrett, J.P. Vary
Spectra and binding energy predictions of chiral interactions for ^7Li
Physical Review C **73** (2006) 064002.
61. H. Polinder, J. Haidenbauer, U.-G. Meißner
Hyperon nucleon interactions: A chiral effective field theory approach
Nuclear Physics A **779** (2006) 244.

62. L. Roca, C. Hanhart, E. Oset, U.-G. Meißner
Testing the nature of the $\Lambda(1520)$ resonance in proton-induced production
European Physical Journal A **27** (2006) 373.
63. D. Rozpedzik, J. Golak, R. Skibinski, H. Witala, W. Glöckle, E. Epelbaum, A. Nogga, H. Kamada
A First estimation of chiral four-nucleon force effects in ^4He
Acta Physica Polonica B **37** (2006) 2889.
64. S. Schneider, S. Krewald, U.-G. Meißner
The reaction $\pi N \rightarrow \pi\pi N$ in a meson-exchange approach
European Physical Journal A **28** (2006) 107.
65. A. Sibirtsev, J. Haidenbauer, H.W. Hammer, S. Krewald
Resonances and final state interactions in the reaction $pp \rightarrow p K^+ \Lambda$
European Physical Journal A **27** (2006) 269.
66. A. Sibirtsev, J. Haidenbauer, H.W. Hammer, U.-G. Meißner
Phenomenology of the Λ/Σ^0 production ratio in pp collisions
European Physical Journal A **29** (2006) 363.
67. A. Sibirtsev, J. Haidenbauer, S. Krewald, U.-G. Meißner
Kaon-deuteron scattering at low energies
Journal of Physics G **32** (2006) R395.
68. A. Sibirtsev, J. Haidenbauer, U.-G. Meißner
Aspects of ϕ -meson production in proton proton collisions
European Physical Journal A **27** (2006) 263.
69. A. Sibirtsev, H.W. Hammer, U.-G. Meißner, A.W. Thomas
 ϕ -Meson Photoproduction from Nuclei
European Physical Journal A **29** (2006) 209.
70. R. Skibinski, J. Golak, H. Witala, W. Glöckle, A. Nogga, E. Epelbaum
Nucleon-deuteron capture with chiral potentials
Acta Physica Polonica B **37** (2006) 2905.
71. A. Wirzba, A. Bulgac, P. Magierski
Casimir interaction between normal or superfluid grains in the Fermi sea
Journal of Physics A **39** (2006) 6815.
72. H. Witala, J. Golak, R. Skibinski, W. Glöckle, a. Nogga, E. Epelbaum, H. Kamada, A. Kievsky, M. Viviani
Testing nuclear forces by polarization transfer coefficients in $d(\vec{p}, \vec{p})d$ and $d(\vec{p}, \vec{d})p$ reactions $E_p^{lab} = 22.7$ MeV
Physical Review C **73** (2006) 044004.

3. Accelerator (including conference proceedings)

73. S. Andrianov, A. Chechenin
The normal form for beam physics in matrix representation
 Proc. EPAC 2006, Edinburgh, Scotland, ISBN 92-9083-278-9, 978-92-9083-278-2, p. 2122.
74. S. Andrianov, A. Chechenin
The high order aberration correction
 Proc. EPAC 2006, Edinburgh, Scotland, ISBN 92-9083-278-9, 978-92-9083-278-2, p. 2125.
75. O. Boine-Frankenheim, R. Hasse, F. Hinterberger, A. Lehrach, A. P. Zenkevich
Cooling equilibrium and beam loss with internal targets in high energy storage rings
Nuclear Instruments and Methods in Physics Research A **560** (2006) 245.
76. A. Chechenin, R. Maier, Yu. Senichev
The Non-linear Space Charge Field Compensation of the Electron Beam in the High Energy Storage Ring of FAIR
 Proc. EPAC 2006, Edinburgh, Scotland, ISBN 92-9083-278-9, 978-92-9083-278-2, p. 2802.

77. A. Chechenin, R. Maier, Yu. Senichev, E. Senicheva
The High Order Non-linear Beam Dynamics in High Energy Storage Ring of FAIR
 Proc. EPAC 2006, Edinburgh, Scotland, ISBN 92-9083-278-9, 978-92-9083-278-2, p. 2083.
78. J. Conradie, A. Botha, P. Celliers, J. Delsink, D. Theunis Fourie, P. Mansfield, P. Rohwer, J. Van Niekerk, J. Dietrich, I. Mohos
Beam Phase Measurement in a 200 MeV Cyclotron
 Proc. EPAC 2006, Edinburgh, Scotland, ISBN 92-9083-278-9, 978-92-9083-278-2.
79. J. Dietrich, V. Parkhomchuk
The Proposed 2 MeV Electron Cooler for COSY-Jülich
 Proc. EPAC 2006, Edinburgh, Scotland, ISBN 92-9083-278-9, 978-92-9083-278-2.
80. F. Esser, R. Eichhorn, B. Laatsch, H. Singer, R. Stassen
First cool down of the Jülich accelerator module based on superconducting half-wave resonators
 Proc. EPAC 2006, Edinburgh, Scotland, ISBN 92-9083-278-9, 978-92-9083-278-2.
81. A. Garishvili, A. Lehrach, B. Lorentz, S. Martin, F. Rathmann, P. Lenisa, E. Steffens
Design study for an antiproton polarizer ring (APR)
 Proc. EPAC 2006, Edinburgh, Scotland, ISBN 92-9083-278-9, 978-92-9083-278-2, p. 223.
82. R. Gebel, O. Felden, R. Maier, P. von Rossen
Recent gain in polarized beam intensities for the cooler synchrotron COSY at Jülich
 Proc. EPAC 2006, Edinburgh, Scotland, ISBN 92-9083-278-9, 978-92-9083-278-2, p. 1705.
83. A.D. Krisch, M.A. Leonova, V.S. Morozov, R.S. Raymond, D.W. Sivers, V.K. Wong, R. Gebel, A. Lehrach, B. Lorentz, R. Maier, D. Prasuhn, A. Schnase, H. Stockhorst, F. Hinterberger, K. Ulbrich
Unexpected enhancement and reduction of rf spin resonance strength
Physical Review ST AB **9** (2006) 051001.
84. A. Lehrach, O. Boine-Frankenheim, F. Hinterberger, R. Maier, D. Prasuhn
Beam performance and luminosity limitations in the High-Energy Storage Ring (HESR)
Nuclear Instruments and Methods in Physics Research A **561** (2006) 289.
85. A. Lehrach, R. Maier, D. Prasuhn, O. Boine-Frankenheim, R.W. Hasse, F. Hinterberger
Beam Performance with Internal Targets in the High-Energy Storage Ring (HESR)
 Proc. EPAC 2006, Edinburgh, Scotland, ISBN 92-9083-278-9, 978-92-9083-278-2, p. 2197.
86. A. Paal, A. Simonsson, J. Dietrich, I. Mohos
Bunched Beam Current Measurements with 100 pA rms Resolution at CRYRING
 Proc. EPAC 2006, Edinburgh, Scotland, ISBN 92-9083-278-9, 978-92-9083-278-2.
87. D. Prasuhn, J. Dietrich, A. Lehrach, B. Lorentz, R. Maier, H. Stockhorst
From COSY to HESR
 Proc. EPAC 2006, Edinburgh, Scotland, ISBN 92-9083-278-9, 978-92-9083-278-2, p. 226.
88. H. Rohdjeß, D. Albers, J. Bisplinghoff, R. Bollmann, K. Blüßer, O. Diehl, E. Dohrmann, H.P. Engelhardt, P.D. Eversheim, M. Gasthuber, J. Greiff, A. Groß, R. Groß-Hardt, F. Hinterberger, M. Igelbrink, R. Langkau, R. Maier, F. Mosel, M. Müller, M. Münstermann, D. Prasuhn, P. von Rossen, H. Scheid, N. Schirm, F. Schwandt, W. Scobel, H.J. Trelle, A. Wellinghausen, W. Wiedmann, K. Woller, R. Ziegler
Determining beam parameters in a storage ring with cylindrical hodoscope using elastic proton-proton scattering
Nuclear Instruments and Methods in Physics Research A **556** (2006) 57.
89. H. Rohdjeß, M. Altmeier, F. Bauer, J. Bisplinghoff, R. Bollmann, K. Büßer, M. Busch, O. Diehl, F. Dohrmann, H. P. Engelhardt, J. Ernst, P.D. Eversheim, K.O. Eyser, O. Felden, R. Gebel, A. Groß, R. Groß-Hardt, F. Hinterberger, R. Langkau, J. Lindlein, R. Maier, F. Mosel, D. Prasuhn, P. von Rossen, N. Scheid, M. Schulz-Rojahn, F. Schwandt, V. Schwarz, W. Scobel, H.-J. Trelle, K. Ulbrich, E. Weise, A. Wellinghausen, K. Woller, R. Ziegler
Upper Limits on Resonance Contributions to Proton-Proton Elastic Scattering in the c.m. Mass Range 2.05 – 2.85 GeV/c²
European Physical Journal A, **28** (2006), 115
90. Yu. Senichev, A. Bogdanov, R. Maier, N. Vasyukhin
Beam dynamics in super-conducting linear accelerator: Problems and solutions
Nuclear Instruments and Methods in Physics Research A **558** (2006) 240.

91. Yu. Senichev, W. Bräutigam, R. Maier, O. Belyaev, Yu. Budanov, V. Stepanov, V. Teplyakov, A. Zherebtsov, I. Zvonarev
Novel H-type rf-deflector
Physical Review ST AB **9** (2006) 012001.
92. Yu. Senichev, N. Vasiukhin
Hamiltonian formalism for halo investigation in high-intensity beams
Nuclear Instruments and Methods in Physics Research A **561** (2006) 166.
93. E. Senicheva, A. Lehrach, D. Prasuhn, D.
The PANDA Insertion Impedance in High Energy Storage Ring of FAIR
Proc. EPAC 2006, Edinburgh, Scotland, ISBN 92-9083-278-9, 978-92-9083-278-2, p. 2865.
94. R. Stassen, R. Eichhorn, F.M. Esser, B. Laatsch, G. Schug, H. Singer
The HW resonators in Jülich
Physica C **441** (2006) 179.
95. H. Stockhorst, B. Lorentz, R. Maier, D. Prasuhn, T. Katayama
Stochastic Cooling for the HESR at the GSI-FAIR Complex
Proc. EPAC 2006, Edinburgh, Scotland, ISBN 92-9083-278-9, 978-92-9083-278-2, p. 231.
96. N. Vasyukhin, R. Maier, Yu. Senichev
The features of high intensity beam dynamics in low energy super-conducting linear accelerator
Nuclear Instruments and Methods in Physics Research A **558** (2006), 333.

C Diploma and Ph.D. Theses

1. Diploma

1. M. Angelstein: *Untersuchungen der Charakteristika eines Szintillatorhodoskopes des Wide Angle Shower Apparatus (WASA) am COoler SYnchrotron" (COSY)*, Fachhochschule Jena
2. M. Evers: *Towards a field theoretically consistent unitatization of quark models*, Universität Bonn
3. B.R. Jany: *Assembly and measurements of the Electromagnetic Calorimeter components for WASA-at-COSY setup*, Jagiellonian University Cracow [arXiv:physics/0606110]
4. E. Matveyev: *Verbesserung der Elektronik einer Emittanzmeßanlage*, Technical University Obninsk
5. M.A. Odoyo: *Development of Software for Slow Control of the High Voltage System of the WASA Central Detector Calorimeter*, Fachhochschule Mannheim.
6. C.F. Redmer: *Groß- und kleinflächige Szintillatorhodoskope in der Teilchen- und Atomphysik*, Ruhr-Universität Bochum
7. D.M. Welsch: *Entwicklung eine Orbitkorrektursystems für den Hochenergie Speicherring HESR im Projekt FAIR*, Universität Bonn
8. L. Yurev: *Performance of the Mini Drift Chamber — The central detector of the experiment WASA*, Voronezh State University

2. Ph.D.

9. I. Keshelashvili: *Kaon pair production in pp collisions at the ANKE spectrometer*, Tbilisi University
10. S. Mikirtychians: *Precision measurement of π^+ and K^+ lifetime*, PNPI Gatchina
11. A. Mussgiller: *Identification and Tracking of Low Energy Spectator Protons*, Universität zu Köln

D Invited Talks and Colloquia

1. Baur, G.
Reaction theory
Nustar Annual Meeting
GSI Darmstadt: 22. – 24.02.2006
2. Baur, G.; Typel, S.
Investigation of subthreshold resonances with the Trojan horse method
Fusion06: International Conference on Reaction Mechanisms and Nuclear Structure at the Coulomb Barrier
S.Servolo Island, Italy: 19. – 23.03.2006
3. Baur, G.
Direct reactions with exotic nuclei, nuclear structure and astrophysics
Erice School on Radioactive Beams, Nuclear Dynamics and Astrophysics
Erice, Italy: 16. – 24.09.2006
4. Büscher, M.
Experimental Program at COSY
Joint Sino-German Symposium on Hadron Physics at COSY and CSR (HPC2)
Lanzhou, China: 13. – 18.01.2006
5. Dietrich, J.
2 MeV Elektronenkühler für COSY-Jülich
Leibnitz-Institut für Polymerforschung, seminar talk
Dresden: 13.10.2006
6. Dietrich, J.
2 MeV Elektronenkühler für COSY-Jülich
Universität Erlangen, Institut für Theoretische Physik, seminar talk
Erlangen: 26.01.2006
7. Dietrich, J.
Measurements of Beam Profile Based on Light Radiation of Atoms Excited by the Particle Beam
iThemba Lab, seminar talk
Faure, South Afrika: 06.12.2006
8. Dietrich, J.
Muon Cooling
Goethe-Universität Frankfurt am Main, Winterseminar Beschleunigerphysik, seminar talk
Riezlern: 05. – 11.03.2006
9. Dietrich, J.
New Experimental Results on Electron Cooling at COSY-Juelich
University of Kyoto, Advanced Research Center for Beam Science, seminar talk
Kyoto, Japan: 07.06.2006
10. Epelbaum, E.
Three-nucleon forces: new developments
2006 APS April Meeting
Dallas, TX: 22. – 26.04.2006
11. Epelbaum, E.
Chiral Forces and Few-Nucleon Systems
Workshop on Exotic Hadronic Atoms, Deeply Bound Kaonic Nuclear States and Antihydrogen: Present Results, Future Challenges
ECT Trento, Italien: 19. – 24.06.2006
12. Epelbaum, E.
Few-Nucleon Forces and Systems in Chiral Effective Field Theory
21st Annual Hampton University Graduate School Program
Jefferson Lab., Newport News: 05. – 23.06.2006

13. Epelbaum, E.
Chiral EFT for Electroinduced Processes in Few-Nucleon Systems Gordon Research Conference on Photonuclear Reactions
Tilton School, Tilton, NH: 30.07. – 04.08.2006
14. Epelbaum, E.
Towards a Systematic Theory on Nuclear Forces and Nuclear Currents
5th International Workshop on Chiral Dynamics: Theory and Experiment
Durham/Chapel Hill, NC: 18. – 22.09.2006
15. Epelbaum, E.
Chiral Extrapolations in Few-Nucleon Systems
Workshop on Lattice QCD, Chiral Perturbation Theory and Hadron Phenomenology
ECT Trento, Italy: 02.10.2006 – 06.10.2006
16. Epelbaum, E.
Isospin Violation in Nuclear Potentials
Carolina Isospin Violation Workshop
Columbia, SC: 01. – 02.12.2006
17. Gillitzer, A.
Experimental access to in-medium properties of η and K mesons
Joint Sino-German Symposium on Hadron Physics at COSY and CSR (HPC2)
Lanzhou, China: 13. – 18.01.2006
18. Gillitzer, A.
Hadrons in the nuclear medium — An experimental review
IVth International Conference on Quarks and Nuclei (QNP06)
Madrid, Spain: 05. – 10.06.2006
19. Gotta, D.
Pionic Hydrogen
The International Workshop Physics with Simple Atomis Systems (PSAS 2006)
Venice, Italy: 13. – 17.06.2006
20. Gotta, D.
Light Antiprotonic Atoms
The International Workshop on Hadronic Exotic Atoms
Trento, Italy: 19. – 23.06.2006
21. Gotta, D.
Pionic Deuterium
The International Workshop on Hadronic Exotic Atoms
Trento, Italy: 19. – 23.06.2006
22. Haidenbauer, J.
Exotica, final-state interactions and the $p\bar{p}$ system
Universität Bonn : Physikalisches Institut; Kolloquium
Bonn: 27.04.2006
23. Haidenbauer, J.
Meson-exchange description of hadronic systems: Recent developments
18th International IUPAP Conference on Few-Body Problems in Physics
Santos, Brasil: 21. – 26.08.2006
24. Haidenbauer, J.
The hyperon-nucleon interaction: conventional versus effective field theory approach
University of Barcelona: Kolloquium
Barcelona, Spain: 31.05.2006
25. Hanhart, C.
CSB pion production, progress in $pn \rightarrow d\pi^0$
Carolina Isospin Violation Workshop
Columbia, SC: 01. – 02.12.2006

26. Hanhart, C.
Dispersive Corrections to the Pion Deuteron Scattering Length
QCD and Few-Hadron Systems
Bad Honnef: 16.11.2006
27. Hanhart, C.
Highlights of the ETA06 Workshop on the Eta-Nucleus System
EtaMesonNet Meeting
Mainz: 03.10.2006
28. Hanhart, C.
Pion reactions on two nucleon systems
Physics and Astrophysics of Hadrons and Hadronic Matter: Lecture series
Shantiniketan, India: 06. – 09.11.2006
29. Hanhart, C.
The pi NN system: Recent progress
5th International Workshop on Chiral Dynamics: Theory & Experiment
Durham, Chapel Hill: 18. – 22.09.2006
30. Hanhart, C.
Towards an understanding of the light scalar mesons
QNP2006
Madrid, Spain: 05. – 10.06.2006
31. Hartmann, M.
The near-threshold production of ϕ mesons in pN collisions
MESON2006: 9th International Workshop on Meson Production, Properties and Interaction
Cracow, Poland: 09. – 13.06.2006
32. Hawranek, P.
Eta physics at GEM
MESON2006: 9th International Workshop on Meson Production, Properties and Interaction
Cracow, Poland: 09. – 13.06.2006
33. Kirilov, D.
Search for eta bound states at COSY
Eta workshop
Jülich: 09.05.2006
34. Kirilov, D.
The eta physics program at GEM
IVth International Conference on Quarks and Nuclear Physics (QNP06)
Madrid, Spain: 05. – 10.06.2006
35. Krebs, H.
Scalar two-loop diagrams on the lattice
Lattice QCD, Chiral Perturbation Theory and Hadron Phenomenology
ECT Trento, Italy: 10. – 14.10.2006
36. Krewald, S.
 N^* physics
Institute of High Energy Physics, Seminar Talk
Beijing, China: 19.01.2006
37. Krewald, S.
Medium modifications of the nucleon-nucleon interaction
XI International Seminar on Electromagnetic Interactions of Nuclei
Moscow, Russia: 21. – 24.09.2006
38. Krewald, S.
Study of N^* excitations with the Juelich model
Thomas Jefferson National Laboratory : N^* Analysis Workshop
Newport News: 04. – 05.11.2006

39. Krewald, S.
Electric Dipole Strength in Heavy Nuclei
QCD and Few-Hadron Systems: 380th International Wilhelm and Else Heraeus Seminar
Bad Honnef, Germany: 13. – 17.11.2006
40. Lorentz, B.
Accelerator constraints for internal experiments
Joint Sino-German Symposium on Hadron Physics at COSY and CSR (HPC2)
Lanzhou, China: 13. – 18.01.2006
41. Machner, H.
Physics with WASA at COSY
Symposium QCD: Facts and Prospects
Oberwölz, Austria: 10. – 16.09.2006
42. Machner, H.
Recent Investigations at BIG KARL
XVIII Baldin ISHEPP
Dubna, Russia: 25. – 30.09.2006
43. Machner, H.
Recent Experiments at Big Karl
Seminar, Helsinki Inst. Physics
Helsinki, Finland: 10.10.2006
44. Meißner, U.-G.
Major Challenges in QCD
Joint Sino-German Symposium on Hadron Physics at COSY and CSR (HPC2)
Lanzhou, China: 13. – 18.01.2006
45. Meißner, U.-G.
Summary Talk of Hadron Physics at COSY and CSR
Joint Sino-German Symposium on Hadron Physics at COSY and CSR (HPC2)
Lanzhou, China: 13. – 18.01.2006
46. Meißner, U.-G.
B-Decays and the Scalar Sector of QCD
Workshop on Three-Body Charmless B Decays
Paris, France: 01. – 03.02.2006
47. Meißner, U.-G.
B-decays and the scalar sector of QCD
Workshop on Scalar Mesons
Bonn, Germany: 27. – 28.03.2006
48. Meißner, U.-G.
Form factors of the nucleon and its pion cloud
Workshop on Shape of Hadrons
Athens, Greece: 27. – 30.04.2006
49. Meißner, U.-G.
Modern Theory of Nuclear Forces
Universität zu Köln: Grosses Physikalisches Kolloquium
Köln: 23.05.2006
50. Meißner, U.-G.
Modern theory of nuclear forces
IVth International Conference on Quarks and Nuclear Physics (QNP06)
Madrid, Spain: 05. – 10.06.2006
51. Meißner, U.-G.
Modern theory of nuclear forces: Status and perspectives
18th International IUPAP Conference on Few-Body-Problems in Physics (FB 18)
Santos, Brazil: 21. – 26.08.2006

52. Meißner, U.-G.
Quark mass dependence of the nucleon mass and axial-vector coupling
Workshop on Soft-Pions in Hard Processes
Regensburg, Germany: 03. – 05.08.2006
53. Meißner, U.-G.
Hadronic atoms
Hadron TH'06 Workshop
Peniscola, Spain : 07. – 09.09.2006
54. Meißner, U.-G.
On the consistency of Weinberg's power counting
5th International Workshop on Chiral Dynamics: Theory and Experiment (CD 06)
Chapel Hill: 18. – 22.09.2006
55. Meißner, U.-G.
Recent developments in chiral perturbation theory
5th International Workshop on Chiral Dynamics: Theory and Experiment (CD 06)
Chapel Hill: 18. – 22.09.2006
56. Meißner, U.-G.
Thoughts on chiral extrapolations for excited states
ECT*-I3HP Workshop on Lattice QCD, Chiral Perturbation Theory, and Hadron Phenomenology
Trento, Italy: 02. – 06.10.2006
57. Meißner, U.-G.
Chiral dynamics with (non)strange quarks
Transregio 16: Tagung des Sonderforschungsbereichs
Bommerholz: 27. – 28.11.2006
58. Meißner, U.-G.
Modern theory of nuclear forces: Status and perspectives
Workshop of the SFB 634
Paradeismühle, Klingenberg: 06. – 08.12.2006
59. Moskal, P.
 η and η' meson production at COSY-11
MESON2006: 9th International Workshop on Meson Production, Properties and Interaction
Cracow, Poland: 09. – 13.06.2006
60. Nikolaev, N.N.
Lectures on factorization theorems for hard processes in a nuclear environment St.Petersburg XL Winter-School on Nuclear and Particle Physics and XII School on Theoretical Physics : St.Petersburg Nuclear Physics Institute St. Petersburg, Russia:
20.02.2006 – 26.02.2006
61. Nikolaev, N.N.
Understanding the Spin Filtering in Storage Rings
Workshop on QCD with Antiprotons
ECT* Trento, Italy: 03. – 08.07.2006
62. Nikolaev, N.N.
QCD Physics with Antiprotons at FAIR GSI
Symposium QCD: Facts and Prospects
Oberwölz, Austria: 10. – 16.09.2006
63. Nikolaev, N.N.
Spin Filtering of Stored (Anti)Protons from FILTEX to COSY to AD to FAIR
17th International Spin Physics Symposium: SPIN2006
Kyoto University, Kyoto, Japan: 02. – 07.10.2006
64. Nogga, A.
Chiral 3N interactions and p-shell nuclei
Los Alamos National Lab, Seminar
Los Alamos: 12.01.2006

65. Nogga, A.
RG and EFT for nuclear forces
ECT* School on RG and Effective Field Theory Approaches to Nuclear Systems: 3 lectures
Trento, Italy: 27.02. – 10.03.2006
66. Nogga, A.
EFT approach
Workshop on Electron-Nucleus Scattering-IX
Isola d'Elba, Italy: 19. – 23.06.2006
67. Nogga, A.
Chirale und Niederimpulswechselwirkungen: ein systematischer Zugang zur Kernphysik
Universität Gießen, Seminar
Gießen: 14.07.2006
68. Nogga, A.
Application of chiral nuclear forces to light nuclei
5th International Workshop on Chiral Dynamics (CD06)
Duke University, Durham, Chapel Hill: 18. – 22.09.2006
69. Nogga, A.
Chiral nuclear interactions: a systematic approach to nuclear structure
University of Vancouver, TRIUMF, Seminar
Vancouver, Canada: 28.11.2006
70. Nogga, A.
Chirale und Niederimpulswechselwirkungen: ein systematischer Zugang zur Kernphysik
Technische Universität München, Seminar
München: 27.10.2006
71. Nogga, A.
Nuclear bound state predictions for chiral interactions
Workshop on QCD and Few-Hadron Systems
Bad Honnef: 13. – 17.11.2006
72. Oelert, W.
Experimente mit der Antimaterie — die geheimnisvolle Materie aus Antiteilchen
Universität Bonn, Kolloquium
Bonn: 28.04.2006
73. Oelert, W.
Experiments on making atoms totally of antimatter — why and how
Silesian University Katowice : Department of Physics, Kolloquium
Katowice, Poland: 17.01.2006
74. Oelert, W.
General thoughts to the Kaon pair production in the threshold region
MESON2006: 9th International Workshop on Meson Production, Properties and Interaction
Cracow, Poland: 09. – 13.06.2006
75. Oelert, W.
Physics with low Energy Antiprotons
Workshop on \bar{p} Physics
Trento, Italy: 06.07.2006
76. Polinder, H.
Hyperon-nucleon interactions in effective field theory
IX International Conference on Hypernuclear and Strange Particle Physics
Mainz: 12.10.2006
77. Polinder, H.
Hyperon-nucleon interactions in effective field theory
Workshop on QCD and Few-Hadron Systems, 380th International Wilhelm und Else Heraeus Seminar
Bad Honnef: 16.11.2006

78. Ritman, J.
Physics with Antiprotons at FAIR
International Graduate School Basel-Tuebingen, Colloquium
Basel, Switzerland: 05.05.2006
79. Ritman, J.
Precision spectroscopy in the charmonium mass region using antiproton annihilation: PANDA at FAIR
Conference on Hadron Physics
Trento, Italy: 07.07.2006
80. Ritman, J.
Investigation of Fundamental Symmetries in Hadronic Systems: WASA at COSY
Technische Universität München, Colloquium
München: 27.07.2006
81. Ritman, J.
Charmonium Physics with PANDA at FAIR
Heavy Quarks and Leptons Conference
München: 17.10.2006
82. Ritman, J.
Symmetrieverletzungen in der Hadronen-Physik
Ruhr Universität Bochum, Colloquium
Bochum: 04.12.2006
83. Schadmand, S.
Hadron Physics at COSY with the WASA Detector
Universität Mainz, Kernphysikalisches Institut, Seminar
Mainz: 02.01.2006
84. Schadmand, S.
Chasing Symmetries with WASA at COSY
Joint Symposium on Hadron Physics, GSI/Mainz, GSI/Darmstadt
Darmstadt: 26. – 27.01.2006
85. Schadmand, S.
Future Physics with WASA at COSY
QNP06: IVth International Conference on Quarks and Nuclear Physics
Madrid, Spain: 05. – 10.06.2006
86. Schadmand, S.
Two Pion Production from Nuclei
New Frontiers in QCD, Exotic Hadrons and Hadronic Matter: Yukawa International Seminar (YKIS) 2006
Kyoto, Japan: 04. – 08.12.2006
87. Speth, J.
Migdal's theory of finite Fermi systems, Nuclear Physics Seminar
Institute of Nuclear Physics, Colloquium
Cracow, Poland: 19.10.2006
88. Speth, J.
From Nuclear Physics to Financial Markets
Institute of Nuclear Physics, Colloquium
Cracow, Poland: 16.11.2006
89. Stassen, R.
Stochastisches Kühlsystem am Beispiel COSY und Weiterentwicklungen für HESR/FAIR
Universität Darmstadt, seminar talk
Darmstadt: 14.11.2006
90. Ströher, H.
Hadron Physics in Germany
Joint Sino-German Symposium on Hadron Physics at COSY and CSR (HPC2)
Lanzhou, China: 13. – 18.01.2006

91. Ströher, H.
Hadron Physics at COSY-Jülich
Universität Basel, Kolloquium
Basel, Switzerland: 04.05.2006
92. Ströher, H.
The Hadron Physics Program at COSY-Jülich
CGSWHP06, Spin in Hadron Physics
Tbilisi, Georgia: 04. – 08.09.2006
93. Ströher, H.
Spin in Hadronic Reactions at Medium Energy
SPIN2006: The 17th International Spin Physics Symposium
Kyoto, Japan : 02. - 07.10.2006
94. Ströher, H.
The Hadron Physics Program at COSY-Jülich
DAE-BRNS06: Physics and Astrophysics of Hadrons and Hadronic Matter
Santiniketan, India: 06. - 11.11.2006
95. Wirzba, A.
Casimir effect and trace formula
Nonlinearities '06 — from Turbulent to Magic
Nordita and Niels Bohr Institute Thematic Workshop
Copenhagen, Denmark: 17. – 20.05.2006
96. Wirzba, A.
Exact and semiclassical solutions to the Casimir effect
Lund University, Mathematical Physics, LTH, Seminar talk
Lund, Sweden: 03.07.2006
97. Wolke, M.
The Physics Case for WASA at COSY
HPC2, Hadron Physics at COSY and CSR
Lanzhou, China: 13. - 18.01.2006
98. Wolke, M.
Physik mit WASA an COSY
TU Dresden, Institut für Kern- und Teilchenphysik, Institutsseminar
Dresden: 13.07.2006
99. Zapatin, E.
Cornell cryostat structural analysis
Cornell LEPP Seminar
Ithaca, NY: 28.08.2006
100. Zapatin, E.
FZJ sc rf cavity developments
FermiLab Accelerator Seminar
Chicago, Ill.: 16.02.2006
101. Zapatin, E.
FZJ superconducting rf cavities
Cornell LEPP Seminar
Ithaca, NY: 14.08.2006
102. Zapatin, E.
High-gradient cavity mid-cell comparison
Cornell LEPP Seminar

E Awards & Offers for Professorships

J. Dietrich: *Dr. h.c.* by JINR Dubna (20.01.2006)

J. Dietrich: *Apl. Professor* by Univ. Dortmund (02.10.2006)

U.-G. Meißner: *Chair in Theoretical Nuclear Physics* by Univ. Mainz (June 2006)

F Funded Projects

Project	Responsible	Partner Institute	Funded by
CARE	R. Tölle		EU/FP6
TA-COSY	D. Grzonka		EU/FP6
Hadron Physics Theory Netzwerk	U.-G. Meißner	Network	EU/FP6
EtaMesonNet	W. Oelert	Network	EU/FP6
Pellet Target	M. Büscher	ITEP, MPEI Moscow (Russia)	EU/FP6
EURONS/EXL	D. Grzonka		EU/FP6
EUROTRANS/NUDATRA	F. Goldenbaum		EU/FP6
DIRAC Secondary Beams	R. Tölle		EU/FP6
DIRAC Secondary Beams PANDA-4	J. Ritman		EU/FP6
DIRAC Second. Beams PANDA-2	J. Ritman		EU/FP6
Strange and Charmed Scalar Mesons	M. Büscher	ITEP, INR Moscow (Russia)	DFG
K^+ Production Mechanisms in Nuclei	H. Ströher	PNPI Gatchina (Russia)	DFG
Light Scalar Resonances $a_0/f_0(980)$	M. Büscher	ITEP, MPEI Moscow (Russia)	DFG
Isospin Violation	M. Büscher	IMP Lanzhou (China)	DFG
Jets in Hard Processes	N.N. Nikolaev	Landau Inst., ITEP Moscow (Russia)	DFG
Properties of Unstable Nuclei	S. Krewald	Petersburg State Univ., IPPE Obninsk (Russia)	DFG
Pion Reactions on Few Nucleon Systems	C. Hanhart	ITEP Moscow (Russia)	DFG
Quark-gluon degrees of freedom in the confinement region of QCD	J. Haidenbauer	UNESP Sao Paulo (Brasil)	DFG
ATRAP	W. Oelert	Univ. Mainz	DFG
Fundamental Research with Hadrons	W. Oelert	Jagellian Univ. Cracow (Poland)	DFG
Broken Symmetries	H. Machner	Univ. Helsinki (Finland)	DAAD
PPP Poland	P.v. Rossen		DAAD
PPP Sweden	H. Ströher	Uppsala Univ. (Sweden)	DAAD
Short-range correlations in nuclear reactions	J. Haidenbauer	JINR Dubna (Russia)	Heisenberg-Landau Program
Eta-Meson Physics	H. Machner	BARC Mumbai (India)	Int. Büro BMBF
Target Development for nuclear physics experiments at COSY and AEA cyclotron	J. Ritman	AEA Cairo (Egypt)	Int. Büro BMBF
Medical Applications of Accelerators	J. Dietrich	iThemba LABS (South Africa)	Int. Büro BMBF
Advanced Residual Gas Profile Monitor	J. Dietrich		INTAS
Advanced Beam Dynamic for Storage Rings	A. Lehrach		INTAS
EM-processes in the peripheral collisions of relativistic and ultrarelativistic heavy ions	G. Baur	Belfast, Tashkent, Arkhangelsk	GSI-INTAS
Polarized Target	F. Rathmann	PNPI Gatchina (Russia)	ISTC
Few Nucleon Systems in χ EFT	E. Epelbaum	Univ. Bonn	HGF
Planare Germanium Detektoren	D. Protic		GSI
Baryon Resonance Analysis	U.-G. Meißner	JLAB (U.S.A.)	JLAB

G COSY-FFE Projects

Project	Responsible	Institute
Θ^+ und Anti-decuplet	Prof. K. Goeke	Univ. Bochum
TOF-Entwicklung und Nutzung	Prof. H. Koch	Univ. Bochum
Frozen Spin Target	Prof. W. Meyer	Univ. Bochum
Zusammenarbeit von HISKP-Bonn an internen Experimenten an COSY	Prof. J. Bisplinghoff	Univ. Bonn
Polarisiertes Target für TOF	Dr. H. Dutz	Univ. Bonn
Theoretical studies of strangeness and charm production at COSY and PANDA/FAIR	Prof. H.-W. Hammer	Univ. Bonn
Entwicklung eines Partialwellenprogrammes für die Analyse von Daten von WASA	Prof. E. Klempt	Univ. Bonn
Zusammenarbeit an COSY H-Strahl Laserdiagnose	Prof. T. Weis	Univ. Dortmund
COSY-TOF detector	Prof. H. Freiesleben	TU Dresden
Bau von Detektoren für ANKE und K^- -Nachweis	Prof. B. Kämpfer	FZ Dresden-Rossendorf
Theoretische Untersuchungen zur künftigen COSY-Physik	Prof. M. Dillig	Univ. Erlangen-Nürnberg
Bau eines Cherenkovdetektors für WASA at COSY	Prof. W. Eyrich	Univ. Erlangen-Nürnberg
Experimente mit COSY-TOF	Prof. W. Eyrich	Univ. Erlangen-Nürnberg
Polarization experiments with ANKE at COSY	Prof. E. Steffens	Univ. Erlangen-Nürnberg
Meson production and resonance properties in the coupled channel K-Matrix approach	Prof. U. Mosel	Univ. Gießen
ANKE Experiment und Auswertung $pp \rightarrow dK^+\bar{K}^0$	Prof. H. Paetz gen. Schieck	Univ. Köln
Schwellenexperimente an COSY-11 und ANKE	Dr. A. Khoukaz	Univ. Münster
Installation und Inbetriebnahme des WASA-Detektors am COSY-Ring und Durchführung von Experimenten an WASA at COSY	Prof. H. Clement	Univ. Tübingen
Experimente an COSY-TOF	Prof. H. Clement	Univ. Tübingen
η -production on heavier nuclei	Dr. R. Tsenov	Univ. of Sofia (Bulgaria)
Polarized internal target for ANKE at COSY	Prof. M. Nioradze	Tbilisi State Univ. (Georgia)
Spin dependence in pd interactions	Prof. P. Dalpiaz	Univ. Ferrara (Italy)
Photonendetektor an ANKE	Prof. A. Magiera	Jagellian Univ. Cracow (Poland)
WASA at COSY	Prof. M. Jezabek	INP Crakow (Poland)
Strange Baryon Produktion at ANKE	Prof. Z. Sujkowski	IPJ Otwock-Swierk (Poland)
Neutron tagging and strangeness production at ANKE	Dr. V. Koptev	PNPI Gatchina (Russia)
Set-up and research with the spectator/vertex detection system at ANKE-COSY	Prof. V. Komarov	JINR Dubna (Russia)
Investigation of scalar meson production in pp , pd and dd collisions	Prof. L. Kondratyuk	ITEP Moscow (Russia)
Development, commissioning and operation of components for the COSY experiments WASA and ANKE and spin-filtering studies at COSY as preparation of the PAX experiment in the framework of the FAIR project at GSI	Dr. A. Vasilyev	PNPI Gatchina (Russia)
Cooperation COSY-WASA for $pp \rightarrow pp\eta$ and $pp \rightarrow pp\eta\pi^0$	Prof. T. Johansson	Uppsala Univ. (Sweden)
Search for mixing between light mesons	Prof. A. Rudchik	INR Kiev (Ukraine)
Unified analysis of meson production in hadronic reactions	Prof. K. Nakayama	Univ. of Georgia (U.S.A.)
SPIN@COSY: Spin-Manipulating Polarized Deuterons and Protons	Prof. A. Krisch	Univ. of Michigan (U.S.A.)

H COSY Summer School CSS2006

From August 28 to September 1 the 3rd COSY Summer School (CSS2006) took place at the conference center Burg Hengebach in Heimbach — organized by the IKP in collaboration with the Universities Dresden and Cracow. It was attended by more than 30 Diploma and Ph.D. students from Germany, France, Ireland, Sweden, Finland, Poland, Ukraina, Russia und China.



Fig. 1: Participants and organizers of the COSY Summer School at Burg Hengebach.

During 12 theoretical and experimental lectures modern techniques and current hot topics in hadron physics were presented with special emphasize on COSY relevant topics. In the second part of CSS2006 the participants were asked to work out — based on the contents of these lectures — experimental COSY proposals. These working groups were especially appreciated since they offered a possibility to apply the new knowledge to a “real case”. The results were finally presented in talks by the students in which they had to “defend” their results against referees (*i.e.* the organizers of CSS2006). All proposals were so well worked out that all of the applied beam times could be “approved”.

The agenda of the Summer School was complemented by an excursion to COSY and its detection systems as well as a hike through the lovely Eifel landscape. Due to the very positive feedback from the participants (one of the foreign guests wrote the organizers: “the best I had so far”), the next COSY Summer School is planned for the year 2008.

Financial support for the CSS2006 by the board of directors of the FZJ is gratefully acknowledged.

I Conferences (co-)organized by the IKP

I.1 HPC², Lanzhou (China)

On January 13–18 2006, the Joint Sino-German symposium on Hadron Physics at COSY and CSR (HPC²) took place in Lanzhou, which is located in central China at the banks of the yellow river. The symposium was jointly organized by the Institute of Modern Physics (IMP) of the Chinese Academy of Sciences, and the IKP, and financed by the Sino-German Center for Research Promotion in Beijing. The workshop was attended by ~80 participants, mostly from China and Germany.



Fig. 2: Some participants of HPC2 in front of the main building of the IMP, Lanzhou.

The IKP has been operating COSY for more than 10 years which provides proton and deuteron beams with momenta up to 3.7 GeV/c. A similar facility — with the CSRM and CSRc rings — has been built at IMP and is now in the commissioning phase.

At COSY several detection systems — like the ANKE dipole spectrometer and the non-magnetic COSY-TOF experiment — are used for hadron physics experiments. A disadvantage of these existing COSY detectors is that they are “photon blind”. This will change with the start of operation of the Wide Angle Shower Apparatus WASA in 2007. WASA is a fixed-target 4π detector and designed for the detection of neutral and charged particles.

On the Chinese side a novel detector, HPLUS, is being prepared for hadron physics experiments. This device is conceptually designed for further studies of baryon resonances, scalar mesons and/or isospin violating effects. The R&D of the whole project has been started in the IMP with participation from other Chinese universities. Once operating, the WASA and HPLUS detectors allow one to investigate basic questions of non-perturbative quantum chromodynamics (“strong QCD”), for example through a precise study of symmetry breaking and very specific investigations of hadron structure. η and η' decays that vanish in the limit of equal light quark masses explore the explicit isospin symmetry-breaking in QCD. Precision measurements of rare η and η' decays can be used to obtain new limits on the breaking of the charge, parity and time symmetries or their combinations.

Last but not least, WASA and HPLUS can contribute to test various models offered to explain exotic and crypto-exotic hadrons — through precise measurements of decay chains and couplings to other hadrons.

These, together with other hot topics of strong QCD were discussed in about 40 talks during the 3-days workshop in order to coordinate the physics programs and share the technological expertise. Further common projects, focussing around measurements with WASA and the preparation of HPLUS, are now being launched.

I.2 International Workshop on η Physics

The International Workshop on Eta Physics was held from May 8–12 2006 at the IKP. The conference was a subgroup meeting of the EtaMesonNet network that coordinates activities and exchanges of information on the study of mesons, especially, η -mesons, at different European accelerator research infrastructures where they are produced with complementary processes.

The idea of this subgroup meeting was to bring together experts on various aspects of the field in order to understand better the complicated many-body problem posed by the η -nucleus dynamics. Most of the time of the meeting we will focus on the related theoretical aspects. However, for the first day we also invited representatives from the various experimental groups involved. There are currently or have been recently strong experimental efforts to investigate the η -nucleus system with various probes at BNL (USA), CELSIUS (Sweden), COSY (Jülich), and MAMI (Mainz). This first day was meant to define the problems to be studied in the following days, to get informed about experimental plans and possibilities, and to initiate the discussions.



Fig. 3: Participants of the η workshop in front of the COSY building.

There were in total 32 participants from 13 countries. The conference was characterized by very intense but constructive discussions. The talks can be found on the conference homepage under <http://www.fz-juelich.de/ikp/etanucleus/> and the results of the meeting as well as the individual talks are summarized in <http://arxiv.org/pdf/nucl-th/0610011>.

The workshop was funded by the European Union and the FZ-Jülich.

I.3 MESON2006, Cracow (Poland)

The 9th MESON conference took place in 2006 as all previous conferences in Cracow, Poland, in the time from June 9–13. The topics covered were

- hadronic meson production in various reactions,
- hadronic meson production in various reactions,
- electromagnetic meson production meson interaction with mesons,
- nucleons and nuclei, structure of hadrons,
- mesons and fundamental symmetries,
- exotic systems.

The conference was organized by Jagellonian University, Cracow, Poland, Polish Academy of Sciences, Cracow, Poland, the Instituto Nazionale di Fisica Nucleare, Frascati, Italy, and the FZJ. It was attended by more than 160 participants. The proceedings will appear as Vol. 22, Nos. 2 & 3 (30 January 2007) in the International Journal of Modern Physics A.



Fig. 4: Participants of the MESON2006 conference in front of the new Audimax of the Jagiellonian University.

I.4 CGSWHP2006, Tbilisi (Georgia)

The possibility of polarizing antiprotons at the upcoming Facility for Antiproton and Ion Research at GSI has stimulated widespread interest within the hadron community. Measuring the Drell-Yan process in high-energy proton-antiproton collisions offers the best way to study the transverse spin structure of protons (transversity). This was the focus at the second Caucasian-German School and Workshop on Hadron Physics (CGSWHP) in Tbilisi, Georgia, on 4-8 September. Around 70 participants attended, from nine countries.

Spin filtering, in which a beam of antiprotons acquires polarization by repeated passage through a polarized hydrogen target, is believed to be the most effective means of producing a useful beam for transversity experiments. CGSWHP'06 discussed preparatory spin-filtering tests using



Fig. 5: Participants relax during an interlude at the highly charged CGSWHP'06 in Georgia.

proton beams. These could be at COSY, where there is an extensive physics programme involving polarized beams and targets. Results from COSY were also presented at the meeting.

Georgian media covered several sessions, as well as the meeting of the organizers with the rector of Tbilisi State University, and some of the social programme. TV interviews publicized the workshop, with local graduate students discussing their research.

The EC Integrated Infrastructure Initiative project, Hadron Physics, supported the workshop, which was themed Spin in Hadron Physics and which was also sponsored by Forschungszentrum Jülich, the International Science & Technology Center, the Joint Institute for Nuclear Research and the Institute for High Energy Physics and Informatization, Tbilisi State University.

I.5 Carolina Isospin Violation Workshop

On December 1st and 2nd the Carolina Isospin Violation workshop was held at the Physics institute of the University of South Carolina located in Columbia, SC. This meeting was one of regular meetings where scientists interested in the subject of isospin violations come together, not only to discuss recent progress in the understanding of isospin violation in nucleon-nucleon and deuteron-deuteron induced pion production (one of the key experiments of WASA at COSY) but also new developments in the field as a whole. Out of the discussions emerged at least two concrete projects that will be carried out in the course of this year.

The workshop was funded by the University of South Carolina.

J Teaching Positions

Institute	Name	University
IKP-1	PD Dr. A. Gillitzer	Bonn
	PD Dr. F Goldenbaum	Wuppertal
	Prof. Dr. H. Machner	Duisburg-Essen
	Prof. Dr. W. Oelert	Bochum
	Prof. Dr. J. Ritman	Bochum
	PD Dr. S. Schadmand	Gießen
IKP-2	PD Dr. M. Büscher	Köln
	PD Dr. D. Gotta	Köln
	PD Dr. F. Rathmann	Erlangen-Nürnberg
	Prof. Dr. H. Ströher	Köln
	Dr. M. Wolke	Bochum
IKP-3	Prof. Dr. G. Baur	Basel
	Prof. Dr. E. Epelbaum	Bonn
	Univ. Doz. Dr. J. Haidenbauer	Graz
	PD Dr. C. Hanhart	Bonn
	Prof. Dr. S. Krewald	Bonn
	Prof. Dr. U.-G. Meißner	Bonn
	Prof. Dr. N.N. Nikolaev	Moscow
	Dr. A. Nogga	Bonn
	PD Dr. A. Wirzba	Bonn
IKP-4	Prof. Dr. Dr. h.c. J. Dietrich	Dortmund
	Dr. A. Lehrach	Bonn
	Prof. Dr. R. Maier	Bonn

K Beam Time at COSY 2006

Date	Experiment	Duration	Reaction
17.02.06–06.03.06	COSY-11	2 weeks	$pn \rightarrow d\eta'$
10.03.–20.03.	GEM	1 week	$pp \rightarrow d\pi^+ / pn\pi^+$
22.03.–29.03.	ANKE	1 week	cell tests
04.04.–02.05.	ANKE	4 weeks	$dd \rightarrow \alpha K^+ K^-$
05.05.–15.05.	GEM	1 week	$\vec{d}p \rightarrow ppn$
19.05.–29.05.	SPIN@COSY	1 week	
21.08.–04.09.	WASA	2 weeks	commissioning
08.09.–25.09.	GEM	2 weeks	$p^6\text{Li} \rightarrow \eta + ^7\text{Be}$
29.09.–23.10.	COSY-11	3 weeks	$pp \rightarrow pp\eta'$
03.11.–20.11.	WASA	2 weeks	commissioning
22.11.–30.11.	ANKE	1 week	$\vec{d}\vec{p} \rightarrow ppn$
Total '06		20 weeks	

L Personnel

L.1 Scientific Staff

Msc. M.-M. Abdel-Bary (IKP-1) (until 31 March, 2006)

DP S. An (IKP-4) (until 28 January, 2006)

DP M. Angelstein (IKP-1) (1 April – 30 Sep., 2006)

F. Ballout (IKP-3) (since 1 July, 2006)

Prof. Dr. G. Baur (IKP-3)

Dr. U. Bechstedt (IKP-4)

Dr. K. Bongardt (IKP-4)

DI N. Bongers (IKP-4)

DI W. Borgs (IKP-2)

DI R. Brings (IKP-4)

PD Dr. M. Büscher (IKP-2)

Dr. R. Castelijns (IKP-1) (until 30 November, 2006)

DP A. Chechenin (IKP-4)

DP D. Chiladze (IKP-2)

Prof. Dr.Dr.h.c. J. Dietrich (IKP-4)

Dr. A. Djalois (IKP-1)

DP A. Dzyuba (IKP-2)

Dr. R. Engels (IKP-2)

Prof. Dr. E. Epelbaum (IKP-3) (since 1 April, 2006)

DI F.-J. Etzkorn (IKP-4)

M. Evers (IKP-3) (until 28 February, 2006)

Dr. P. Fedorets (IKP-2)

Dr. O. Felden (Rs)

M. Freunek (IKP-3) (since 1 July, 2006)

Dr. W. Gast (IKP-1)

Dr. R. Gebel (IKP-4)

PD Dr. A. Gillitzer (IKP-1)

PD Dr. F. Goldenbaum (IKP-1)

PD Dr. D. Gotta (IKP-2)

Dr. F. Grümmer (IKP-3)

Dr. D. Grzonka (IKP-1)

DI W. Günther (IKP-4)

Univ. Doz. Dr. J. Haidenbauer (IKP-3)

PD Dr. C. Hanhart (IKP-3)

Dr. M. Hartmann (IKP-2)

Dr. V. Hejny (IKP-2)

DI K. Henn (IKP-4)

Dr. F. Hügging (IKP-1)

D. Jamanidze (IKP-2) (1 April – 30 September, 2006)

Dr. V. Kamerdjiev (IKP-4)

Dr. I. Keshelashvili (IKP-2)

DP D. Kirillov (IKP-4)

DP P. Klaja (IKP-1) (since 1 February, 2006)

A. Klingler (IKP-2) (since 1 April, 2006)

DP A. Kowalczyk (IKP-1) (since 6 November, 2006)

Dr. H. Krebs (IKP-3) (since 1 April, 2006)

Prof. Dr. S. Krewald (IKP-3)

DI K. Kruck (IKP-4)

Dr. A. Lehrach (IKP-4)

DP V. Lensky (IKP-3)

DP V. Leontyev (IKP-2)

DP M. Lesiak (IKP-1) (until 31 August, 2006)

Dr. B. Lorentz (IKP-4)

Prof. Dr. H. Machner (IKP-1)

Dr. Y. Maeda (IKP-2) (until 31 March, 2006)

Prof. Dr. R. Maier (IKP-4)

J. Majewski (IKP-2)

Dr. S. Martin (IKP-4) (until 30 April, 2006)

Prof. Dr. U.-G. Meißner (IKP-3)

DP M. Mertens (IKP-1) (since 16 October, 2006)

M. Mittag (IKP-2) (1 April – 30 September, 2006)

DI I. Mohos (IKP-4)

Dr. H.-P. Morsch (IKP-1) (until 31 December, 2006)

Dr. M. Nekipelov (IKP-2)

Prof. Dr. N.N. Nikolaev (IKP-3)

Dr. A. Nogga (IKP-3)

DP M. Odoyo (IKP-1) (1 March – 31 August, 2006)

Prof. Dr. W. Oelert (IKP-1)

DP D. Oellers (IKP-2)

Dr. H. Ohm (IKP-2)

DI N. Paul (IKP-1)

Dr. C. Pauly (IKP-1) (since 1 September, 2006)

DP F. Pavlov (IKP-3) (until 20 August, 2006)

DP B. Piskor-Ignatowicz (IKP-1) (until 28 Feb., 2006)

DP P. Podkopal (IKP-2)
 Dr. H. Polinder (IKP-3)
 Dr. D. Prasuhn (IKP-4)
 DP D. Protic (Dt)
 DP J. Przerwa (IKP-1) (since 1 February, 2006)
 PD Dr. F. Rathmann (IKP-2)
 DP Ch.F. Redmer (IKP-1)
 DI A. Richert (IKP-4)
 Prof. Dr. J. Ritman (IKP-1)
 Dr. E. Roderburg (IKP-1)
 Dr. P. v. Rossen (IKP-4) (until 31 December, 2006)
 DI J. Sarkadi (El)
 DP P. Saviankou (IKP-3)
 Dr. H. Schaal (IKP-1)
 PD Dr. S. Schadmand (IKP-1)
 E. Schlauch (IKP-3) (since 15 August, 2006)
 Dr. R. Schleichert (IKP-2)
 Dr.-Ing. A. Schnase (IKP-4) (until 30 September, 2006)
 DI H. Schneider (IKP-4)
 DI G. Schug (IKP-4)
 Dr. Th. Sefzick (El)
 DI E. Senicheva (IKP-4)
 Dr. Y. Senichev (IKP-4)

DI M. Simon (IKP-4)
 Dr. A. Sokolov (IKP-1)
 Dr. R. Stassen (IKP-4)
 Dr. H. Stockhorst (IKP-4)
 Dr. T. Stockmanns (IKP-1)
 DP Th. Strauch (IKP-2) (since 1 June, 2006)
 Prof. Dr. H. Ströher (IKP-2)
 T. Tolba (IKP-1) (since 1 August, 2006)
 Dr. R. Tölle (IKP-4)
 DP Y. Valdau (IKP-2)
 DI T. Vashegyi (IKP-4)
 Dr. N. Vasiukhin (IKP-4)
 DP P. Vlasov (IKP-1)
 Chr. Weidemann (IKP-2) (since 1 November, 2006)
 DP D. Welsch (IKP-4)
 Dr. P. Wintz (IKP-1)
 PD Dr. A. Wirzba (IKP-3)
 DI J.-D. Witt (IKP-4)
 Dr. M. Wolke (IKP-2)
 L. Yurev (IKP-2)
 Dr. E. Zaplatin (IKP-4)
 DP D. Z. Zhang (IKP-1)

L.2 Technical and Administrative Staff

C. Berchem (El)	St. Nießen (Dt)
P. Birx (IKP-4)	H. Pütz (IKP-4)
M. Böhnke (IKP-4)	G. Roes (Ad)
H. Bongen (IKP-1) (since 22 February, 2006)	N. Rotert (IKP-4)
J. Borsch (Rs)	D. Ruhrig (IKP-4)
P. Brittner (IKP-4)	T. Sagefka (IKP-4)
J. But (Ws)	F. Scheiba (IKP-4)
M. Comuth-Werner (Ad)	H. Schiffer (El)
B. Dahmen (IKP-4)	J. Schmitz (IKP-4)
C. Deliege (IKP-4)	F. Schultheiß (Ws)
W. Derissen (Co)	K. Schwill (Dt) (until 30 June, 2006)
N. Dolfus (El)	H. Singer (IKP-4)
G. D'Orsaneo (IKP-2)	D. Spölggen (IKP-2)
R. Dosdall (IKP-1)	G. Sterzenbach (IKP-1)
R. Enge (IKP-4)	J. Strehl (Ws)
B. Erkes (IKP-4)	R. Stumm (IKP-1) (until 31 January, 2006)
W. Ernst (El)	J. Uehlemann (IKP-1)
K. Esser (Ad)	P. Wieder (IKP-2)
H.-P. Faber (IKP-4)	Th. Willems (IKP-2) (until 31 January, 2006)
G. Fiori (Dt)	J. Wimmer (IKP-1)
H.-W. Firmenich (Ws)	H. Zens (IKP-4)
J. Göbbels (Rs)	
H. Hadamek (Ws)	
R. Hecker (IKP-4)	
E. Heßler (Co)	
M. Holona (Ws)	
H.-M. Jäger (IKP-1)	
H. J. Jansen (Ws)	
M. Karnadi (IKP-2)	
A. Kieven (IKP-4)	
Ch. Krahe (Ws)	
M. Kremer (Ws)	
Th. Krings (Dt)	
G. Krol (IKP-4)	
M. Küven (Ws)	
K.-G. Langenberg (IKP-4)	
H. Metz (Dt)	
S. Müller (Ad)	
R. Nellen (El)	

Ad = Administration
Co = Construction
Dt = Detectors
El = Electronics
Rs = Radiation Safety
Ws = Workshop

M List of Authors

- Ackens, A., 31
Amaro, F., 61
Anagnostopoulos, D.F., 61
ANKE collaboration, 1, 3–7, 9, 10, 13, 15, 56
- Bühler, P., 61
Büscher, M., 5, 54, 143
Balanutsa, V., 143
Barion, L., 56
Baru, V., 118, 119
Baumeister, H., 48
Baur, G., 93–97
Belov, A.S., 131
Belushkin, M., 63
Berchem, C., 153
Bernard, V., 76
Biegun, A., 104
Birnbaumer, P., 135
Bodek, K., 104
Borasoy, B., 66, 68, 69, 72
Borsch, H., 135, 136
Boukharov, A., 143
Brings, R., 133
Brittner, P., 140, 141
Bruns, P.C., 66
Bulgac, A., 98, 102
- Calén, H., 31, 35
Capiluppi, M., 58
Chernetsky, V., 143
Chiladze, D., 11, 13
Choudhury, D., 105
Ciepal, I., 104
Clement, H., 20
Contalbrigo, M., 59
COSY-11 collaboration, 39–47, 49
COSY-TOF collaboration, 17, 19, 20
Covita, D., 61
Cvitanović, P., 100
Czerwiński, E., 35, 43, 49
Czyżykiewicz, R., 35, 39
- Deltuva, A., 104, 108
Demekhin, A., 143
Devidze, G., 71
Dietrich, J., 126, 128, 129
Dolfus, N., 153
Doroshkevich, E., 20
dos Santos, J.M. F., 61
Duniec, D., 35
Duweke, C., 108
Dymov, S., 6, 11, 13
Dzyuba, A., 5
- Egelhof, P., 152
Ehrhardt, K., 19, 20
- Emmerich, R., 108
Engels, R., 11, 13
Epelbaum, E., 104, 106, 108, 113–115
Erhardt, A., 20
Ernst, W., 153
Erven, W., 31
Eyrich, W., 17
- Fedorets, P., 143
Felden, O., 131, 133, 136
Fonseca, A.C., 108, 111
Fransson, K., 31, 35
Frink, M., 67
- Göbbels, J., 136
Garishvili, A., 146
Gebel, R., 131, 133
GEM - KVI/UJ/US/UT collaboration, 52
GEM collaboration, 37, 50, 51
Gerasimov, A., 143
Glöckle, W., 104, 107–110, 113–115
Golak, J., 104, 107–110, 113–115
Goldenbaum, F., 27
Gotta, D., 61
Grevén, R., 140
Grigoriev, K., 11, 13
Grishina, V.Yu., 54
Gruber, A., 61
Grzonka, D., 27, 43, 47–49
Gusev, D., 11
Gusev, L., 143
Gustafsson, L., 31
Gårdestig, A., 111
- Haberzettl, H., 117
Haidenbauer, J., 79–89, 118, 119
Hammer, H.-W., 63, 79, 83, 84, 106
Hanhart, C., 73, 87, 111, 118, 119
Hecker, R., 135
Heczko, A., 35
Heim, T., 97
Heimbach, H., 140
Hejny, V., 31
Hencken, K., 96, 97
HESR consortium, 138, 145
Hinterberger, F., 36, 53
HIRES collaboration, 53
Hirtl, A., 61
Hodana, M., 29
Horowitz, C.J., 111
- Igashira, M., 109
Imig, A., 108
Indelicato, P., 61
Ivanov, G., 28
- Jansen, P., 11

Janusz, M., 28, 29, 149
 Jany, B.R., 21

 Kämmerling, P., 31
 Kacharava, A., 11, 13
 Kalantar-Nayestanaki, N., 104
 Kalashnikova, Yu., 87
 Kamada, H., 104, 107, 109, 110, 113, 115
 Katayama, T., 120
 Kemmerling, G., 31
 Keshelashvili, I., 23
 Khoukaz, A., 7, 9, 10, 32, 48
 Kieven, A., 131, 133
 Kievsky, A., 115
 Kikuchi, T., 109
 Kis, M., 104
 Kistryn, S., 104
 Klaja, P., 35, 40, 44
 Klehr, F., 11
 Kleines, H., 11, 31, 58
 Klos, B., 104
 Kobayashi, T., 109
 Kobets, A., 126, 128
 Komarov, V., 6
 Kondratyuk, L.A., 54
 Koptev, V., 5
 Kozela, A., 104
 Krebs, H., 72
 Krewald, S., 74, 85, 116, 117
 Krings, T., 151, 152
 Kruck, K., 135
 Kubis, B., 70
 Kucurkarlan, A., 75
 Kudryavtsev, A.E., 87, 118, 119
 Kulessa, P., 28, 29, 149
 Kulikov, A., 6
 Kupść, A., 34, 35
 Kupsc, A., 31
 Kurbatov, V., 6
 Kuros-Zolnierczuk, J., 104
 Kyryanchuk,, 37

 Lähde, T.A., 65
 Le Bigot, E.-O., 61
 Lee, D., 72
 Lee, T.-S.H., 89
 Lehrach, A., 138, 145
 Lenisa, P., 56, 58, 146
 Lensky, V., 118, 119
 Leontyev, V., 15
 Lewis, R., 66
 Ley, J., 108
 Liparteliani, A., 71
 Loevenich, H., 31
 Lomidze, N., 59
 Lorentz, B., 11, 146

 Müller, E.H., 70
 Macharashvili, G., 6, 59, 148

 Machner, H., 37
 Magierski, P., 98, 102
 Mahjour-Shafiei, M., 104
 Maier, R., 120, 126, 128
 Majewski, J., 28, 29, 149
 Makii, H., 110
 Malarz, A., 35
 Marciniowski, P., 31
 Martin, S., 146
 Maryshev, I., 143
 Meißner, U.-G., 63, 65–85, 88, 99, 104, 106, 108, 118, 119
 Mersmann, T., 7, 9, 10
 Merzliakov, S., 15
 Meshkov, I., 126, 128
 Micherdzinska, A., 104
 Mielke, M., 7, 9, 10
 Migdal, W., 35
 Mikirtychyants, M., 11, 13
 Mikirtychyants, S., 11
 Milke, N., 32
 Miller, G.A., 111
 Mishima, K., 110
 Mittag, M., 23
 Mohos, I., 151
 Moskal, P., 34, 35, 39, 40, 42–46, 49
 Miller-Veggian, M., 152

 Nagai, Y., 109, 110
 Naito, S., 110
 Nakayama, K., 89, 117
 Nass, A., 58
 Nawrot, A., 35
 Nefediev, A.V., 87
 Nekipelov, M., 1, 5, 61
 Nellen, R., 31, 153
 Niessen, S., 152
 Nikolaev, N.N., 90–92
 Niskanen, J.A., 111
 Nißler, R., 68, 69
 Nogga, A., 104–115

 Oelert, W., 27
 Oellers, D., 15, 56
 Ohgaki, H., 110
 Ohm, H., 28, 29, 31, 149
 Oset, E., 73

 Paetz gen. Schieck, H., 108
 Papenbrock, M., 7, 9, 10
 Parkhomchuk, V.V., 129
 Paul, N., 35
 Pauly, C., 26, 35
 PAX collaboration, 56, 59, 145
 Petukhov, Y., 149
 Phillips, D.R., 105
 PISA collaboration, 55
 Piskor-Ignatowicz, C., 42
 Podchasky, S., 143
 Podkopal, P., 24, 28

Polinder, H., 88, 103
 Pollacco, E.C., 152
 Povtoreyko, A., 36
 Prasuhn, D., 11, 120, 126, 128
 Pricking, A., 35
 Protić, D., 151, 152
 Przerwa, J., 35, 45, 46
 Pysz, K., 28, 29, 149

 Raha, U., 77, 78
 Rakhimov, A.M., 99
 Rathmann, F., 11, 13, 56, 58, 146
 Rausmann, T., 7, 9, 10, 32
 Redmer, C.F., 27
 Rejdych, B., 46
 Richert, A., 135
 Ritman, J., 33, 36
 Roca, L., 73
 Rotert, N., 131, 133
 Rozpedzik, D., 113
 Ruhrig, D., 135
 Rusetsky, A., 77, 78

 Sarkadi, J., 11, 58, 153
 Sauer, P.U., 104, 108
 Schäfer, W., 90–92
 Schiffer, H., 153
 Schleichert, R., 15, 56
 Schlessner, S., 61
 Schmid, P., 61
 Schmitz, J., 135
 Schneider, H., 135
 Schneider, S., 74
 Schug, G., 140, 141
 Sefzick, T., 27, 31, 153
 Semenov, A., 143
 Serdyuk, V., 28, 29, 149
 Seyfarth, H., 11, 13
 Shima, T., 109, 110
 Sibirtsev, A., 79–85
 Sidorin, A., 126, 128
 Simons, L.M., 61
 Singer, H., 140, 141
 Siudak, R., 36, 37, 53
 Skibinski, R., 104, 107, 109, 110, 113–115
 Smirnov, A., 126, 128
 Smyrski, J., 41, 42
 Soubotin, V. B., 116
 Spillmann, U., 151
 Stöhlker, Th., 151
 Stassen, R., 120, 140, 141
 Statera, M., 146
 Steffens, E., 58
 Steffens, E., 56
 Stein, H.J., 126, 128
 Stephan, E., 104
 Stockhorst, H., 120
 Ströher, H., 56, 58
 Strauch, Th., 61

 Sworst, R., 104

 Täschner, A., 7, 9, 10, 32, 48, 49
 Tabidze, M., 59
 Takaoka, K., 109
 Tamura, K., 110
 Thorndahl, L., 140
 Tikhomirov, V., 28
 Tolba, T., 33
 Toyokawa, H., 110
 Trautmann, D., 96, 97
 Trusov, S., 15
 Tselyaev, V. I., 116
 Tsirkov, D., 6
 Typel, S., 93–95

 Uzikov, Yu., 6, 86

 Valdau, Yu., 4
 van Kolck, U., 111
 Vasilyev, A., 11, 13
 Veloso, J.F.C.A., 61
 Vinas, X., 116
 Viviani, M., 115
 Vlasov, P., 36
 von Rossen, P., 131, 133

 Wüstner, P., 31
 Wagner, G.J., 20
 WASA collaboration, 21, 23, 24, 26–37
 Weglorz, W., 30
 Wilkin, C., 13, 86
 Winnemöller, A., 32
 Wirzba, A., 98–102
 Witala, H., 104, 107–110, 113–115
 Wolke, M., 31

 Yakhshiev, U.T., 99
 Yongseok Oh, 89
 Yuan, X., 5
 Yurev, L., 28, 29, 149

 Zakharov, B.G., 92
 Zejma, J., 104
 Zieliński, M., 34, 35
 Zipper, W., 104
 Zmeskal, J., 61
 Zoller, V.R., 92
 Zvoll, K., 31
 Zychor, I., 3

